NAME OF AUTHOR... *John   G   Samson* ....

TITLE OF THESIS....... *Spectral   Characteristics* ... *of   PC 4   and   PC 5   Geomagnetic*

.. *Micropulsations* ....

UNIVERSITY.... *Alberta* ....

DEGREE FOR WHICH THESIS WAS PRESENTED.......... *Ph. D.* ....

YEAR THIS DEGREE GRANTED...... *1971* ....

(Signed)... *J. G. Samson* ....

PERMANENT ADDRESS:

.. *556   Rochester Ave*

.. *Coquitlam, New Westminster*

.. *British   Columbia*

DATED.. *Sept 29* 19 *71*

THE UNIVERSITY OF ALBERTA

SPECTRAL CHARACTERISTICS OF

Pc 4 AND Pc 5 GEOMAGNETIC MICROPULSATIONS

by

$\copyright$ JOHN C. SAMSON

A THESIS

SUBMITTED TO THE FACULTY OF GRADUATE STUDIES AND RESEARCH

IN PARTIAL FULFILMENT OF THE REQUIREMENTS FOR THE DEGREE

OF DOCTOR OF PHILOSOPHY

DEPARTMENT OF PHYSICS

EDMONTON, ALBERTA

FALL, 1971

UNIVERSITY OF ALBERTA

FACULTY OF GRADUATE STUDIES AND RESEARCH

The undersigned certify that they have read,
and recommend to the Faculty of Graduate Studies and
Research for acceptance, a thesis entitled SPECTRAL
CHARACTERISTICS OF Pc 4 AND Pc 5 GEOMAGNETIC MICRO-
PULSATIONS submitted by John C. Samson in partial
fulfilment of the requirements for the degree of
Doctor of Philosophy.

....
Supervisor

....

....

....

....

Date........................

....
External Examiner

ABSTRACT

In the summer of 1969 a line of seven magnetic stations was established in western Canada between the geomagnetic latitudes of 58.5° and 77.0°N and within 2° of 302°E corrected geomagnetic longitude. This thesis gives an analysis of the general, spectral characteristics (including the three-dimensional polarizations and station-to-station phases) of Pc 4 and Pc 5 geomagnetic micro-pulsations recorded at these stations in 1969 and 1970.

A change in the horizontal sense of polariz-ation of the micropulsations, occurring around 1100 to 1200 local geomagnetic time, indicates that Pc 4's and Pc 5's are generated through the development of Kelvin-Helmholtz instabilities at the magnetopause. The power spectra and polarizations of the micropulsations exhibit marked latitudinal changes, implying that much of the micropulsation energy is distributed in resonant oscil-lations of magnetic shells. The existence of distinct Pc 4 and Pc 5 spectral bands may be the result of prefer-ential coupling of energy into magnetic shells near the auroral oval and near the plasmapause, with Pc 5's occurring primarily in the auroral regions and Pc 4's near the plasmapause.

ACKNOWLEDGEMENTS

TABLE OF CONTENTS

LIST OF TABLES

LIST OF ILLUSTRATIONS

1. INTRODUCTION

1.1 Geomagnetic micropulsations, definition and classification

Geomagnetic micropulsations are transient, ultra low frequency oscillations of the earth's magnetic field. Low frequency micropulsations ($\approx 10^{-3}$ Hz) often have amplitudes of hundreds of gammas at the earth's surface although high frequency micropulsations (≈ 1 Hz) seldom have amplitudes larger than a fraction of a gamma (γ). The structure of the pulsations may be very irregular and ragged or almost sinusoidal (Figure 1). In some cases the pulsations continue over many cycles, with some low frequency pulsation trains lasting for hours. At other times the pulsations disappear after only one or two oscillations. It is now commonly believed that continuous micropulsations originate within the magnetosphere as hydromagnetic waves, although there is considerable uncertainty about the energy sources and modes of propagation of these waves.

Micropulsations are normally classified in three characteristic ways, by their morphological properties (frequency, wave form, etc.), by their correlative properties, and by their genetical properties [*Jacobs*,1970]. At present
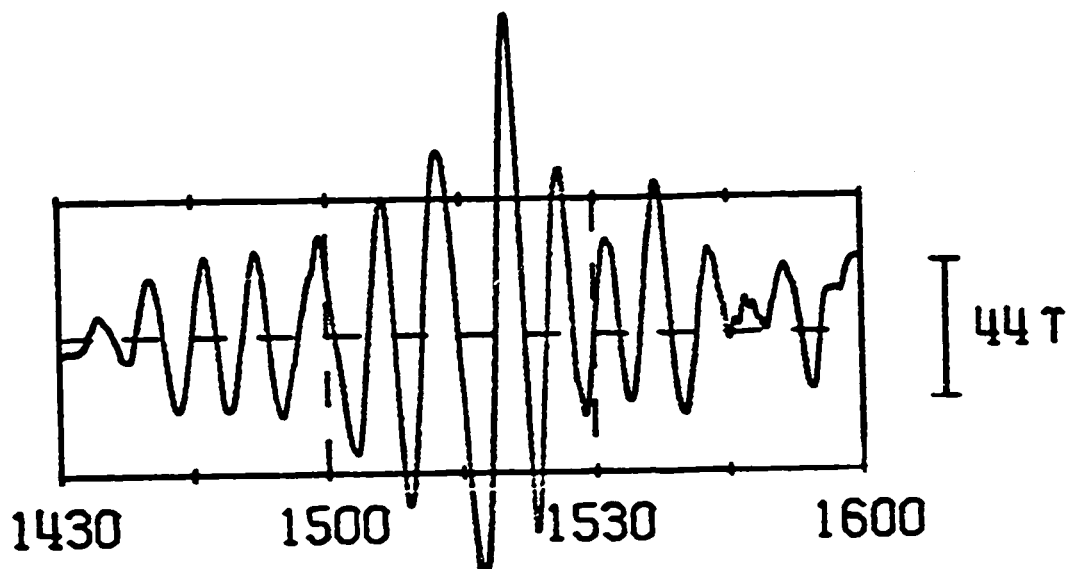
Fig. 1. An example of low frequency, continuous micro-pulsations. This event was recorded in the interval 1430-1600 UT, 1970.

both the correlative and genetical properties form a poor basis for classification in that correlative properties have been observed in only a few cases and, as mentioned above, the specific origins of many types of micropulsations are uncertain. A classification system based on the frequency of the oscillations and the wave form of the pulsation train is now commonly accepted. In this system regular, continuous pulsations are denoted by the term Pc and irregular, impulsive pulsations by the term Pi. Both the Pc and Pi classes are divided into frequency ranges based on other physical and morphological properties [*Jacobs et al.*, 1964]. Table 1 gives a list of these classifications. *Hultqvist* [1966] gives a more comprehensive description of the different classification systems.

TABLE 1. Micropulsation Classifications

Notation	Frequency (mHz)	Period (Sec)	Notation	Frequency (mHz)	Period (Sec)
Pc1	200-5000	0.2-5			
Pc2	100- 200	5-10	Pi1	25-1000	1-40
Pc3	22.2- 100	10-45	Pi2	6.7-25	40-150
Pc4	6.7-22.2	45-150			
Pc5	1.7-6.7	150-600			

The experiment outlined in this thesis was designed to study the morphological features of continuous micropulsations in the spectral range 1-30 mHz (Pc4 and Pc5) at a series of ground stations set at different latitudes along a geomagnetic meridian. For comparative purposes the analysis includes a number of nighttime Pi micropulsation events. We have reduced the data by means of a generalized spectral analysis of the micropulsation signals. In this method of analysis the autospectra and cross spectra are arranged in the form of 3x3 matrices, based on the three spatial components, and from these matrices the intensities, polarizations, and station-to-station phase characteristics of the micropulsations are calculated. This type of analysis allows a more objective and complete approach and puts the results in a format which is more compatible with the literature on the theory of micropulsations.

The analysis indicates that much of the energy of dayside Pc 4's and Pc 5's, and perhaps some of the energy of nightside Pc's, comes from Kelvin-Helmholtz instabilities at the dawn and dusk magnetopause. At least some of this energy is coupled into resonant oscillations of magnetic shells within the inner "dipole" region of the earth's magnetic field. The formation of distinct Pc 4 and Pc 5

spectral bands may be the result of preferential coupling of energy into magnetic shells near the auroral oval and near the plasmapause, with Pc 5's occurring primarily in the auroral regions and Pc 4's near the plasmapause.

1.2 Review of the observational results

Since *Stewart* [1861] first reported micropulsations, a great diversity of papers has appeared in the literature. The largest increase in the output of papers came about in the late 1950's after the I.G.Y. In the 1960's satellite data first appeared but, as yet, the number of reports of micropulsations is limited. The purpose of this review is to discuss very briefly the observations which are most pertinent to the data presented in this thesis. The first section deals with ground-based observations of Pc 4's and Pc 5's and the second section with recent satellite observations. *Troitskaya* [1967], *Campbell* [1967], *Saito* [1969], *Dungey and Southwood* [1970], and *Jacobs* [1970] have given more comprehensive reviews in these areas.

(A) Ground-Based Observations

— Both Pc 4's and Pc 5's have maximum amplitudes and occurrence frequencies in the auroral zones (65°-70° geomagnetic latitude) [*Jacobs and Sinno*, 1960; *Obertz and Raspopov*, 1968; and *Hirasawa*, 1970] although *Kato and Saito*

[1962] have noticed a second Pc 4 peak at 50°. The amplitudes of Pc 5's often reach hundreds of gammas in the auroral region, decreasing to about 1/5 of this value at 80° and 50°. Pc 4 amplitudes, on the other hand, are seldom greater than 10γ. The longitudinal extent of both Pc 4's and Pc 5's far exceeds the latitudinal extent and follows roughly an east-west direction along the auroral zone [*Eleman*, 1966]. *Obertz and Raspopov* [1968] observed that the characteristic longitudinal extent of Pc 5's is 60° with most activity centred between 0600 and 0900 LMT.

The diurnal variation of the occurrence frequency of auroral zone Pc 5's differs from that of midlatitude Pc 5's (40°-55°). In the auroral zones the activity peak is sharply defined and centred near 0400-1000 LMT, with a small second peak in the afternoon [*Saito*, 1964; *Hirasawa*, 1970] (see Figure 2). In sub auroral regions the occurrence frequency is double peaked with a second peak in the afternoon [*Ol'* 1963; *Saito*, 1964]. In midlatitude regions Pc 5's occur with equal probability over most of the day.

The amount of Pc 4 activity usually has a broad maximum in the daytime at midlatitudes [*Saito*, 1964] whereas the maximum is at 0300-0600 LMT in the auroral zones [*Saito*, 1964; *Stuart and Usher*, 1966; *Annexstad and Wilson*, 1968].
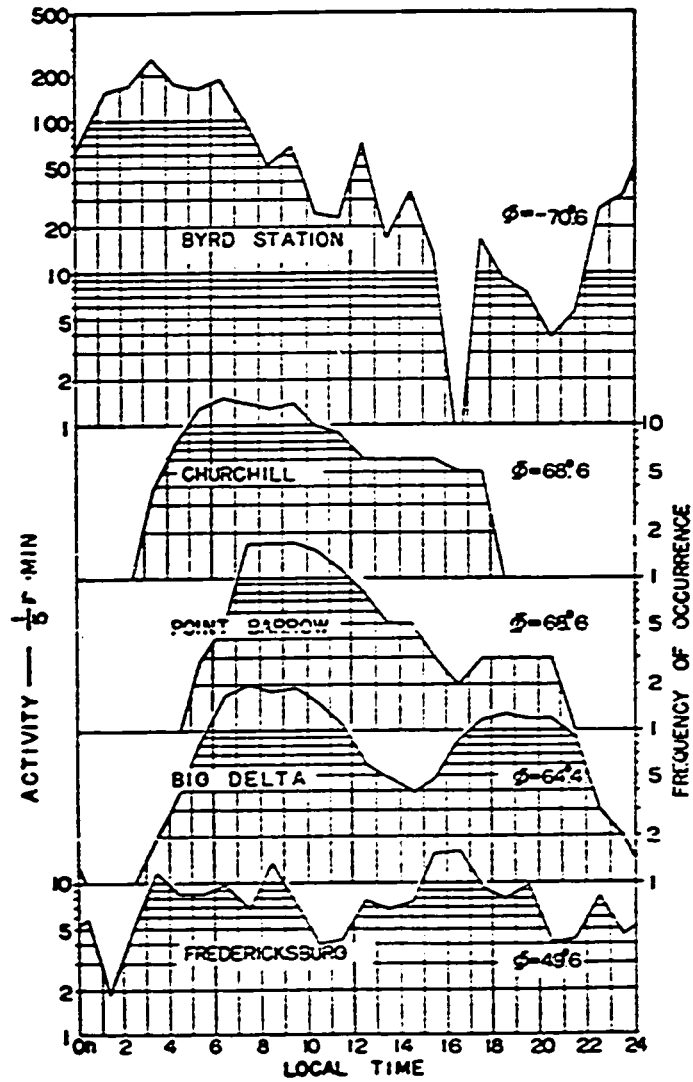
Fig. 2. The transition of Pc 5 occurrence frequencies
from a single maximum at high latitudes to a double
maximum at low latitudes (after *Saito* [1964]).

In general both Pc 4's and Pc 5's are most sinusoidal in
the morning and early afternoon, the greater part of the
evening and nighttime activity having only a few damped
cycles in the wave train [*Jacobs and Wright*, 1965].

Statistical studies by *Obayashi and Jacobs* [1958],
Oguti [1963] and *Ol'* [1963] show that the periods of Pc 4's
and Pc 5's increase with increasing latitude (Figure 3).
Ol' concluded that the average period T is given by the
equation

$$T = C \cdot \sec^2 \phi$$

where ϕ is geomagnetic latitude and C is a constant
depending on diurnal and solar cycle effects. Normally,
however, a given micropulsation event has the same frequency
at all latitudes [*Ellis*, 1960; *Obertz and Raspopov*, 1968].
The latitude-dependent Pc's noted by *Voelker* [1968] are
exceptions to this rule. These micropulsations exhibit a
systematic increase in the dominant period of the H component
with increasing latitude. This particular type of event will
be discussed in more detail in the analysis of data in this
thesis.

Saito [1969] postulated that although the frequency
of a specific micropulsation event is the same at all latitudes
(see profiles a and b in Figure 4), the statistically
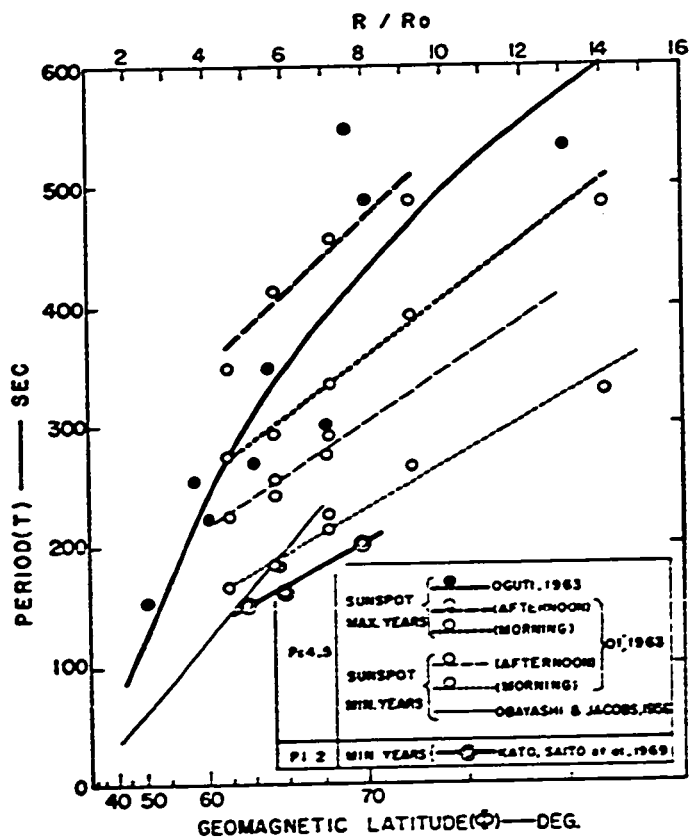
Fig. 3. The latitudinal dependence of the periods of Pc 4's and Pc 5's. The values R/R_0 are the equatorial radii of the field lines in units of earth radii (after *Saito* [1969]).
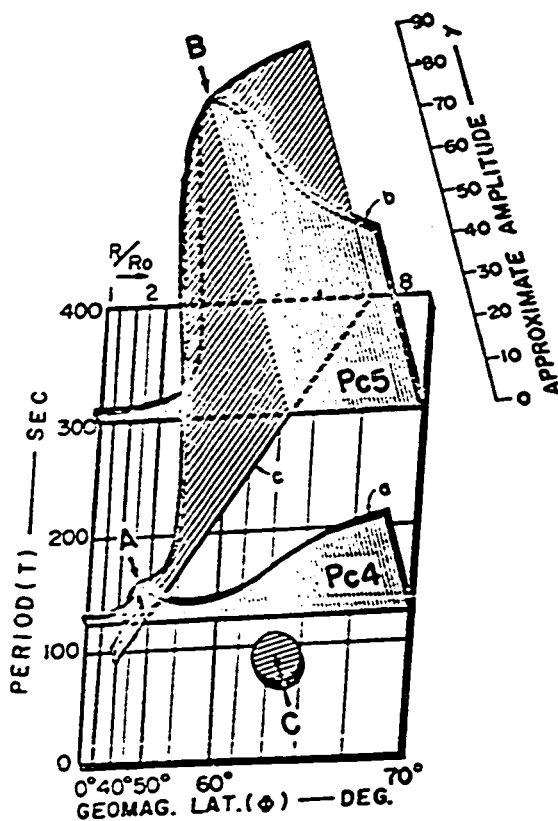
Fig. 4. Latitudinal and period dependence of Pc 4 and Pc 5 amplitudes. The curves *a* and *b* represent the latitudinal dependence of the amplitudes of Pc 4's and Pc 5's respectively. When the geomagnetic activity increases, the curves *a* and *b* move along line *c* to lower latitudes. Peaks A, B, and C belong to Pc 4, Pc 5, and giant pulsations respectively (after *Saito* [1969]).

determined frequencies can decrease with increasing latitude. He suggested that if the intensity peak of a Pc 4 or Pc 5 micropulsation train moves southward, due to increasing magnetic activity, then the frequencies of the pulsations increase (i.e. the peaks A and B move along line c in Figure 4). The analysis of *Obertz and Raspopov* [1968] supports Saito's model.

In general both Pc 4's and Pc 5's have higher frequencies during the day than at night. At midlatitude stations the Pc 4 frequency reaches a broad maximum centred near 1200 LMT [*Christoffel and Linford,* 1966; *Saito,* 1964]. The maximum frequency, occurring during the day, is 30-50 mHz and the minimum frequency, occurring at night, is 10-15 mHz. *Hirasawa and Nagata* [1966] and *Nagata and Fukunishi* [1968] found that the midlatitude Pc 4's actually occupy two distinct spectral bands, one centred at 15 mHz and the other at 30 mHz. The 30 mHz band is most evident during the day. Both bands show pronounced diurnal variations in frequency (Figure 5). During periods of low magnetic activity (Kp 0∿1) the highest frequencies occur around 1500 LMT and during periods of high activity (K_p 5∿7) around 0700 LMT. In the auroral zones, Pc 5's have their highest frequencies around 0600 LMT [*Saito,* 1964; *Hirasawa,* 1970] but in sub
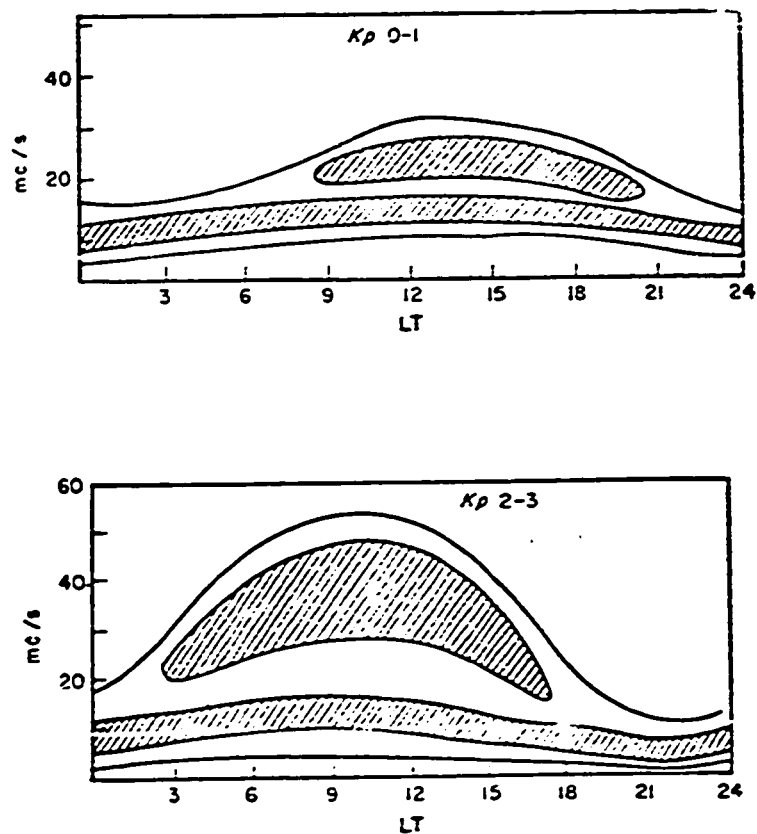
Fig. 5. Average sonograms of geomagnetic micro-pulsations recorded at Kakioka.

(a) Quiet conditions, $K_p = 0 \sim 1$;

(b) Slightly disturbed conditions, $K_p = 2 \sim 3$

(after *Nagata and Fukunishi* [1968]).

auroral and midlatitude regions they have their highest
frequencies around 1200 LMT [*Kitamura*, 1963; *Kato and
Saito*, 1962].

Both Pc 4's and Pc 5's show polarization char-
acteristics which change with latitude and time. Normally
the vertical component is the smallest but it does reach
appreciable amplitudes in the auroral regions [*Eleman*, 1966].
A complete analysis of the polarization characteristics of
micropulsations requires the determination of the projec-
tions of the polarization ellipse on three planes. Unfor-
tunately, this has only been done for a few events [*Paulson
et al.*, 1965; *Wilson*, 1966; *Annexstad and Wilson*, 1968].
To date most analyses have dealt only with the horizontal
projections of the polarization ellipses.

In northern high latitude regions (> 60°), the
horizontal components of Pc 5's are polarized in a CC
(counterclockwise)sense in the morning (looking down on
the earth), with 8-10 hours of predominantly CW (clockwise)
polarization during the afternoon and evening. The transition
between the morning and afternoon sectors typically occurs
around 1100 local geomagnetic time [*Kato and Utsumi*, 1964;
see Figure 6]. The morning section of CC polarization is
the clearest and the afternoon section most confused, having
an appreciable amount of both CW and CC polarization. These
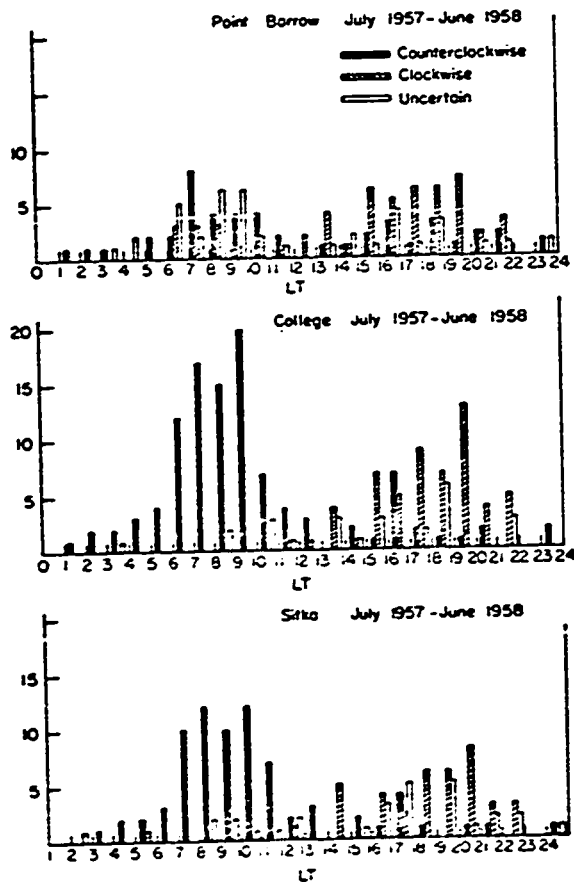
Fig. 6. Local time distribution of Pc 5's in
Alaska, showing the rotation sense of the disturbance
field vector in the horizontal plane (after *Kato and
Utsumi* [1964]).

diurnal polarization characteristics are reversed in the southern auroral regions [Saito, 1969]. In middle latitudes, the diurnal polarization characteristics of Pc 5's are more complex, with four sectors alternating from CW to CC [Saito, 1964].

The diurnal polarization pattern of high latitude Pc 4's matches the Pc 5 pattern (see Figure 7). One striking feature of Figure 7 is that the sense of polarization of Pc 2, 3's (30-100 mHz) is always opposite to that of Pc 4, 5's. Pc 2's and Pc 3's have CW polarization in the morning with a pronounced change to CC polarization in the afternoon. In northern midlatitudes Mather et al. [1964] found CW polarization for daytime Pc 4's and CC polarization for nighttime Pc 4's. This observation agrees with the southern, midlatitude Pc 4 polarizations determined by Christoffel and Linford [1966] (i.e. CC during the day and CW during the night, looking down at the earth).

In addition to diurnal changes in polarization, Pc 4, 5's exhibit pronounced latitudinal changes in their sense of polarization. Kaneda et al. [1964] and Obertz and Raspopov [1968] reported that Pc 5's at Barrow (68.6°) often had CW polarizations in the horizontal plane when the polarizations at Sitka (60.0°) and College (64.7°)
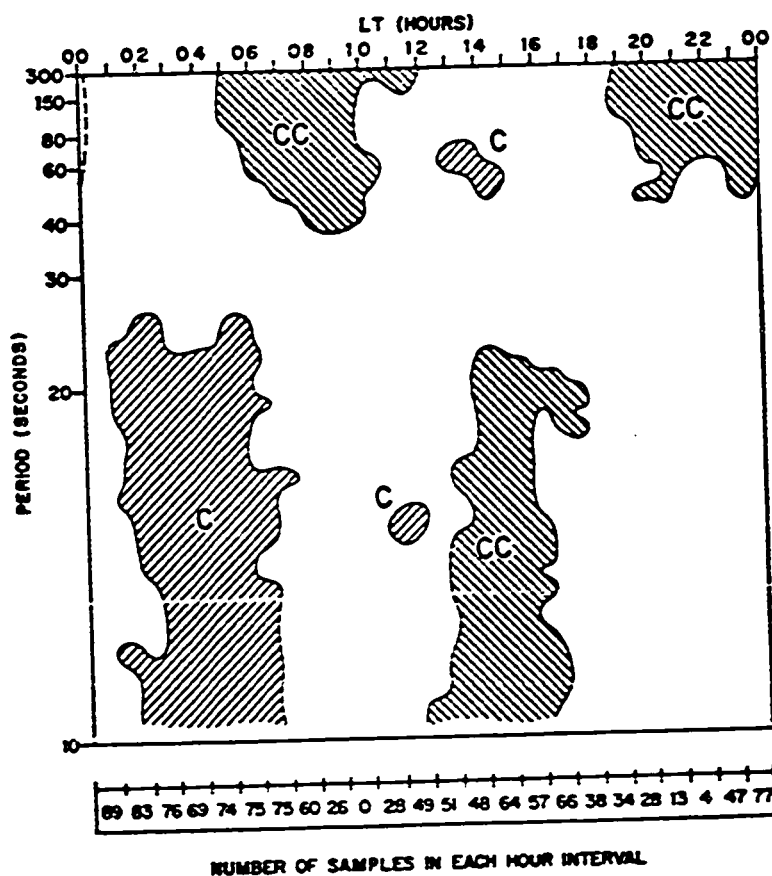
Fig. 7. Average senses of polarization in the horizontal plane of micropulsations in the spectral range 3.3 - 100 mHz. The shaded regions marked C have predominantly clockwise polarization and those marked CC have predominantly counterclockwise polarization. The unshaded regions have no predominant sense of polarization (after *Rankin and Kurtz* [1970]).

were CC. An appreciable latitudinal phase shift in the H
component accompanied the polarization reversal. In
addition, the opposite sense of polarization appeared only
when the centre of activity was between College and Barrow.
Eleman [1966] found similar latitudinal changes in the senses
of polarization of Pc 3, 4's, and *Sakurai* [1970] found
similar characteristics for Pi 2's.

Conjugate observations of pulsation waveforms and
polarizations are important since they directly relate
micropulsations to the magnetosphere. Studies by *Nagata*
et al. [1963] and *Jacobs and Wright* [1965] showed similar
Pc 5 pulsations occurring simultaneously at conjugate points.
They found, in addition, that the senses of polarization
were conserved along the geomagnetic lines of force. *Annex-*
stad and Wilson [1968] observed the same characteristics
for higher frequency (10-15 mHz) Pc 4's.

(B) Satellite Observations in the Magnetosphere

To date few observations of micropulsations have
been made by satellites and even fewer observations have been
related to ground-based data. Pioneers I and V and Explorer
6 recorded some of the earlier observations of pulsations
in the magnetosphere [*Coleman et al.*, 1960; *Sonett et al.*,
1962; *Judge and Coleman*, 1962]. *Patel and Cahill* [1964]

and *Patel* [1965] reported irregular 5.5-8.3 mHz (120-180 sec period) transverse oscillations recorded simultaneously both in the magnetosphere by Explorer 12 and at the ground on the same magnetic field line at College, Alaska. The waves needed 1 1/2 min to travel from the satellite to the ground. Patel and Cahill also found that the polarizations, frequencies, and amplitudes of the pulsations at College agreed with those at the satellite. In addition Patel found a local-time-dependence for the polarization at the satellite which was substantially in agreement with ground-based Pc 5 observations (i.e. CC before 1100 local geomagnetic time, CW after). *Dungey and Southwood* [1970], in an analysis of magnetic field data from Explorer 33, determined the same diurnal polarization rule for fluctuations inside the magnetosphere near the magnetopause (Figure 8).

One of the first reports on observations of continuous pulsations in the magnetosphere was made by *Cummings et al.* [1969] using records from the geostationary satellite ATS 1. These pulsations occurred during magnetically quiet periods, mostly in the interval 0400-1600 LMT. The oscillations were very sinusoidal and many continued for 10-400 min before disappearing (Figure 9). The observed frequencies
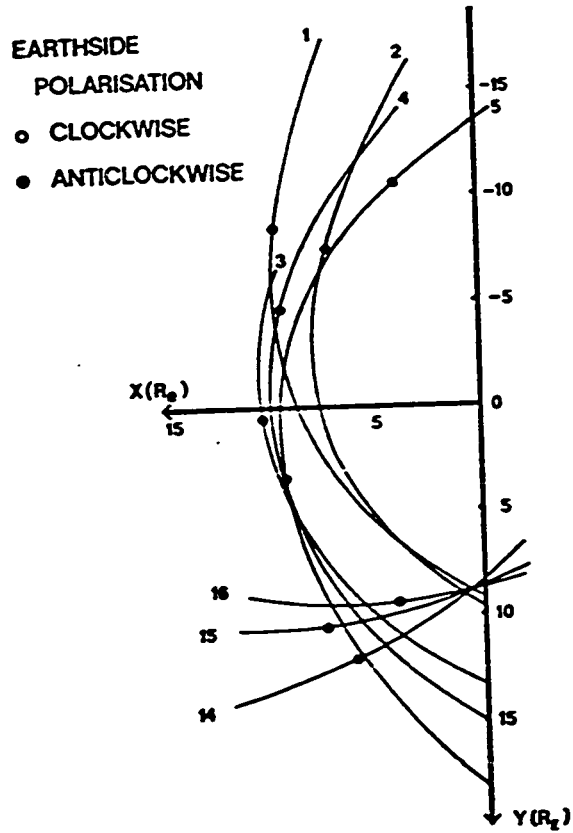
Fig. 8. Orbits of Explorer 33 projected on the ecliptic plane. The magnetopause crossings and the polarizations of the micropulsations are marked by open or closed circles (after *Dungey and Southwood*, [1970]).
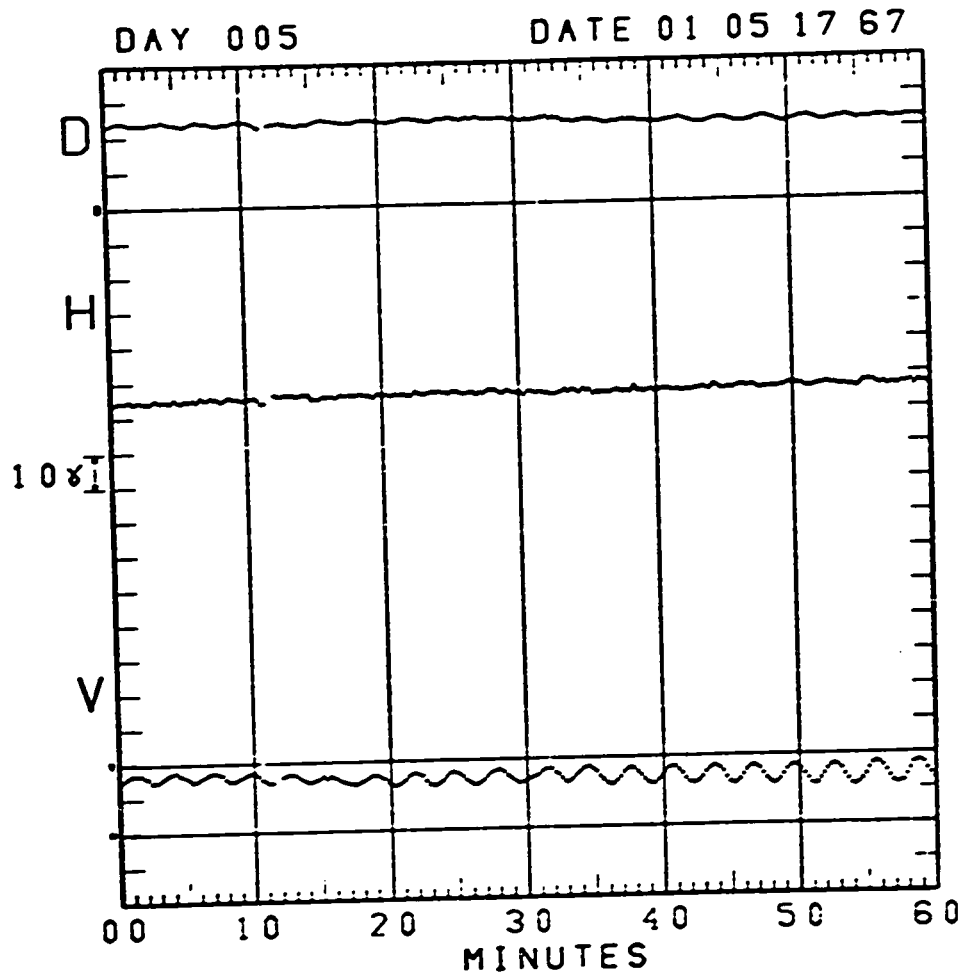
Fig. 9. An example of the transverse oscillations observed at ATS 1. The starting time (UT) is in the upper right corner of the diagram (month, day, hour, year). The D component is positive eastward, the V component is positive outward from the earth, and the H component is positive northward (perpendicular to the equatorial plane) (after *Cummings et al.* [1969]).

occupied two broad bands, one centred at 10 mHz (102 sec period) and the other at 5.3 mHz (209 sec period). Most of the pulsations were elliptically polarized in a plane transverse to the main magnetic field. More recently *Barfield et al.* [1971] have reported an observation of compressional Pc 4 micropulsations at ATS 1. Both the magnetic field intensity and energetic electron fluxes exhibited sinusoidal modulations at 9.4 mHz. These oscillations lasted for nearly seven hours. The largest pulsations reach 8γ (peak to peak) in the direction of the main magnetic field, with almost no magnetic variations transverse to the main field.

1.3 Excitation mechanisms proposed for continuous micropulsations

Continuous micropulsations are now thought to originate as hydromagnetic (hm) waves in the magnetosphere but there is still considerable uncertainty concerning the sources of energy which excite these waves. Some of the current theories are those based on

(a) gradients in particle and ionization densities [*Swift*, 1967].

(b) non neutral plasma distributions [*Nishida*, 1964; *Kimura and Matsumoto*, 1968].

(c) resonant interactions of particles and
waves [*Parker,* 1961; *Dungey,* 1965; *South-
wood et al.,* 1969; *Dungey and Southwood,*
1970]

(d) surface wave motions at the boundaries
between two regions of different plasma
concentrations [*Dungey,* 1954; *Sen,* 1965;
Atkinson and Watanabe, 1966; *Southwood,*
1968].

These mechanisms are discussed in some detail in the follow-
ing sections.

The energy in a gradient instability is derived
from the free energy of the inhomogeneous plasma [*Swift,*
1967]. The instability results in the generation of electro-
static waves in the magnetosphere which couple to electro-
magnetic waves in the ionosphere. The electrostatic waves
have CW polarization (looking in the direction of the
magnetic field) in a region of enhanced plasma density and
CC polarization in a depleted region.

Instabilities due to non neutral plasma distrib-
utions are excited by an electron or ion beam (such as
precipitating auroral particles) passing through some part
of the magnetosphere [*Kimura and Matsumoto,* 1967]. The
frequency of this instability depends only on the magnitude

of the excess charge and can be as low as the Pc 5 spectral band. A negative excess charge causes an instability in the Alfvén mode whereas a positive excess causes an instability in the modified Alfvén mode.

The most natural wave-particle instability for Pc 4's and Pc 5's is one involving bounce resonance [Dungey and Southwood, 1970]. Southwood et al. [1969] have shown that this resonance can occur in the magnetosphere under certain, very specific conditions. They found that quasi-transverse hm modes of large m can be excited by the exchange of energy with energetic particles. (The azimuthal variations of the wave are taken as $e^{im\phi}$ where ϕ is the azimuthal angle and m is an integer.) The change in the energy of a particle is directly proportional to the magnetic shell coordinate (L) of the particle and is independent of the particle's energy or pitch angle. The dominant parameter in energy exchange is the tilting of field lines and under certain conditions the growth rate of the waves can be very large.

The surface wave or Kelvin-Helmholtz instability at the magnetospheric boundary has long been a popular mechanism for the excitation of low frequency micropulsations [Dungey, 1954]. The surface waves are generated near the sun side of the equatorial magnetopause by the tangential flow of

the solar wind around the magnetosphere, flowing to the west on the morning side of 1100 local geomagnetic time and to the east on the evening side [*Atkinson and Watanabe,* 1966]. This tangential flow of the wind forces fluid elements in the magnetosphere to rotate in the manner shown in Figure 10. Since the magnetospheric plasma in this region is a good conductor the magnetic field is "frozen" into the plasma and is forced to rotate with it. Thus we expect the polarization configuration of Figure 11, with CC polarization before 1100 local geomagnetic time and CW polarization after 1100. These polarizations agree with both satellite and ground-based observations [*Dungey and Southwood,*1970]. *Southwood* [1968] deduced that in fact the magnetospheric boundary can be unstable. He showed that in equatorial regions, away from the subsolar point, the first growing hm modes propagate perpendicular to the geomagnetic field and are circularly polarized in a plane perpendicular to the main magnetic field.

1.4 Normal modes of oscillation in the magnetosphere

The theoretical treatment of hm modes in the earth's magnetosphere is extremely difficult. The problem is obscured by mathematical difficulties, by the complexity of the resonant cavities within the magnetosphere, and by
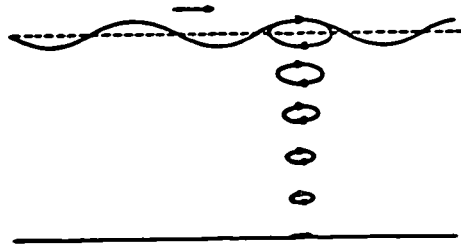
Fig. 10. Motion of fluid elements in a free surface wave (after *Atkinson and Watanabe* [1966]).
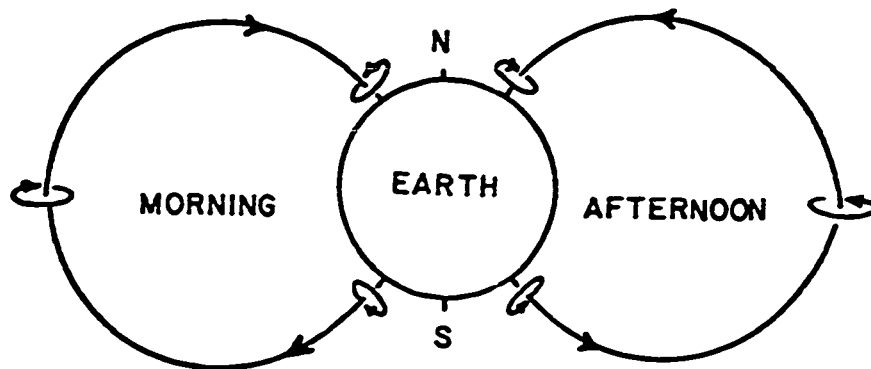
Fig. 11. The senses of polarization of geomagnetic micropulsations induced by a Kelvin-Helmholtz instability at the magnetopause.

uncertainties in the correct boundary conditions. Up to
the present, most theoretical treatments have considered
the resonant modes of an axially symmetric magnetosphere
[*Dungey*, 1954; *Jacobs and Westphal*, 1964]. If we further
assume that the disturbance field is axisymmetric, then
two simple hm modes exist. The toroidal mode has the
perturbation magnetic field polarized in an azimuthal
(east-west) direction and corresponds to a torsional oscil-
lation of a magnetic shell. The second mode, the poloidal
mode, corresponds to a compressional oscillation of the
whole magnetosphere. Normally, however, these modes are
not good approximations to actual conditions since most
observations show that the longitudinal (azimuthal) extent
of Pc 4, 5's is limited. *Dungey* [1954, 1967] and *Radoski*
[1967] have discussed very briefly some of the characteristics
of highly asymmetric perturbations.

The basic configuration of the magnetosphere and
its resonant cavities is depicted in Figure 12. The earth-
ionosphere boundary is usually considered a perfect reflector
for low frequency hm waves because of the high apparent
conductivity of the earth at these frequencies. *Dungey* [1970]
has indicated, however, that this assumption is open to some
doubt.
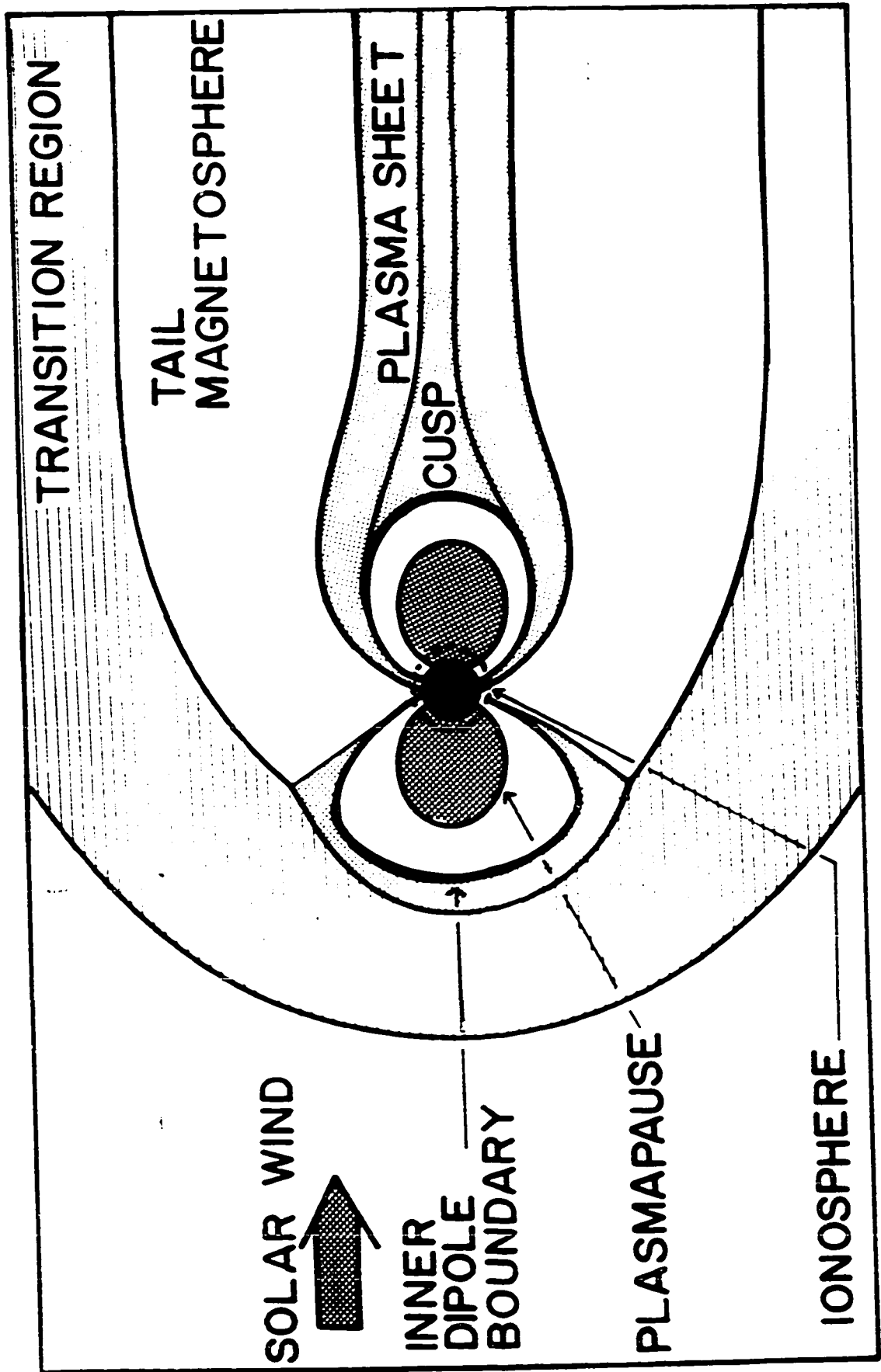
Fig. 12. The configuration of the earth's magnetosphere (meridian cut).

A problem related to the reflection of hm and electromagnetic waves within the earth and ionosphere is the determination of ground level magnetic fields which result when hm waves interact with the ionosphere. This problem is particularly important if we wish to relate ground-based observations to magnetospheric phenomena. Consequently the transmission and reflection of hm waves in the ionosphere has been considered in detail in a number of theoretical discussions, including those by *Prince and Bostick* [1964], *Field and Greifinger* [1965], *Greifinger and Greifinger* [1965] and *Inoue and Schaeffer* [1970].

The plasmapause (Figure 12) is a field-aligned density discontinuity which separates the plasmasphere, a region of relatively high plasma density ($\sim$ 100 electrons/cm^3), from the plasma trough (density $\sim$ 1 electron/cm^3). In the plasma trough the number density of electrons decreases as r^{-4} whereas inside the plasmasphere the density is determined by diffusive equilibrium [*Angerami and Carpenter,* 1966]. During periods of moderate magnetic activity ($K_p \approx$ 2-4), the geocentric distance to the dayside plasmapause is about 3.5 R_E (earth radii) whereas the distance to the nightside plasmapause is as great at 5.5 R_E. *Carpenter* [1970] and

Chappell et al. [1970] have given detailed descriptions
of the dynamic behavior of the plasmasphere and plasma-
pause.

Near the magnetic poles the geomagnetic field
loses its approximate dipole shape and the field lines are
swept back into the magnetotail configuration. This region
also includes part of the plasma sheet and the electron
densities are higher than those in the plasma trough
(0.3-30 el/cm^3[*Vasyliunas,* 1968a]). The outer limits of
the geomagnetic field are marked by the magnetopause. In
the solar direction the geocentric distance to the magneto-
pause is typically 10 R_E although distances ranging from
13 R_E to 8 R_E have been observed.

Most theoretical treatments of magnetospheric
oscillations use hm equations to describe the perturbation
magnetic and electric fields. For simplicity and convenience
we will follow this precedent and use these equations in
this discussion, even though it is not always clear that
the assumptions applicable to hm (or magneto-hydrodynamic)
equations are justified within the magnetosphere. *Hultqvist*
[1966], *Holt and Haskell* [1965], and *Rossi and Olbert* [1970]
have given comprehensive accounts of the conditions necessary
for the application of the hm equations.

The linearized, hm wave equation for a plasma with infinite conductivity is

$$\frac{\partial^2 \vec{E}}{\partial t^2} = \vec{v}_A \times \vec{v}_A \times \nabla \times \nabla \times \vec{E} \qquad (1)$$

(gaussian units)

where $\vec{E}$ is the perturbation electric field, $\vec{v}_A = \vec{B}_0 (4\pi\rho)^{-\frac{1}{2}}$ and $\vec{B}_0$ is the unperturbed magnetic field. The component equations are best analysed by first expressing them in orthogonal curvilinear coordinates (x_1, x_2, x_3) with the unit vector $\hat{x}_1$ in the direction of $\vec{B}_0$. Displacements along the three coordinates are given by the relation

$$dS_i = h_i dx_i \qquad (2)$$

where the scale factors h_i are in general functions of x_1, x_2, and x_3. In the analysis presented here we assume that the system is axisymmetric with respect to x_3. (In the earth's field, x_3 is geomagnetic longitude). If we further assume a time-dependence of the form $e^{i\omega t}$, then the component equations for an axisymmetric system are

$$\frac{1}{h_1}\left\{ \frac{\partial}{\partial S_3} \left[h_1 \left(\frac{1}{h_3} \frac{\partial}{\partial S_2}(h_3 E_3) - \frac{1}{h_2} \frac{\partial}{\partial S_3}(h_2 E_2) \right) \right] \right.$$

$$\left. - \frac{h_1}{h_3} \frac{\partial}{\partial S_1} \left[\frac{h_3}{h_2} \frac{\partial}{\partial S_1}(h_2 E_2) \right] \right\} = \frac{\omega^2}{v_A^2} E_2 \qquad (3)$$

$$\frac{1}{h_1}\left\{-\frac{\partial}{\partial S_2}\left[h_1\left(\frac{1}{h_2}\frac{\partial}{\partial S_3}(h_2 E_2) - \frac{1}{h_3}\frac{\partial}{\partial S_2}(h_3 E_3)\right)\right]\right.$$

$$\left.-\frac{h_1}{h_2}\frac{\partial}{\partial S_1}\left[\frac{h_2}{h_3}\frac{\partial}{\partial S_1}(h_3 E_3)\right]\right\} = \frac{\omega^2}{v_A^2} E_3 \qquad (4)$$

Equations (3) and (4) are coupled and consequently are very difficult to solve except in a few simple cases.

Since the system is axisymmetric with respect to x_3, E_i can be represented by a summation of modes. More precisely,

$$E_i = \sum_{m=0}^{\infty} {}^m N_i \, e^{imx_3} \qquad (5)$$

In solving for the mode in which $m = 0$ (the mode in which the perturbation fields are also axisymmetric), two decoupled equations result.

$$\frac{1}{h_3}\frac{\partial}{\partial S_1}\left[\frac{h_3}{h_2}\frac{\partial}{\partial S_1}(h_2 {}^0 N_2)\right] = \frac{-\omega^2}{v_A^2} {}^0 N_2 \qquad (6)$$

$$\frac{1}{h_2}\frac{\partial}{\partial S_1}\left[\frac{h_2}{h_3}\frac{\partial}{\partial S_1}(h_3 {}^0 N_3)\right] + \frac{1}{h_1}\frac{\partial}{\partial S_2}\left[\frac{h_1}{h_3}\frac{\partial}{\partial S_2}(h_3 {}^0 N_3)\right]$$

$$= \frac{-\omega^2}{v_A^2} {}^0 N_3 \qquad (7)$$

Equation (6) describes the toroidal mode of oscillation and equation (7) the poloidal mode. The toroidal mode appears to be a "guided" mode since there are derivatives only along a field line. Equation (6) can be solved by using the W.K.B. approximation where applicable [*Radoski*, 1966]. By using the W.K.B. approximation and assuming that the earth is a perfect reflector, we find that the resonant frequencies of this mode are given by the relation

$$\omega \int_{\phi_1}^{\phi_2} \frac{dS_1}{V_a} = n\pi \qquad n = 1, 2, 3... \qquad (8)$$

where ϕ_1 and ϕ_2 are the points where the field line intercepts the earth. From this equation it appears that ω is a function of position and this violates the assumptions used to obtain equations (3) and (4). (i.e. we assumed that $\frac{\partial}{\partial x_i}(\omega) = \omega\frac{\partial}{\partial x_i}$.) *Bruška* [1968] and *Kahalas* [1969] have shown that this dilemma can be resolved by a closer inspection of the physical parameters in the problem. Since the integral in equation (8) normally increases with increasing geomagnetic latitude, the expected frequency of the toroidal mode must decrease with increasing latitude [*Dungey*, 1954; *Jacobs and Westphal*, 1964].

The perturbation magnetic field $\vec{B}$ is found using Faraday's Law

$$\nabla \times \vec{E} = - \frac{1}{c} \frac{\partial \vec{B}}{\partial t} \tag{9}$$

More explicitly

$$\left(B_1, B_2, B_3\right) =$$

$$c(i\omega)^{-1} \left[\frac{1}{h_2 h_3} \frac{\partial}{\partial x_2} (h_3^0 N_3), \frac{1}{h_1 h_3} \frac{\partial}{\partial x_1} (h_3^0 N_3), \frac{1}{h_1 h_2} \frac{\partial}{\partial x_1} (h_2^0 N_2) \right] \tag{10}$$

Equation (10) shows that the magnetic field of the toroidal mode is polarized in the x_3 direction (east-west) and that the poloidal mode has components along the field and in the x_2 direction. The poloidal mode will not be discussed in any more detail here since this mode has very complex analytic solutions. *Kato and Akasofu* [1955], *Jacobs and Westphal* [1964], and *Carovillano et al.* [1966] have given comprehensive discussions of this mode.

Another simple but interesting case occurs when the disturbance has an extreme longitudinal asymmetry (modes of large m). The magnetic disturbance then becomes transversely polarized in the x_2 direction and obeys an equation very similar to the toroidal wave equation. *Radoski* [1967] called this mode a guided poloidal mode.

Unfortunately the picture presented above is drastically simplified. The magnetosphere is clearly not symmetric and the approximations used to obtain the hm equations and equation (1) are open to considerable debate. A more realistic approach to the problem would be to consider the effects of finite conductivity and finite Hall currents in the Ohm's law relation and possible viscous effects in the equation of motion. Inclusion of any of these terms couples the wave equations. Even in the simple axisymmetric case, the toroidal and poloidal modes are coupled. Magnetospheric oscillations with mode coupling have been considered briefly by *Bruska* [1968, 1969] and *Kahalas* [1969] and in more detail by *McClay* [1970].

2. EXPERIMENTAL DETAILS

2.1 The magnetic stations

In the summer of 1969 a line of 7 magnetic stations was established in Alberta and the Northwest Territories of Canada (see Figure 13) to record polar substorms and low frequency (1-20 mHz) micropulsation activity. In 1970 the station at Penhold was moved to Leduc and an additional station was established at Fort Reliance to give a total of eight stations. The stations lay within 2° of 302° corrected geomagnetic longitude [*Hakura*, 1965]; the southernmost station was at Calgary (58.5°N) and the northernmost at Cambridge Bay (77°N) (see Table 2). Each station used three-component fluxgate magnetometers oriented in (H, D, Z) coordinates (Figure 14).
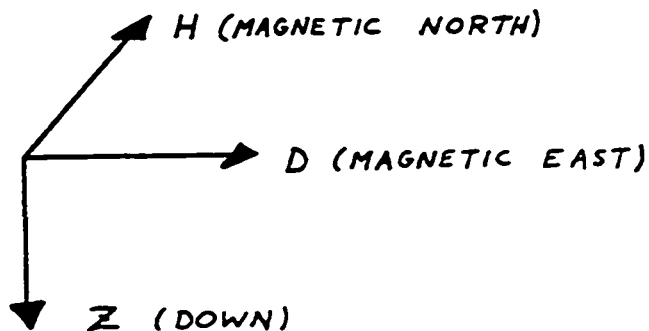
Fig. 14.   The magnetic coordinates
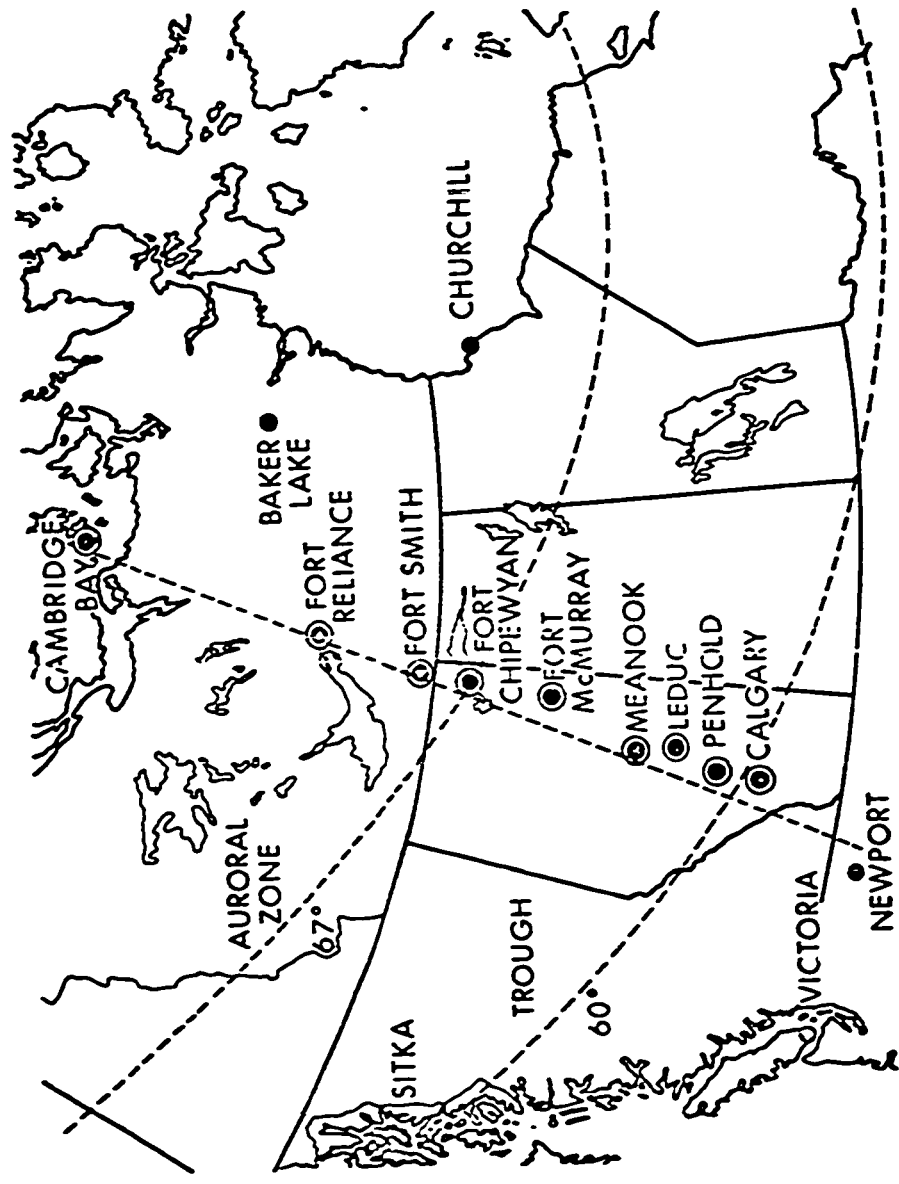
Fig. 13. Locations of the magnetic stations (double circles) used in this experiment. Standard magnetic observatories are shown as solid circles. The approximate positions of the auroral zone and the plasma trough are indicated by dotted lines.

Data were recorded digitally on 7-track, magnetic tapes
at a rate of 1 sample/component/sec in 1969, and at a
rate of 1 sample/component/2 sec in 1970, To time the
records, each system recorded WWVB directly on tape every
16 hr 23 min in 1969 and every 7 hr 38 min in 1970.
Appendix A6 gives a more complete description of the
instrumentation.

The most common source of lost data originated
from failures in the digital systems. Any large transients
in line power caused lost data blocks with subsequent data
gaps and inaccurate timing. This problem was especially
severe in 1969 since the digital system had to be restarted
manually after every power failure. An automatic restart
mechanism was incorporated into the system in 1970. At RELI,
nearby radio transmitters caused large amounts of digital
and magnetometer noise. The number of transients in the
magnetic data from RELI is so great that no data from this
station are included in the spectral analysis. Other
difficulties occurring in the magnetometers resulted in
lost data at SMIT, MCMU, and MENK. At MENK a malfunction
in the D component amplifier during most of the summer of
1970 caused sporadic changes in the gain of the channel.

TABLE 2 The Magnetic Stations

Station	Code Name	Corrected Geomagnetic Coordinates		Time Interval in Operation	
				1969	1970
Calgary	CALG	58.7°N	302.0°E	Aug-Nov	May-Nov
Penhold	PENH	59.5	301.4	Aug-Nov	---
Leduc	LEDU	61.2	301.5	---	June-Nov
Meanook	MENK	62.5	301.2	Sep-Nov	May-Nov
Fort McMurray	MCMU	65.0	304.0	Aug-Nov	May-Nov
Fort Chipewyan	FTCH	67.0	303.0	Aug-Nov	May-Nov
Fort Smith	SMIT	68.5	302.0	Aug-Nov	May-Nov
Fort Reliance	RELI	71.4	300.0	---	July-Oct
Cambridge Bay	CAMB	77.0	301.0	Aug-Nov	June-Oct

2.2 Geoelectric characteristics of the earth in central Canada: Associated induction effects

The geoelectric properties of the earth in central Canada are summarized in Figure 15. The electrical properties of the substrata in southern Alberta and southern British Columbia are well known since many magnetotelluric and geomagnetic depth sounding surveys have been made in these regions

Figure 15. Geological and geoelectric regions
of central Canada

The numbers in parenthesis on the map are the surface resistivities of the regions in units of ohm meters.

Legend

1. The Cordilleran Region, Paleozoic sediments, Tertiary volcanics, Mesozoic and Cenozoic intrusives.
    *Surface resistivity 100-1000 Ω M.

2. Lower and Upper Cretaceous marine and non marine sedimentary rocks.
    *resistivity 5-400 Ω M.

3. Proterozoic intrusions, acidic rocks, granodiorite, granite, quartz diorite.
    *resistivity 5000-20000 Ω M.

4. Devonian sedimentary and volcanic rocks.
    *resistivity 100-2000 Ω M.

5. Ordovician and Silurian sedimentary rocks
    *resistivity 50-200 Ω M.

* The resistivities in regions 1 and 2 were obtained from *Rankin and Reddy* [1969], *Peeples* [1969] and *Cochran and Hyndman* [1970]. The resistivities for the rocks in other regions were obtained from *Keller and Frischknecht*[1966].
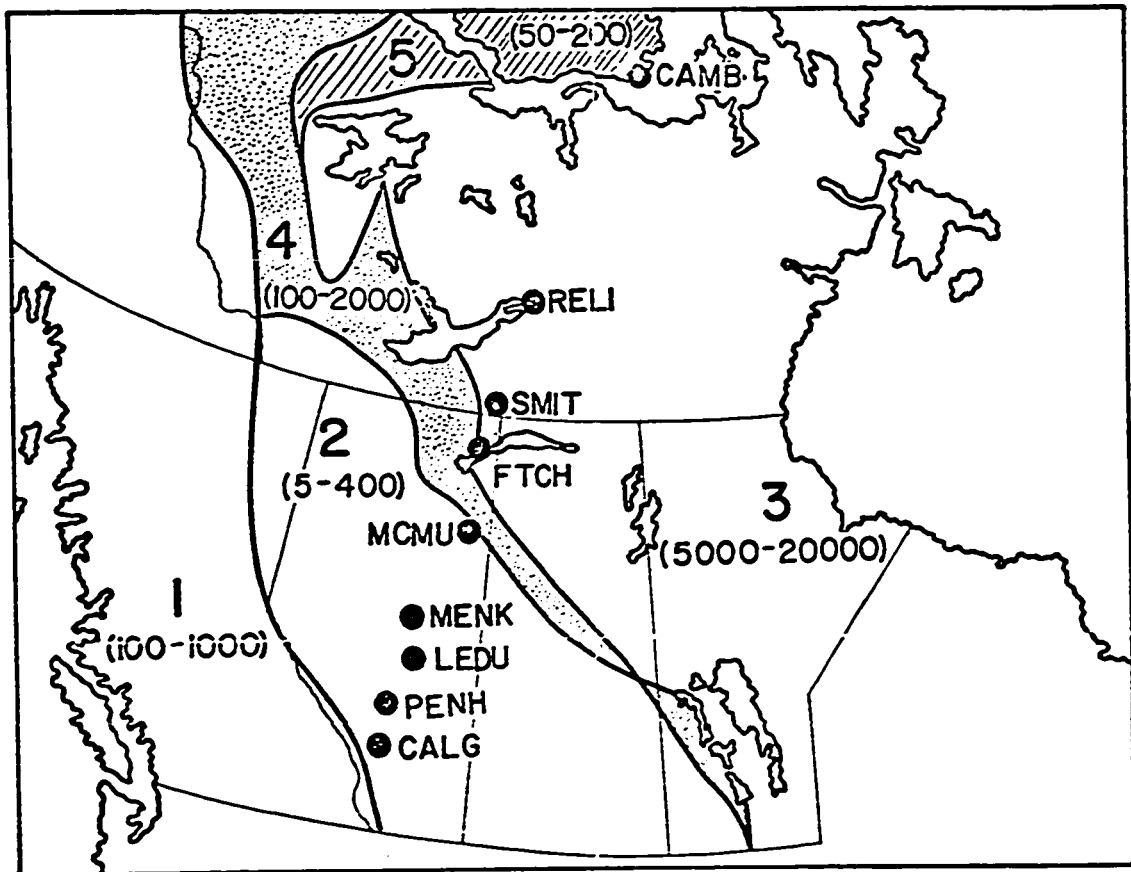
Fig. 15.

[*Caner et al.*, 1969; *Rankin and Reddy*, 1969; *Peeples*,
1969; *Cochran and Hyndman*, 1970]. In the mountains of
southern British Columbia (region 1 on Figure 15) a thin
(10-20 km) layer of resistive rocks overlies a thick
(20-40 km) region of rocks with very low resistivities
(5-15 ΩM). Conversely over most of southern Alberta (region
2) a thin (1-2 km) layer of conducting sediments (5-10 ΩM)
overlies layers of more resistive (200-400 ΩM) Cretaceous
sedimentary rocks [*Rankin and Reddy*, 1969; *Peeples*, 1969].
There is no doubt that in the mountain regions induced
earth currents strongly affect the magnetic fields of Pc 4
and Pc 5 micropulsations. These effects might extend as
far east as Calgary. Induction should also be noticeable in
the Pc4 micropulsation band at all the stations in southern
Alberta (see Appendix A7). Highly resistive intrusive rocks
occupy most of the Canadian Shield (region 3) and, depend-
ing on the thickness of these rocks, the induction effects
at FTCH, SMIT, and RELI should be negligible. Ocean waters
should produce the most substantial induction at CAMB. There
is also evidence for a shallow,conducting anomaly to the far
north on Ellesmere Island [*Praus et al.*, 1971] but the
exact extent of this anomaly is not yet known. In summary
we expect induction to be noticeable at all our stations
except the three on the Canadian Shield.

2.3 Method of data analysis

Many researchers in the field of micropulsations estimate wave characteristics such as mean periods, mean amplitudes, and polarization hodographs directly from amplitude-time recordings. These methods are often cumbersome and the results misleading. (See for example *Pope* [1964], *Egeland* [1965].)In addition, the necessity for clean monochromatic events drastically limits the selection of data. Finally, the results of such analyses are often difficult to compare with the theoretical literature since most theories are developed in terms of the spectral components of the wave forms (i.e. the time dependence is of the form $e^{i\omega t}$). Clearly an alternative presentation of the data is needed.

Correlation and cross spectral matrices offer useful, alternate formulations for micropulsation data (see Appendix A1). Data pertaining to quasi-monochromatic waves are easier to interpret by considering the spectra of the waves and the geometric figures traced out by the waves' disturbance vector. In the simple case of a monochromatic signal the endpoint of the disturbance vector traces out an ellipse. The parameters of the polarization ellipses can be computed directly from the cross spectral matrix $J_{ij}(\vec{r}_1,\vec{r}_1,f)$ (see Appendix A1 for an explanation of the

symbols) and the relative phases of the vector components at different stations can be calculated directly from $J_{ij}(\vec{r}_1,\vec{r}_2,f)$. Considerable care must be exercised in using these methods, however, since many hazards are involved in estimating the spectral parameters from real data (see Appendices A2, A3 and A4).

In the analysis of the data presented in this thesis the following parameters were calculated.

(A) Polarization Parameters

(a) R_1 is the ratio of the apparent plane polarized signal intensity to the total signal intensity (see equation (A17)). The definition of plane polarization used here is not the same as that used in optics. By plane polarization we mean that at one point in space the vector is restricted to motion on a given plane. For example, suppose that we have sinusoidal pulsations with powers a, b, and c in the H, D, and Z directions respectively and that a totally random signal, with power d in each direction is then superimposed on the pulsations. Since the motion of the disturbance vector of three-dimensional, sinusoidal oscillations describes an ellipse in a given plane, the intensity of the plane polarized signal is (a+b+c) and

$$R_1 = \frac{(a+b+c)}{(a+d) + (b+d) + (c+d)} \qquad (11)$$

(b) R_2 is the ratio of the completely coherent signal intensity to the plane polarized signal intensity (see equation (A20)) R_2 is equivalent to the polarization ratio defined by *Born and Wolf* [1954] and *Fowler et al.* [1967].

(c) The intensity I is the total power of the coherent signal (equation (A22)). In the above example

I = a+b+c.

The projection of the polarization ellipse (equation(A21)) was determined for each of three planes (H-D, H-Z, D-Z) by using the rotation matrix R (equation (A14) and the cross spectra P_{ij} (equation (A18)).

(d) In each plane, the ellipticity is the ratio of the minor to the major axis of the polarization ellipse. Looking at the plane from a direction in which the coordinates form a left handed system (downward on the horizontal H-D plane), the ellipticity is considered positive if the polarization is counter-clockwise (Figure 16). Zero ellipticity (E=0) represents linear polarization while unity represents circular polarization.

ELLIPTICITY = A_i / B_i

E = -1

E = 0

E = +1
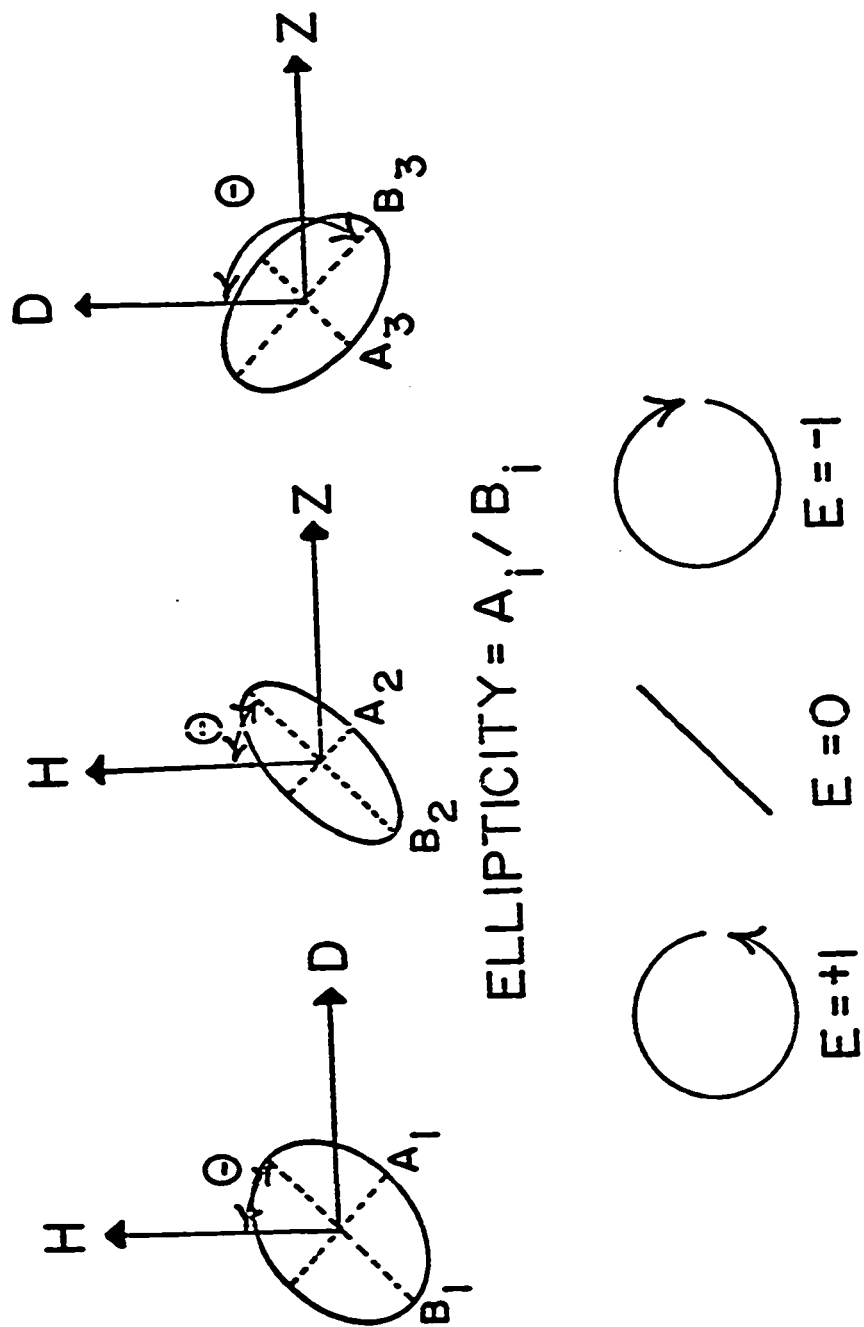
Fig. 16. The polarization parameters.

(e) The polarization angle θ is the angle, measured
clockwise, between the major axis of the ellipse
and the H direction in the H-D plane, the major
axis and the H direction in the H-Z plane, and
the major axis and the D direction in the D-Z plane.

(B) <u>Station to Station Correlations: Coherency and Phase</u>

(a) The coherency $K_{ij}(r_1, r_2)$ is a measure of the cor-
relation of component i at station r_1 with
component j at station r_2 (see equation (A27)).
This might be, for example, a correlation of the
H component at SMIT with the Z component at MCMU.

(b) The phase estimator $F_{ij}(r_1, r_2)$ is a measure of the
phase difference between component i at station
r_1 and component j at station r_2. If F_{ij} is
positive then component i leads component j.

To prevent needless repetition in the calculations of the
phases and coherencies only six component-to-component
comparisons were made for each pair of stations. These were
$H(r_1) \cdot H(r_2)$, $H(r_1) \cdot D(r_2)$, $D(r_1) \cdot D(r_2)$, $D(r_1) \cdot Z(r_2)$, and
$Z(r_1) \cdot Z(r_2)$. For the sake of brevity, not all these
estimates are given in this thesis. In most cases one
station was used as a base and the coherency and phase
parameters of all other stations calculated with respect
to that station.

In the actual analysis, two data windows were
used. One was one hr long and was used in the analysis
of low frequency Pc 5 micropulsations. The other was
1/2 hr long and was used in the analysis of Pc 4 micro-
pulsations. A more complete description of these data
windows and the associated spectral windows is given in
Appendices A2, A3 and A4.3.

The lengths of the data windows were dictated
by the scale size of the temporal variations of the
micropulsation spectral parameters. Normally Pc 4's and
Pc 5's have stationary spectral characteristics over periods
of 1/2 hour to hours, with perhaps some fluctuations in
amplitude over periods of 10-20 min [*Saito*, 1967]. There
is generally no consistent and pronounced dispersion in
the spectra and no consistent short term changes in the
sense of polarization. The long term stability of these
parameters is illustrated in Figure 17. Apparently the
ellipticity and central frequency of this event remained
stationary for over an hour. This feature was generally
the case in almost all the events analysed in this fashion.
It appears then, that the spectral changes are based on a
time scale greater than 1-2 hr, perhaps a time scale of
diurnal length. With these considerations in mind, a window

Fig. 17. Contours of the intensity, $\log_{10}$ (intensity), and ellipticity in the H-D plane of a micropulsation event occurring on day 163, 1970 and recorded at LEDU. Intensities are in units of γ^2.

ELLIPTICITY

LOG INTENSITY

INTENSITY
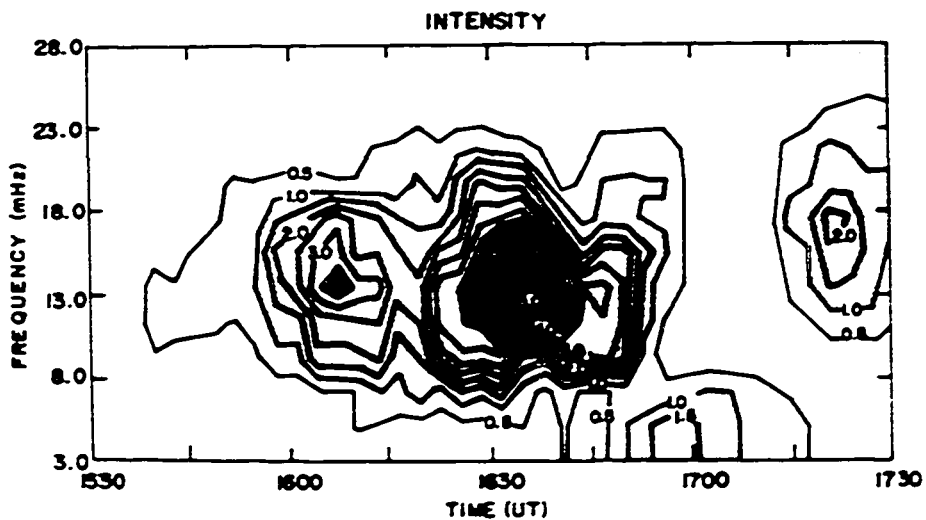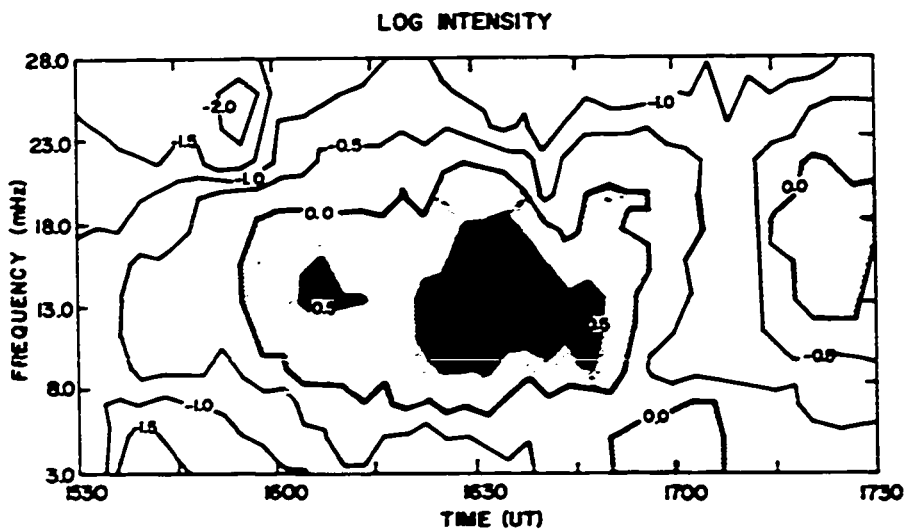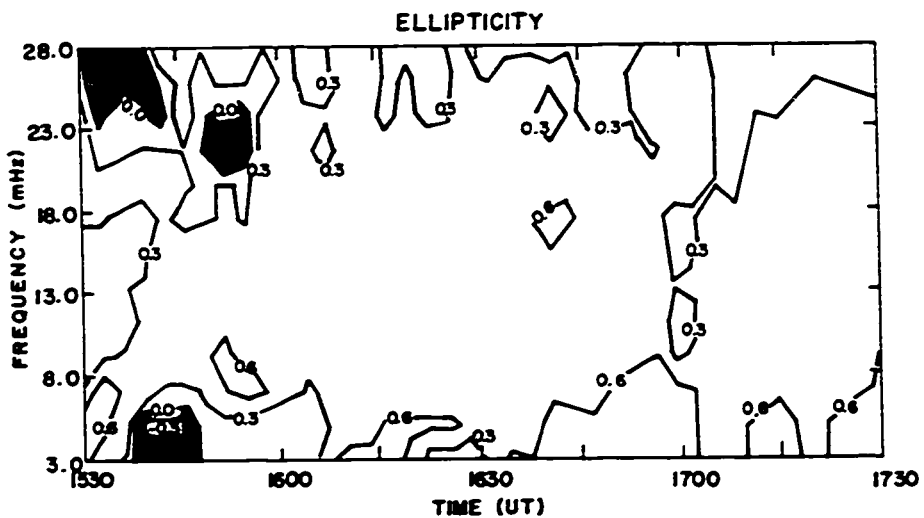
Fig. 17.

length of 1/2 - 1 hr apparently gives the best compromise between temporal resolution and the amounts of data analysed.

Computer programs were written to determine the elements of the cross spectral matrix (equations (A12), (A25)) and from these, the polarization, phase and coherency estimates were computed. Appendix A4 outlines the practical considerations in the evaluation of these parameters. To facilitate analysis, the computer programs were also designed to pick quasi-monochromatic spectral peaks (corresponding to quasi-sinusoidal micropulsation events). The quasi-monochromatic restriction specifies that the micropulsations have a spectral peak of mean frequency ν with a peak width $\Delta\nu$ (measured between half power points) such that $\frac{\Delta\nu}{\nu} \ll 1$. In practice, peaks with $\Delta\nu/\nu > 0.5$ were rejected. The best resolution used in separating peaks is given by the relation $\Delta\nu_s/\nu > 0.1$ where $\Delta\nu_s$ is the separation of the two spectral peaks and ν their mean frequency. For example, peaks at 100 and 110 mHz would be analysed separately whereas peaks at 100 and 105 mHz would be averaged to give an estimate at $\sim$ 103 mHz. In the selection of the polarization parameters by the computer, events with R_1 or $R_2 < 0.75$ were rejected (see Appendix A3). In the selection of station - to - station phase

estimates, events with all coherencies less than 0.45 were rejected. In other words if $K_{ij}(r_1,r_2,f_0) < 0.45$, then the phase estimates in the comparison of station r_1 with station r_2 at frequency f_0 were rejected. This selection rule gives an approximate 95 per cent confidence interval in the rejection of unwanted random signals. The selected polarization parameters were stored on data cards and later used in a statistical analysis of the polarization parameters.

The selection of spectral peaks by the computer did not, however, completely alleviate the tedious task of visually checking the computer outputs. Often the spectral peaks and polarization ratios (R_1, R_2) of an event differed considerably from station to station. In extreme cases a spectral peak at one station might be nonexistent at another station. To find the polarization parameters of a given event at all stations, it was then necessary to make direct comparisons of the spectra and the amplitude-time plots of the micropulsations.

Only the two horizontal components (H and D) of the 1969 data were analysed. *Samson et al.* [1971] have summarized the results from this data. A more generalized analysis was carried out with the 1970 data in that the three-dimensional polarization, coherency, and phase para-

meters were calculated. We must remember, though, that induced earth currents substantially affect the polarization characteristics in the H-Z and D-Z planes and that horizontal changes in geoelectric properties substantially affect the station-to-station phase spectra. These considerations will be discussed in more detail in the analysis of the data.

2.4 Selection of micropulsation events

Micropulsation events were selected from periods with low to moderate activity $(K_p < 4)$ and with evident Pc 4 or Pc 5 micropulsation activity lasting for an hour or more. The Meanook standard magnetograms were used in the initial determination of these intervals since the sensitivites of the component magnetograms (H $\equiv$ 10.3 γ/mm, D $\equiv$ 1.6'/mm, Z$\equiv$ 9.4γ/mm) allow the detection of most large amplitude Pc 4 and Pc 5 micropulsations. Digital plots of the data from our stations were then made in the selected time intervals. Those micropulsation events which satisfied the following simple criteria were selected for analysis.

(a) There must be at least four stations with no data gaps and with timing accurate to within $\sim$ 5 sec in the interval of interest.

(b)   There must be apparent micropulsation activity
at three or more of these stations and this
activity must last for more than an hour. No
restrictions were placed on the shape of the
pulsation waveforms although some events were
selected specifically because of their sinu-
soidal appearance. We placed no restrictions
on the local time of occurrance of the events.

(c)   The micropulsations must have amplitudes of at
least 2γ (peak to peak on one component) at
three or more stations. Lower amplitudes lead
to sizeable quantizing errors in the spectral
estimates (see Appendix A5). Due to the natural
falloff of power in the geomagnetic spectrum this
restriction limited the highest selected frequencies
to $\sim$ 30 mHz.

Table 3 lists the events selected for analysis, and Table
4 gives a summary of the K_p indices during the selected days.
Indices corresponding to the time intervals analysed are
underlined.

TABLE 3. Micropulsation Events Selected for Analysis

Event Number	Time			Stations
	Year	Day	Hour (UT)	
1	1969	219	0400-2400	CAMB, SMIT, FTCH, MCMU, CALG
2	1969	262 263	0900-0400	CAMB, SMIT, FTCH, PENH (0900-1700), CALG
3	1969	270	0300-2400	CAMB, SMIT, FTCH, PENH, CALG
4	1970	157 158	1300-0900	CAMB, FTCH, MENK (1700-0500), LEDU, CALG
5	1970	163 164	1500-0200	CAMB, SMIT, FTCH (1500-2000), MCMU (1530-1730), MENK (1500-2000), LEDU, CALG
6	1970	167 169	1600-0300	CAMB, SMIT, FTCH, MCMU, MENK (168,0000-1200), LEDU, CALG
7	1970	186 187	1400-0400	CAMB, SMIT, FTCH, MCMU, MENK (1700-0400), LEDU
8	1970	191	1400-1900	CAMB, SMIT, FTCH, MCMU, MENK, LEDU, CALG
9	1970	193 194	1200-1200	CAMB, SMIT, FTCH, MCMU, MENK, LEDU, CALG
10	1970	195	1930-2330	CAMB, SMIT, FTCH, MCMU, MENK, LEDU, CALG (2030-2330)
11	1970	262 263	1800-0200	CAMB, SMIT, FTCH, MCMU, MENK (2200-2300), LEDU, CALG
12	1970	269	1800-2200	CAMB, SMIT, FTCH, MCMU {1800-2100}, MENK (200-2200), LEDU, CALG {2000-2200}

TABLE 4. K_p Indices on the Days Selected for Analysis

Year	Day	K_p							
		1	2	3	4	5	6	7	8
1969	219	2-	2	2-	2+	2	1	3-	3-
1969	262	3	4-	2	2	2	1	1	2+
1969	263	2	2-	3-	2+	2	3+	2-	1-
1969	270	0	0+	0+	0	1	1	1+	4+
1970	157	1	1	1+	2-	0+	0+	0+	0
1970	158	0	1-	1-	1-	1	3-	3+	4+
1970	163	2-	1+	1+	1	1-	1	2-	1+
1970	164	1-	1	3-	3	3+	3-	2-	2
1970	167	2+	3	2	1+	2+	2	1+	3-
1970	168	1+	0+	3-	3-	4-	3+	3+	3
1970	169	3+	2+	4+	4+	5+	4	3	4
1970	186	3-	4+	4-	2-	3+	3	2+	3-
1970	187	4-	3+	4-	4-	4	1	1-	1-
1970	191	7-	2	2-	1+	4-	5	5	4
1970	193	3+	3+	2+	3-	2+	2+	4-	3+
1970	194	3	3	2	1+	1+	3-	3-	2+
1970	195	3-	2+	3-	2-	1+	2	3-	3-
1970	262	1	5-	4	3+	2+	3	3+	3
1970	263	2	4-	4-	4-	2+	3-	2+	3+
1970	269	1-	3-	2-	2	1+	1+	2-	2

3. OBSERVATIONS

3.1 <u>Introduction</u>

The data presented here occupy two distinct sections. The first section contains a statistical analysis of the three-dimensional polarization parameters of the selected micropulsation events (see Table 3). The second section contains a complete, detailed discussion of a number of individual micropulsation events. The statistical results are presented first in order to develop a good perspective for the analysis of the complicated characteristics of individual events.

The statistical analysis summarizes the average characteristics of the intensities, ellipticities and polarization angles (see Section 2.3) of quasi-monochromatic Pc 4's and Pc 5's. The variation of these parameters with time, latitude, and frequency is considered. Since the number of parameters is very large we will not attempt to discuss all the data but will present only those results which are representative and illuminating. The selection of polarization parameters is discussed in detail in Sections 2.3 and A4 and will not be repeated here. Unless otherwise indicated all the statistical results pertain to the 1970 data.

Figure 18 summarizes the total number of data hours in each hour of Universal Time. Histograms (1) and (2) pertain to data which were subjected to polarization analysis using the 1/2 hour and 1 hour data window respectively. Histograms (3) and (4) pertain to data which were subjected to station-to-station phase comparisons using the 1/2 hour and 1 hour window respectively. Most of the data are found during the daytime hours reflecting the local-time-dependence of the occurrance frequency of the micropulsations. Normally data from the morning events are the clearest and the easiest to analyse, showing very predictable ellipticities and polarization angles at all the stations. Because of the relatively small amounts of data from the nighttime, inferences from data during this time should be considered very cautiously. There is also the problem that some of the nighttime events are composed of short-lived impulsive trains much like Pi's. These events may have characteristics that are fundamentally different from Pc 4 or Pc 5 characteristics.

Data from MENK are included in the analysis even though the gain of the D component at this station changed sporadically. To correct this varying gain we compared our D component data with standard magnetograms from Meanook.
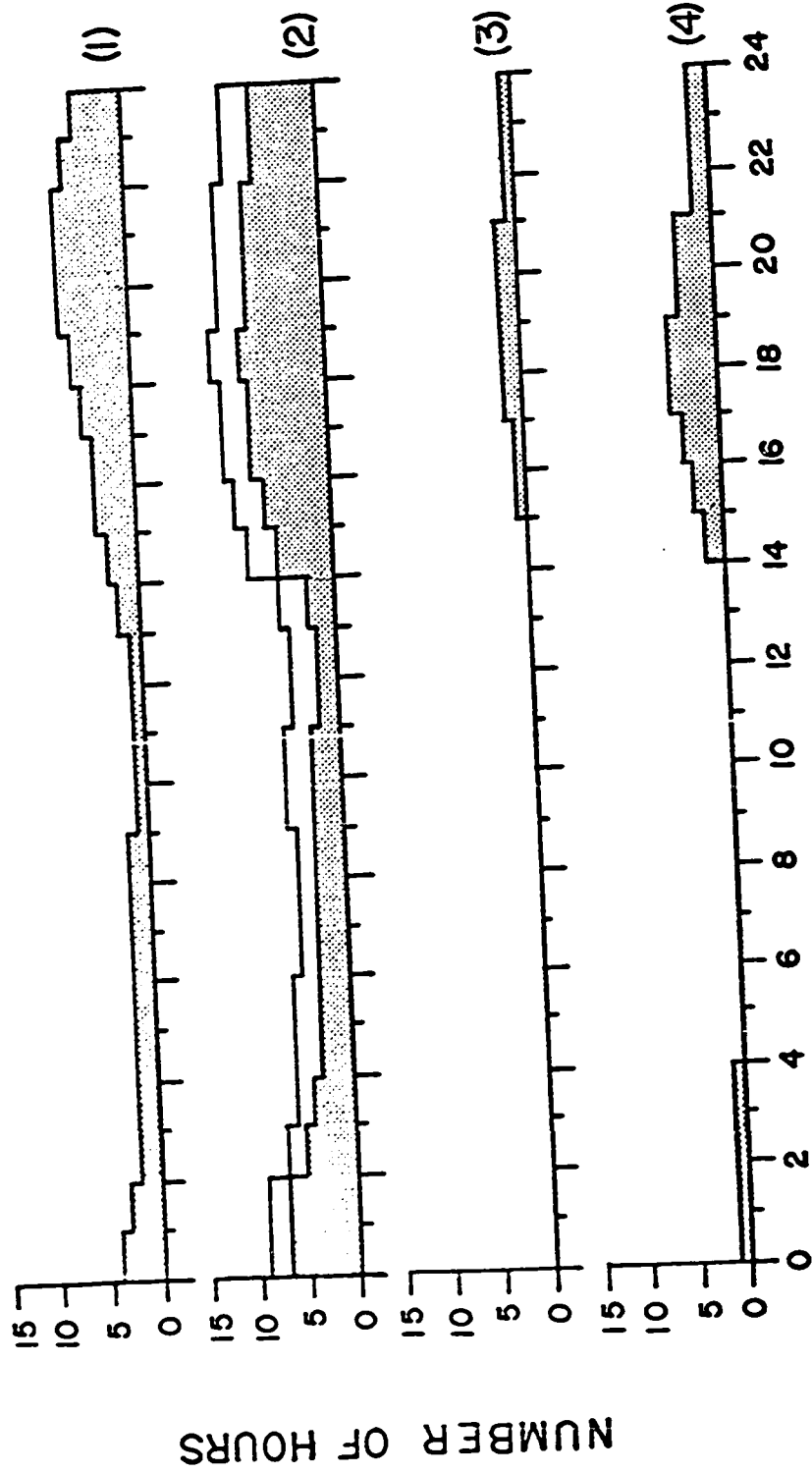
Fig. 18. Histograms showing the number of data hours in each hour of Universal Time. The labels are explained in the text. The unshaded region in histogram (2) pertains to the 1969 data.

After calculating an average value for the gain of the
D component we corrected the MENK data by multiplying
by this average gain. On an event to event basis this
leads to rather variable characteristics. The statis-
tical averaging of the events should, however, give mean-
ingful results. In fact we find that the sense of polar-
ization at this station is consistent with the results at
the other stations although there are some variations in
intensities, ellipticities, and polarization angles
calculated at this station.

A complete discussion of the polarization and
station-to-station phase characteristics of five represent-
ative events is given after the statistical analysis. The
frequencies of the micropulsations in these events range
from 1.3 mHz to 20.3 mHz and thus cover the whole spectrum
of interest here. The events all occurred during the day-
time, the earliest between 1400-1700 UT and the latest
between 2300-2400 UT. The event on day 186 is the most
intriguing, having very sinusoidal oscillations with peak
to peak amplitudes of nearly 180 γ in the H component at
SMIT. These large amplitudes permit the use of this event
in a worldwide analysis of the spectral characteristics.
The longitudinal dimension inherent in a worldwide analysis
is especially helpful in evaluating the statistical, diurnal

characteristics obtained from the data at our line of stations. We accordingly digitized magnetograms from 13 other magnetic observatories in the northern hemisphere and used this data to determine the polarization character- istics of the event at those observatories. Since standard magnetograms normally have poor temporal resolution, these polarization characteristics must be considered with care

In the presentation of the data that follows corrected geomagnetic coordinates are used throughout. All latitudes in the text and all latitudes in the figures are corrected geomagnetic latitudes. *Hakura* (1965) gives a complete description of the computation of these coordinates on a worldwide basis. For simplicity we have plotted all temporal variations in Universal Time. Unless otherwise indicated, Universal Time is used throughout the text. An approximate conversion to local geomagnetic time (LGT) at our stations can be made by substracting 8 1/2 hours from the given Universal Times.

3.2 A statistical analysis of the polarization parameters

In the analysis of the data it soon became apparent that almost all Pc 4's and Pc 5's have frequencies which are latitude-independent. No gradual latitudinal changes in frequency are evident, though two or more micropulsation

trains of different frequencies often occur at the same time. This feature is evident from a visual inspection of the magnetograms, from power spectra calculated for the stations, and from the spectral peaks selected through use of the computer programs (see Section 2.3). This evidence supports the observations of *Ellis* [1960] and *Obertz and Raspopov* [1968] who also found no latitudinal changes in frequency. Exceptions to the above rule do occur, however, and an example of an event with latitude-dependent frequencies is given in Section 3.3.

3.2.1 <u>Intensities</u> The iso-intensity contours in Figure 19 summarize the daily variations in the relative intensities of 1-3 mHz micropulsations occurring in our 1970 data. We have used only those events with distinct spectral peaks (selected by the computer) at three or more stations. The intensities at the other stations were determined by visually inspecting the computer outputs of the spectral parameters (see Section 2.3). The intensities at each station were then summed in hourly intervals and the average intensities, I_i, in these intervals calculated. If I_m is the largest of the intensities at all the stations in a given interval, then the relative intensity at station i is defined by I_i/I_m.
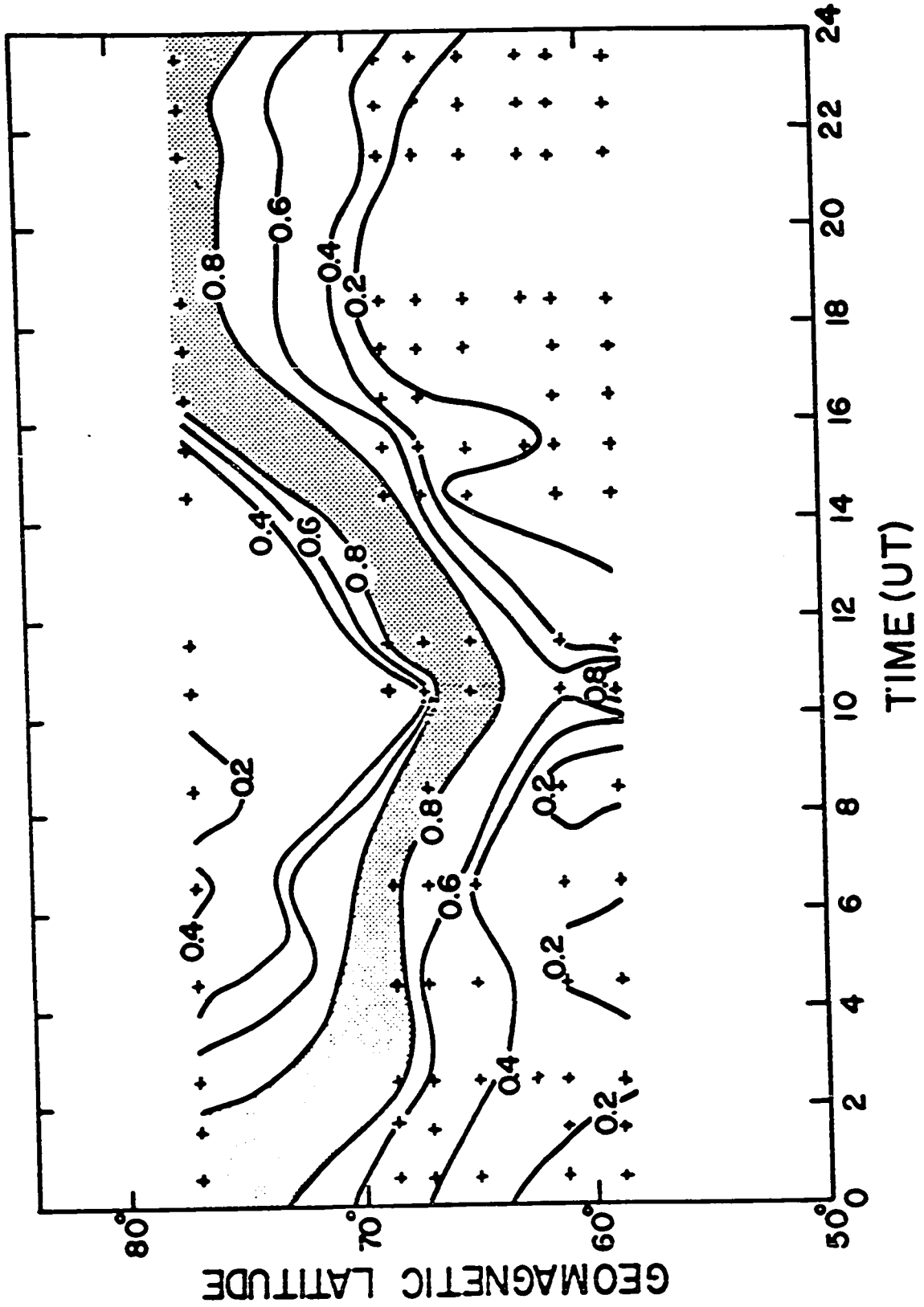
Fig. 19. Contours of equal relative intensity of micropulsations in the 1-3 mHz spectral band. The crosses represent sample points.

The intensity is clearly localized in latitude and moves northward during the day. The maximum intensity is at 65°-68^ON during the early morning, moving to $\sim 75^O$N between 0830 and 1530 LGT (1700-2400 UT). These diurnal variations closely resemble those of the auroral oval. The resolution in the northern regions is poor since CAMB and SMIT are 9° apart and consequently the position of the maximum is uncertain in the interval 1700-2400. Equivalent diurnal trends also appear in the intensity maxima of 3-8 mHz Pc 5's but the maxima are south of those in Figure 19. Pc 4 micropulsations, on the other hand, have rather complex iso-intensity contours.

Latitude plots of the relative intensities of micropulsations in given spectral bands indicate that low frequency Pc 5's have most of their energy concentrated north of 70^ON, whereas Pc 4's have their largest intensities and most energy south of 60-62^ON. Figure 20 presents latitude plots of relative intensities in 7 spectral bands ranging from 0-2 mHz to 15-20 mHz. To obtain these plots we calculated the relative intensities for each individual event occurring in 1970, sorted the events into the 7 spectral bands, and then averaged the relative intensities at each station. We have not included MENK data in this
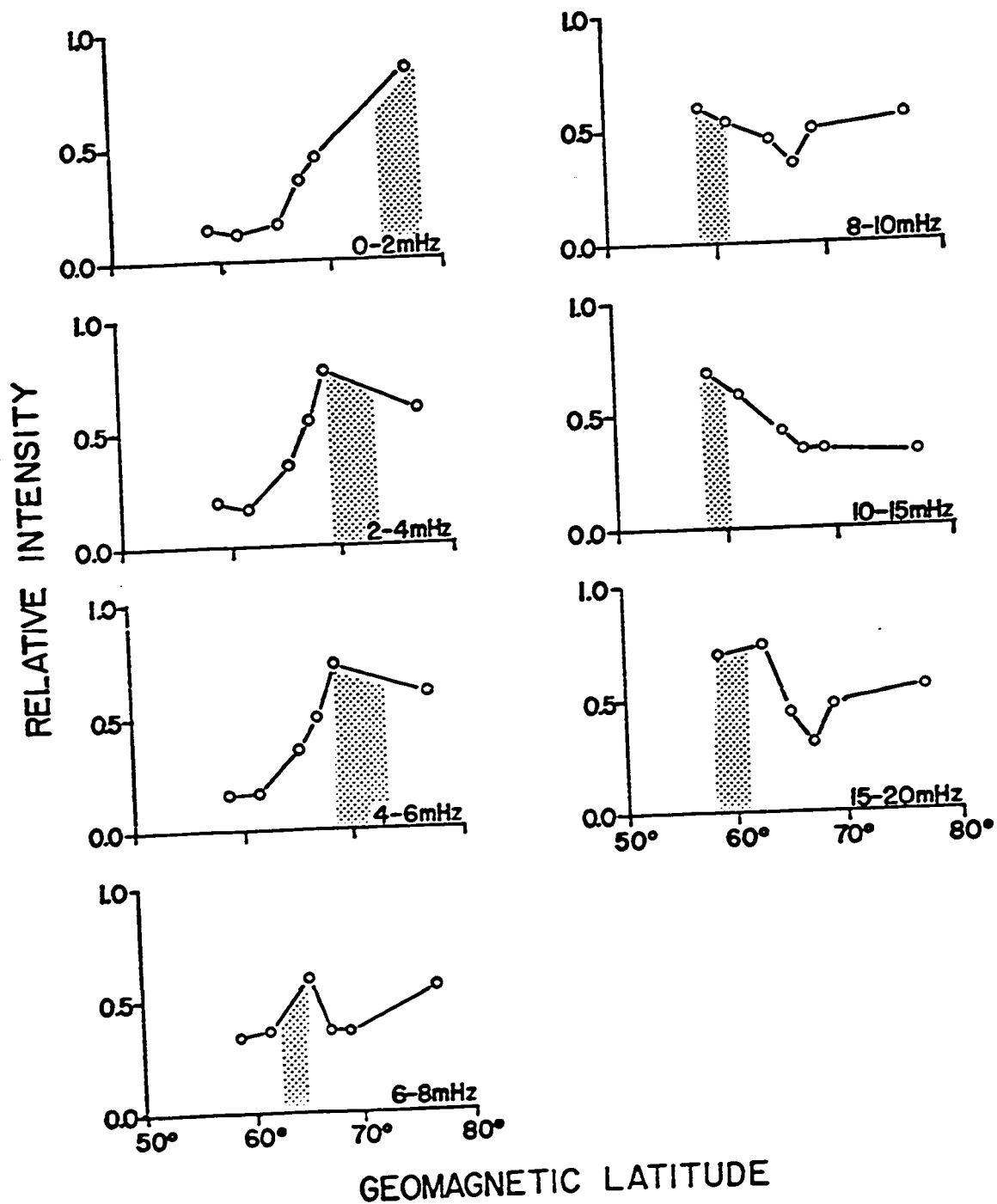
Fig. 20. Intensity - latitude profiles of micro-pulsations in seven spectral bands. The shaded areas are the estimated positions of the intensity peaks.

plot because of the anomalous D component at this station. The shaded areas in Figure 20 outline the regions where we estimate the peak intensities occur. In the 0-2 mHz spectral band the shaded region is a southern limit and in the three Pc 4 spectral bands the shaded regions are northern limits. Clearly the latitude of the intensity peaks depends on the frequencies of the micropulsations, the peaks for the highest frequencies occurring at the southernmost latitudes. One difficulty in interpreting the data in these plots arises from the fact that the averages are taken from events occurring at any time during the day. Diurnal effects such as those noted in Figure 19 definitely broaden the latitude ranges of the intensity peaks and make the peaks more difficult to resolve.

An alternative method of depicting the intensity data is to construct scatter plots showing the estimated latitudes of the intensity peaks of micropulsations of all frequencies. Figures 21 and 22 show the results of such an analysis. In making these scatter plots the day was divided into two sectors, based on the diurnal variations noted in Figure 19.The first sector extends from 0200 to 1600 and the second from 1600 to 0200. We determined the latitudes of the intensity peaks by noting the station
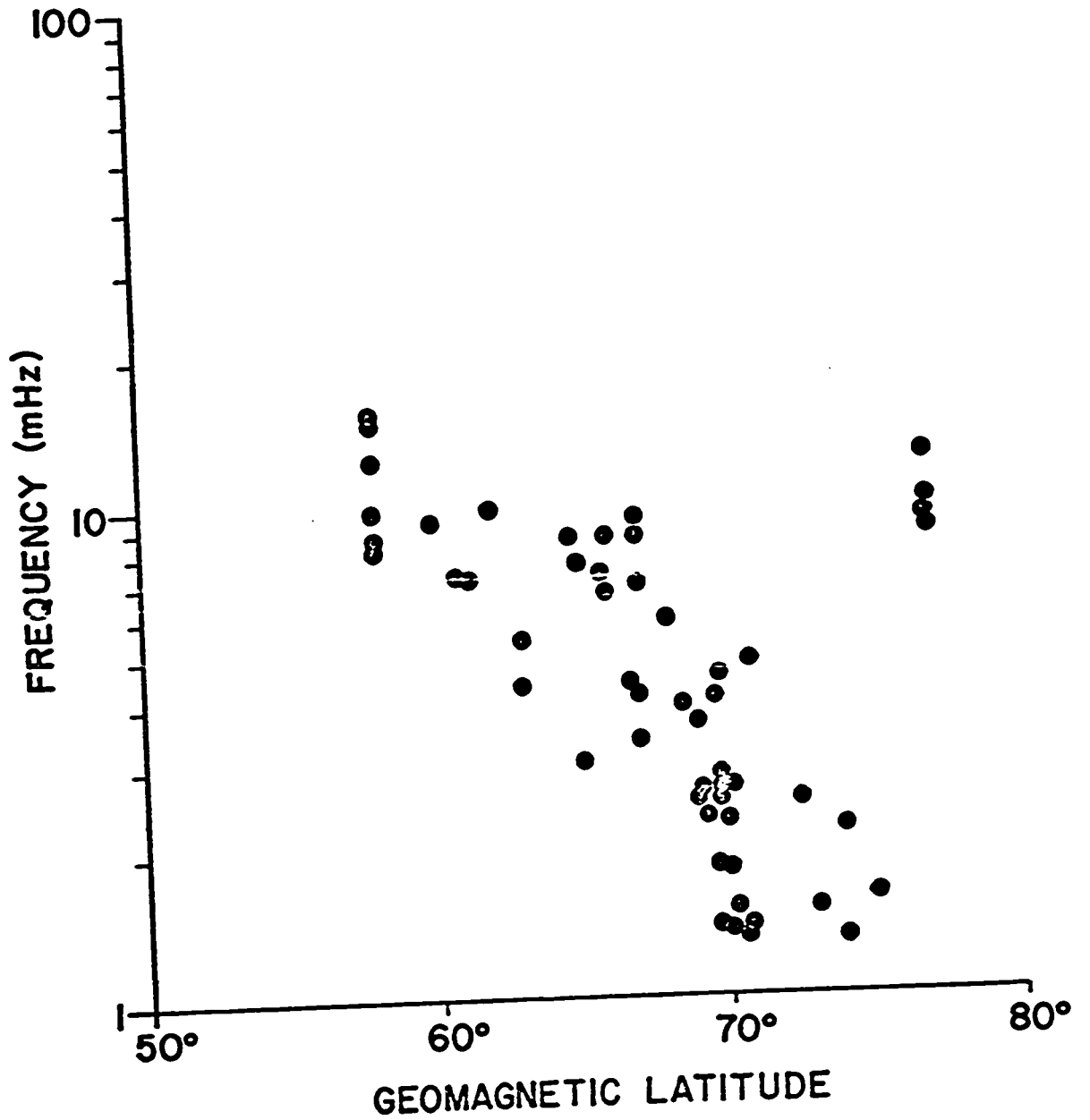
Fig. 21. Estimated latitudes of the intensity peaks of micropulsations occurring between 0200 and 1600 UT.
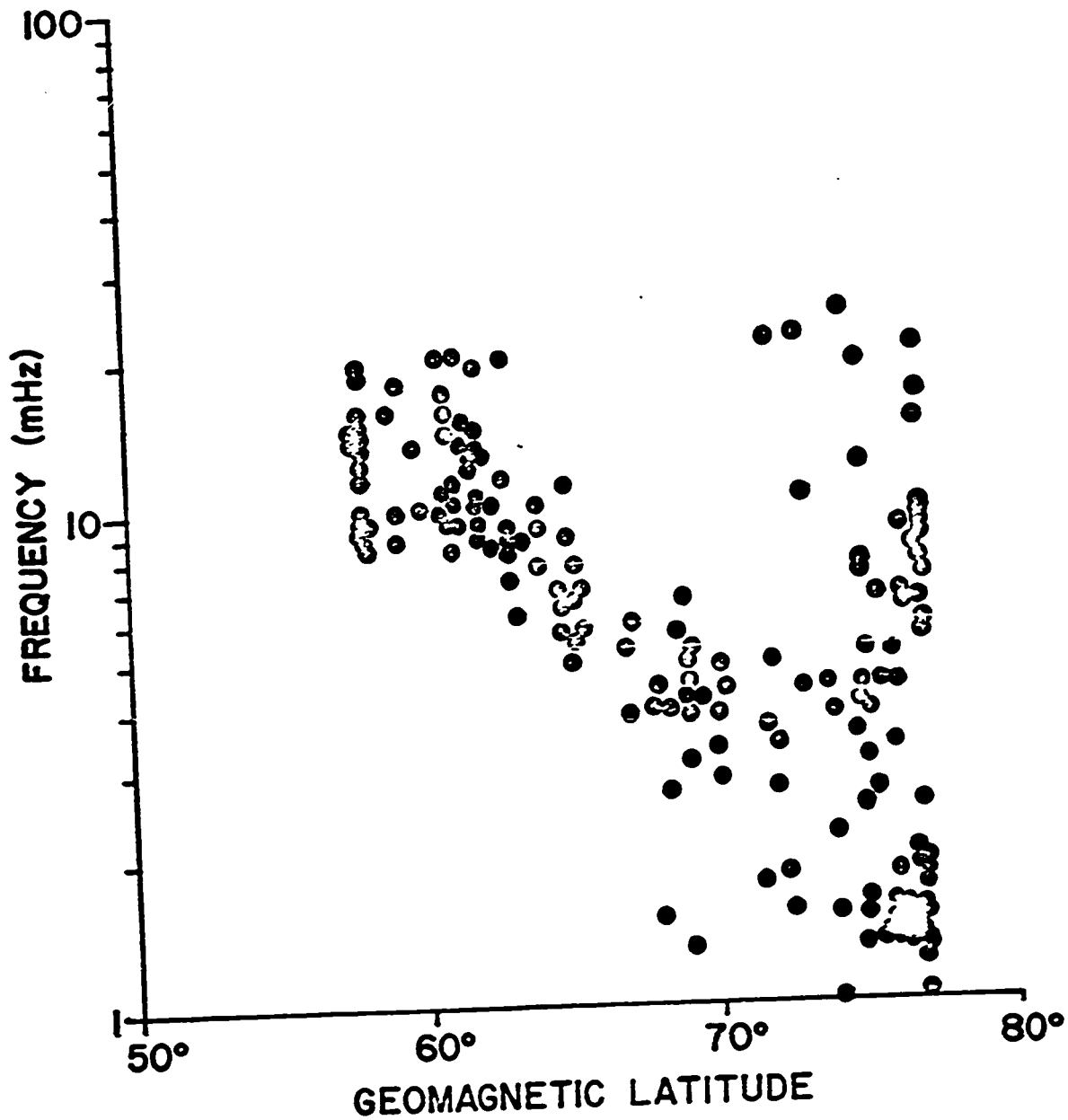
Fig. 22.   Estimated latitudes of the intensity peaks
of micropulsations occurring between 1600 and 0200 UT.

with an obvious maximum in intensity for a given micro-pulsation event. If the intensity showed peaks near two different stations then the latitudes of both these peaks were plotted, even though one peak might be larger than the other . If there were more than two peaks or if there were no clear peaks, we rejected the event. Since the two northern stations are separated by 9° the latitudes of peaks occurring between these stations were determined by extrapolation, the peak being proportionally closer to the station with the greatest intensity. In some instances the intensity increases monotonically across the array of stations. These events, which clearly have maxima beyond the latitude of the array,have their peaks plotted at 58^oN or 77^oN depending on the direction of increasing intensity.

The most obvious feature in each plot is a strong latitude-frequency correlation in the grouping of the estimates below 72°. In Figure 21 (0200-1600) the peaks are centred near 10 mHz at 60^oN, decreasing continuously to about 2 mHz at 71^oN. In Figure 22 (1600-0200) the peaks are centred near 15 mHz at 60^oN, decreasing continuously to 2 mHz at $70-75^o$N. A cluster of intensity peaks which covers all frequencies and is localized in northern latitudes (72°-77°) is also apparent in Figure 22. This

region corresponds to the approximate position of the auroral oval during this time interval (see Section 4.1). The high latitude cluster does not appear in Figure 21 but this might be expected since the nightside segment of the auroral oval is usually at latitudes south of 70°N. The absence of any high latitude cluster in Figure 21 also indicates that nightside micropulsations might have different energy sources than those causing dayside micropulsations.

3.2.2 Ellipticities   Figures 23 to 29 summarize the diurnal characteristics of Pc 4 and Pc 5 ellipticities. Most of the data are from 1970 although some of the H-D plane data are from 1969. The estimates used in this analysis and in the analysis of the polarization angles were all selected by computer, subject to the constraints listed in Section 2.3. These plots are based on averages over four-hour intervals and are calculated for all 3 planes (H-D, H-Z, D-Z). The circles in the plots are at the centres of the four-hour intervals.

The ellipticities at MENK in the H-D and H-Z planes appear somewhat more linear than those at LEDU and CALG. This feature is probably due to the malfunctioning of the D component at MENK. The diurnal trends in the ellipticities at MENK do, however, agree with those at CALG. and LEDU.

In the H-D plane, the low frequency Pc 5 micropulsations (0-6 mHz) show the simplest and most consistent polarization patterns. At all stations from SMIT southward

Fig. 23. A summary of the ellipticities in the three planes of micropulsations recorded at CALG. The data points are based on averages in 4-hr intervals.

Fig. 24. A summary of the ellipticities at LEDU.

Fig. 25. A summary of the ellipticities at MENK.

Fig. 26. A summary of the ellipticities at MCMU.

Fig. 27. A summary of the ellipticities at FTCH.

Fig. 28. A summary of the ellipticities at SMIT.

Fig. 29. A summary of the ellipticities at CAMB.

Fig. 23.

Fig. 24.

ELLIPTICITY

TIME (UT)

H-D   H-Z   D-Z

0-2mHz
2-4mHz
4-6mHz
6-8mHz
8-10mHz
10-15mHz
15-20mHz

+0.5
-0.5

Fig. 25.

Fig. 26.

D-Z

H-Z

H-D

0-2mHz

2-4mHz

4-6mHz

6-8mHz

8-10mHz

10-15mHz

15-20mHz

+0.5

-0.5

ELLIPTICITY

2 6 10 14 18 22 2

2 6 10 14 18 22 2

2 6 10 14 18 22 2

TIME (UT)
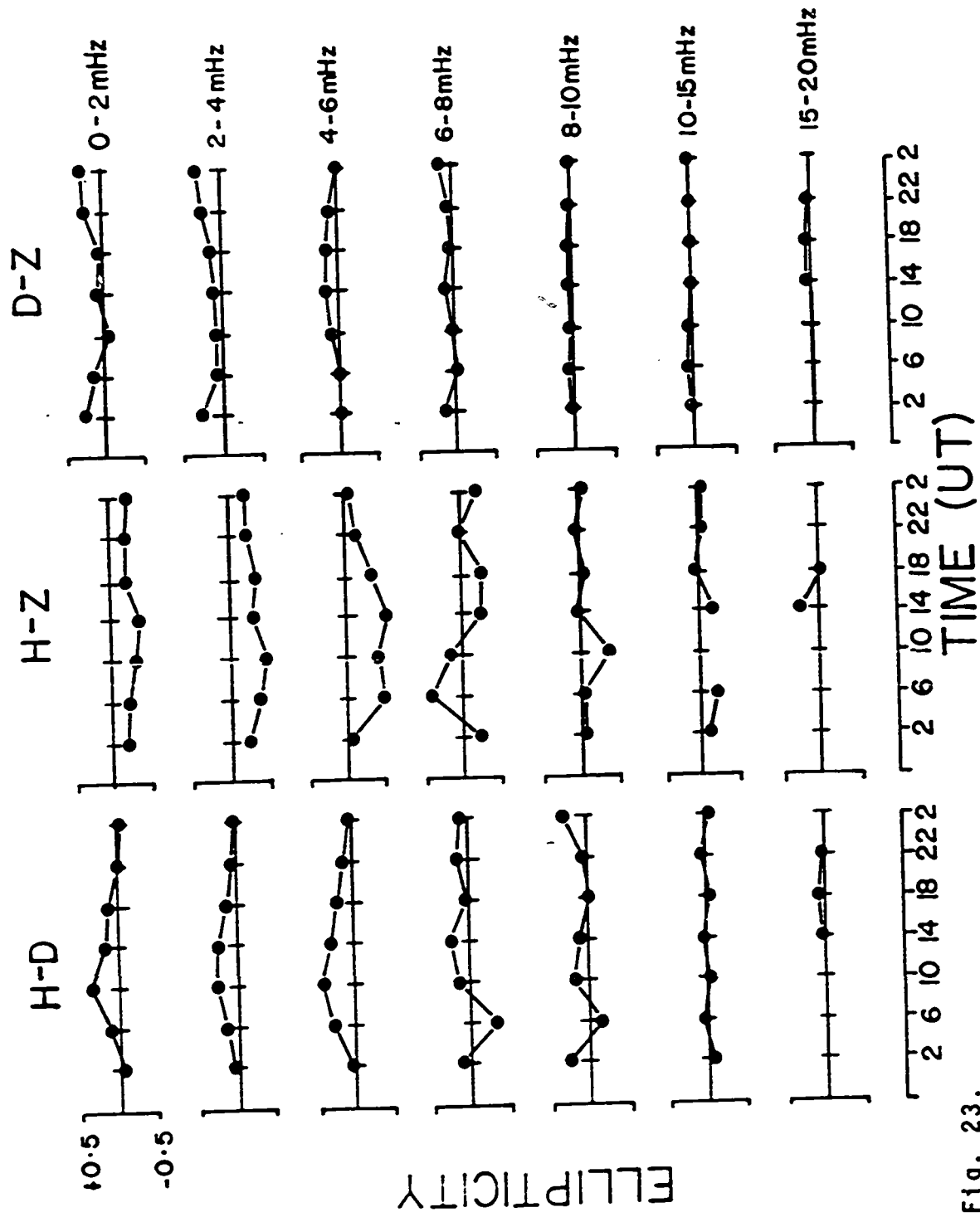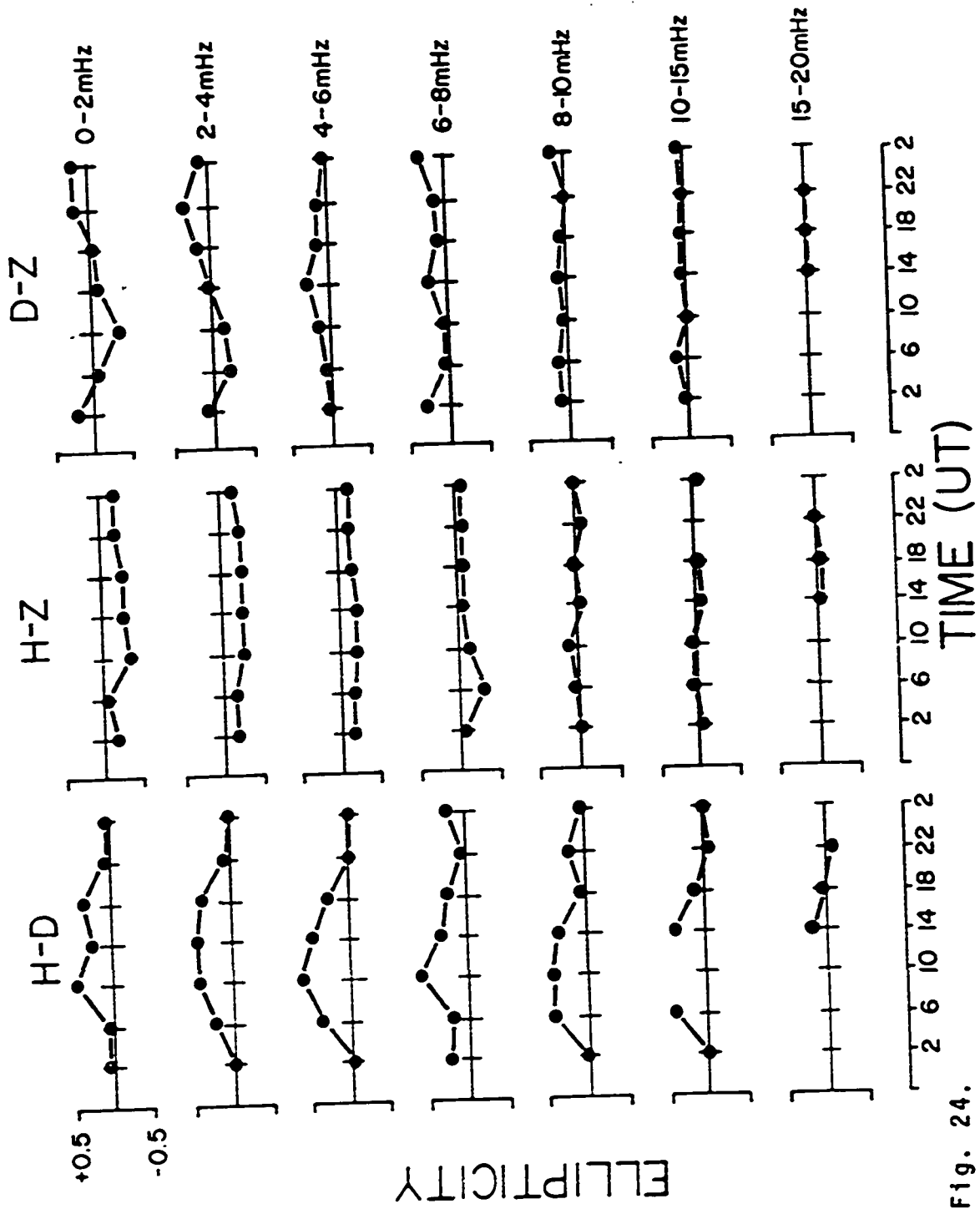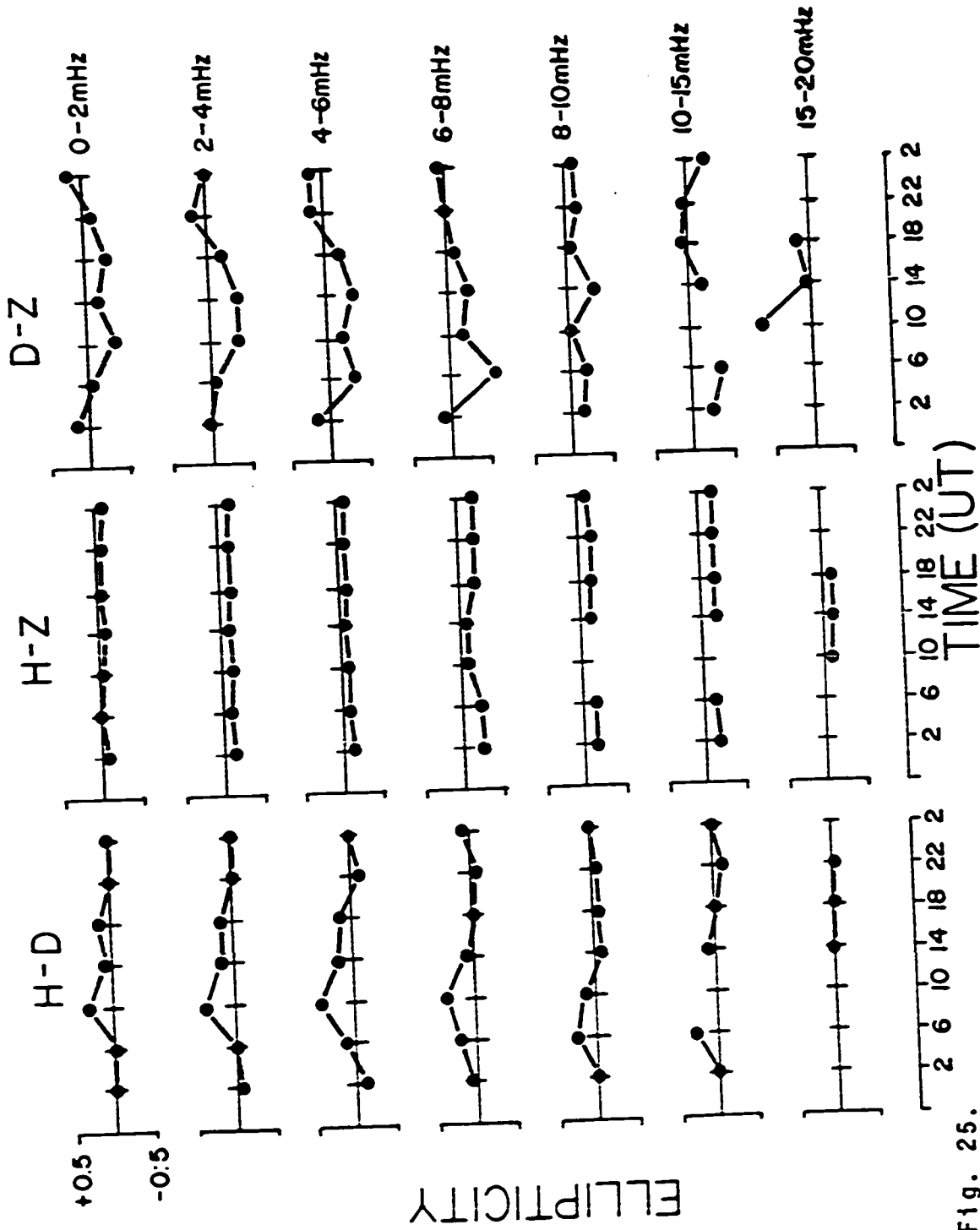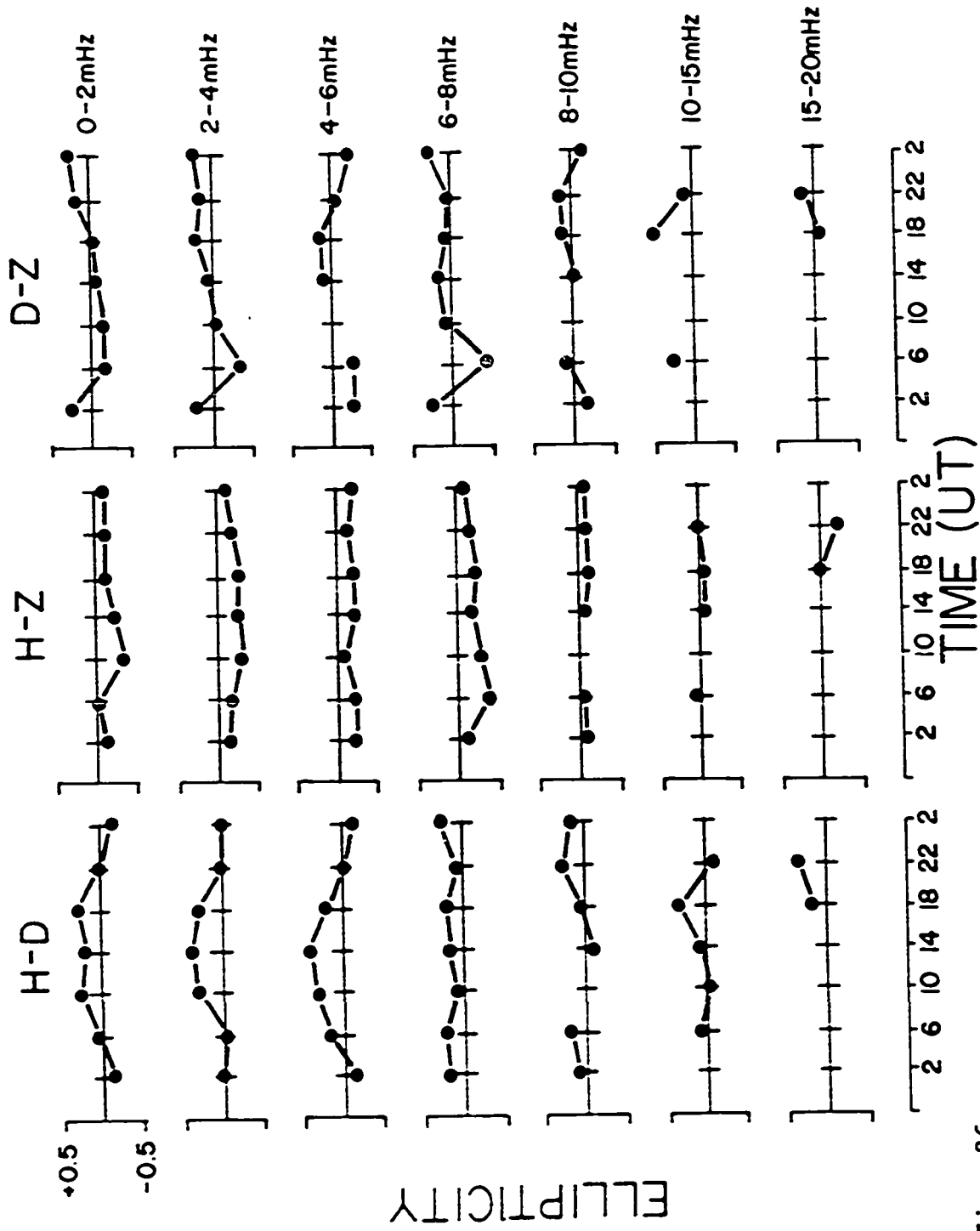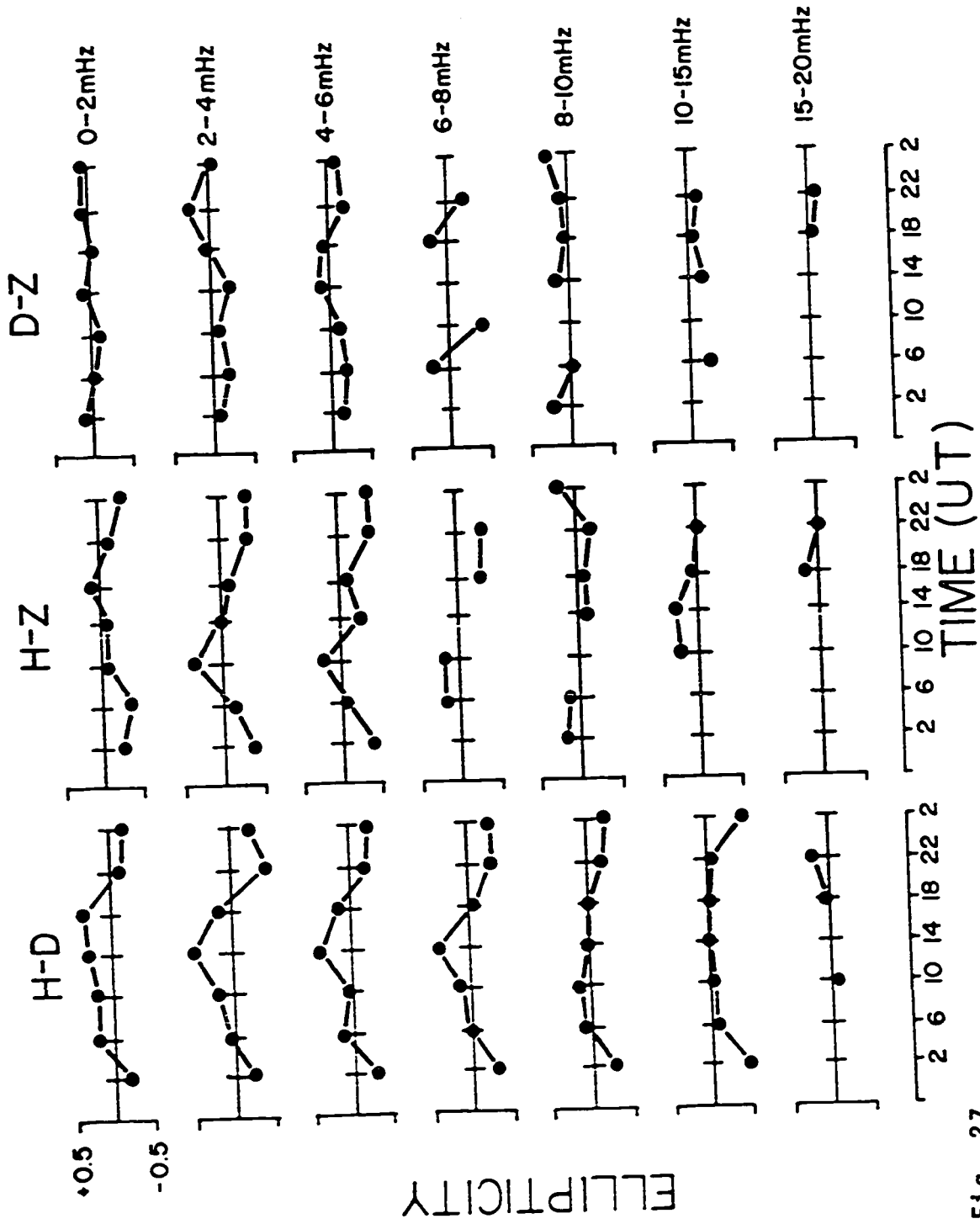
Fig. 27.
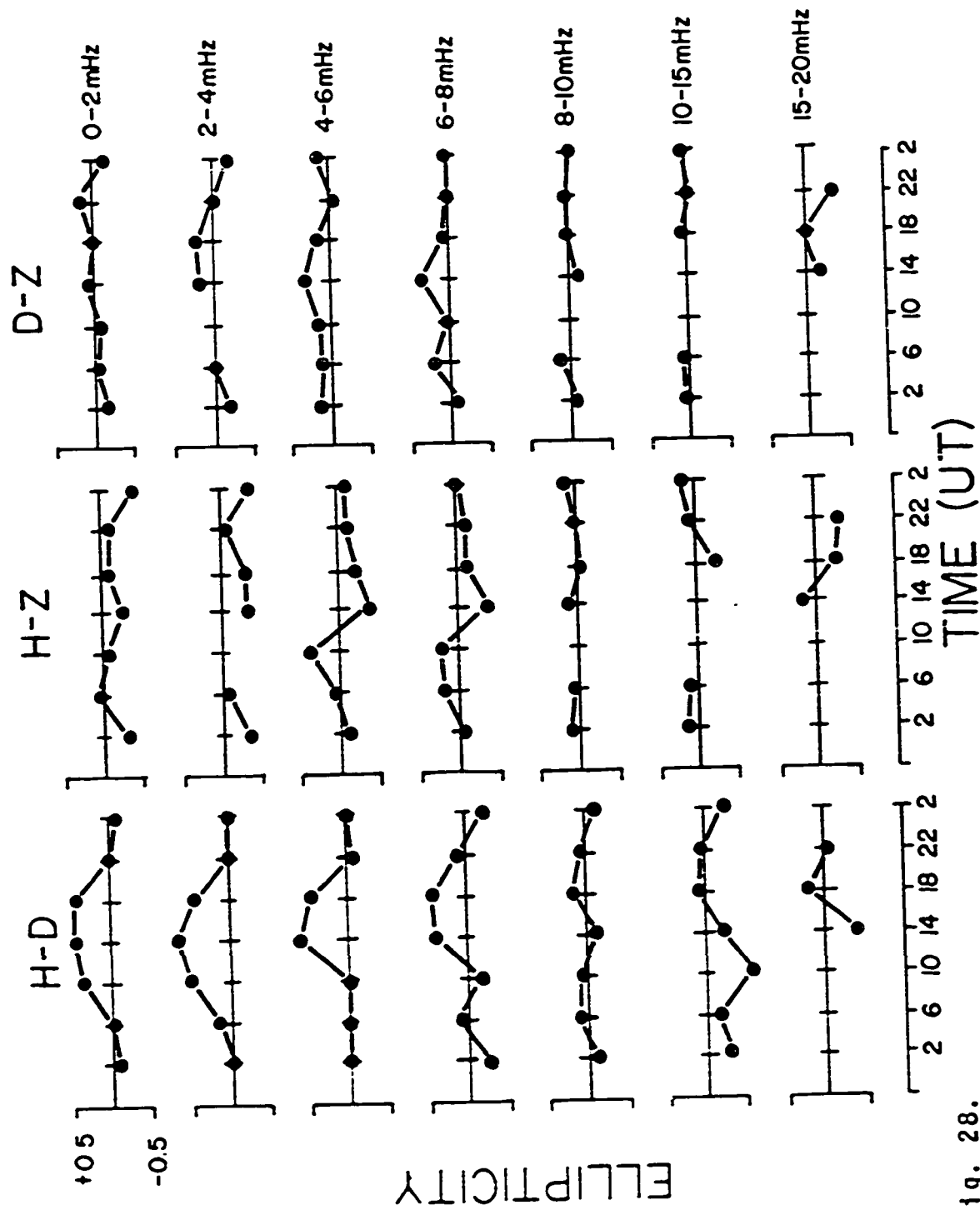
Fig. 28.
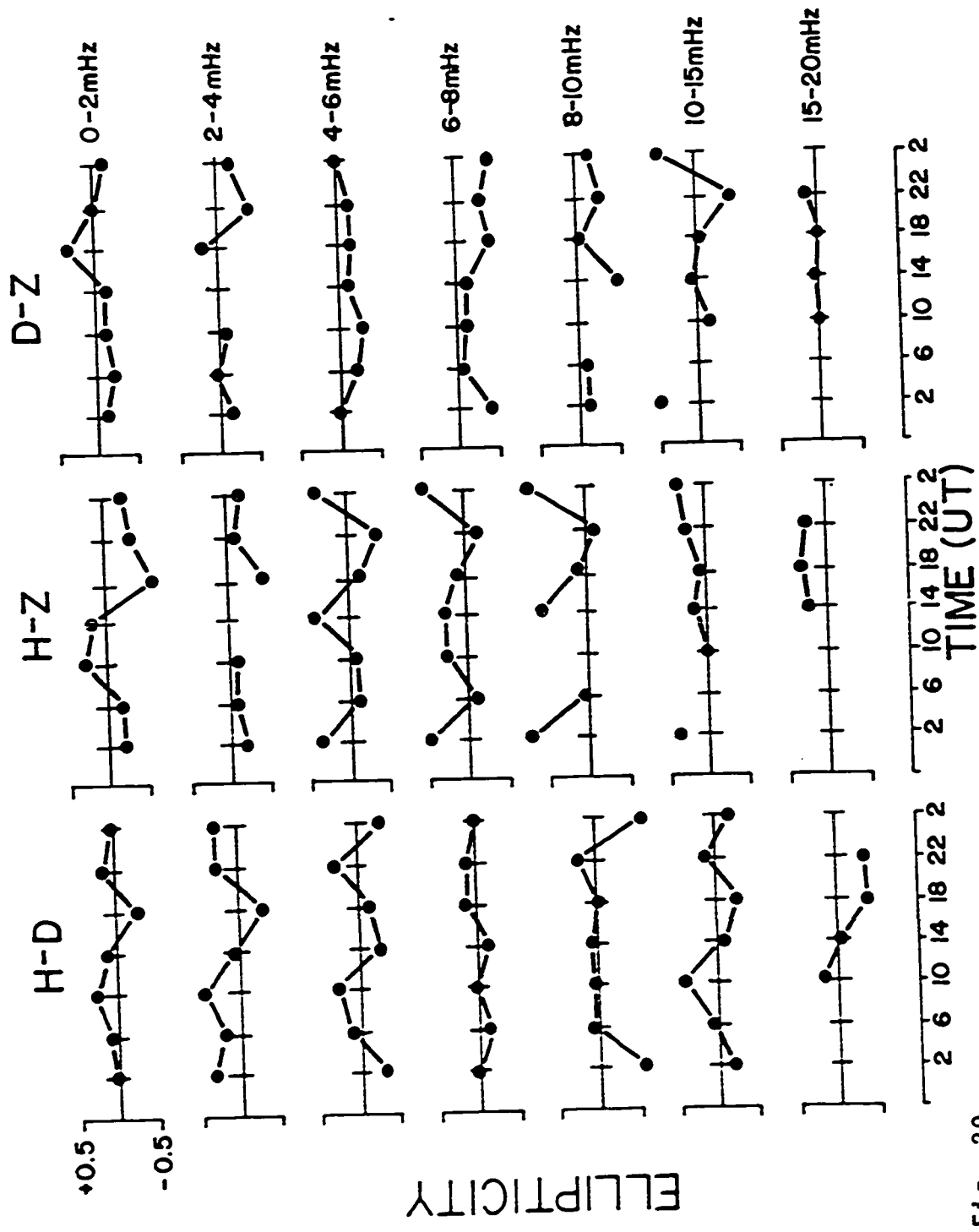
Fig. 29.

the sense of polarization is CC (counterclockwise) over most of the day with a period of CW (clockwise) polarization occurring between 2000-0400 (1130-1930 LGT). The period of CW polarization is most evident at FTCH, where the ellipticity decreases to -0.5. This polarization pattern corresponds remarkably well to those computed by *Kato and Utsumi* [1964] and *Rankin and Kurtz* [1970]. The micropulsations at CAMB are the exception to this diurnal polarization rule, having CW polarization from 1200-2000 and CC polarization outside this time interval. These diurnal polarization characteristics will be discussed in greater detail later.

Pc 4 micropulsations, on the other hand, appear to have rather complex polarizations in the H-D plane. It should be noted that the data used to construct the Pc 4 plots are rather limited, especially during the nighttime hours (0200-1400). Morning Pc 4 micropulsations appear to have some predictable polarization characteristics and these will also be discussed in detail later.

The low frequency Pc 5's show relatively simple polarization changes in the H-Z plane. Micropulsations at most of the stations have CW polarization over the whole day, with short periods of CC polarization occurring in

the interval 0800-1200   at CAMB, SMIT, and FTCH. The
patterns at MCMU, MENK, and LEDU are the simplest having
almost constant CW polarization throughout the day. With
the exception of a short period of CC polarization in the
6-8 mHz band from 0400-1200, Pc 5's at CALG also have
CW polarization throughout the day. The polarization
patterns at CAMB are somewhat more complex than those at
the other stations but distinct similarities between CAMB,
SMIT, and FTCH do exist, especially in the 0-4 mHz band.

In the H-Z plane changes in the ellipticities
of Pc 4's have more complicated characteristics than do
those of Pc 5's. The Pc 4 patterns are also confused by
sketchy data in this spectral band, especially at the
northern stations. Generally speaking, polarizations
at the southern stations are very linear, with little
apparent structure. This characteristic may be a mani-
festation of earth induction effects in the southern
prairie regions.

Polarizations in the D-Z plane show the least
predictable characteristics. At CALG and LEDU polarizations
in the Pc 5 band change slowly over the day. At these two
stations the greater part of the day has CC polarization,
with the exception of a short period of CW polarization
at LEDU in the interval 0400-1200. Polarizations are

most elliptical around 2000-2400 at which time the
ellipticity is +0.3 at CALG and LEDU. The period of
CW polarization becomes more pronounced at MENK and
extends from 0800-2000. At SMIT and FTCH, Pc 5 polar-
ization patterns are very complex, changing rapidly
with time and frequency. The pattern in the 0-4 mHz band
at SMIT resembles that in the H-D plane. More precisely
polarizations are CC throughout most of the day with
a short section of CW polarization from 2000-0400. Pc 5
micropulsations at CAMB show predominantly CW polarization
with a short section of CC polarization occurring between
1600 and 2000. Once again micropulsations in the Pc 4
band show predominantly linear polarizations at the
southern stations. The linear polarizations are almost
always due to the small Z components at these stations.

Figure 30 illustrates the temporal polarization
features of the very low frequency Pc 5 micropulsations
(0-4 mHz). The samples are based on averages over two-
hour intervals and the circles in the plot are at the
centres of these intervals. This figure shows that these
micropulsations obey rather simple polarization rules in
all three planes. In the H-D plane the ellipticities
follow an inverted U-shaped diurnal variation (based on

Fig. 30. A summary of the ellipticities of micropulsations in the 0-4 mHz band (Pc 5). The data are from 7 stations and are based on averages in 2-hr intervals.
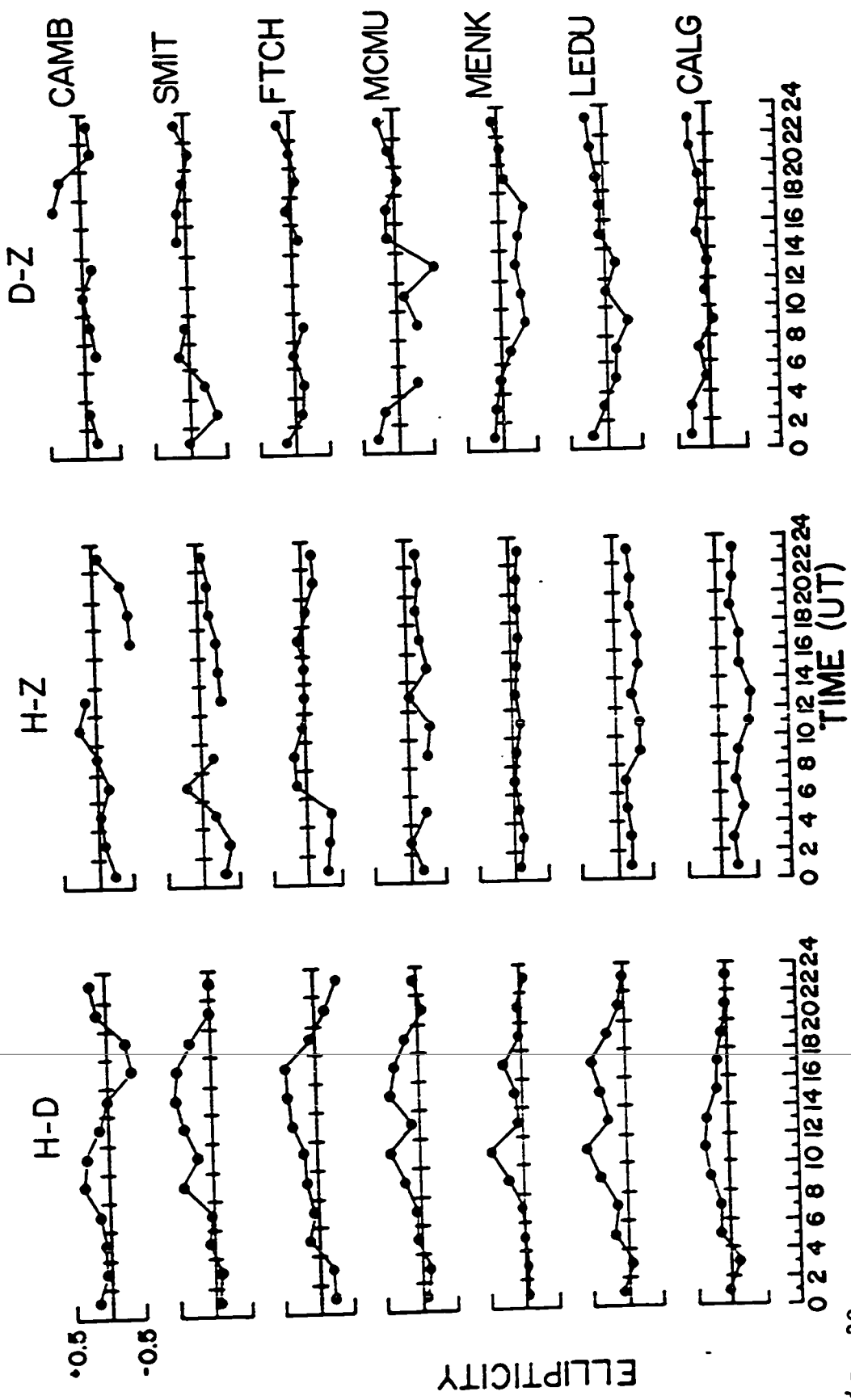
Fig. 30.

a universal day) at all stations except CAMB. Polarizations are most elliptical in the period 1000-1800 having ellipticities as large as +0.5 at SMIT and FTCH. At all stations from SMIT southward micropulsations are polarized in a CC sense during the evening and morning hours with a 7 to 8-hour period of linear and CW polarization occurring between 2000 and 0400 (1130-1930 LGT). This corresponds to the period of CW polarization noted by *Kato and Utsumi* [1964] for Pc 5's at high latitude stations. During the daytime, micropulsations at CAMB have a reversed sense of polarization as compared to the other stations. This implies that during the daytime there exists a given latitude across which the sense of polarization reverses. We shall refer to this latitude as the *demarcation line*. The existence of a demarcation line in this frequency band suggests that we plot latitude profiles of ellipticities in other frequency bands to determine whether this reversal exists for all frequencies. This problem will be dealt with in detail later.

Polarizations in the H-Z plane are predominantly CW throughout the day. Pulsations at stations from MCMU southward always remain CW whereas pulsations at FTCH, SMIT and CAMB show periods of pronounced CC polarizations at

0600-1000, 0600-0800 and 1000-1400 respectively. There is no evidence for a consistent latitudinal reversal in the sense of polarization as there is on the H-D plane.

Ellipticities in the D-Z plane are somewhat more complex than those in the other two planes but some predictable patterns are evident. At CALG, LEDU, MENK and MCMU the ellipticities show a U-shaped diurnal variation, being mostly CC from 2200-0200 and CW from 0600-1400. At FTCH, SMIT and CAMB the polarizations are more confused. Micropulsatons at FTCH are linearly polarized for most of the day, whereas at SMIT they show a diurnal variation very similar to that in the H-D plane. In fact, Pc 5's at both SMIT and CAMB have diurnal variations which are the reverse of those at the southern stations. More precisely they have CC polarization in the morning hours (0600-2000) with a tendency toward CW polarization in the afternoon and evening.

Figure 31 shows plots of ellipticity versus latitude in the H-D plane for the morning hours 1200-1600 and 1600-2000. Data from MENK are not included since the ellipticities at that station are inaccurate. Pc 5 micropulsations show an evident reversal in the sense of polarization occurring somewhere between 70°N and 75°N. Unfortunately the station spacing in this region is very
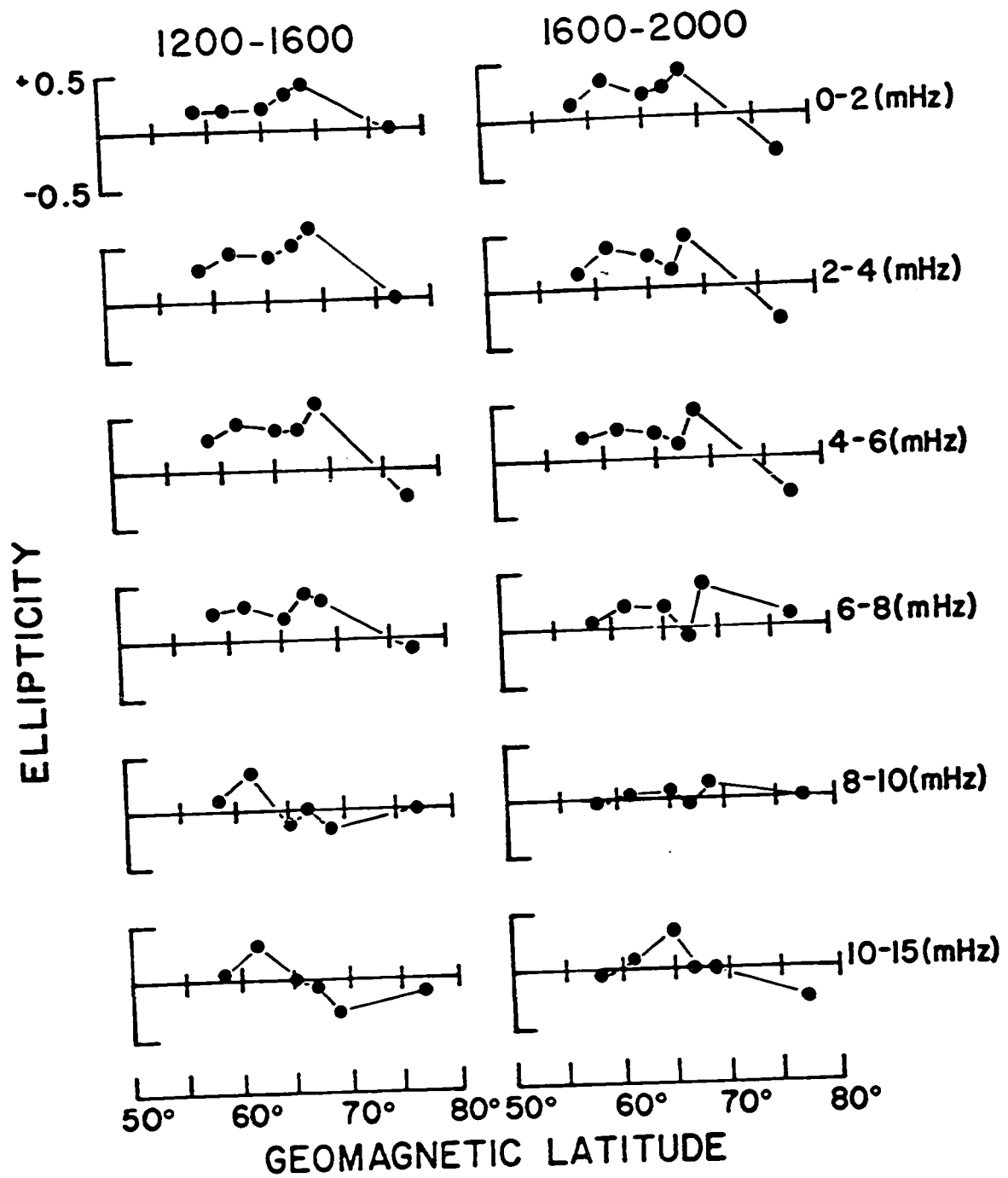
Fig. 31. Latitude profiles of ellipticities in the H-D plane. The data are based on the average ellipticities in the intervals 1200-1600 UT and 1600-2000 UT.

poor (CAMB and SMIT are 9° apart) and consequently we cannot determine from these plots if there is any latitude-.frequency dependence of the demarcation line. *Obertz and Raspopov* [1968] noted that the demarcation line apparently moves southward as the frequency of the micropulsations increases. *Samson et al.* [1971] have also shown that for selected, individual events there appears to be a latitude-frequency dependence of the demarcation line. In the Pc 4 band the latitudinal characteristics of the ellipticities appear more complex. There are, however, indications that these micropulsations have a demarcation line between 60° and 65°. This feature is most evident in the interval 1200-1600.

We can obtain additional, useful information by plotting ellipticity as a function of frequency for the seven stations. Figure 32 indicates that a frequency-dependent change in the sense of polarization in the H-D plane is evident at SMIT, FTCH, and MCMU. At SMIT micro-pulsations with frequencies less than 7 mHz have CC polarization while those with frequencies greater than 7 mHz have CW polarization. At FTCH and MCMU the change occurs at ∿ 9 mHz. CAMB does not show any distinct changes in polarization and micropulsations at most frequencies

Fig. 32. Ellipticities in the H-D plane plotted against frequency at 7 stations. All the data are from the interval 1200-1600 UT. The solid lines have been fitted to the data by taking averages over 2 mHz bandwidths at intervals of 1 mHz.
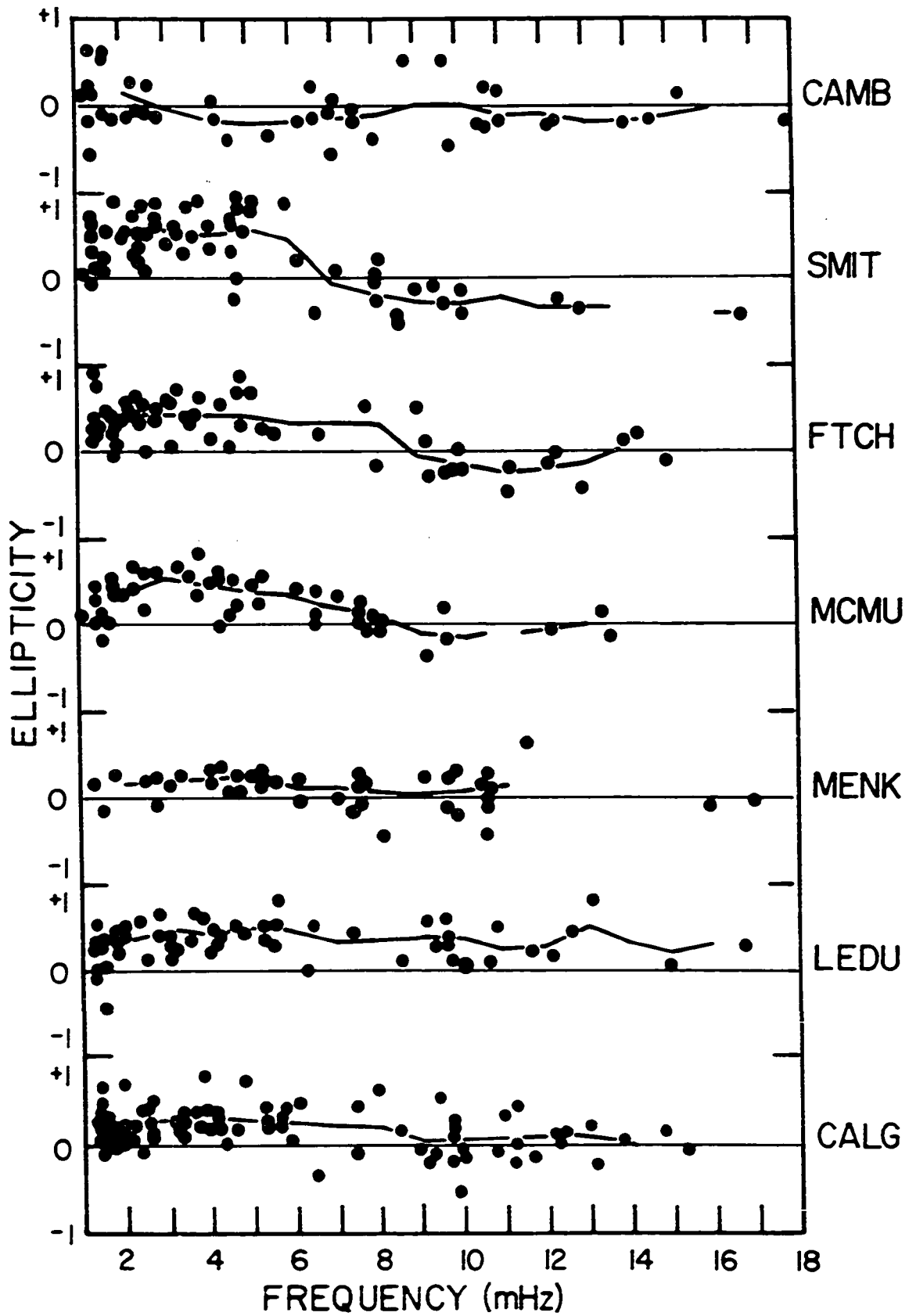
Fig. 32.

are nearly linearly polarized. There is, however, some
indication of a change at 2-3 mHz. The average ellipt-
icities at the three southern stations (MENK, LEDU, and
CALG) do not show any change in sign. If a change does
occur at these stations it must be only at frequencies
greater than 15 mHz. In fact, *Rankin and Kurtz* [1970]
found that at Leduc a change in the sense of polarization
occurs near 20-40 mHz. Some caution should be used in
interpreting the Calgary data, however, since there are
a considerable number of events above 9 mHz which have
CW polarization. Ellipticity plots from data recorded
in the late morning and afternoon indicate that the change
in sense is seen at higher frequencies at this time (see
Figure 33). This trend might be expected from the diurnal
variation of the intensity maxima shown in Figure 19.

The plots in Figure 32 allow us to estimate
the latitude of the polarization demarcation line as a
function of frequency. The frequency at which the sense
of polarization changes (e.g. 7 mHz at SMIT) corresponds
to the frequency of micropulsations that have a demarcation
line at that station. These estimates eliminate the poor
latitude resolution inherent in ellipticity-latitude
profiles computed from data from widely separated stations.
The weakness of this method is that it demands large
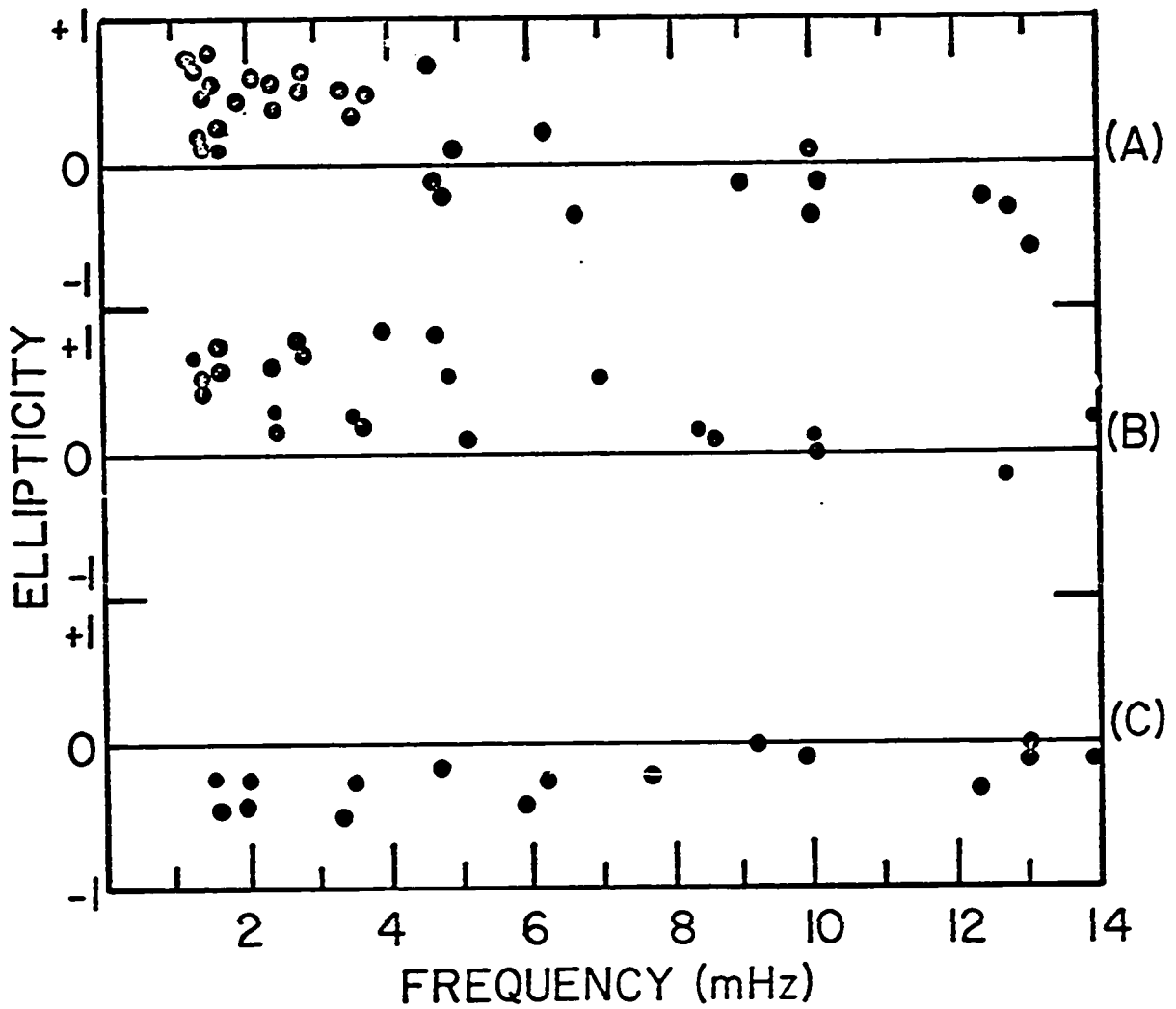
Fig. 33. Ellipticities in the H-D plane of micro-
pulsations recorded at SMIT in 1969. The intervals
of time in the plot are (A) 0800-1600 UT, (B) 1600-
1900 UT, (C) 2300-0300 UT.

amounts of micropulsation activity at one time or station-
ary geomagnetic conditions over long intervals. Neither
condition prevails very often and consequently the data
are scattered and frequency resolution is lost. Figure
34 shows the estimated frequencies of the polarization
reversals plotted against latitude. The solid line gives
the approximate trend of the intensity peaks plotted in
Figures 21 and 22. Evidently there is a correlation between
the ellipticity reversals and the intensity peaks.

3.2.3 Polarization angles A simple plot of average
polarization angles is not possible because of the cyclical
nature of these parameters. The distributions of the angles
are conveniently presented in the form of circular bar
histograms. The lengths of the bars give the expectation
of finding the polarization angle in the given intervals.
For the data presented here we have used the six intervals
shown in Figure 35. A bar of length 1.0 indicates that
all measured angles were in the given interval. For clarity
in the following histograms bars with lengths of less than
0.1 are not plotted.

Not all the data will be presented here since
this would require the construction of over 1200 histograms,
based on intervals of 4 hr x 2 mHz. In general the polar-
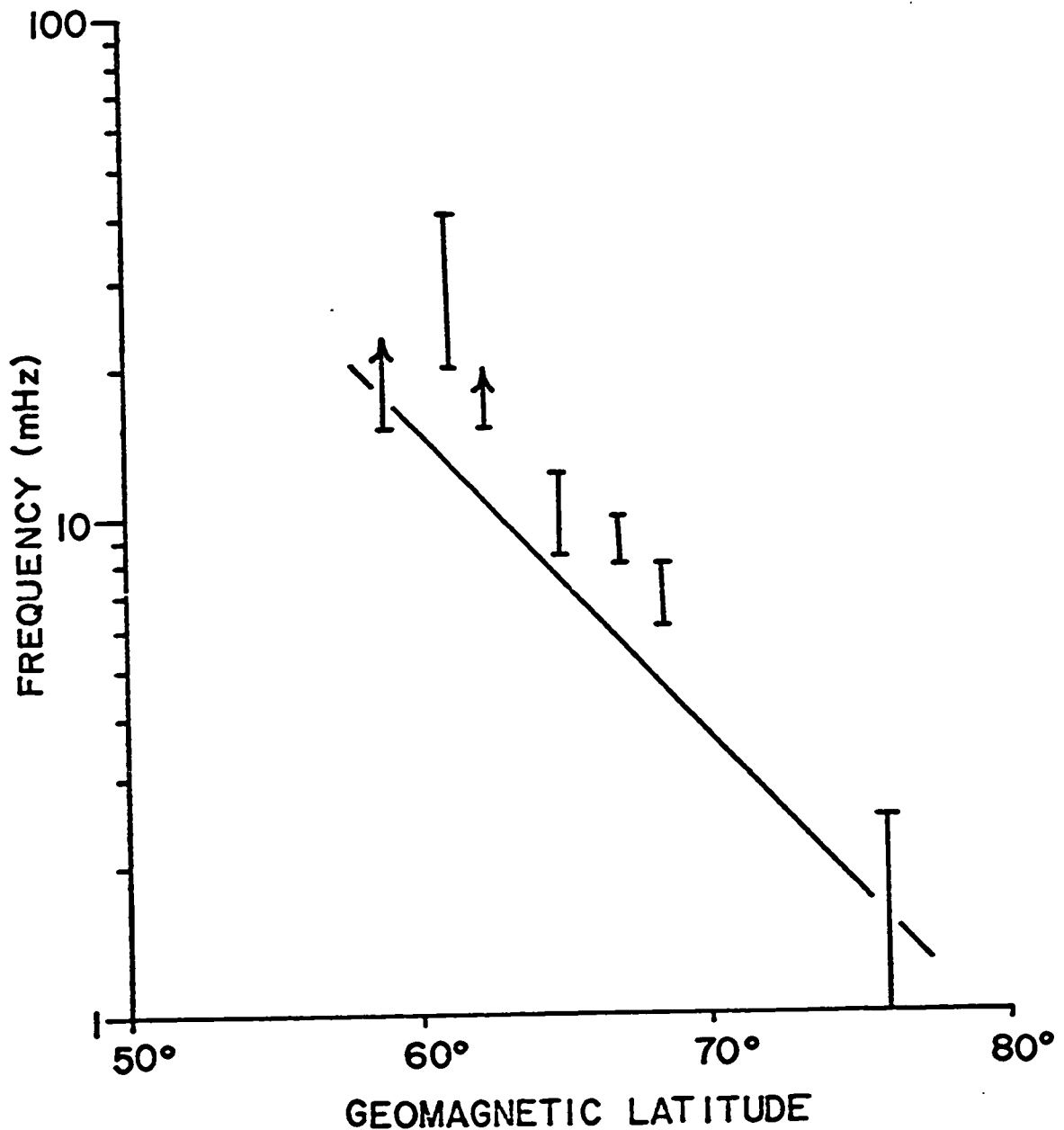
Fig. 34. Estimated frequencies of the polarization reversals at the stations. The arrows at CALG (58.7°) and MENK (62.5°) indicate that the reversals occurred at frequencies higher than those marked by the horizontal bars. The frequency range of the reversals at LEDU (61.2°) was determined from the data given by *Rankin and Kurtz* [1970]. The solid line shows the approximate trend of the intensity peaks plotted in Figure 22.
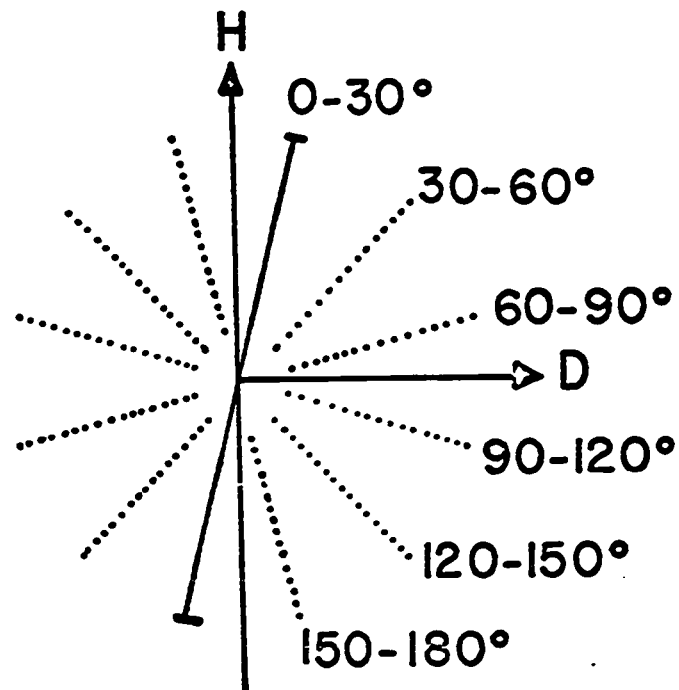
Fig. 35. The ranges of the polarization angles in the circular histograms. In this example we have assumed that all the polarization angles are in the 0-30° range.

ization angles of the low frequency Pc 5's are the most predictable; the angles in the Pc 4 band show considerable scatter. In the H-D plane the polarization angles of Pc 5's indicate that the magnetic fields at CALG are strongly affected by induced earth currents, the most probable cause being a deep conducting anomaly in the Cordillera region. The following histograms give summaries of the H-D, H-Z, and D-Z polarization angles of 0-4 mHz pulsations and a summary of the H-D polarization angles of micropulsations in the 10-15 mHz band. We have omitted the Pc 4 data in the H-Z and D-Z planes because of the small amplitudes of the Z component in this band and because of induction effects on the Z components.

In the 0-4 band, the polarization angles in the H-D plane (Figure 36) show simple diurnal variations at all stations except CALG. The H direction predominates over most of the day with tendencies for polarization in the D direction at CAMB, SMIT, and FTCH between the hours of 0800 to 2000. This interval marks the time during which pulsations at these stations have the most elliptical polarization in the H-D plane (Figure 30). The tendency for polarization in the D direction is most pronounced in the interval 0800-1200 at CAMB changing to 1200-2000 at

SMIT and FTCH. The major axes at MCMU and LEDU are clustered around the H direction throughout the day and show only slight diurnal variations in direction. From 0400 to 1200 the angles favor the 0°-30° interval and for the rest of the day they favor the 150°-180° interval.

The polarization angles at CALG differ substantially from those at the other stations. The major axes are grouped in the 120°-150° region and there is little variation over the entire day. In fact, the major axes are parallel to the strike dividing the plains from the mountains. The direction of the strike is $\sim 30^{\circ}$ west of geographic north or 53° west of magnetic north (corresponding to a polarization angle of 143°). This type of polarization would be expected if CALG were on the resistive side of a vertical geoelectric discontinuity (see Appendix A7, Figure A21). This supposition is supported by magnetotelluric and geomagnetic depth sounding data in southern Alberta (see Section 2.3).

The polarization angles in the H-Z plane (Figure 37) have very simple diurnal characteristics. At all stations the preference is for the H direction although there is some change of angle with latitude. At FTCH, MCMU, LEDU and CALG most angles lie in the 0°-30° interval

whereas at SMIT the angles are in the 150°-180° interval. These histograms and the ellipticity plots show that the pulsation magnetic fields are definitely not polarized transverse to the main geomagnetic field. For example, transversely polarized waves at LEDU would have polarization angles grouped around 167° whereas the actual angles are grouped around 15°. Pc 5's at CAMB show more confused characteristics than those at the other stations. Even so the major axes of the polarization ellipses generally point in the H direction.

The characteristics of the polarization angles in the D-Z plane (Figure 38) show pronounced diurnal variations at every station except CALG. Conditions in the interval from 1200 to 1600 are the clearest with the major axes at most stations favoring the D direction. Micropulsations occurring during this time interval must have large D components since they are also polarized in the D direction in the H-D plane. At other times of the day, the polarization in the D-Z plane is more confused, especially at FTCH and MCMU. During these times the D and Z components are probably of comparable magnitude. The intervals of confused polarization are most pronounced between 0000-0800 at FTCH, MCMU, and LEDU. The polar-

Fig. 36. Polarization angles in the H-D plane of micropulsations in the 0-4 mHz spectral band. The sample intervals are 4 hr long. The horizontal bar at the top of the diagram is 1 unit long.

Fig. 37. Polarization angles in the H-Z plane of micropulsations in the 0-4 mHz spectral band.

Fig. 38. Polarization angles in the D-Z plane of micropulsations in the 0-4 mHz spectral band.
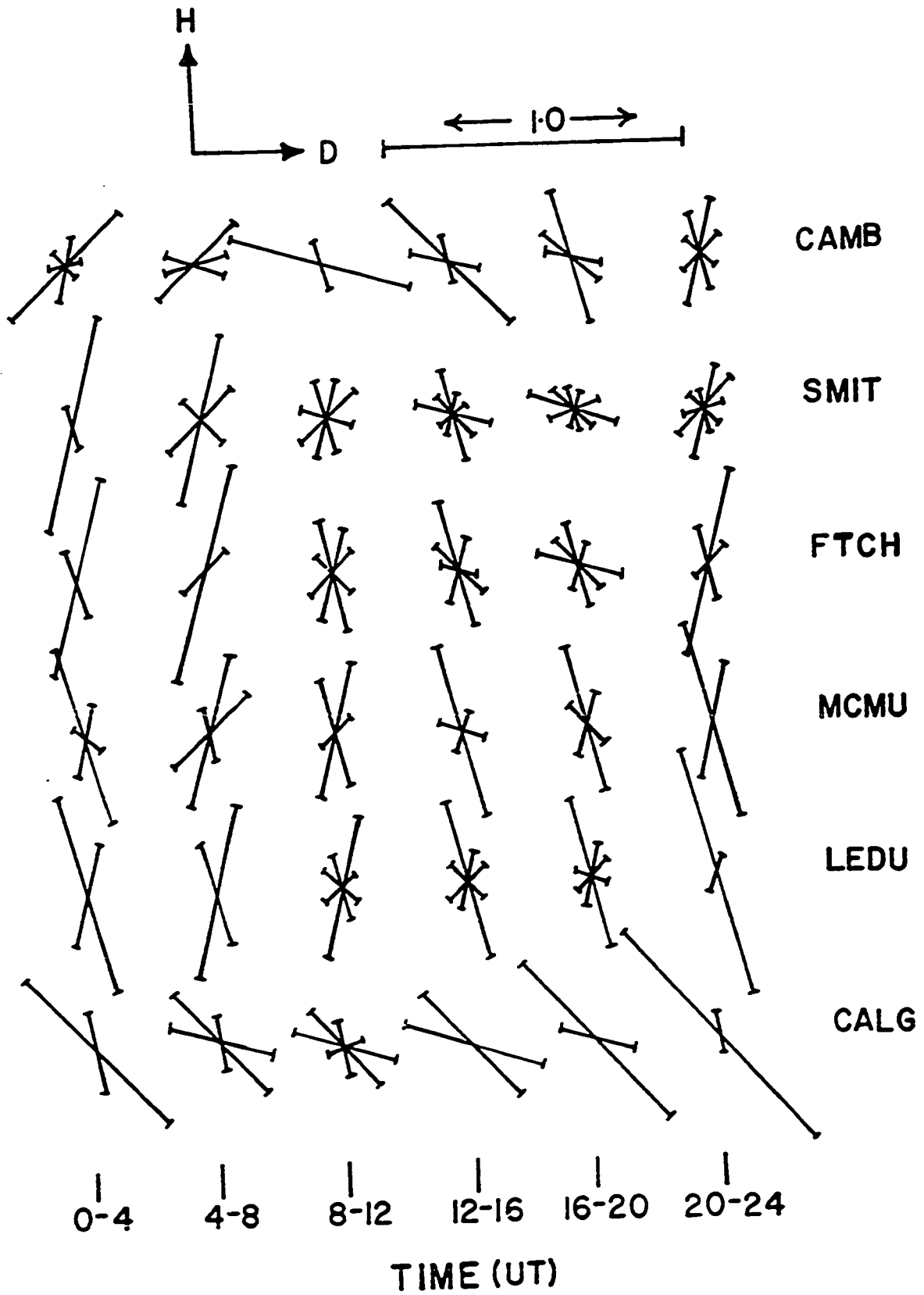
Fig. 36.
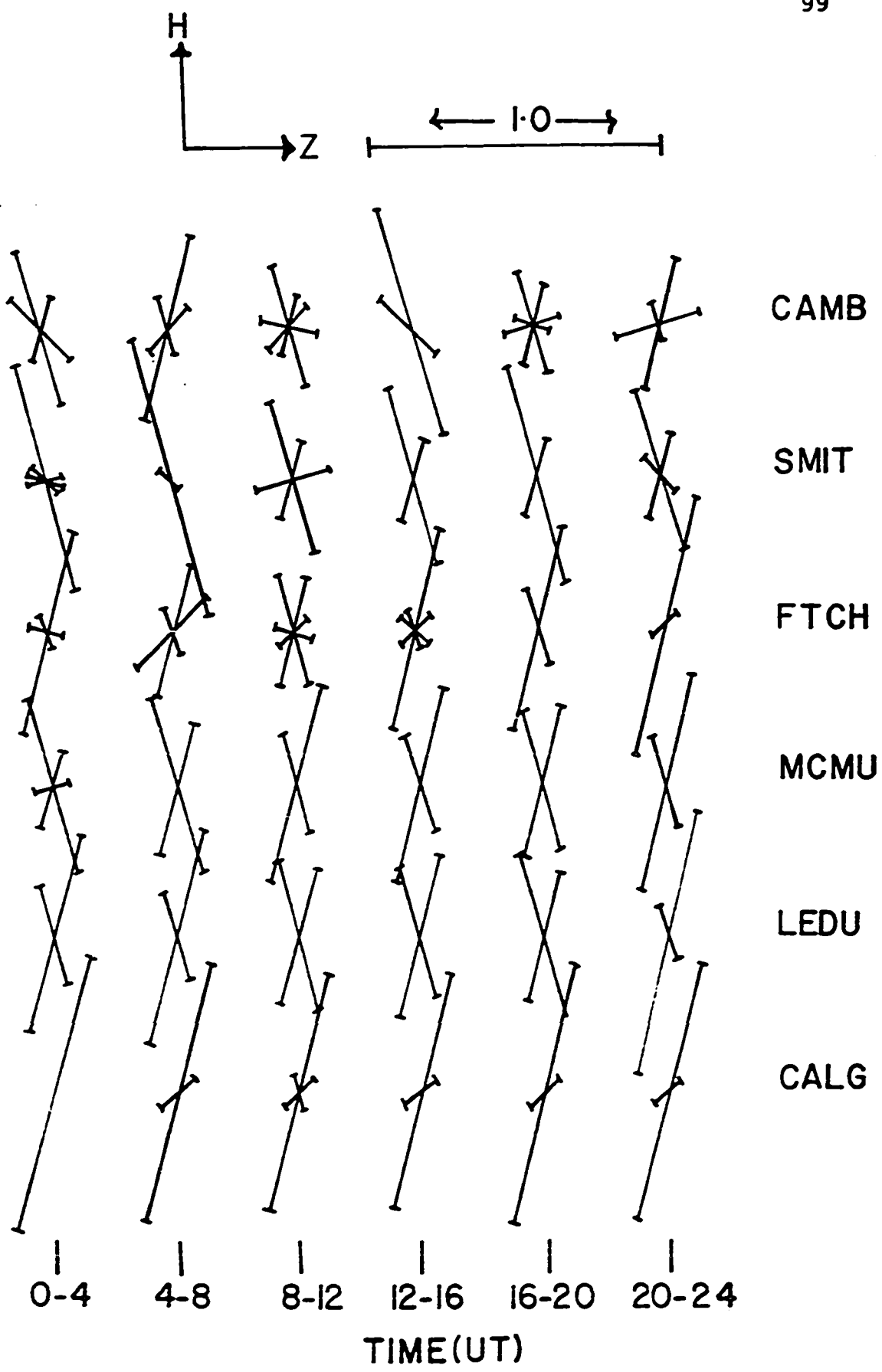
Fig. 37.
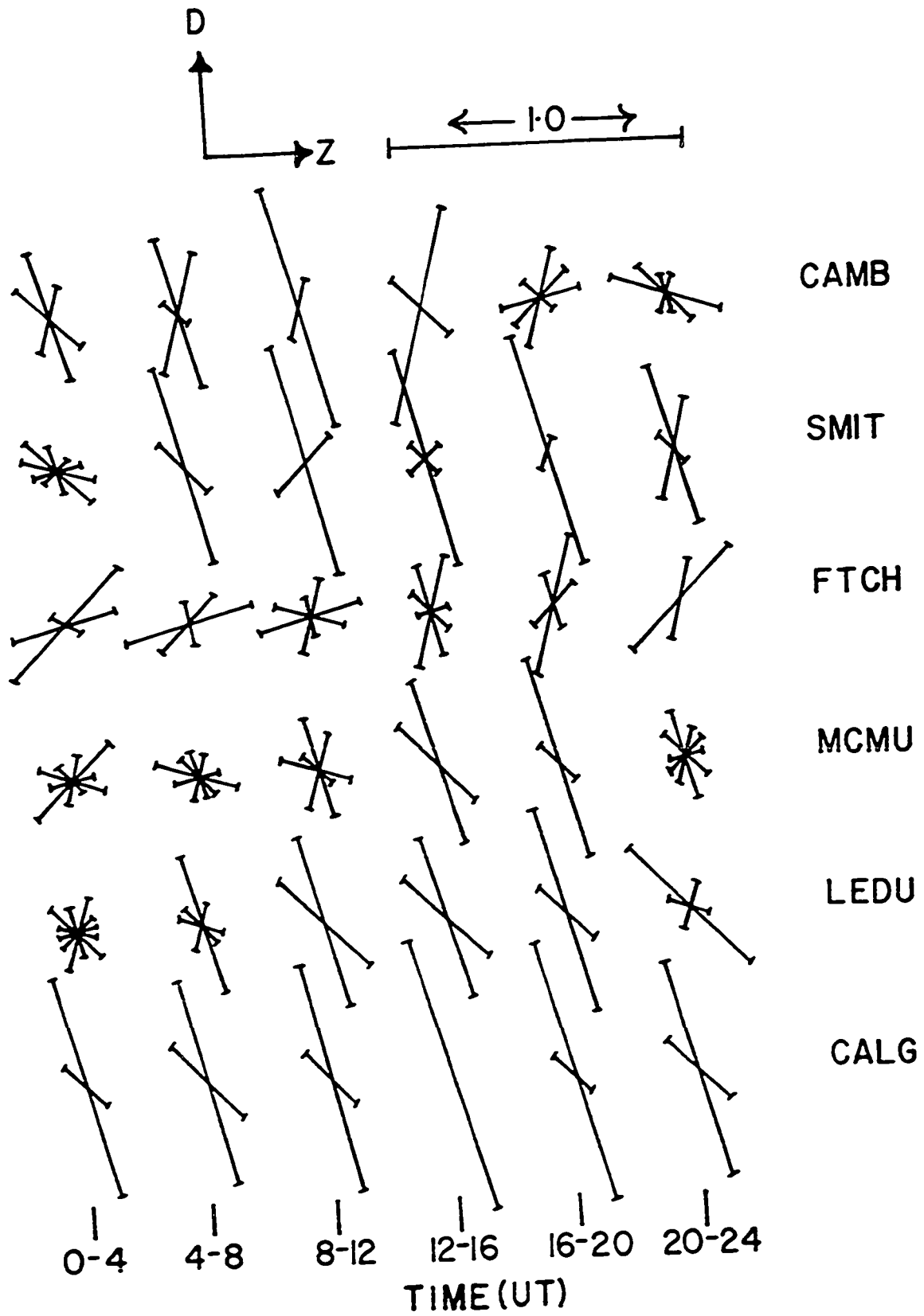
Fig. 38.

ization angles of Pc 5's at FTCH also favor the Z direction in this time interval. On the other hand, the angles of Pc 5's at CAMB favor the Z direction in the interval 2000-2400.

Figure 39 summarizes the diurnal polarization characteristics in the H-D plane of low frequency (0-4 mHz) Pc 5 micropulsations. Data from CALG are not included in this plot because of their anomalous behavior. The dotted line on the plot gives an estimate of the position of the intensity maximum as a function of time (see Figure 19). The polarization patterns show some strikingly simple features, especially when they are correlated with the diurnal variation of the intensity maxima. The major axes of all the ellipses tend to line up perpendicular to this line. This is most evident for those stations closest to the intensity maxima (CAMB, SMIT, and FTCH) although the trend does show at MCMU and LEDU as well. Generally speaking, polarizations become most elliptical when a given station is near the line of maximum intensity, although there is also a tendency for more elliptical polarizations at the southern stations in the morning hours (0800-2000). In addition, if the line
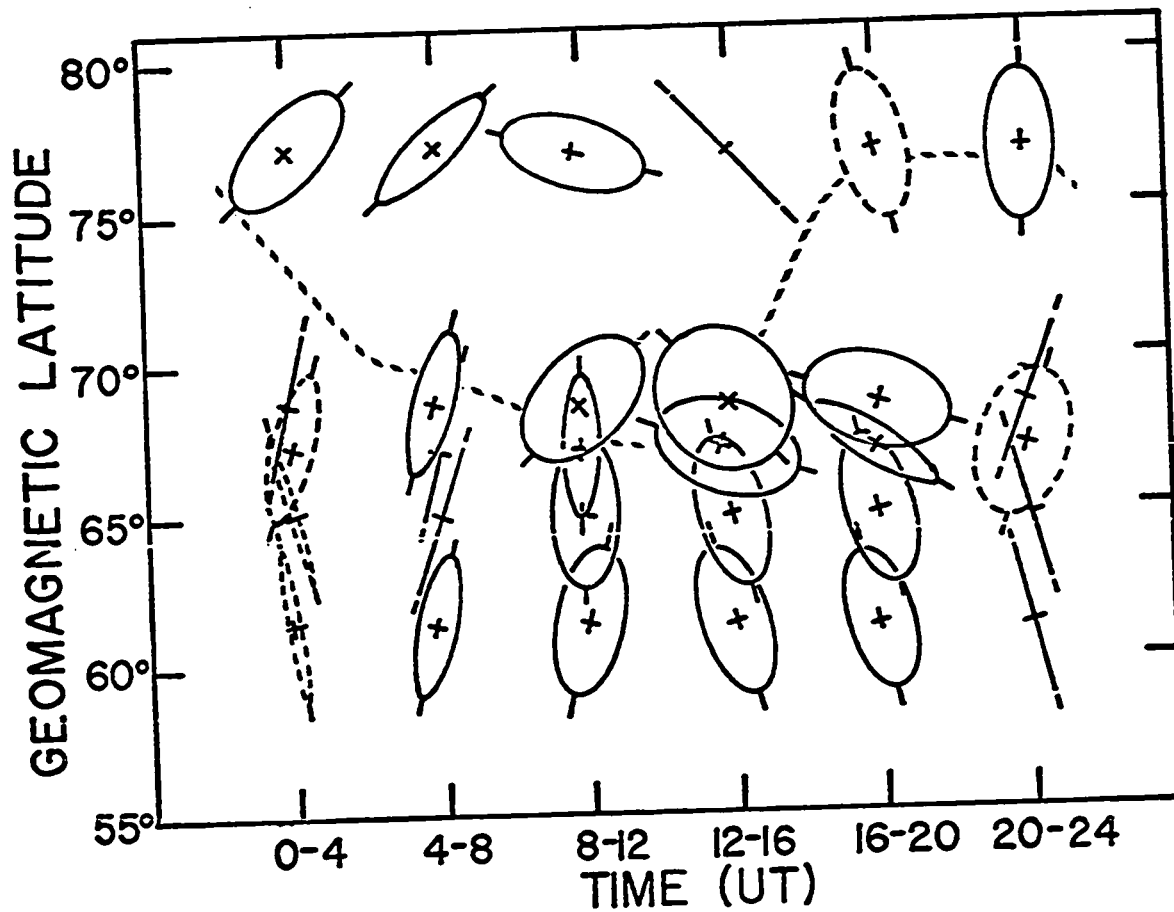
Fig. 39. A summary of the polarization parameters in the H-D plane of micropulsations in the 0-4 mHz spectral band. Ellipses with solid lines depict CC polarization and ellipses with dotted lines depict CW polarization. The dotted curve shows the position of the intensity maximum. The sizes of the ellipses are not scaled to the average intensities and all the major axes have the same length. The centres of the ellipses are at the latitudes of the stations from which the data were obtained (CAMB, SMIT, FTCH, MCMU, LEDU).

of maximum intensity is midway between CAMB and SMIT, both SMIT and FTCH have a sense of polarization opposite to that at CAMB. In the early morning hours, when the activity centre is near SMIT (0400-1200),all stations including CAMB have the same sense of polarization. Some caution should be exercised in correlating the polarization angles of Figure 39 with the line of maximum intensity since the polarization angles in the figure are *spatial* orientations whereas the intensity line is a plot of *temporal* variation.

We conclude this study of polarization angles with a short discussion of the polarizations of Pc 4's in the H-D plane (see Figure 40). The characteristics of these micropulsations are rather complex and our data sketchy so that we will mention only a few of the more evident trends. The most noticeable feature in Figure 40 is the consistent polarizations in the D direction at CALG. This feature may once again be a manifestation of induced earth currents, although the angles do not align with the strike of the Rocky Mountains. LEDU also shows a predominance of angles in the D direction so it may be that these polarizatons are truly a reflection of the source configurations. All the other stations have very complex polarization characteristics, which differ from station to
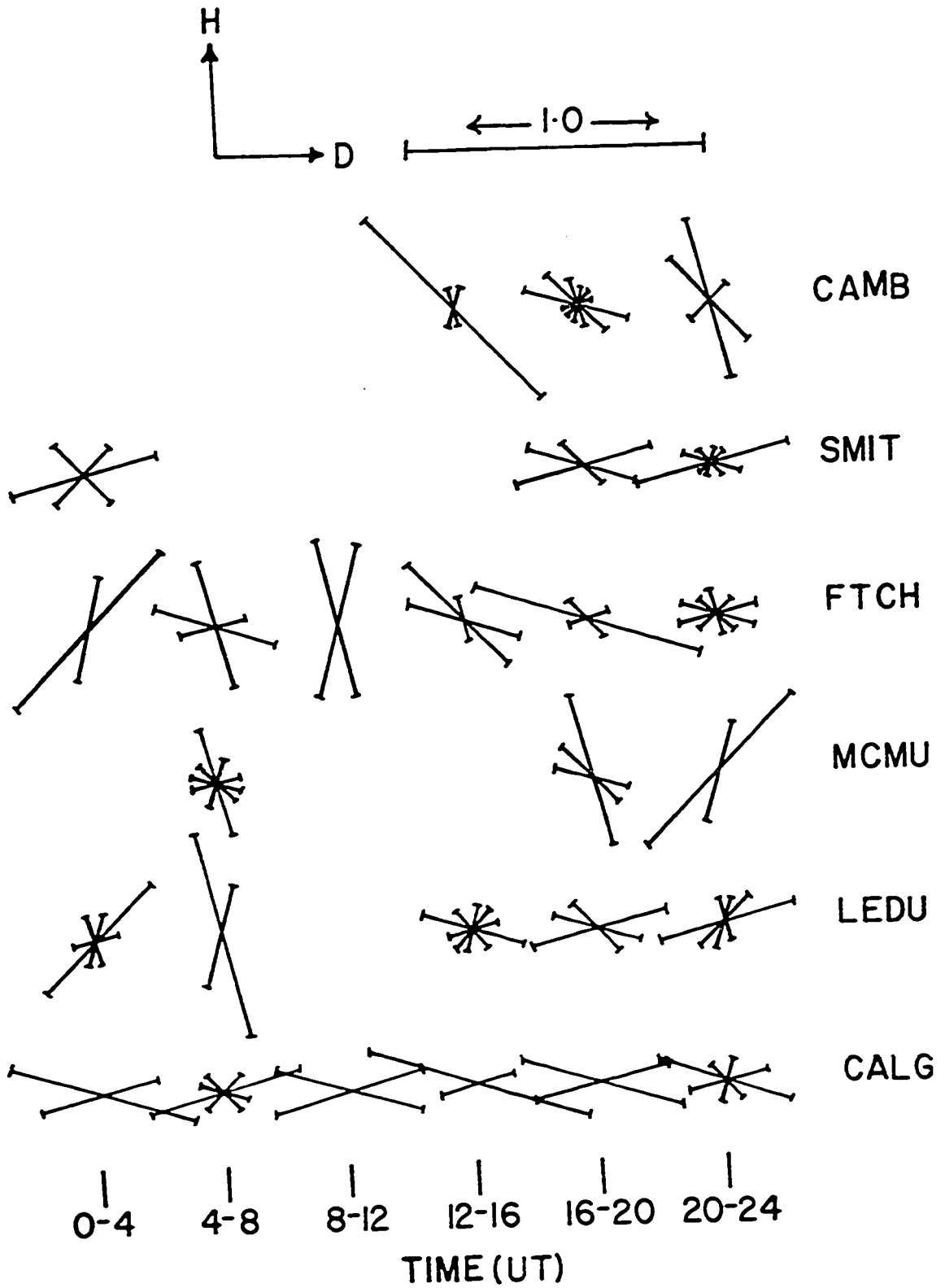
Fig. 40. Polarization angles in the H-D plane of micropulsations in the 10-15 mHz spectral band (Pc 4).

station and from time to time. The polarization angles
do, however, favor the H direction during the interval
0000-1200 and the D direction during the interval 1200-2400.
Pc 4's at FTCH show this feature most clearly whereas at
MCMU the angles tend to align with the H direction through-
out the day.

3.3 Some individual micropulsation events

This section contains the analysis of five events
which were individually selected for their clear sinusoidal
micropulsations. The following pages outline the general
spectral characteristics of these micropulsations, includ-
ing the power spectra, station-to-station phase spectra,
and polarization parameters.

To reduce the amount of data presented in this
section the only phases we have plotted are those given
by $F_{ii}(\vec{r}_1, \vec{r}_2, f)$ (see Section 2.3). CAMB is used as the
reference station and all phases are calculated with respect
to this station. The estimates F_{11}, F_{22} and F_{33} compare
the phases of the H, D and Z components respectively at
all stations. For example, if the H components at FTCH
and SMIT lead the H component at CAMB by 20° and 40°
respectively, then F_{11} at FTCH is -20°, and F_{11} at SMIT
is -40°. In plotting the phases, we have subtracted the
corresponding median value from each estimate of F_{11}, F_{22},
and F_{33} in order to centre the data on the grids. Thus

the estimates of F_{ii} at CAMB often do not have the value 0°.

It must also be remembered that the phases of the magnetic fields can be severly affected by horizontal changes in the geoelectric properties of the earth (see Appendix A7). Large latitudinal phase shifts in the data may not be due to the source configuration of the micro-pulsations but may perhaps be due to a vertical contact separating two regions with very different conductivities. However, we did not note any pronounced and consistent phase changes in our data at any given latitude. The latitudes of the most apparent phase changes varied from event to event, and probably reflected the source fields of the micropulsations.

The events selected for analysis here are from five separate days in 1970 (days 163, 167, 186, 195 and 262). All the events occurred during the daytime, the earliest event occurring at 1400 (0630 LGT) and the latest at 2300 (1430 LGT).

As already mentioned, the frequency of a given micropulsation train is usually independent of latitude. With the exception of the event occurring on day 262, this is the case for all the events discussed here. Analysis of the event from day 262 shows that the dominant frequency in the H component apparently decreases with increasing latitude.

The event on day 186 merits special attention because of its sinusoidal appearance and large amplitudes. The magnetograms from 13 standard observatories were digitized and these data are included in the discussion of this event. It is interesting to compare the spatial features of this event with the average polarization characteristics of the 1969 and 1970 data (Figure 39).

The events are discussed in chronological order and the magnetograms are reproduced in the following pages (Figures 41 to 45).

(a) Day 163, 1600-1700 UT

This interval shows distinct 12 mHz,Pc 4 micropulsations and distinct 1.0 mHz,Pc 5 micropulsations. The Pc 5 activity is most evident at CAMB where it attains peak to peak amplitudes of ∿ 30γ in the D and Z components. Note that the D component at MENK may be too small because of the malfunctioning of the magnetometer. The Pc 4 activity has a distinct latitude-dependence in the powers in the three components (Figure 46A), especially in the D component. The D components at LEDU and CALG are far larger than those at any other of the stations. Conversely the Pc 5 event has its greatest power at CAMB (Figure 47A), with very little power at the southern stations. The H-D ellipticities of both micropulsation trains show marked latitude reversals (Figures 46C, 47C). The change in the sense of polarization

Fig. 41. Magnetograms of the event occurring on day 163. The records have been detrended with a 1-20 mHz digital filter (see Section A4.3). The time scale is marked in hours of Universal Time.

Fig. 42. Magnetograms of the event occurring on day 167. The records have been detrended with a 1-20 mHz filter.

Fig. 43. Magnetograms of the event occurring on day 186. The records have been detrended with a 1-20 mHz filter.

Fig. 44. Magnetograms of the event occurring on day 195. The records have been detrended with a 2.5-100 mHz filter.

Fig. 45. Magnetograms of the event occurring on day 262. The records have been detrended with a 1-20 mHz filter.

DAY 163,1970
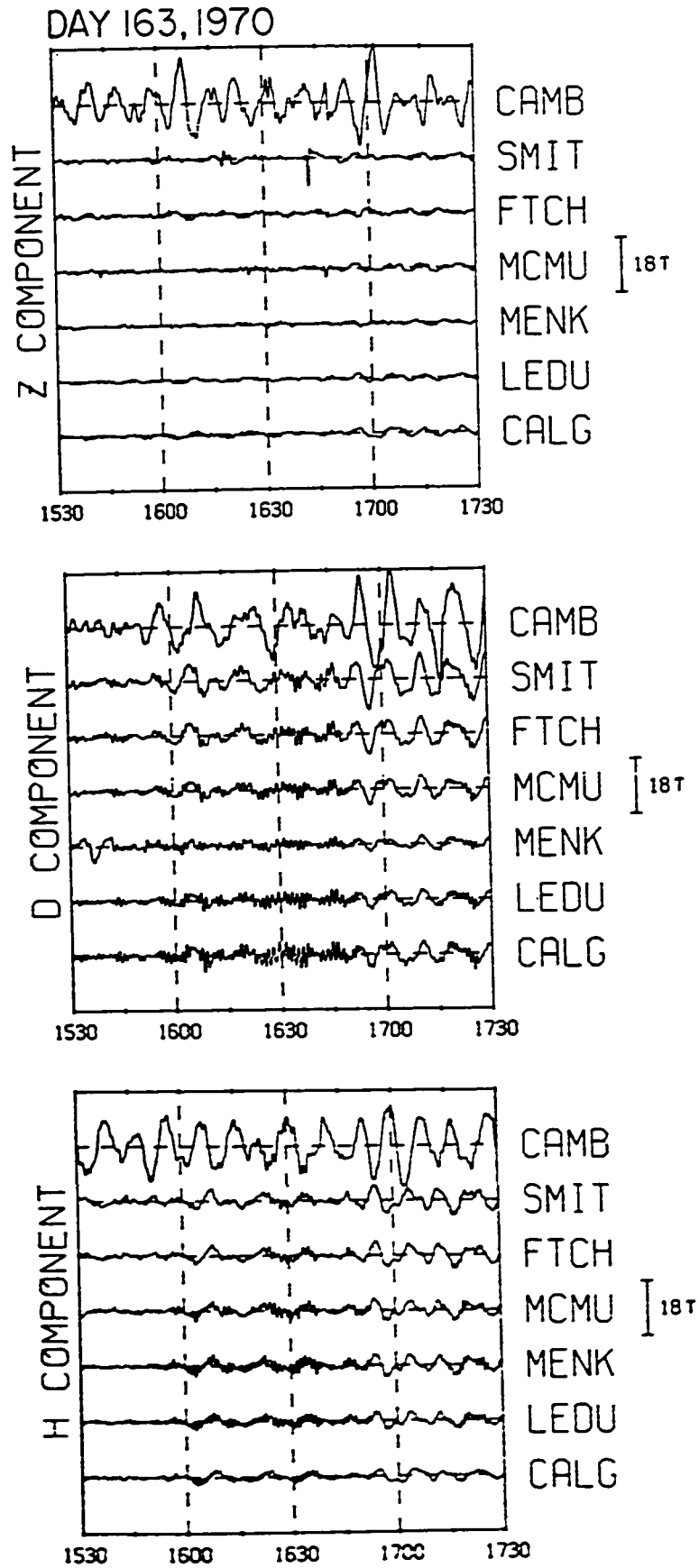
Fig. 41.
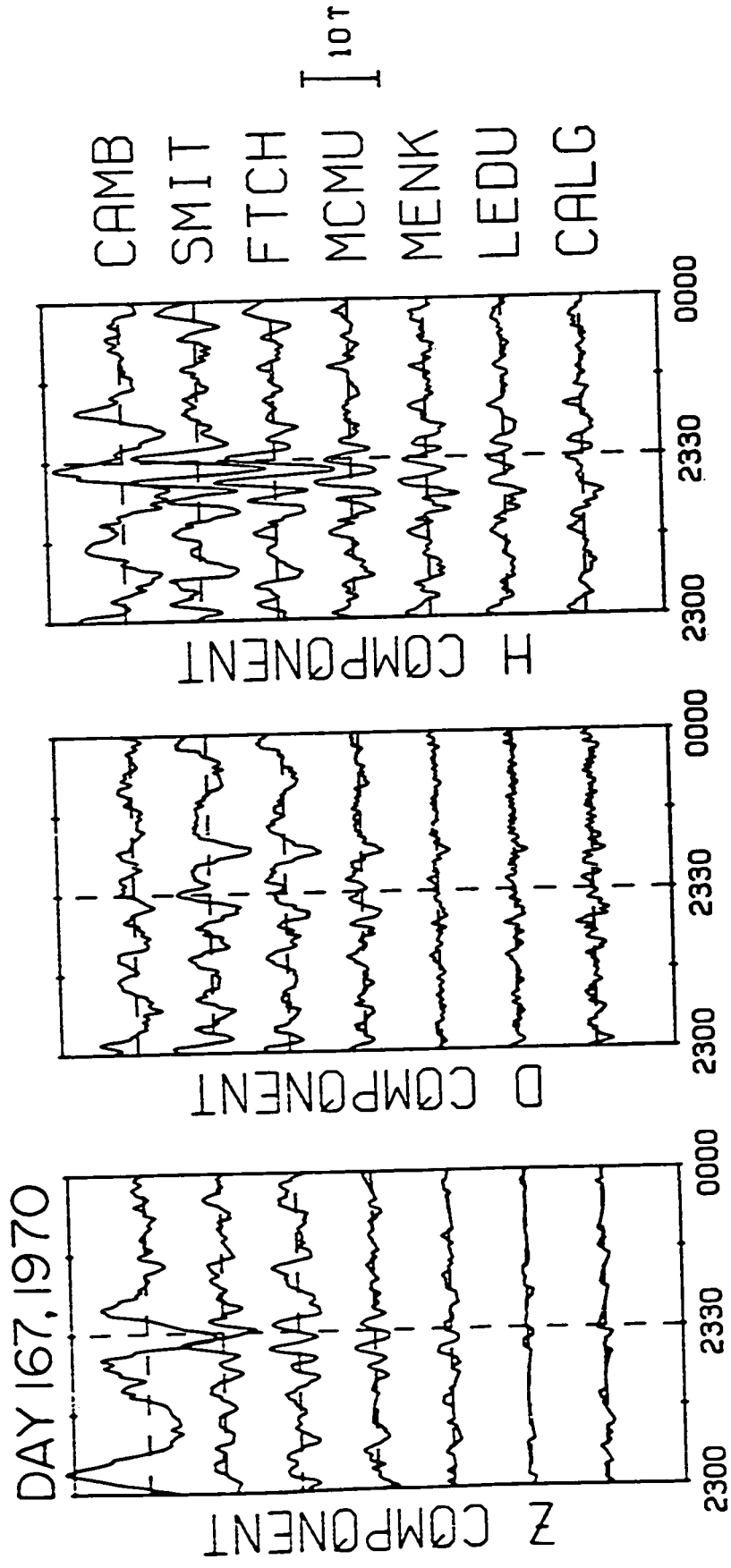
Fig. 42.
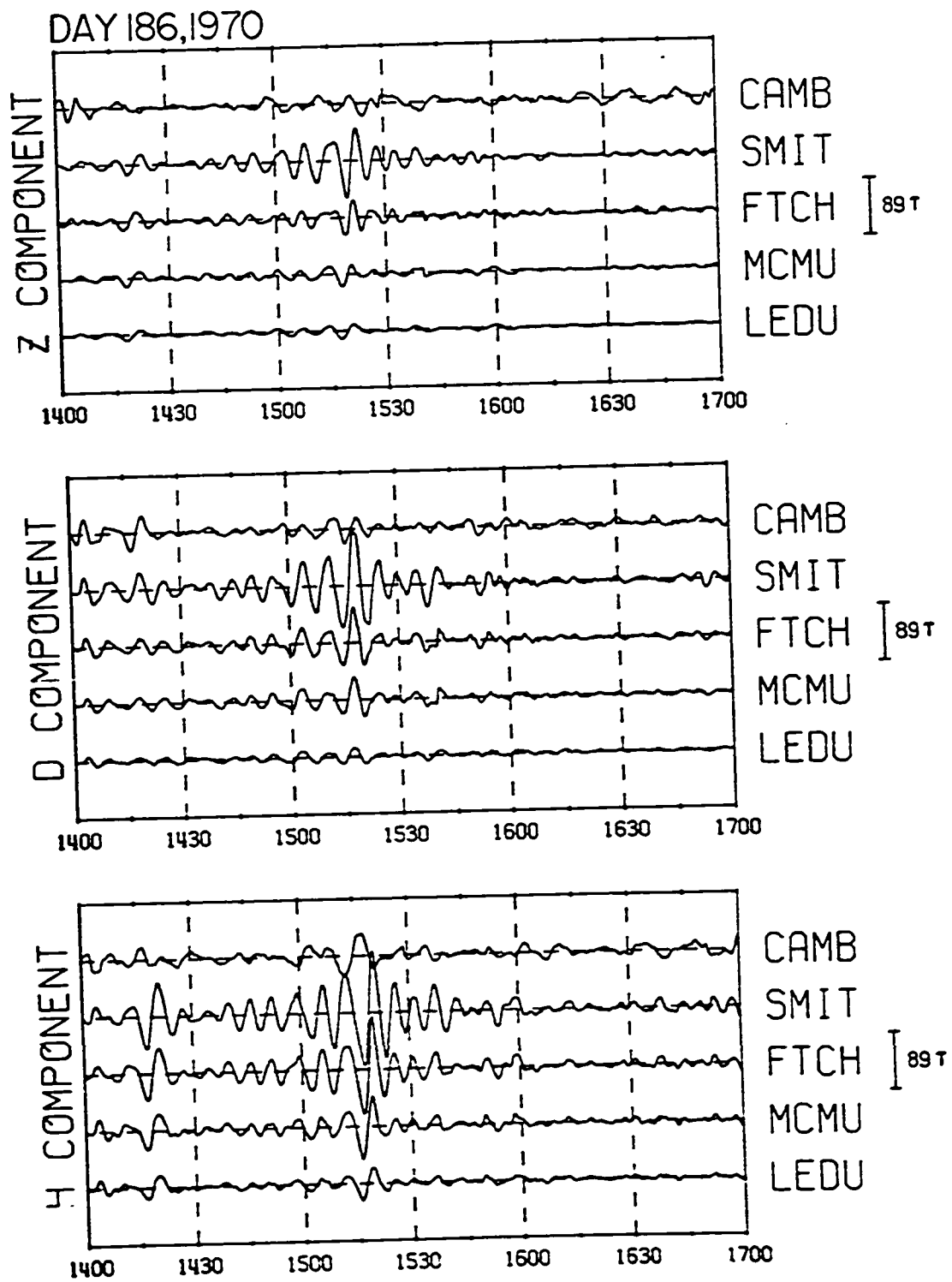
Fig. 43.
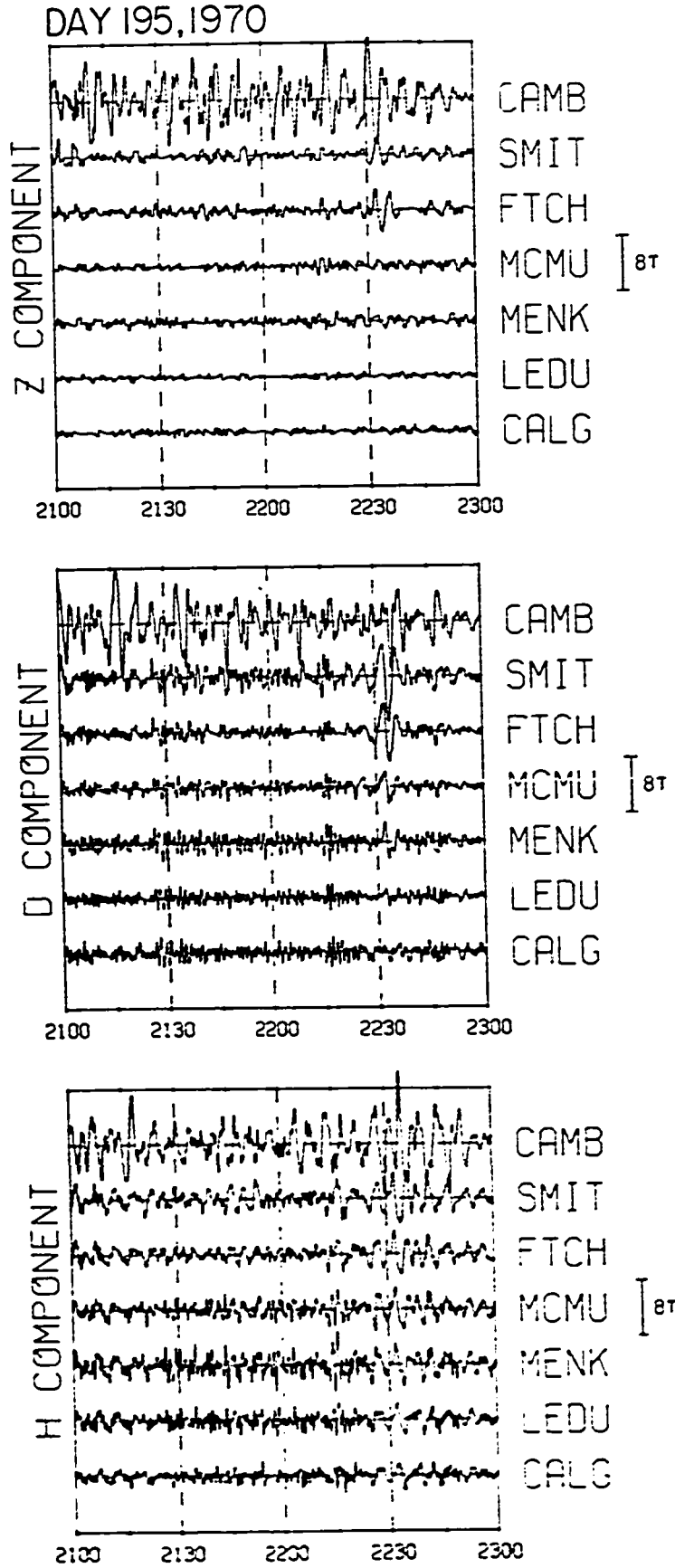
Fig. 44.
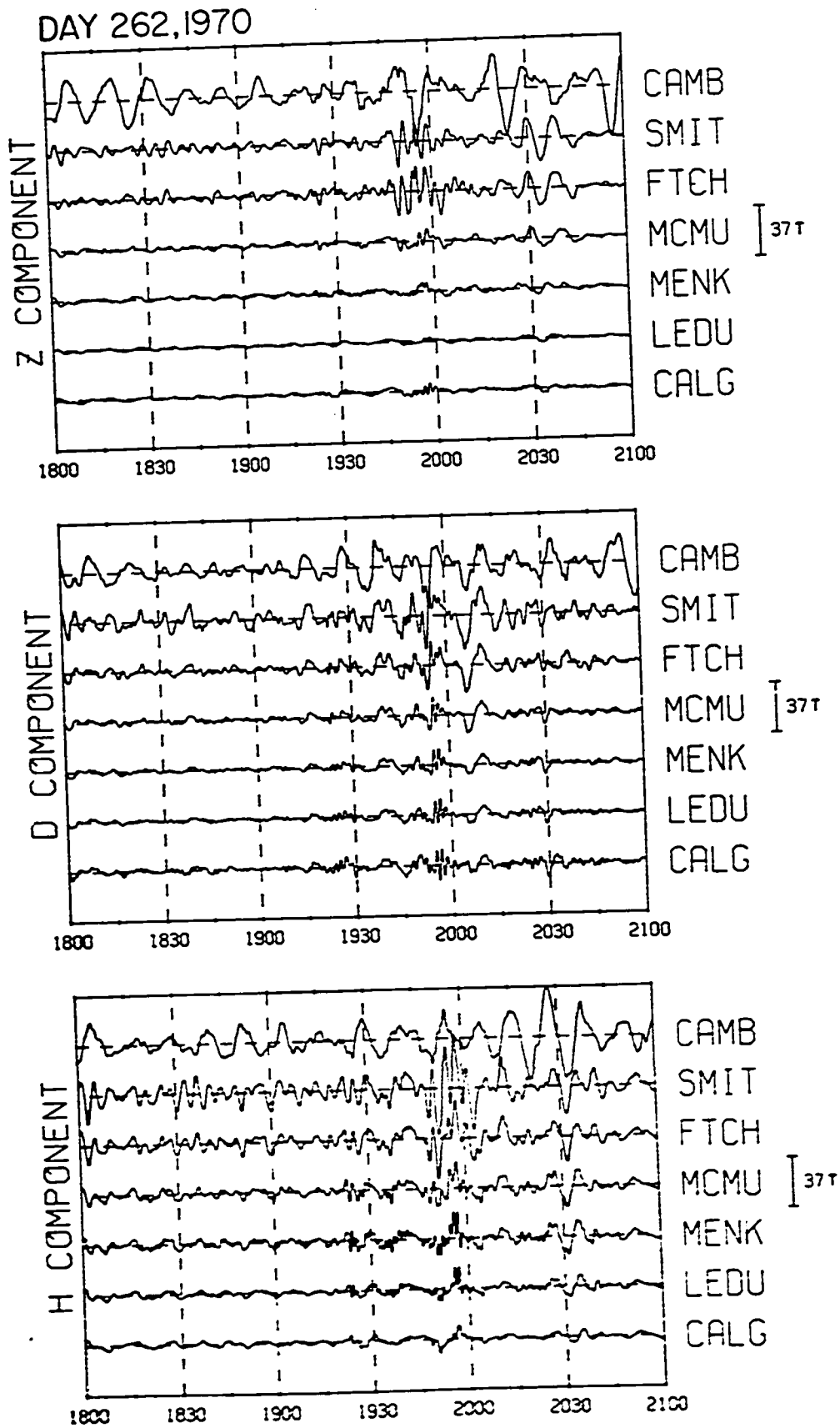
Fig. 45.

Fig. 46. Latitude-dependence of the spectral parameters of the 12 mHz micropulsations (day 163, 1600-1630). The phases of the Z components are not plotted because of the low amplitudes of this component at the southern stations.

(A) Power plotted as a function of latitude

—●— H.

—O— D.

—Δ— Z.

(B) Relative phases of each component

● $\equiv F_{11}$ (H component phases).

O $\equiv F_{22}$ (D component phases).

Δ $\equiv F_{33}$ (Z component phases).

The estimates F_{11}, F_{22}, and F_{33} compare the phases of the H, D, and Z components respectively. In plotting these estimates we have subtracted the corresponding median value from each estimate of F_{ii} in order to centre the data on the grid.

(C) Ellipticities.

(D) Polarization angles.
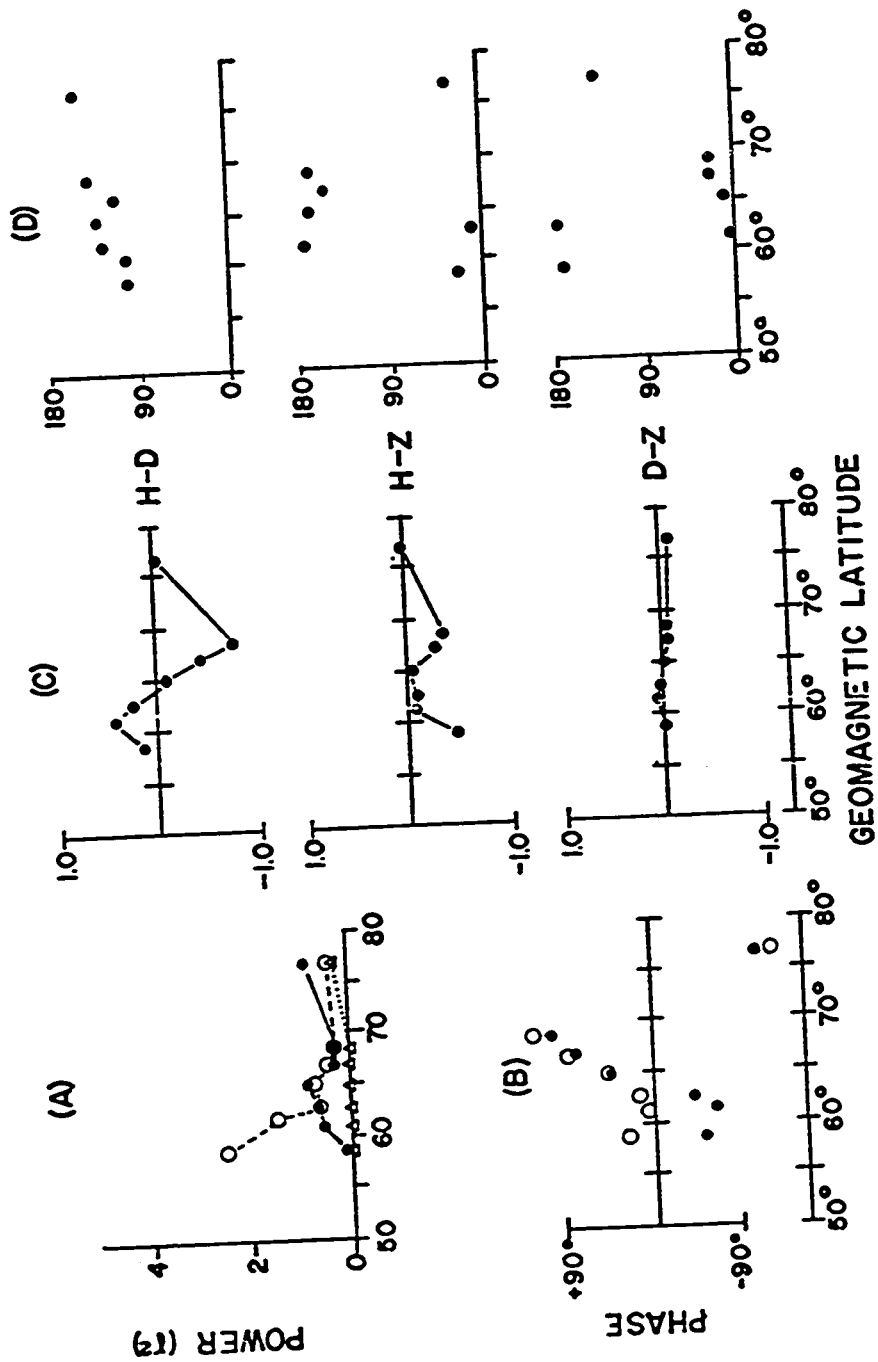
Fig. 46.
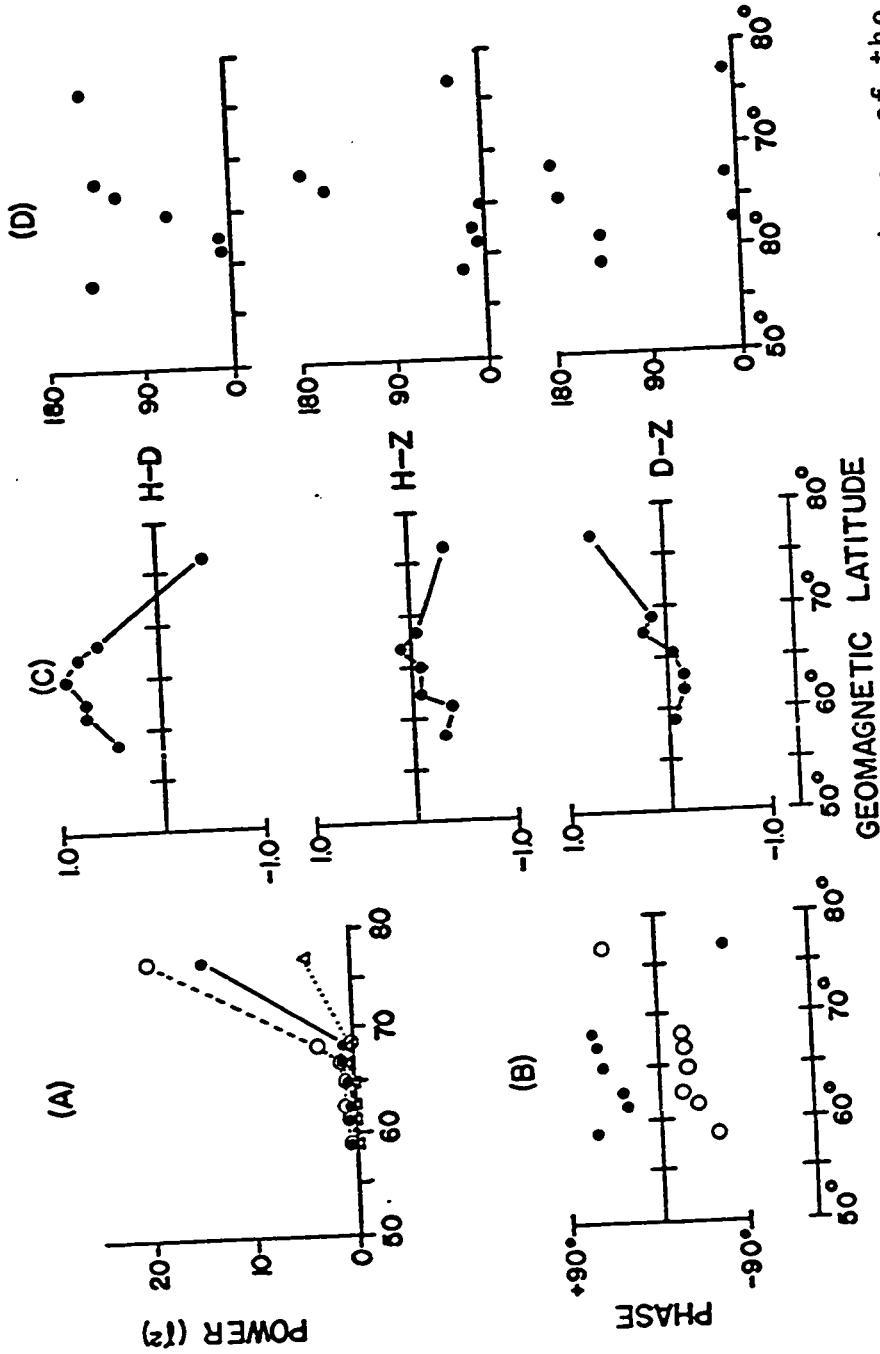
Fig. 47. Latitudinal plots of the spectral parameters of the 1.0 mHz micropulsations (day 163). The symbols are defined in the caption for Figure 46. The phases of the Z components are not plotted because of the low amplitudes of this component at the southern stations.

of the Pc 4 event occurs at 63-65°N whereas the change

in the sense of the Pc 5 event occurs between SMIT and

CAMB (68-77°N). Inspection of Figure 46B indicates

that the polarization reversal of the Pc 4 event is caused

by a rapid change in the phase of the H component, occur-

ring between MCMU and LEDU. A more abrupt phase change

occurs between SMIT and CAMB but both the H and D phases

change by the same amount. Consequently the sense of

polarization is conserved. On the other hand, the phases

of the H and D components of the Pc 5 event remain constant

at the southern stations (Figure 47B). Between SMIT and

CAMB there are sudden changes in the phases of both

components but the changes are opposite in sign and con-

sequently the sense of polarization at CAMB differs from

that at the other stations.

(b) Day 167, 2300-2400 UT

This is a very simple event, consisting of only

4 or 5 sinusoidal pulsations with a mean frequency of

4.5 mHz. The pulsations are most evident in the H and Z

components. A plot of power versus latitude (Figure 48A)

shows that the centre of activity is sharply defined with

its maximum at FTCH in both the H and Z components. At

all the stations except CAMB and CALG the power in the D
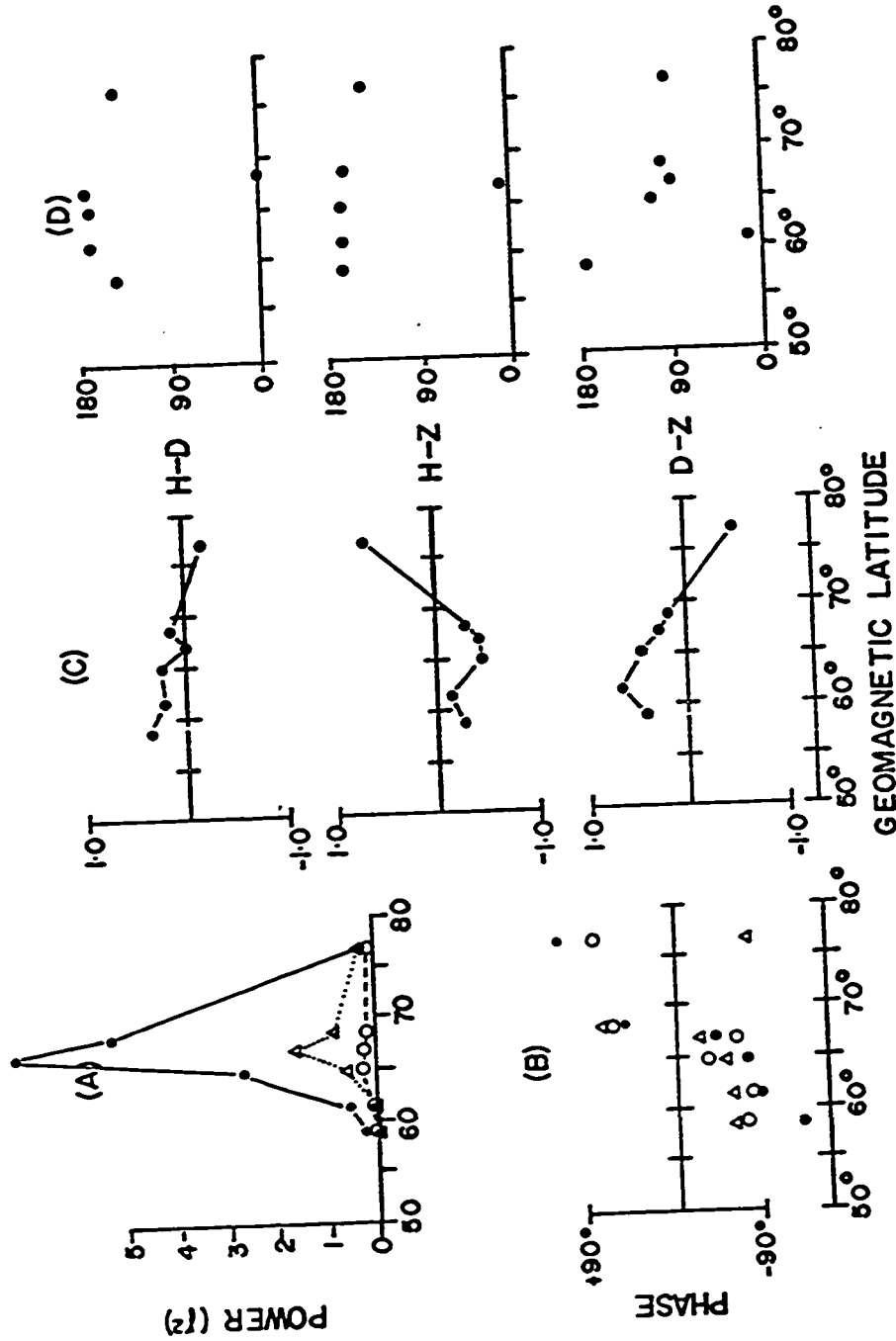
Fig. 48. Latitudinal plots of the spectral parameters of the 4.5 mHz micropulsations (day 167).

component is much less than that in either the H or Z
components. This observation is consistent with the
statistical results for the polarization parameters in
that we expect micropulsations occurring in this time
interval to be nearly linearly polarized in the H
direction on the H-D plane. The pulsations at the south-
ern stations have CC polarization (Figure 48C) even
though we might expect CW polarization from the statistical
results. In reality, though, the afternoon sector is
complicated, showing a large number of events with either
sense of polarization. When many events are averaged,
however, a slight tendency for CW polarization is evident
(see Figure 30). This event has a change in the sense
of polarization in the H-D plane, occurring near FTCH
or SMIT. The H-Z and D-Z planes also show changes in the
sense of polarization, with pulsations at CAMB having
polarizations opposite to those at the southern stations.
Figure 48B shows that both the H and D components have
substantial changes in phase between SMIT and FTCH but
in this case it is the D component which has the largest
change.

(c) Day 186 1400-1700 UT

This event has an unusual series of sinusoidal oscillations with peak to peak amplitudes of 180γ in the H component at SMIT. The large amplitudes and low frequency of this event ($\simeq$ 2 mHz) allow the use of standard magnetograms in the evaluation of the morphological features of the pulsations. Consequently we decided to analyse this event on a worldwide basis and obtained standard magnetograms from 16 stations around the world. At 13 of these stations, the temporal resolution was accurate enough, and the pulsations large enough to allow fairly precise spectral analysis of the data. These stations are listed in Table 5 and their positions mapped in Figure 49. We subsequently digitized the magnetograms at 1 min intervals and used the digitized data in an analysis of the polarization parameters of the micropulsations. Magnetograms plotted from the digitized data are shown in Figure 50. No attempt has been made to ascertain the true accuracy of the relative timing of the components at these observatories so that the data must be evaluated with caution. It is interesting, nevertheless, to compare the longitudinal characteristics of this event with the diurnal averages of the polarization parameters (Figure 39).

TABLE 5.   Magnetic Observatories used in the Analysis
of Data for Day 186

Observatory	Code Name	Corrected Geomagnetic Coordinates	
		Latitude	Longitude
College	COLL	64.6	256.3
Sitka	SITK	59.8	276.6
Victoria	VICT	53.9	292.6
Newport	NEWP	55.3	299.5
Resolute	RESO	84.3	306.0
Baker Lake	BAKE	73.8	314.8
Churchill	CHUR	70.0	326.0
Great Whale River	WHAL	68.2	353.8
Ottawa	OTTA	58.9	355.7
St. John	JOHN	57.7	29.8
Leirvogur	LEIR	66.2	72.3
Lovo	LOVO	55.9	97.9
Kiruna	KIRU	65.2	116.0
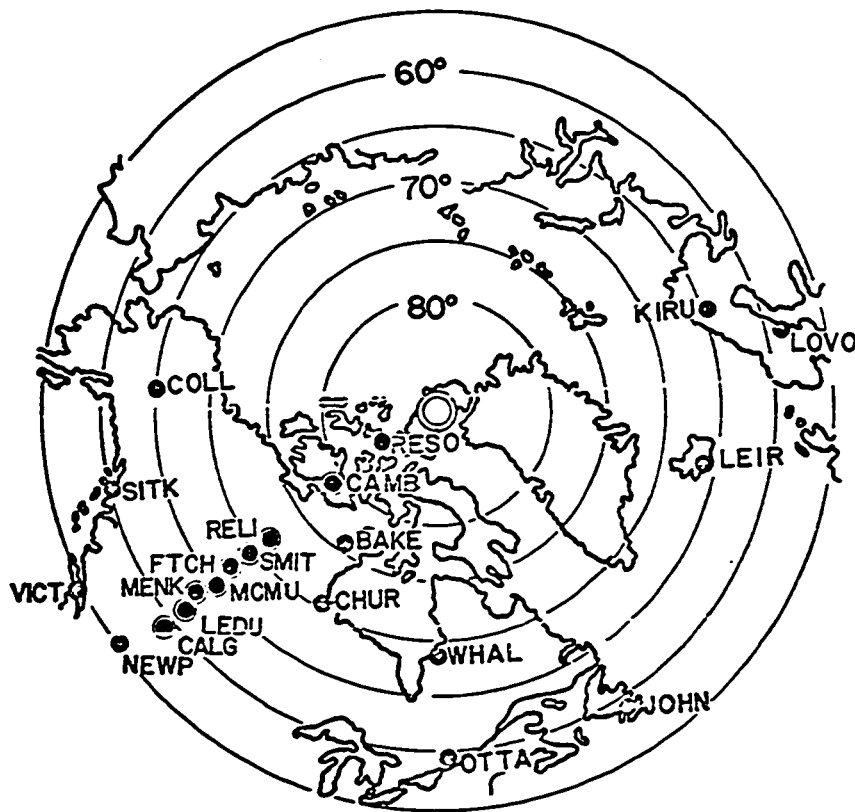
Fig. 49. The positions of the observatories used in the analysis of the micropulsations occurring on day 186. The circular grid lines show the corrected geomagnetic latitudes. The code names of the observatories are given in Table 5. This map is based on the nomograph drawn by *Whalen* [1970].

Fig. 50. Magnetograms of the digitized magnetic data from 13 observatories. The records have been detrended with a 1-5 mHz filter.
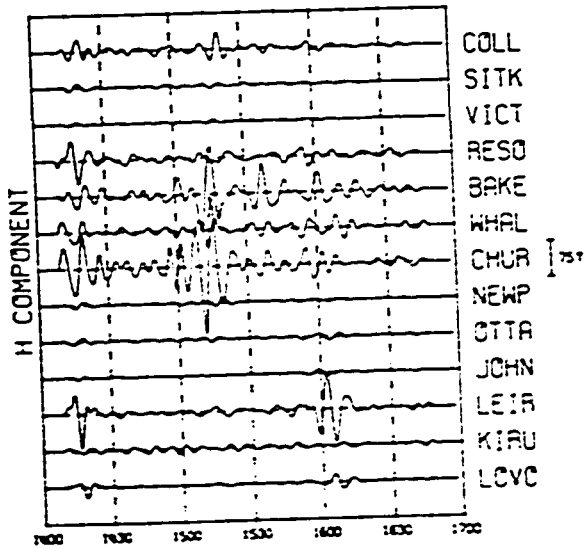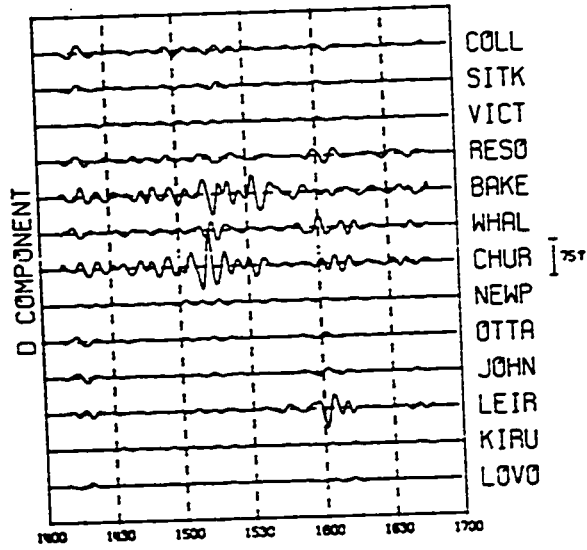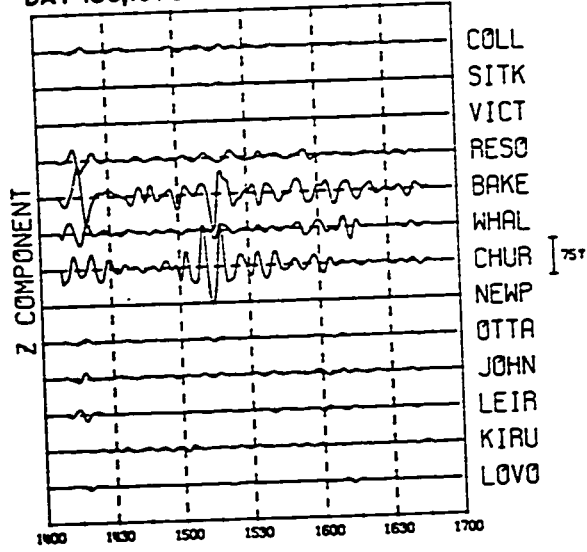
Fig. 50.

Table 6 summarizes the polarization character-
istics of the event at our stations and at the observ-
atories in the interval 1500-1600. The pulsations are
clearly localized in latitude, having intensities of
$4160\gamma^2$ and $7870\gamma^2$ at SMIT and Churchill respectively.
(Intensity is defined in Section 2.3.) This localization
is illustrated in Figure 51. The powers in all three
components show sharp peaks at SMIT dropping to half their
peak values only 2-3° to the north or south. At Baker
Lake (Figure 50) the pulsations have already lost their
sinusoidal appearance and at Resolute they are barely
perceptible. Similarly, in the south at MCMU (Figure 43)
the pulsations look irregular and at LEDU show clearly
for only two or three cycles.

Figure 52 shows the power spectra for our stations
and the two observatories, Baker Lake and Churchill, which
are nearest to the centre of activity of the micropulsation
event. With the exceptions of CAMB and Baker Lake, all
the H and D component power spectra show distinct peaks
at 2.1-2.2 mHz. Normally the power in the Z component is
the smallest but it does reach appreciable values at
Churchill. Micropulsations recorded at this observatory
may be influenced by coastal induction since the observatory

TABLE 6. The Polarization Parameters (1500-1600 UT, Day 186)

Station or Observatory	Intensity	Polarization Parameters					
		H - D		H - Z		D - Z	
		Ellip.	Polar Ang.	Ellip.	Polar Ang.	Ellip.	Polar Ang.
CAMB	$250.0\gamma^2$	-.40	145°	+.10	157°	-.45	19°
SMIT	4150.0	+.74	146	-.43	163	+.32	154
FTCH	1560.0	+.53	164	-.25	0	+.12	158
MCMU	608.0	+.63	160	-.37	4	+.05	151
LEDU	179.0	+.57	168	-.47	0	+.12	142
COLL	191.0.	+.28	166	+.20	5	-.45	21
SITK	17.6	+.63	86	+.48	5	-.02	17
VICT	6.8	+.66	51	-.22	0	-.09	169
RESO	---	---	---	---	---	---	---
BAKE	1380.0	-.16	156	-.13	150	-.05	51
WHAL	230.0	+.44	156	-.24	173	+.34	164
CHUR	7870.0	+.28	167	-.53	156	+.46	108
NEWP	21.1	+.46	139	0.0	0	0.0	0
OTTA	12.8	+.02	153	+.00	31	-.02	129
JOHN	10.8	+.32	90	-.11	81	-.23	115
LEIR	34.4	-.22	150	-.06	0	+.08	4
KIRU	22.5	-.08	13	-.04	159	-.23	122
LOVO	---	---	---	---	---	---	---

Fig. 51. Latitudinal plots of the spectral parameters of the
2.1 mHz micropulsations (day 186, 1500-1600 UT).
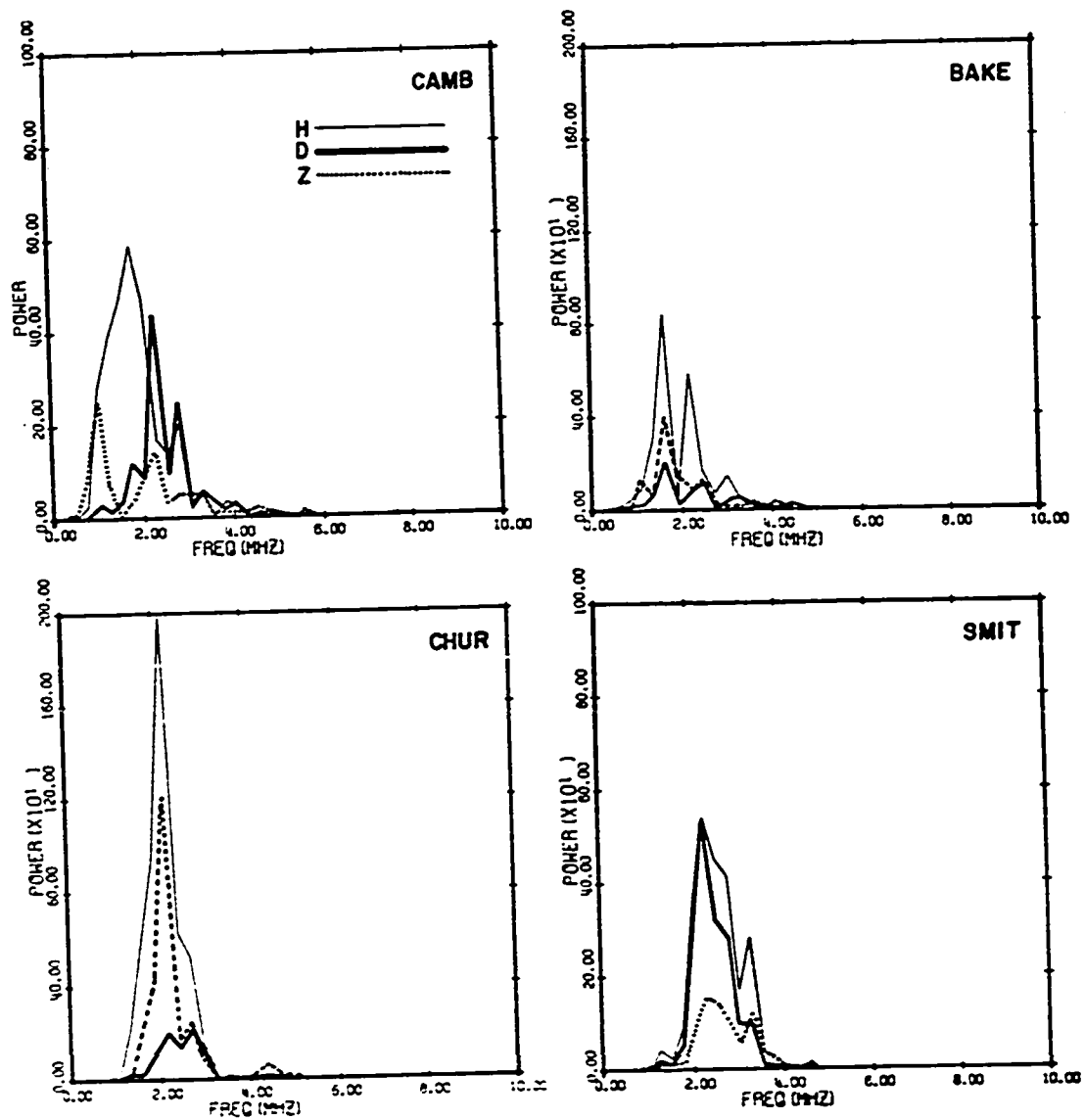
Fig. 52. Power spectra of the 3 magnetic components at our stations and at Baker Lake and Churchill. The spectra were calculated from data recorded in the interval 1500-1600 UT (day 186). The records were detrended with a 1-20 mHz filter. The power is in units of γ^2 sec.
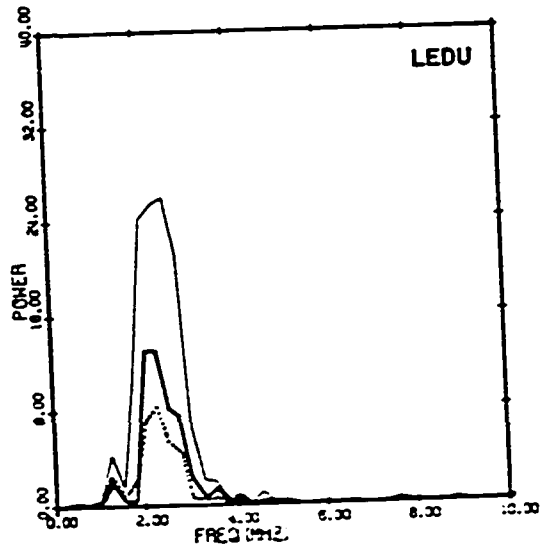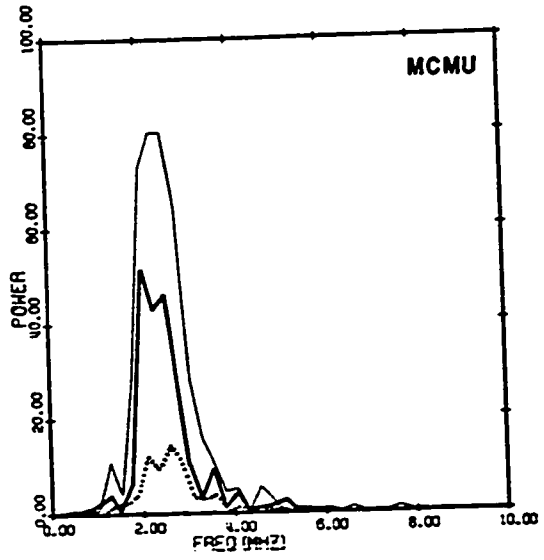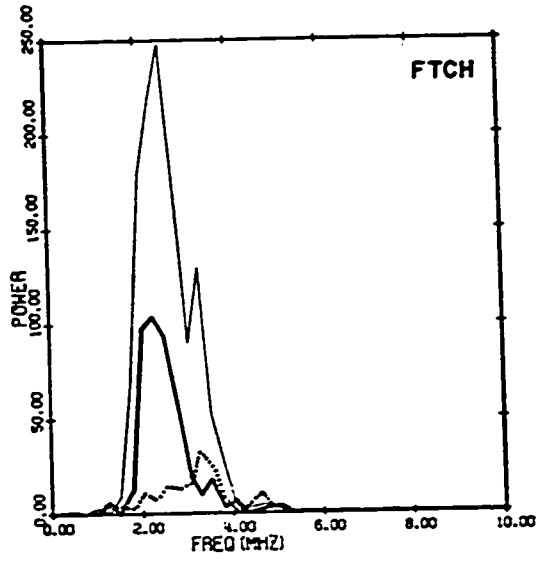
is situated near Hudson Bay. An indication of a second
large spectral peak is evident near 3.0 mHz at Churchill,
SMIT, and FTCH. At CAMB and Baker Lake at least three
spectral peaks are evident. These peaks are at ∿ 1.5 mHz,
2.1 mHz, and 3.0 mHz with the low frequency peak most
dominant at both CAMB and Baker Lake. Micropulsations
at CAMB have the most complex spectra and the least power,
with two distinct peaks in the D component and one broad
low frequency peak in the H component. Based on the
spectra from our stations and these two observatories,
there appears to be a dividing line separating a southern
region with sinusoidal pulsation trains from a northern
region with complex wave forms and spectra. This line
must be somewhere near 72°N with Baker Lake directly to
the north of the line and SMIT and Churchill directly to
the south. As we will see later, this line coincides with
the demarcation line.

The latitude-dependent characteristics of the
powers,phases, and polarization parameters, associated with
the 2 mHz Pc 5's are summarized in Figure 51. Data from
the observatories at Newport and Baker Lake have been
included in the plots since these observatories are situated
near 302° geomagnetic longitude. The powers in all three

components reach a sharp peak at SMIT (Figure 51A),
both the H and D components having comparable powers
at this station. To the north and south of SMIT the
D component power decreases the most rapidly of the
three. The ellipticities (Figure 51C) also show very
distinct latitudinal characteristics. The senses of
polarization in all three planes show distinct reversals
occurring between SMIT and Baker Lake. From SMIT south-
ward the micropulsations are polarized in a CC sense in
the H-D plane, agreeing with the statistical results
presented in Section 3.2. Most of the stations have
CW polarization in the H-Z plane. In the D-Z plane,
the polarizations are the same as those in the H-D
plane with stations from SMIT southward having CC polar-
ization and Baker Lake and CAMB having CW polarization.
The changes in the senses of polarization in the H-D
and H-Z planes are apparently caused by an abrupt 160°
phase change in the H component,occurring between CAMB
and SMIT (Figure 51B). This phase change is also evident
in the magnetograms of the micropulsations (Figure 43).

The worldwide distributions of the polarizations
in the H-D plane are summarized in Figure 53. Note that
in this figure the sizes of the polarization ellipses
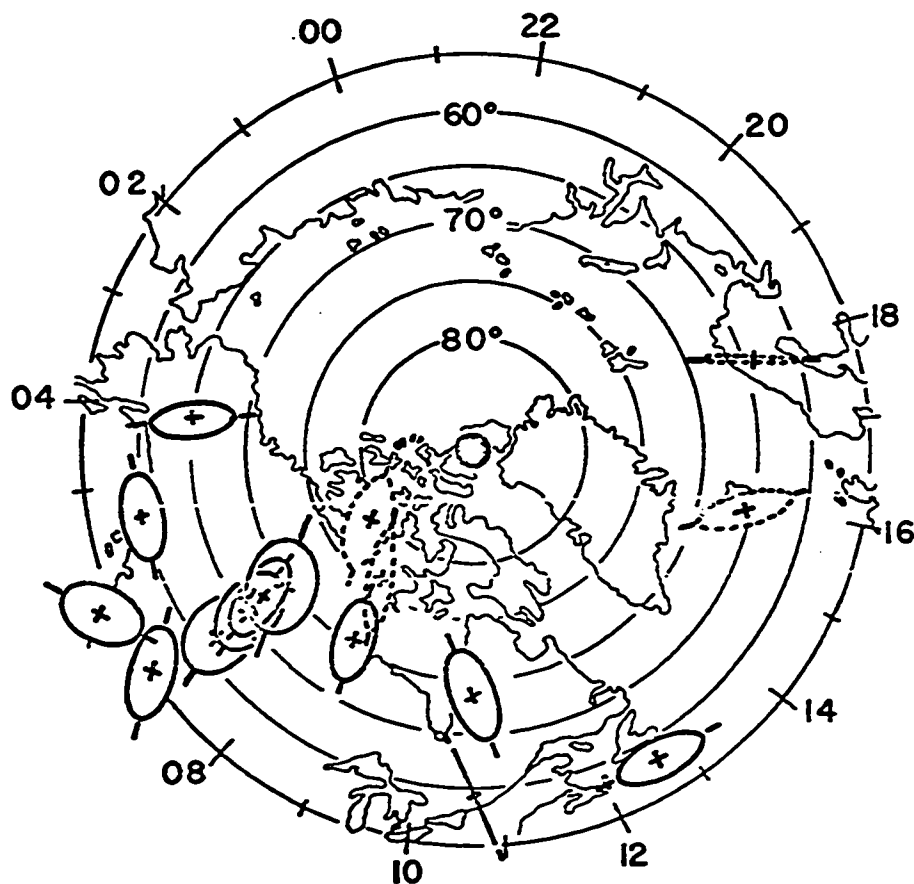
Fig. 53. A summary of the latitudinal and longitudinal H-D polarization characteristics of the 2 mHz micropulsations (day 186) plotted in local geomagnetic time. The times were determined by using the nomograph drawn by *Whalen* [1970]. The centre of each ellipse is at the position of the corresponding observatory or station. Ellipses with dotted lines indicate CW polarization and ellipses with solid lines indicate CC polarization.

are not scaled to the intensity of the pulsations at the stations. Comparison of Figure 39 with Figure 53 shows that the spatial distribution of the polarization parameters of this event agrees remarkably well with the statistical, diurnal variations obtained at our line of stations. The polarizations at the observatories on coastlines must be considered carefully, however, because of possible ocean induction effects (Appendix A7). There is certainly complete agreement between the statistical diurnal variations in the senses of polarization (Figure 39) and the data shown here (Figure 53). All the stations and observatories south of 72°N and west of 1300 LGT have CC polarization. Both Baker Lake and CAMB have CW polarization as expected and Leirvogur, which is east of 1300 LGT, has rather elongated but CW polarization. The polarization angles at all stations and observatories, with the exceptions of the coastal observatories at Sitka, Victoria, and St. John, are also consistent with those expected from the statistical, diurnal variations at our stations.

(d) Day 195 2200-2230 UT

This interval shows a preponderance of very high frequency Pc 4 micropulsations. Two spectral peaks are evident at most of the stations, one at 12.7 mHz, the other

at 20.3 mHz. The 20.3 mHz micropulsations have intensities less than $.2\gamma^2$ at CAMB, SMIT, FTCH, and MCMU and consequently the polarization parameters for these stations may be in considerable error. Figures 54A and 55A indicate that the H component-powers of both the 12.7 and 20.3 mHz micropulsations have sharp peaks at MENK. The 12.7 mHz pulsations also have a marked increase in power in the D component at CALG and in the power in the Z component at CAMB. The latitudinal characteristics of the ellipticities of these two micropulsation trains are complicated and do not show any obvious latitudinal reversals in sense. The micropulsations exhibit CW polarization in the H-D plane at the southern stations MCMU, MENK, LEDU, and CALG. Each micropulsation event has two abrupt latitudinal phase changes in the H component (Figure 54B, 55B). These changes occur at $\simeq 65°N$ and at $70-75°N$. The phase changes between SMIT and CAMB may not be meaningful since both events have low amplitudes and complex spectra at these latitudes.

(e) Day 262 1900-2000 UT

This interval is a complicated but interesting one. The activity here differs from most other micropulsation events in that the dominant frequency in the H component decreases with increasing latitude. There are at least four distinct frequency peaks in the H components, and each frequency is dominant in a narrow latitudinal range. This feature is evident even from a quick, visual inspection of the magnetograms
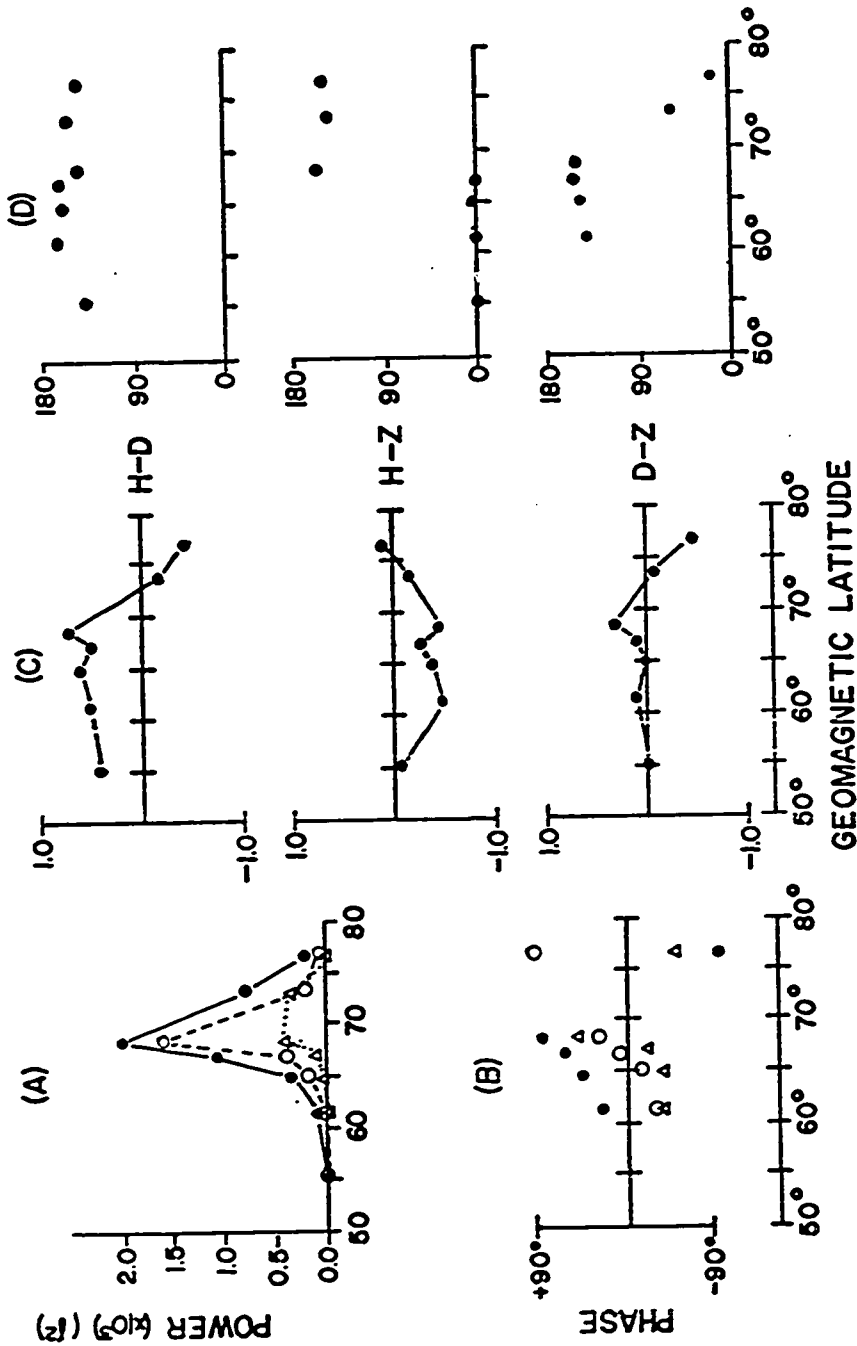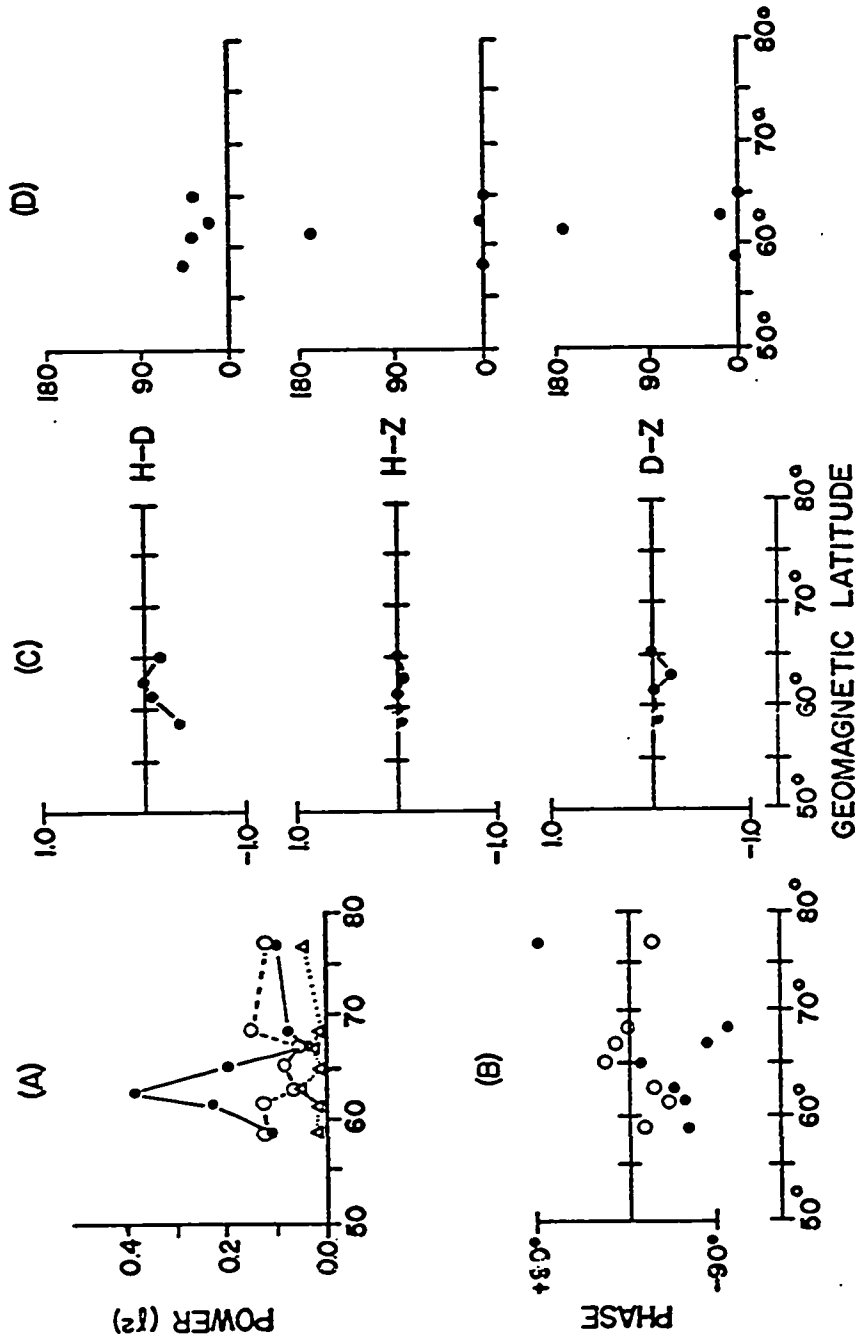
Fig. 54. Latitudinal plots of the spectral parameters of the 20.3 mHz micropulsations (day 195). The polarization angles and ellipticities of the micropulsations recorded at FTCH, SMIT and CAMB are not plotted because of the low amplitudes of the micro-pulsations at these stations.
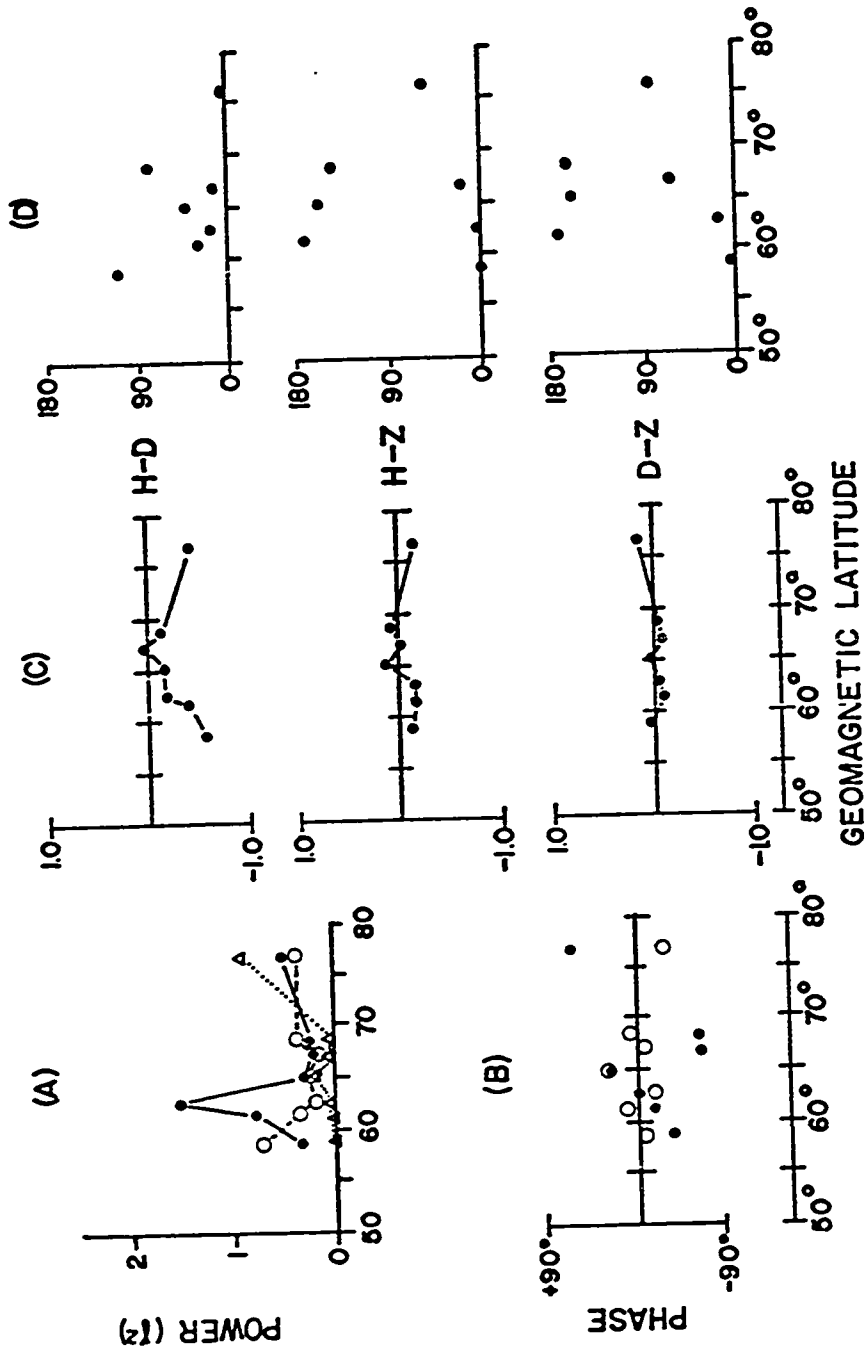
Fig. 55. Latitudinal plots of the spectral parameters of the 12.7 mHz micropulsations (day 195).

(Figure 45). This marked latitude-dependence of the H component frequency makes latitudinal plots of polarization parameters based on a spectral peak at one frequency rather meaningless. Consequently we will show no plots of the latitudinal polarization parameters, with the exception of those for a 1.0 - 1.3 mHz micropulsation train which is evident at all the stations. The power spectra from the 7 stations shows that there are 4 distinct spectral peaks in the H components (Figure 56). A 1.3 mHz peak predominates at CAMB (this peak does not show in the figures since the data were detrended using the 2.5-100 mHz filter), a 4.1 mHz peak predominates at SMIT and FTCH, a 6.6 mHz peak predominates at MCMU, and a 14.7 mHz peak predominates at MENK and LEDU. CALG does not have any distinct spectral peaks in the H component. These spectral peaks and the latitudinal ranges in which they are most dominant are plotted in Figure 57. There is obviously a distinct correlation in the latitude-dependence of these peaks and the statistical results derived from the intensity peaks (Figure 22). This observation is discussed in more detail in Section 4.1.

The Z components at MCMU, FTCH, SMIT, and CAMB have many of the characteristics of the H components, showing the same pronounced peaks and the same latitude-frequency dependence. In fact, at FTCH the 4.1 mHz power
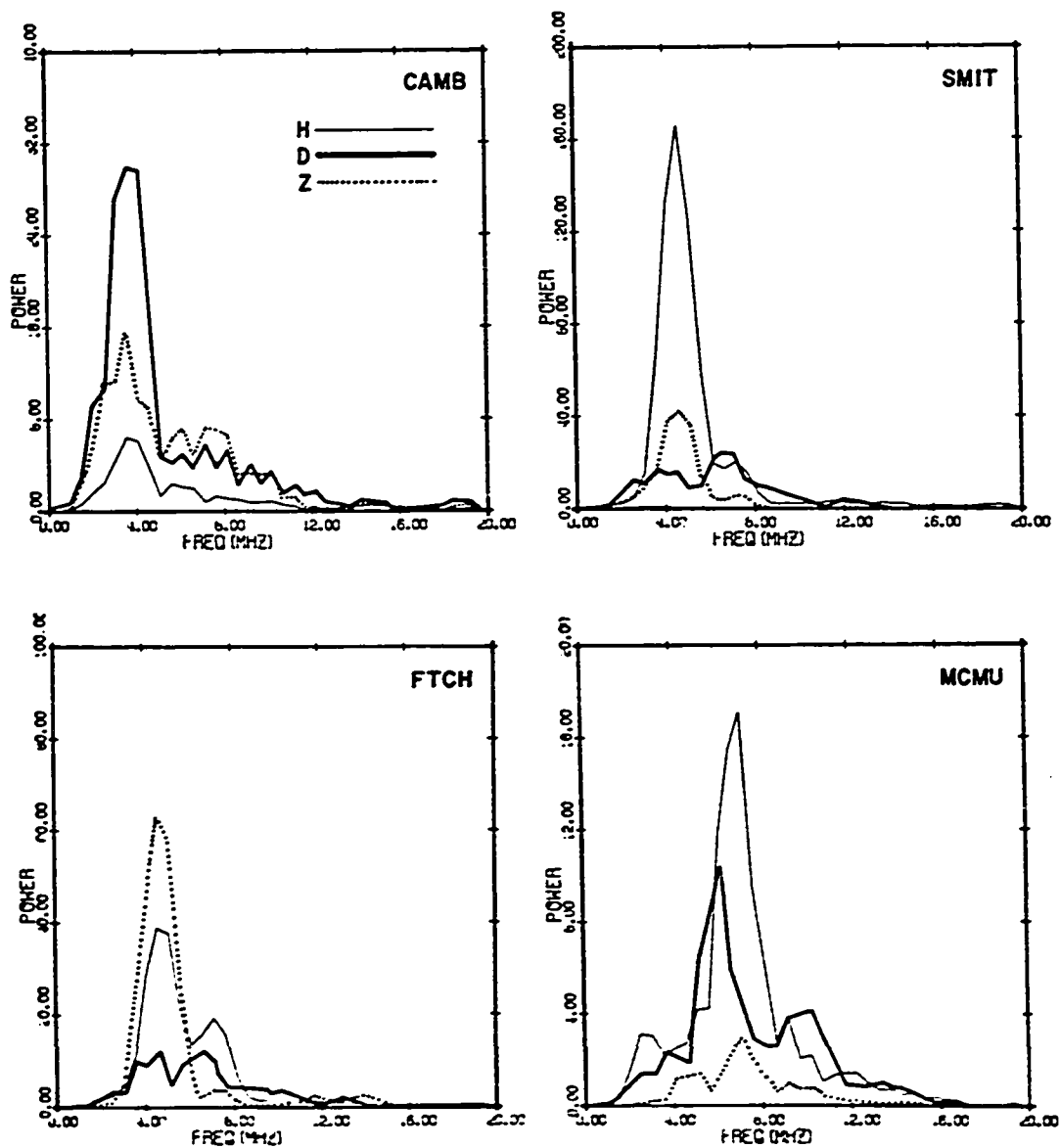
Fig. 56. Power spectra of the 3 magnetic components at the stations. The data are from the interval 1930-2000 UT (day 262) and the records were detrended with a 2.5 - 100 mHz filter. The power is in units of γ^2 sec. (continued on page 139).
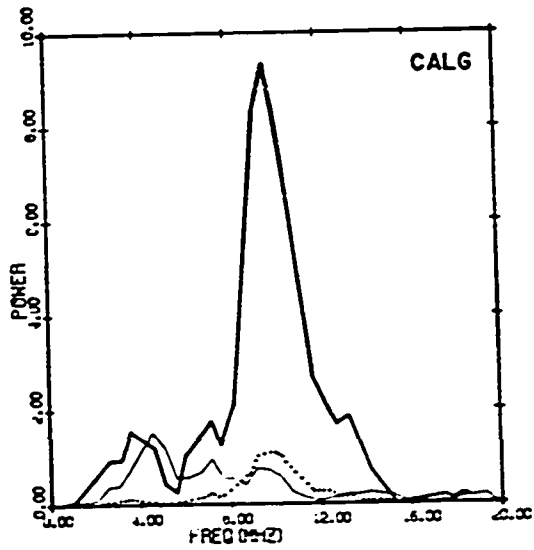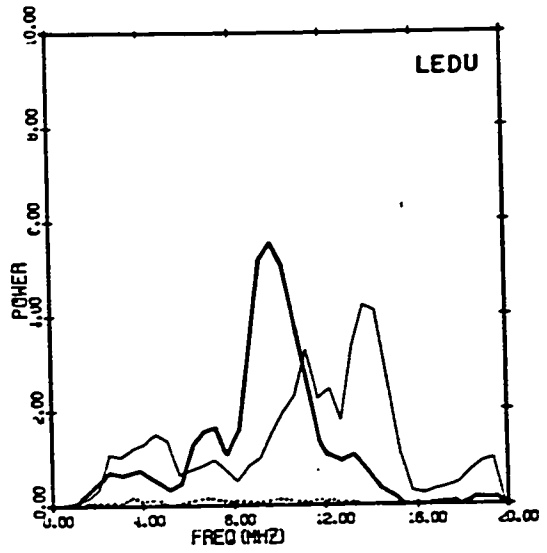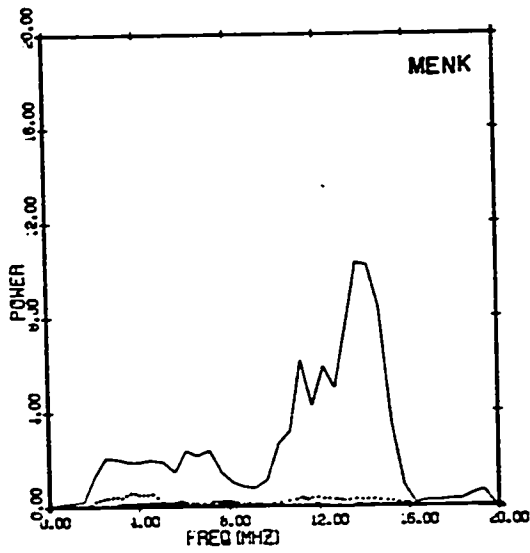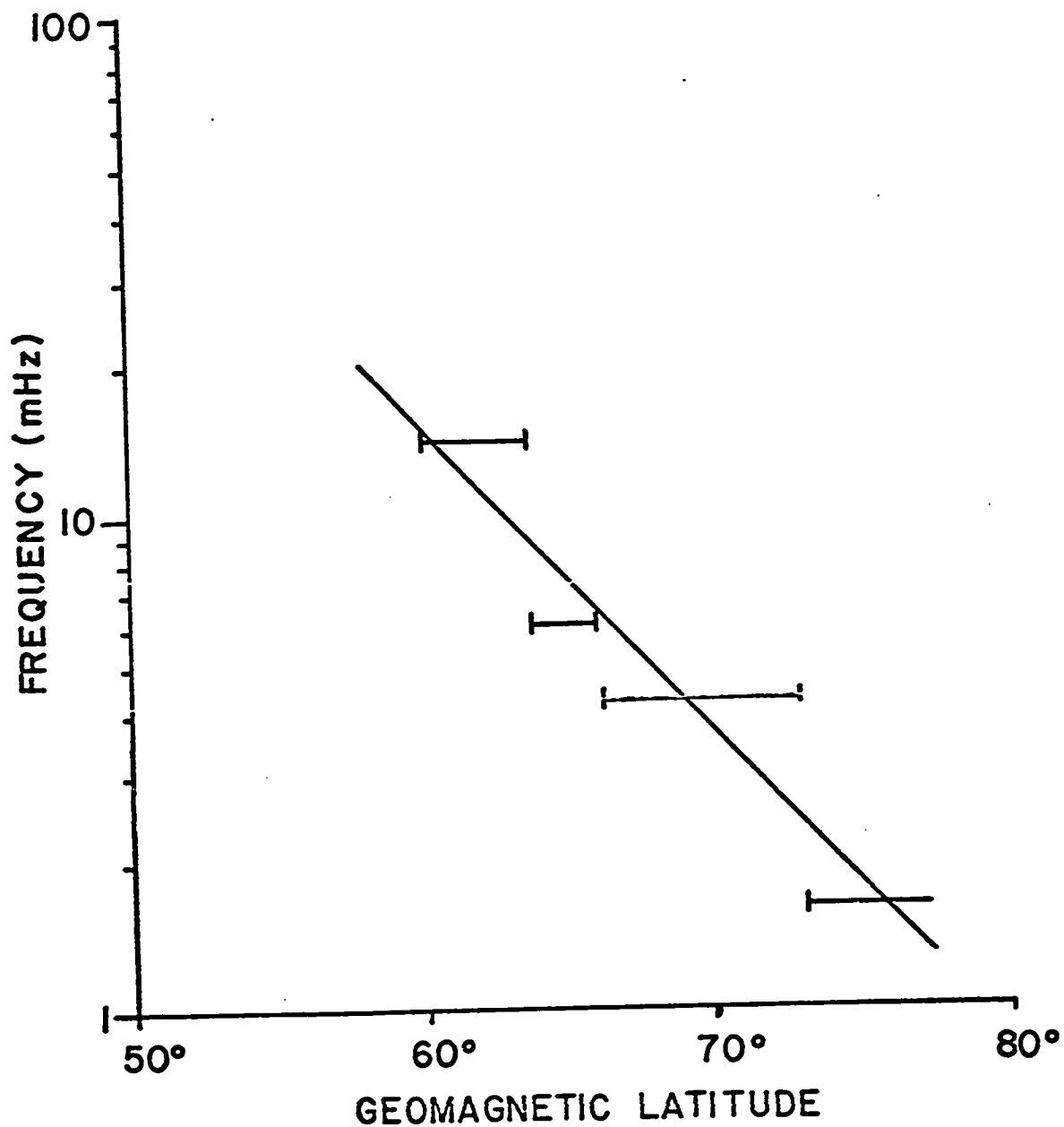
Fig. 57. Latitudinal ranges of the dominant peaks in the power spectra of the H components (Figure 56). The solid line shows the approximate trend of the intensity peaks plotted in Figure 22.

in the Z component far exceeds that in the H component. At MENK, LEDU and CALG however, the powers in the Z components are negligible. The power spectra of the D components differ completely from the other spectra. A single distinct peak shows at 9.6 mHz at CALG, LEDU, and MCMU. The behavior of the powers in the D components at the northern stations is somewhat more complex and no dominant spectral peaks show at FTCH and SMIT.

As already mentioned the 1.3 mHz spectral peak occurs at all stations. Latitudinal plots of the powers of the three components and the polarization parameters associated with this peak are shown in Figure 58. The powers in all three components increase monotonically with latitude to a maximum at CAMB (Figure 58A). The sense of polarization in the H-D plane (Figure 58C) is CW at CAMB and CC at all other stations. In the H-Z and H-D planes the senses of polarization are CW at all stations including CAMB. The apparent change in the sense of polarization in the H-D plane is caused by a gradual latitudinal change in the phase of the D component. The phase of the H component changes very little with latitude.
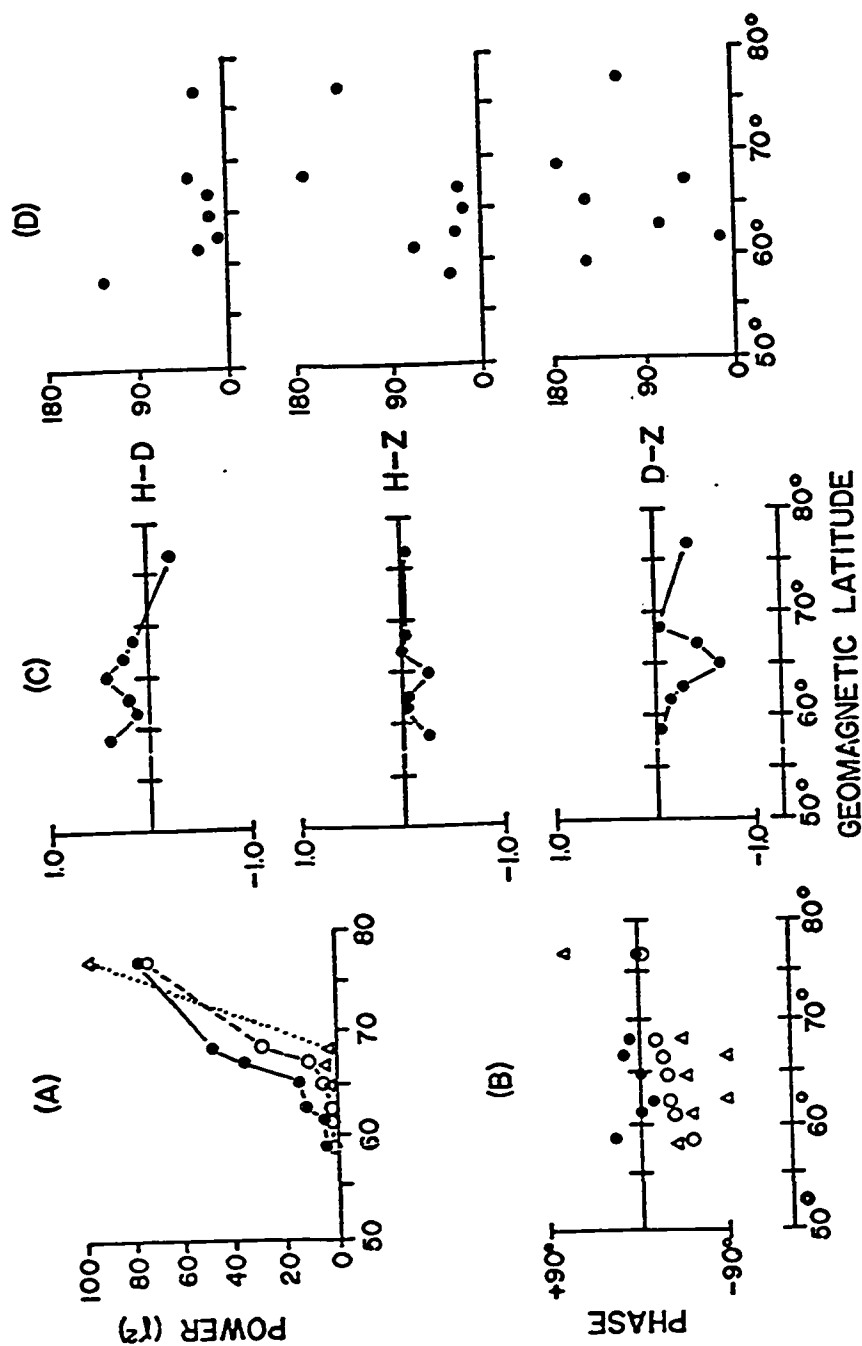
Fig. 58. Latitudinal plots of the spectral parameters of the
1.3 mHz micropulsations (day 262).

4. CONCLUSIONS

4.1 Discussion of the observations

The number and complexity of the parameters affecting geomagnetic micropulsations make it almost impossible to deduce a simple model which explains all the observed features of Pc 4's and Pc 5's. We can only hope to eliminate those theories which obviously conflict with the experimental data and perhaps select a few which show good qualitative agreement. The most promising source of energy for both Pc 4's and Pc 5's appears to be Kelvin-Helmholtz instabilities at the dawn and dusk sections of the magnetopause. Evidence exists to show that some of this energy is coupled into resonant oscillations of magnetic shells, although the simple toroidal mode discussed in Section 1.3 does not explain the apparent polarizations of the micropulsations. The existence of discrete Pc 4 and Pc 5 peaks in the geomagnetic spectrum is probably due to the preferential coupling of micropulsation energy into magnetic shells near the auroral oval and near the plasmapause. At present the spatial characteristics of the micropulsation fields are too poorly understood to explain with any accuracy the observed polarizations in the H-Z and D-Z planes.

In the discussion of micropulsation intensities in Section 3.2.1 we noted that the intensity maxima of Pc 5's follow the auroral oval (Figure 19). This observation is clarified in Figure 59 which shows a polar plot of the positions of the intensity maxima, together with the auroral oval and the average position of the plasmapause [*Carpenter*, 1966]. Except around local noon, the auroral oval and the zone of maximum intensity overlap. At local noon, however, the centre of activity has obviously moved north of 70°N and unfortunately we have no stations between 68°N and 77°N. Consequently the mismatch in the positions of the auroral oval and the activity centre may not be real. Another interesting feature is the proximity of the plasmapause to the auroral oval in the interval 2000-2200 LGT. This bulge in the plasmapause could considerably affect the propagation of the dayside micropulsation energy to the nightside of the earth. The bulge would certainly complicate any latitude-dependent characteristics of micropulsations occurring on the duskside of the earth.

Fairfield [1968] has shown that the dayside segment of the auroral oval maps along geomagnetic field lines to the magnetopause. In addition, *Frank* [1971] has shown that field lines at these high latitudes lie very close to the dayside polar cusp. Both these features indicate that the energy of low frequency Pc 5's might be derived from
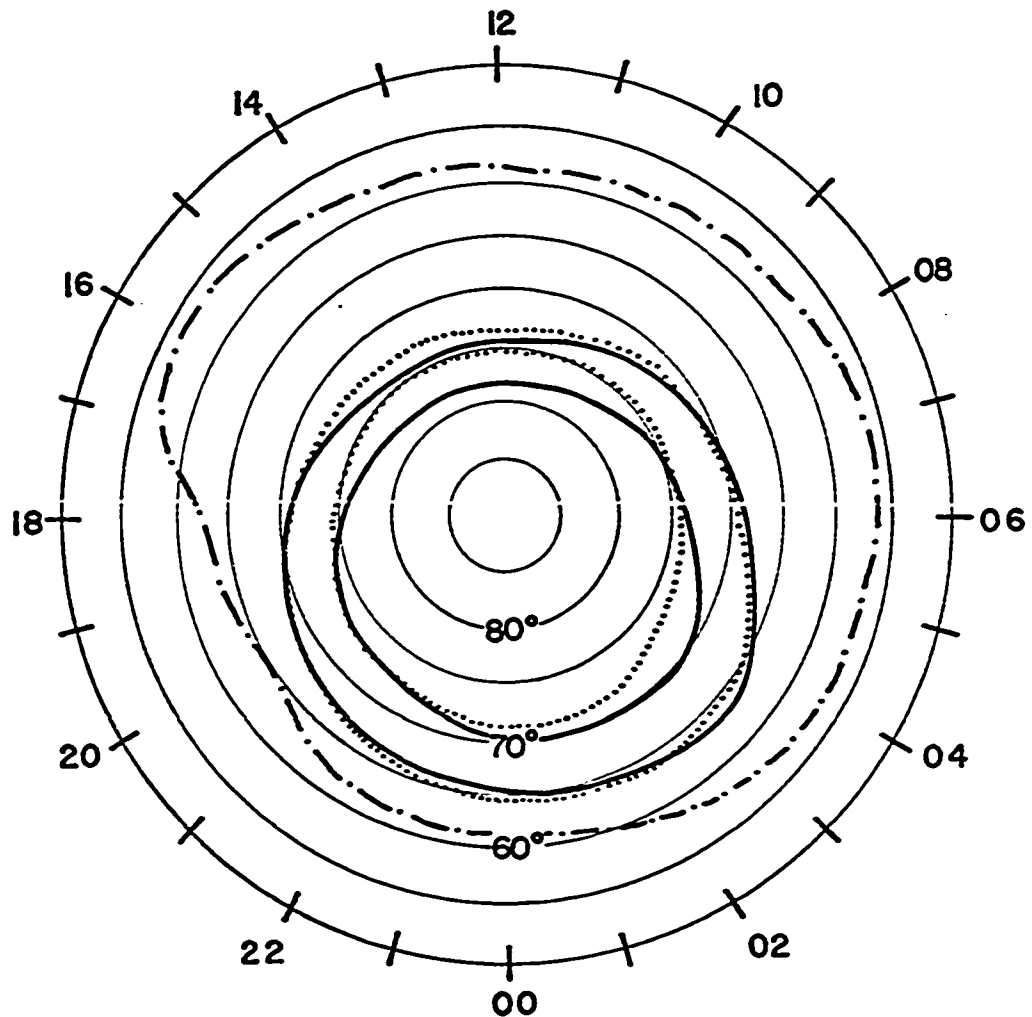
Fig. 59. Polar plots of the auroral oval (between dotted lines), the intensity maxima of Pc 5's (between solid lines), and the plasmapause (dashed line). The auroral oval corresponds to the oval deduced by *Feldstein* [1967] for periods with moderate activity (Q = 3). The circular grid lines show the corrected geomagnetic coordinates. The time scale is marked in hours of corrected geomagnetic local time.

an interaction of the solar wind with the earth's magneto-
sphere. We will show later that our polarization studies
suggest that this interaction sets up a Kelvin-Helmholtz
instability near the magnetopause, and that this energy
is guided along field lines to the earth's surface. If
the energy does indeed come from the solar wind, we still
have the problem of explaining why the centre of activity
follows the auroral oval on the evening side of the earth.
One possible explanation is that the micropulsation energy
is coupled into the "inner dipole" region of the geomagnetic
field and that this whole region oscillates in response to
the energy input on the dayside. Since the auroral oval
lies near the region of the transition from open to closed
field lines and the beginning of the plasma sheet [*Vasyliunas,*
1968], any micropulsation energy north of the auroral oval
on the nightside would not be expected. This is especially
true since the plasma sheet effectively absorbs micropul-
sation energy [*Barnes,* 1966; *Tamao,* 1968].

An alternative explanation for the micropulsation
energy in the nightside auroral oval is that the energy
originates in the magnetotail and reaches the earth by
propagating along field lines [*Rostoker,* 1967]. *Tamao* [1968]
and *Saito and Sakurai* [1970] suggested that this energy
might be derived from hm instabilities near the inner
boundary of the plasma sheet.

In the plots of intensity versus latitude (Figure 20) we noted that Pc 4's have proportionally greater intensities at low latitudes than Pc 5's. The lowest frequency Pc 5's (0-2 mHz) have maximum intensities near 75°N whereas Pc 4's (10-20 mHz) have maxima near 60°N. This frequency-dependent transfer of energy to lower latitudes suggests that at least some of the energy of the micropulsations is distributed in resonant oscillations of magnetic shells similar to the toroidal mode discussed in Section 1.3. Micropulsations at CAMB have considerable energy in all spectral bands, indicating once again that the field lines in this region are near the source of micropulsation energy.

The latitude-frequency dependence of the intensity peaks is shown better in the scatter plots of Figures 21 and 22. Both these figures show distinct latitude-frequency trends in the groupings of the intensity peaks. Figure 22 also shows a substantial cluster of peaks covering all frequencies from 1-20 mHz at latitudes above 75°. This high latitude cluster indicates once again that stations at these latitudes lie near the source of dayside micropulsation energy. This feature does not appear on the nightside plot (Figure 21) and most of the intensity peaks are south of 72°. The four Pc 4 peaks at CAMB (77°N) may

simply indicate energy input from the tail region and may not have any connection with micropulsations at lower latitudes.

The second feature evident on both plots is the latitude-frequency correlation of the intensity peaks south of 75°. This feature certainly indicates that micropulsation energy is distributed in resonant oscillations of magnetic shells. The frequency estimates in Figures 21 and 22 are higher than the fundamental toroidal eigenfrequencies calculated by *Dungey* [1954] for a normal dipole field in a constant density plasma ($\rho = 10^{-22} g \ cm^{-3}$), but agree better with the eigenfrequencies of a compressed dipole field in a cavity of radius $8 \ R_E$ with a plasma density of $6.5 \times 10^{-22} \ g \ cm^{-3}$ [*Westphal and Jacobs,* 1962].

At this point we might ask which component, if any, shows the most distinct and predictable latitudinal dependence in its intensity peaks. Actually the particular component seems to depend both on local time and the frequency of the given micropulsations. Both the H and D components of Pc 5's show strong latitudinal peaks in the morning, but normally the H component shows the most distinct latitudinal peaks in the afternoon (see for example Figures 48 and 51). Pc 4's on the other hand often show strong latitudinal peaks in the D component in the morning (see for example Figure 46).

These features certainly do not describe a simple toroidal oscillation. In addition, the limited longitudinal extent of most pulsations precludes the use of the toroidal equation for a description of the modes of oscillation. The asymmetric, guided poloidal mode is also not a good approximation since it predicts linear polarization in the H direction, and both Pc 4's and Pc 5's normally have elliptical polarizations in the H-D plane.

We might intuitively expect that since the symmetric toroidal mode is polarized in the D direction and the highly asymmetric poloidal mode is polarized in the H direction (at the earth's surface), more generalized modes of resonant oscillations of magnetic shells would be elliptically polarized in a plane perpendicular to the main field. *Cummings et al.* [1969] have reported micropulsations with this type of polarization in magnetic data from the satellite ATS 1. This satellite is in an equatorial orbit at 6.6 R_E situated on field lines which intercept the earth's surface at $\sim 67^O$N. The micropulsations detected by the satellite occupied two frequency ranges, one centred at 5.3 mHz and the other at 9.8 mHz. The frequencies of these spectral bands agree qualitatively with the frequencies of the micropulsations we find with intensity peaks at 67^ON.

Since the micropulsations observed at ATS 1 were transversly polarized we should perhaps consider the hm wave equations with the additional constraint

$$b_1 = 0$$

where b_1 is the perturbation magnetic field in the direction of the main field. *Cummings et al.* [1969] and *Namgaladze and Brunelli* [1970] have considered in some detail the resulting simplifications in the wave equation resulting from this constraint. The constrain $b_1 = 0$ (using the coordinate system introduced in Section 1.4) and Faraday's Law

$$\nabla \times \vec{E} = -\frac{1}{C} \frac{\partial \vec{B}}{\partial t}$$

indicate that

$$\frac{\partial}{\partial x_2}(h_3 E_3) - \frac{\partial}{\partial x_3}(h_2 E_2) = 0 \qquad (11)$$

Consequently equations (3) and (4) become

$$\frac{1}{h_3} \frac{\partial}{\partial S_1}\left[\frac{h_3}{h_2} \frac{\partial}{\partial S_1}(h_2 E_2)\right] = \frac{-\omega^2}{V_A^2} E_2 \qquad (12)$$

$$\frac{1}{h_2} \frac{\partial}{\partial S_1}\left[\frac{h_2}{h_3} \frac{\partial}{\partial S_1}(h_3 E_3)\right] = \frac{-\omega^2}{V_A^2} E_3 \qquad (13)$$

Equation (12) is equivalent to the equation for the toroidal mode: equation (13) describes the highly asymmetric or guided poloidal mode. Both these equations describe the resonant oscillations of magnetic shells and there are derivatives only along the field lines (i.e. $\frac{\partial}{\partial S_1}$). To solve these wave equations we must once again apply the boundary condition $E = \underline{0}$ at the earth's surface. We then find that the modes can exist only for certain discrete frequencies, and that in both cases the fundamental frequency decreases with increasing latitude. Cumming et al. determined, however, that the fundamental frequencies of E_2 and E_3 are different. Thus equation (11) can never be satisfied for the fundamental mode. This they construed as meaning that the fundamental mode cannot exist. They found, however, that all the higher harmonics of E_2 and E_3 have almost equal frequencies. In other words, if the harmonics of E_2 and E_3 are $^2\omega_i$ and $^3\omega_i$ respectively then

$$^2\omega_i \simeq {}^3\omega_i \qquad\qquad i \neq 1$$

If the plasma density in the plasma trough varies as r^{-4} and if the equatorial number densities are in the range 1-5 el/cm^3, then according to the calculations of

Cummings et al. the expected frequencies of the second harmonics occurring at 67° are in the range 17-38 mHz. These frequencies are much higher than we would expect from our data. For the frequencies to match those in our data the equatorial densities of electrons would have to be 10 - 30 el/cm^3. These densities are clearly much too high. In fact, the calculated frequencies of the fundamental modes compare best with our data.

Up to the present there has been considerable confusion regarding the possibility of a latitudinal dependence in the frequencies of micropulsations. Our analysis shows that with few exceptions a micropulsation train has the same frequency at all latitudes, although the latitude of the peak intensity tends to decrease with increasing frequency. The earlier work of *Ellis* [1960] and *Obertz and Raspopov* [1968] confirm these observations. Conversely, many researchers have found, through statistical analysis, that the average frequency of micropulsations decreases with increasing latitude. (Compare Figure 3 with our data in Figure 22.) These statistical results do not necessarily contradict our observations since those events which have a frequency equivalent to the resonant frequency of a given magnetic shell would typically have thier greatest amplitudes at the latitude

of that shell. Averaged over many events the larger
amplitudes at this resonant frequency would tend to give
more weight to events with this frequency. Since the
resonant frequencies of the magnetic shells decrease with
increasing latitude, a latitude-dependence in the average
frequencies of the micropulsations would be evident.

In special cases, when considerable broad band
energy is introduced into the magnetosphere (e.g. a sudden
impulse), there might be a pronounced latitudinal depen-
dence in the frequency of a given micropulsation event.
For example, suppose the input energy has spectral peaks
at 3 distinct frequencies f_1, f_2, and f_3 (Figure 60). This
energy is coupled into resonant oscillations of magnetic
shells with energy of frequency f_3 at the lowest latitude
and f_1 at the highest. Consequently micropulsations in
region c (Figure 61) have an apparent frequency f_1, in
region b they have an apparent frequency f_2, and in
region a an apparent frequency f_3. Thus there is an
evident decrease in frequency with increasing latitude.

In reality the situation is more complex since
the spectral peaks of the input energy are controlled not
only by the source mechanism, but also by the size and
shape of the magnetosphere. The boundary at the outside
of the magnetosphere forces the whole magnetosphere to
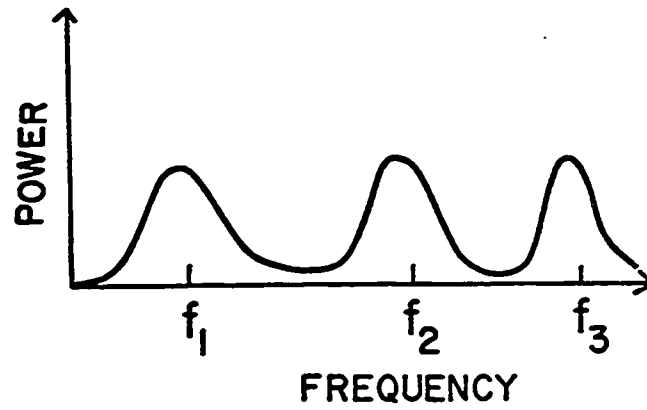
Fig. 60. An example power spectrum of a broad band source of micropulsation energy.
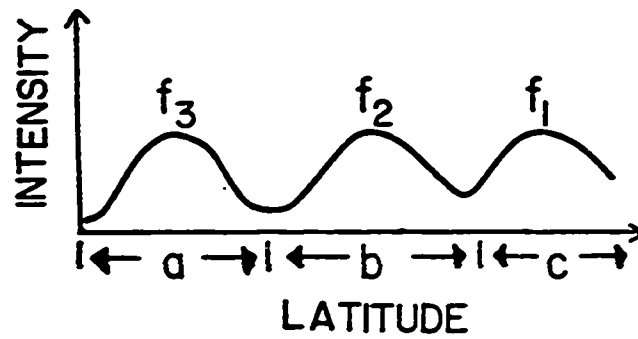
Fig. 61. The latitudinal distribution of the energy and frequency of the micropulsations.

oscillate at preferred frequencies. In an axisymmetric magnetosphere the modes of oscillation would be very similar to the simple poloidal mode [*Kato and Akasofu*, 1955; *Jacobs and Westphal*, 1964; *Carovillano et al.*, 1966]. This poloidal energy is coupled into resonant magnetic shell oscillations with the lowest frequencies near the auroral oval.

The event occurring on day 262 shows a distinct latitudinal dependence in the frequency of the H component and may, according to the above discussion, be caused by a broad band energy source. This event is similar to the micropulsations for which *Voelker* [1968] found latitude-dependent frequencies in the H components. In fact the latitude-frequency dependence found by Voelker compares remarkably well with our data (Figure 57). Since these events have a pronounced latitude-frequency dependence only in the H component, they could be manifestations of the guided poloidal mode. Equation (13) describes the perturbation electric field for this mode. Cummings et al., in determining the resonant frequencies of this mode, have shown that the harmonics have the same frequencies as the harmonics of the toroidal mode. Even the fundamental frequency of the guided poloidal mode is not too different from that of the toroidal mode (e.g. 17 and 12 mHz respec-

tively at 67°N for a r^{-4} distribution of the density of electrons). Consequently we would expect the guided poloidal mode to show essentially the same latitude-frequency dependence as the toroidal mode.

Siebert [1964] proposed another explanation for the latitude-dependent frequencies in the H components of some micropulsations. He postulated that latitudinal changes in frequencies are a result of field-aligned hm oscillations in the magnetosphere. For these oscillations to occur, the magnetospheric plasma density must have a lamellar structure, with the density changing continuously along geomagnetic field lines and changing abruptly in directions perpendicular to the field lines.

In any case, the energy for the latitude-dependent oscillations probably comes from a sudden compression of the dayside magnetosphere by the solar wind. Voelker has shown that SSC's and Si's associated with pulsations with latitude-dependent frequencies occur near local noon (as does our event), thus giving additional support to the compressional model.

If the energy of Pc 4 and Pc 5 micropulsations originates on field lines in the auroral oval and is coupled into resonant magnetic shell oscillations at lower latitudes, it is difficult to see why there should be distinct Pc 4

and Pc 5 classifications. *Saito* [1964] and *Campbell* [1967] have shown, however, that there is a natural division of the average geomagnetic spectrum into Pc 4 and Pc 5 bands. Both these authors have computed spectra which show substantial peaks in both the Pc 4 and Pc 5 bands. In addition, inspection of Figure 22 shows that in our data there is an obvious concentration of micropulsations in the Pc 4 band, most of the intensity peaks being south of 65°.

The division of the geomagnetic spectrum into Pc 4's and Pc 5's possibly indicates that these micropulsations have different sources of energy. Pc 4's, for example, might derive their energy from a bounce resonance interaction of particles and waves (Section 1.3), whereas most Pc 5's derive their energy from instabilities at the magnetopause. The sinusoidal appearance and long wave trains of many Pc 4's make the bounce resonance theory particularly appealing [*Dungey and Southwood,* 1970]. On the other hand Pc 4's and Pc 5's often obey the same diurnal polarization rules (see for example Figure 24 and *Rankin and Kurtz* [1970])suggesting that they have the same energy sources.

The formation of distinct Pc 4 and Pc 5 spectral peaks might also result from the preferential coupling of energy into given magnetic shells, say at the plasmapause

and near the auroral oval. *Hirasawa and Nagata* [1966]
proposed that Pc 4's are caused by a strong coupling of
energy into resonant oscillations of magnetic shells near
the plasmapause. *Tamao* [1968, 1969] suggested that a
trough in the spatial distribution of the Alfvén velocity
serves as a trapping region for hm waves. Such a trough
exists just inside the plasmapause [*Dungey*, 1967] and we
might expect a large number of micropulsations with
frequencies equivalent to the resonant magnetic shell
frequencies in this region (∿ 10-20 mHz).

Figure 62 summarizes the diurnal polarization
characteristics of Pc 5's in the H-D plane and should be
compared with Figure 39. Figure 62 shows the polarization
characteristics of micropulsations with mean frequencies
near 5 mHz. The features of the diagram must be moved
to the south for micropulsations with higher frequencies
and to the north for lower frequencies. Actually the
diagram is probably a good indicator of the characteristics
of polarizations of Pc 4's as well. The vertical line at
2000-2100 (∿ 1130-1230 LGT) marks the temporal reversal
noted simultaneously at all our stations [*Samson et al.*,
1971]. This reversal also shows in the data of *Kato and
Utsumi* [1964]. A second reversal at approximately 0300-
0400 (1830-1930 LGT) is at the edge of the diagram.
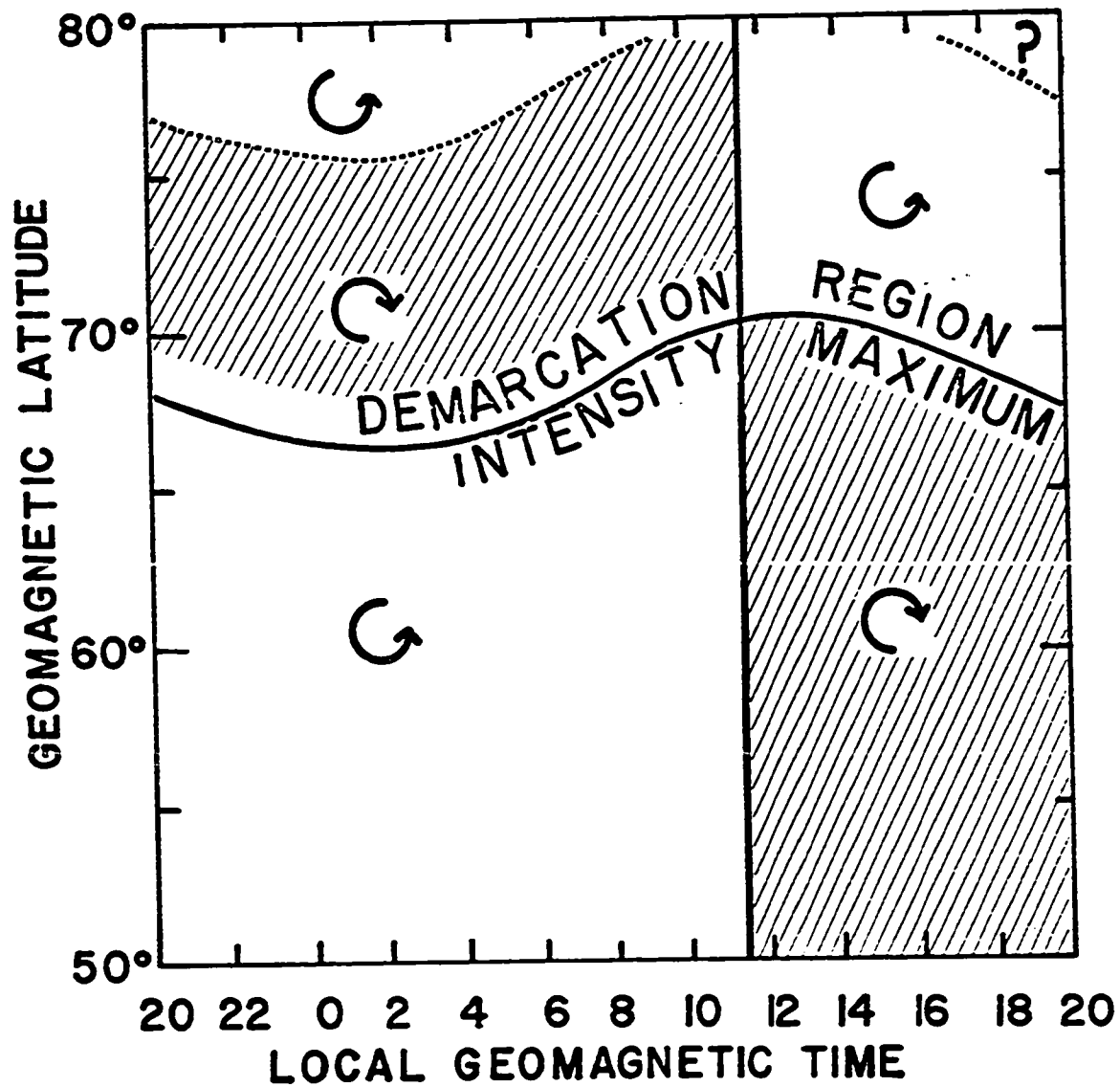
Fig. 62. The latitudinal and diurnal variations of the H-D polarizations of 5 mHz Pc 5's.

The short period (7-8 hr) of CW polarization occurring at the southern stations in the afternoon suggests that the day be divided into 3 sectors: late morning (0700-1200 LGT), afternoon (1200-1900 LGT) and night (1900-0700 LGT). The nightside and morning sectors have the same polarization configurations but different energy outputs. Impulsive Pi micropulsations dominate much of the activity in the nightside whereas continuous Pc micropulsations dominate most of the activity in the morning.

A plausible explanation of the polarization reversal at 1130-1230 LGT is that the energy of daytime micropulsations originates from a Kelvin-Helmholtz instability at the magnetopause [Atkinson and Watanabe, 1966; see also Section 1.3]. The sense of polarization of Pc 5's occurring at stations south of CAMB is CC in the morning and CW in the afternoon in agreement with the sense predicted by this theory. The large input of energy at all frequencies on the dayside auroral oval (see Figure 22) gives further support to this theory. Unfortunately this model does not explain the latitudinal change in the sense of polarization.

The demarcation line lies in the curved region above the line of maximum intensity. (The demarcation line has been labeled demarcation region in Figure 62 because of the inaccuracy in determining the position of this line with respect to the latitude of the maximum intensity.) The second line (dotted curve) at high latitudes is necessary since certain

times exist during the evening when Pc 5's at all our stations, including CAMB, have the same sense of polarization in the H-D plane. Unfortunately the two northernmost stations are 9° apart and the region of reversed polarization (directly above the demarcation line) is sometimes not evident in the evening data.

At first we may be tempted to associate the polarization demarcation line with the position of the auroral oval, especially since most low frequency Pc 5's have their maximum intensities and their demarcation lines in this region. This feature does not always appear to be the case, though, since there is a close correlation between the frequency of a micropulsation train and the latitude of its demarcation line (Figure 34). Many Pc 4's have demarcation lines well south of the auroral oval (see for example Figure 46), although in general Pc 4's have rather complex latitudinal polarization characteristics. Clearly more stations are needed in the region between 68°N and 77°N in order to compare the latitudes of the demarcation lines of Pc 5's with their intensity centres and the auroral oval.

The station-to-station phase comparisons indicate that abrupt, latitudinal phase changes in either the H or D component may be more useful than polarization reversals in determining the position of the demarcation line. In

some cases the relative latitudinal phase changes in these components are very large but not large enough to cause a change in the sense of polarization.

As mentioned in Section 3.2.2 there is a strong diurnal variation in the frequencies of micropulsations with demarcation lines at a given station (see for example Figure 33). Figure 63 is a composite of diurnal polarization data from SMIT and FTCH and shows the sense of polarization as a function of time and frequency. The dotted line indicates the frequencies of micropulsations with demarcation lines near these stations (we shall call this the demarcation frequency). This frequency is as low as 4 mHz in the interval 1000-1200 rising to a maximum of 14 mHz from 1800 to 0400. Evidently the diurnal variation in the demarcation frequency is closely associated with the latitudinal motion of the auroral oval. At our stations the oval is furthest south between 0800-1200 (2330-0330 LGT) and moves quickly northward at approximately 1500-1700 (0630-0830 LGT) (see Figure 59). Although not evident in our data a diurnal trend in the demarcation frequency is apparent in micropulsations recorded at LEDU [*Kurtz*, 1969]. (The frequency-dependent reversal is not noticeable in our data since our system cannot detect many micropulsations with
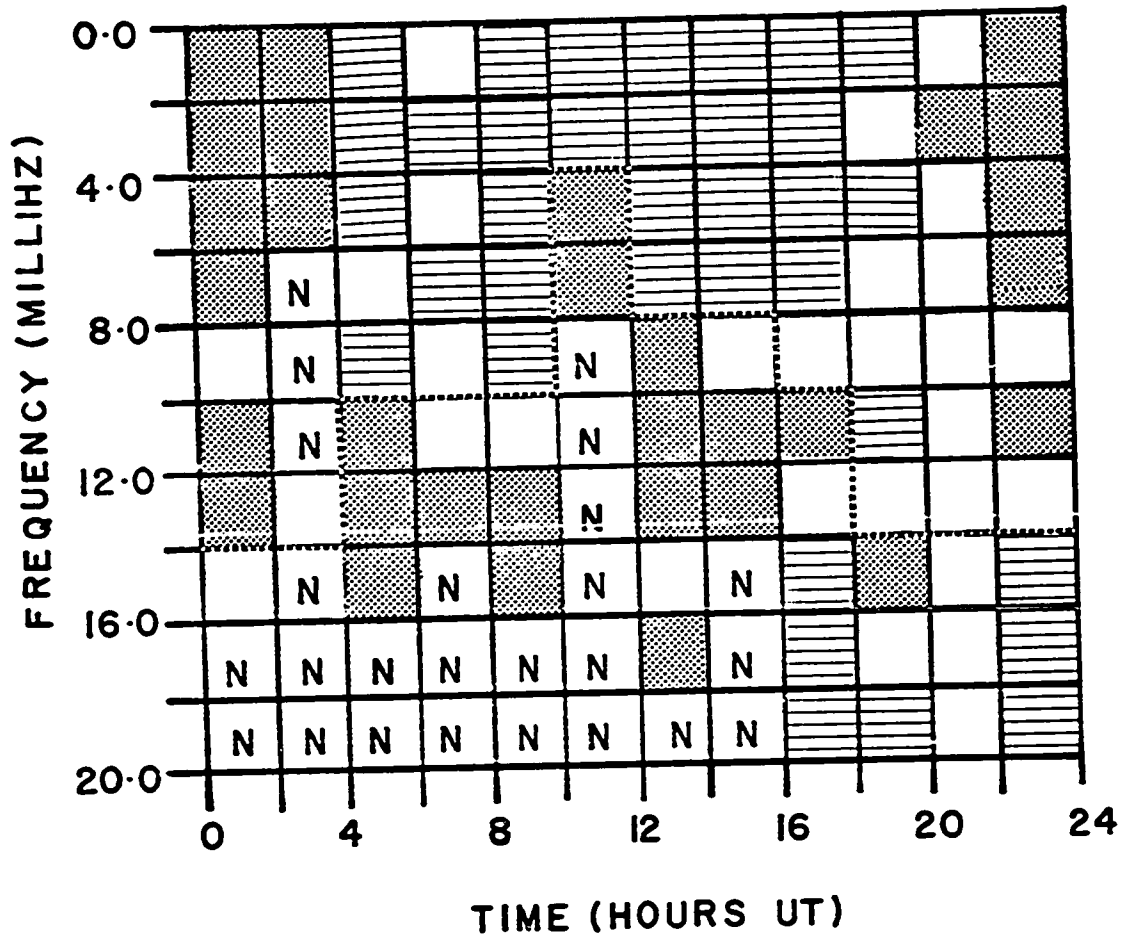
Fig. 63. The frequency-dependent and time-dependent changes of the H-D ellipticities of micropulsations recorded at FTCH and SMIT. In the dotted regions, the ellipticities are less than -0.1 and in the lined regions, the ellipticities are greater than +0.1. The demarcation frequency is indicated by the dotted line. Spaces with an N have no data.

frequencies greater than 20 mHz). Figure 64 shows a comparison of the diurnal variations of the demarcation frequencies at LEDU and at SMIT, FTCH. Evidently the demarcation frequency at LEDU is much higher than that at SMIT and FTCH. The difference in the demarcation frequencies would be expected if the latitudes of the demarcation line were associated with the intensity peaks. Since many Pc 4's have intensity peaks near and south of LEDU, we could expect that LEDU would show ellipticity reversals in the Pc 4 spectral band whereas SMIT and FTCH would show reversals in the Pc 5 band. The diurnal variation of the demarcation frequency at LEDU also does not have the same shape as that at SMIT and FTCH. This might be a result of the close proximity of LEDU to field lines following the plasmapause (from 1800-0100 LGT, LEDU is actually south of the expected position of the plasmapause).

The dotted line in Figure 64 shows the high frequency limit of the two spectral bands noted by *Hirasawa and Nagata* [1966] and *Nagata and Fukunishi* [1968] in their analysis of micropulsation data from Kakioka ($36^\circ N$) (see Section 1.2). They attributed the spectral band centred at 15 mHz to eigenoscillations of magnetic shells near the plasmapause since the diurnal variation in the mean frequency of the band followed the diurnal variation in the latitude
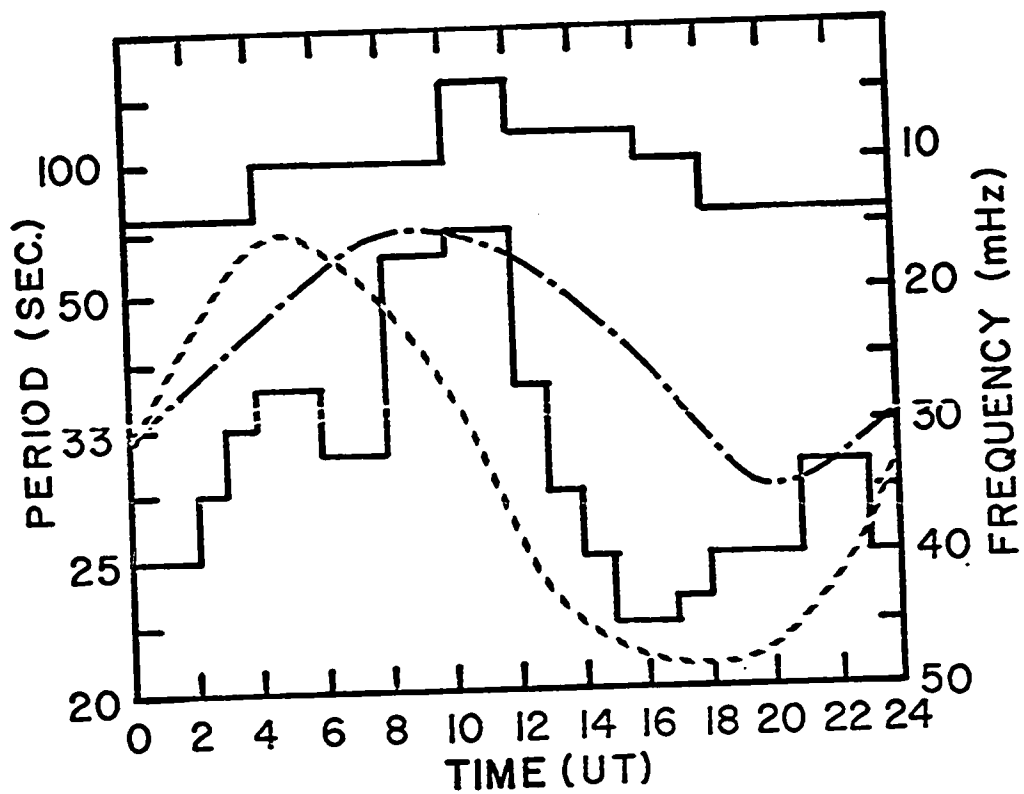
Fig. 64. The diurnal variation of the demarcation frequency at SMIT and FTCH (upper solid curve) and at LEDU (lower solid curve). The dashed line shows the high frequency limit of the two spectral bands noted by *Nagata and Fukunishi* [1968] during periods of low magnetic activity ($K_p \sim 0$-1) and the dotted line shows the upper limit during periods of moderate activity ($K_p \sim 2$-3).

of the plasmapause. On the other hand, they attributed the 30 mHz band to hm modes trapped between the plasmapause and the ionosphere. An obvious correlation exists between the demarcation frequency at LEDU and the two spectral bands noted by the above authors. It appears, then, that the ellipticity reversal at LEDU is related to the Pc 4 resonance near the plasmapause whereas the ellipticity reversal at SMIT and FTCH is related to the Pc 5 resonance in magnetic shells near the auroral oval.

The polarization demarcation line and the associated frequency-dependent senses of polarization now appear to be fundamental characteristics of magnetospheric modes of oscillation of Pc 4's and Pc 5's. *McClay* [1970], in solving the problem of coupled toroidal and poloidal modes of oscillation in a hm wedge, found that resonances appear on given magnetic shells and that the sense of polarization of the perturbations changes across the resonance region. The whole cavity oscillates at a given frequency and both toroidal and poloidal modes are evident throughout the cavity. The toroidal modes, however, have spatial resonances on given magnetic shells. The positions of these shells are determined by the eigenfrequencies appropriate to the shells. The polarizations derived from this model agree at least qualitatively with the latitude-dependent senses of polarization found in our data.

The diurnal variations of the polarization angles in the H-D plane, shown in Figures 36 and 39, indicate that the ellipses of Pc 5 micropulsations are oriented in the H direction throughout most of the day. It might be conjectured that this is an ionospheric effect, perhaps due to the latitudinal localization of the micropulsation field [*Inoue and Schaeffer*, 1970]. Satellite data indicate, however, that polarizations in the H direction are characteristic of the magnetospheric modes of propagation. Cummings et al. noted that sinusoidal micropulsations recorded at ATS 1 normally had much larger radial than azimuthal field components (see Figure 9). In their data the average orientation of the major axis was 30° east of the radial (outward) direction. *Patel* [1965] also noted a preference for greater amplitudes in the radial direction near local noon. He found, however, that the azimuthal component of the pulsations increased toward the dawn side of the magnetosphere. His observations agree with our data since we find elliptical polarization in the early morning with a preference for polarization in the D direction at SMIT and FTCH in the interval 1600-2000 (0730-1130 LGT). (See also *Samson et al.* [1971].)

In addition to being the time of the most circular polarizations, the early morning also has the greatest occurrence frequency of Pc 5 micropulsations (see Section 3.2.2). Field lines which intersect the earth's surface in the early morning sector are swept back from the sun and meet the magnetopause at a position where the solar wind flows tangentially [*Fairfield*, 1968]. Since the magnetopause is most susceptible to a Kelvin-Helmholtz instability in this region [*Southwood*, 1968], we would expect most of the micropulsation energy and most circular polarizations in this region.

If the energy for daytime Pc 4 and Pc 5 micropulsations originates from a Kelvin-Helmholtz instability at the magnetopause, it is difficult to explain the apparent difference between micropulsation activity occurring in the morning and in the evening. The morning sector usually has the greatest number of sinusoidal pulsations and has consistent, sometimes almost circular, CC polarization. The afternoon sector, on the other hand, usually shows very few sinusoidal pulsation trains, a mixture of polarization senses, and a predominance of almost linear polarization in the H direction. Intuitively we would expect that a Kelvin-Helmholtz instability would be equally probable in the morning and afternoon sectors of the magnetopause and

that this instability would produce micropulsations with
equally elliptic polarizations but with opposite senses
in these two regions (see Figure 11). The actual asymmetry
in micropulsation activity might be caused by the attenu-
ation of the CC or right handed mode in the ionosphere or
magnetosphere [*Field and Greifinger*, 1965; *Inoue and Schaeffer*,
1970]. Cummings et al. found, however, that most of their
events occurred before 1200 LMT, in agreement with ground-
based observations of the occurrence frequency. Further
comparisons of satellite and ground-based data should
clarify this point.

One other possible cause of the asymmetry in
micropulsation characteristics is the dawn-dusk asymmetry
in the plasma sheet [*Vasyliunas*, 1968b]. The plasma sheet
is well defined near the dusk magnetopause whereas in the
morning sector plasma densities change continuously from
the plasmatrough to the magnetopause. A sharp discontinuity
in the density of the plasma might result in considerable
absorption of micropulsation energy in the evening sector.

The Z components of micropulsations observed on
the ground are undoubtedly due to spatial gradients in the
currents induced in the ionosphere by hm waves. It is
illuminating to consider current systems compatible with
the H and D components recorded on the ground and to compare

the predicted Z variations and polarizations with those we have observed experimentally. *Wilson* [1966] used a rotating line current as a model for the current systems induced in the ionosphere by hm waves. In most cases this model does not explain our observations, especially the variation in the sense of polarization in the H-D plane with latitude. This model also does not predict a large Z component at the latitude of the maximum in the intensity of the horizontal components, which we often find to be the case in our data (see for example Figures 47, 50, 53). *Eleman* [1966] also noted this discrepancy between Wilson's model and the intensities of the Z component.

The large latitudinal phase shift occurring in the two horizontal components is indicative of a rather strong shear flow in ionospheric currents. Since the phase shift is usually most noticeable in the H component [*Kaneda et al.* 1964; *Obertz and Raspopov*, 1968], especially during morning Pc 5 activity (see for example Figure 51), the shear must occur during that part of the pulsation cycle with strong east-west currents. This shear is evident in the equivalent current system for Pc 5's given by *Jacobs and Sinno* [1960]. Normally, however, the current patterns must change during the pulsation cycle in order to produce the elliptical polarizations observed at the earth's surface.

Consider now a micropulsation event with nearly circular polarization in the H-D plane. The latitudinal dependence of the phases and powers are shown in Figure 65. (Compare Figure 65 with Figures 51B, 55B.) Since there is a very rapid latitudinal phase change in the H component we would expect an equivalent current system similar to that shown in Figures 66 and 67. The moving current vortices proposed by Obertz and Raspopov could possibly cause the changes in direction of the current flow shown in Figure 66. However, it is not easy to see how their current vortices could produce sinusoidal oscillations. We will call the region of shear flow the demarcation line because of its association with the polarization reversal. Directly to the south of the demarcation line the Z component is 180° out of phase with the H component (Figure 67) and directly to the north of the demarcation line the Z component is in phase with the H component. The maximum amplitude of the Z component occurs very close to the demarcation line. Thus we expect linear polarization in the H-Z plane with the value of the polarization angle depending on whether the station is to the north or south of the demarcation line.

172
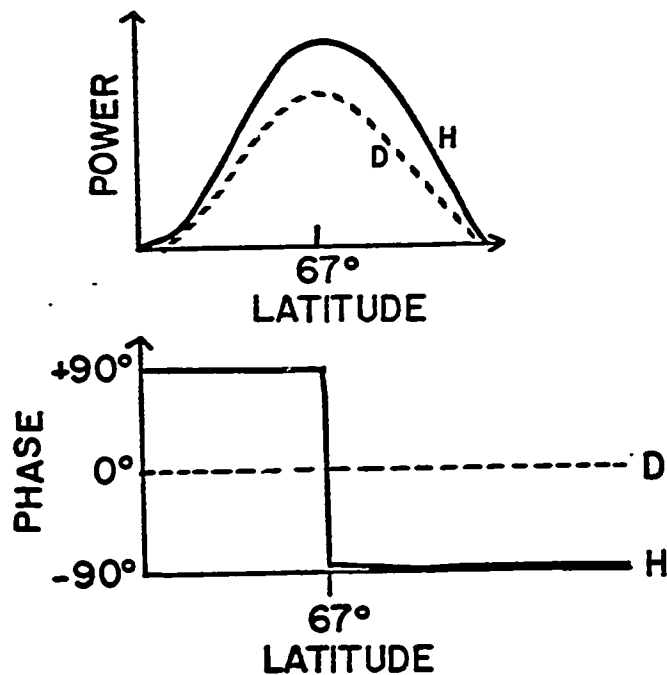
Fig. 65. Latitudinal plots of the powers and phases of the H and D components of a model micropulsation event.
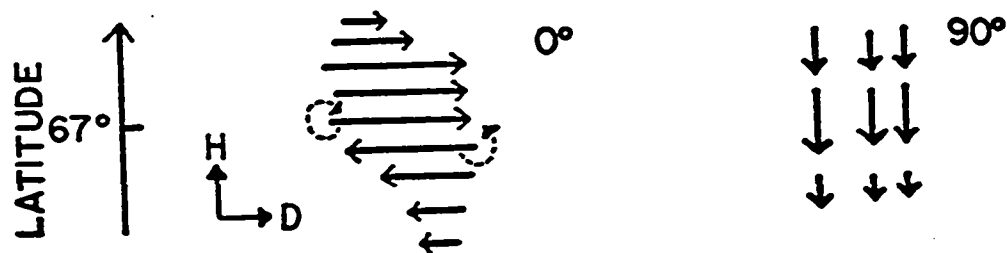
Fig. 66. The equivalent ionospheric currents of the model micropulsation event (viewed from above). This diagram shows the equivalent currents during two parts of the cycle which are 90° apart. The dotted circles show the direction of the rotation of the current vectors.
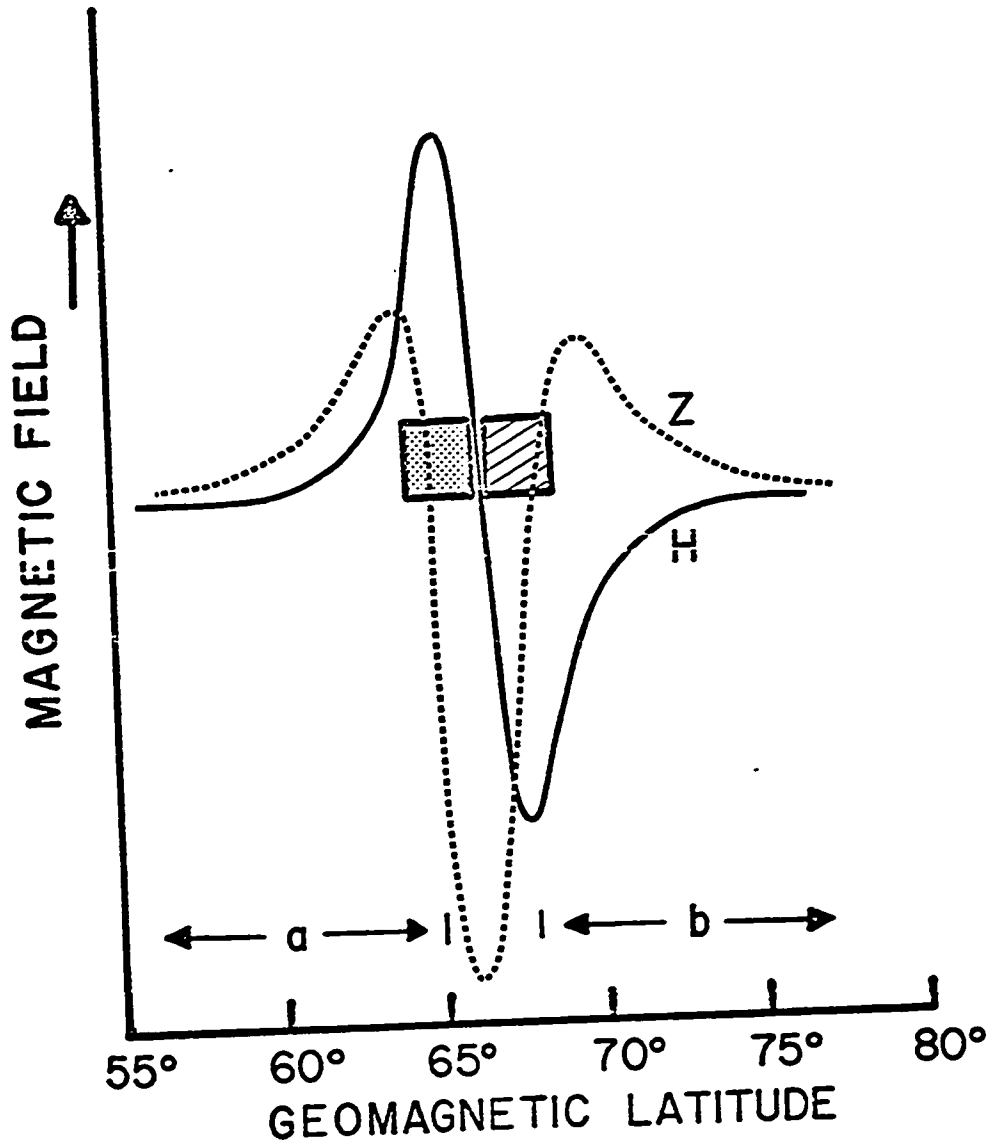
Fig. 67. The magnetic perturbations of the H and Z components of equivalent currents flowing to the west (dotted region) and to the east (lined region) in the ionosphere. This figure corresponds to the 0° equivalent current system shown in Figure 66.

Further south of the demarcation line, the Z component is again in phase with the H component (region a Figure 67). In this region the polarizations in the D-Z plane should be opposite to those in the H-D plane. This is evident in Figure 30. All the stations which are far south of the centre of activity for Pc 5's (MCMU, MENK, LEDU, and CALG) have polarizations in the D-Z plane which are essentially opposite to those in the H-D plane. This observation is particularly evident if we consider the diurnal trends in the ellipticities. The ellipticities in the H-D plane have a U-shaped diurnal variation, whereas in the D-Z plane they have an inverted U-shaped variation.

The above model is of course an over simplification. In general the polarizations will be highly elliptical and the actual demarcation line will run at an angle to the D direction. We also have not considered three-dimensional current models such as those proposed for polar magnetic substorms [*Bonnevier et al.* 1970]. Our model does suffice, however, to explain some of the more evident latitude - dependent characteristics of Pc 5's and, to some degree, those of Pc 4's. In order to establish this current model for Pc 5's we need more magnetic stations between 68°N and 77°N.

The analysis of the model of ionosphere currents is considerably simplified by computing instantaneous, latitudinal profiles of the amplitudes of the three components. These can be calculated directly from the cross spectral estimates $F_{ij}(r_1, r_2, f)$. We have computed amplitude profiles for a few of the events in this thesis but there are usually too few stations north of the demarcation line of Pc 5 events to clearly establish the latitudinal dependence of the components. The latitudinal profiles of Pc 4's are generally very complex possibly because the Z components are strongly affected by induction.

4.2 Summary

From the analysis of the data in our experiment, several features of Pc 4's and Pc 5's have been determined. First, most micropulsation trains have frequencies which are independent of latitude. However, micropulsation trains with apparent latitude-dependent frequencies in the H component do occur. The guided poloidal mode appears to satisfactorily describe these latitude-dependent micropulsations.

At least some of the energy of Pc 4 and Pc 5 micropulsations is distributed in resonant oscillations of magnetic shells. However, the simple toroidal mode does not adequately describe the spatial features of the micro-

pulsations. The latitude-dependent frequencies of resonant oscillations of magnetic shells are evident in two ways.

(a) The latitudes of the intensity maxima of spectral components of micropulsations decrease with increasing frequency.

(b) The sense of polarization of micropulsations changes across the demarcation line. The latitude of the demarcation line decreases as the frequency of the micropulsations increases. Actually an abrupt latitudinal phase shift in either the H or D component is probably more useful than the polarization change for determining the latitude of the demarcation line.

The existence of distinct Pc 4 and Pc 5 peaks in the average geomagnetic spectrum is probably due to the preferential coupling of energy into magnetic shells near the auroral oval and near the plasmapause. Pc 5's occur predominantly in the auroral zones whereas Pc 4's occur predominantly near the plasmapause.

The reversal in the sense of polarization which occurs between 1130-1230 LGT in the H-D plane gives strong evidence in support of a Kelvin-Helmholtz instability as the source of energy for daytime Pc 4's and Pc 5's. The

large influx of power at all frequencies in the daytime
auroral oval further supports this theory. Unfortunately,
the theory does not explain the apparent differences
between the morning and afternoon micropulsation activity.
It is also difficult to see how any hm instability could
produce the very sinusoidal Pc 4's which often occur in
our data.

The Z components and the related polarizations
in the H-Z and D-Z planes of micropulsations observed at
the ground are undoubtedly caused by spatial gradients
in the ionospheric currents associated with the micropul-
sations. During part of the pulsation cycle, strong shear
currents flow to the east and the west in the ionosphere.
Unfortunately, the wide spacing of our stations in the
northern regions and the complexities in the diurnal
variations of the polarization parameters have limited
our interpretation to a very simple ionospheric current
model. An accurate current model would be very useful
in relating ground-based observations to the hm modes in
the magnetosphere.

There are a number of obvious ways to supplement
the data collected in this experiment. In the region
between 68°N and 77°N a closer spacing of stations would
help in comparing the relative positions of the intensity

maxima and the demarcation lines of Pc 5's. A closer
spacing would also help to develop a more accurate model
of the ionospheric current systems of Pc 5's. Since our
fluxgate magnetometers are inherently limited to micro-
pulsation frequencies below 20-30 mHz, it would be helpful
to complement our fluxgate records with data obtained from
other instruments such as induction coils. Finally,
stations positioned along an east-west line are necessary
in order to compare the phases of the H, D, and Z components
at different longitudes, and to compare longitudinal polar-
ization characteristics with the diurnal characteristics,
found in this experiment. These stations must be established
in regions with uniform geoelectric characteristics, other-
wise earth induction effects could mask the true source
configuration of the micropulsations. Knowledge of longi-
tudinal phase changes would allow the development of a more
accurate model of ionospheric currents.

REFERENCES

Alpaslan, T., *Spectral behavior of short period body waves and the synthesis of crustal structure in western Canada*, M.Sc. thesis, Edmonton, Department of Physics, University of Alberta, 1968.

Angerami, J. J., and D. L. Carpenter, Whistler studies of the plasmapause in the magnetosphere, *J. Geophys. Res.*, *71*, 711-725, 1966.

Annexstad, J. O., and C. R. Wilson, Characteristics of Pg micropulsations at conjugate points, *J. Geophys. Res.*, *73*, .1805-1818, 1968.

Atkinson, G., and T. Watanabe, Surface waves on the magnetospheric boundary as a possible origin of long period geomagnetic micropulsations, *Earth Planet. Sci. Lett.*, *1*, 89-91, 1966.

Barfield, J. N., L. J. Lanzerotti, C. G. Maclennan, G. A. Paulikas, and M. Schulz, Quiettime observation of a coherent compressional Pc-4 micropulsation at synchronous altitude, *J. Geophys. Res.*, *76*, 5252-5258, 1971.

Barnes, A., Collisionless damping of hydromagnetic waves, *Phys. Fluids*, *9*, 1483-1495, 1966.

Bendat, J. S., and A. G. Piersol, *Measurement and Analysis of Random Data*, John Wiley and Sons, New York, 1966.

Bennett, W. R., Spectra of quantized signals, *Bell Syst. Tech. J.*, *27*, 446-472, 1948.

Blackman, R. B., and J. W. Tukey, *The Measurement of Power Spectra*, Dover Publication, New York, 1958.

Bonnevier, B., R. Boström, and G. Rostoker, A three-dimensional model current system for polar magnetic substorms, *J. Geophys. Res.*, *75*, 107-121, 1970.

Born, M., and E. Wolf, *Principles of Optics*, Pergamon Press, New York, 1959.

Campbell, W. H., Geomagnetic pulsations, in *Physics of Geomagnetic Phenomena*, edited by S. Matsushita and W. H. Campbell, Academic Press, New York, 821-909, 1967.

Caner, B., P. A. Camfield, F. Andersen, and E. R. Niblett, A large-scale magnetotelluric survey in Western Canada, *Can. J. Earth Sci.*, *6*, 1245-1262, 1969.

Carovillano, R. L., H. R. Radoski, and J. F. McClay, Poloidal hydromagnetic plasmaspheric resonances, *Phys. Fluids*, *9*, 1860-1864, 1966.

Carpenter, D. L., Whistler studies of the plasmapause in the magnetosphere, 1. Temporal variations in the position of the knee and some evidence of plasma motions near the knee, *J. Geophys. Res.*, *71*, 693-709, 1966.

Carpenter, D. L., Whistler evidence of the dynamic behavior of the duskside bulge in the plasmasphere, *J. Geophys. Res.*, *75*, 3837-3847, 1970.

Chappell, C. R., K. K. Harris, and G. W. Sharp, A study of the influence of magnetic activity on the location of the plasmapause as measured by OGO 5, *J. Geophys. Res.*, *75*, 50-56, 1970.

Christoffel, D. A., and J. G. Linford, Diurnal properties of the horizontal geomagnetic micropulsation field in New Zealand, *J. Geophys. Res.*, *71*, 891-897, 1966.

Cochrane, N. A., and R. D. Hyndman, A new analysis of geomagnetic depth sounding data from western Canada, *Can. J. Earth Sci.*, *7*, 1208-1218, 1970.

Coleman, P. J., C. P. Sonett, D. L. Judge, and E. J. Smith, Some preliminary results of the Pioneer 5 magnetometer experiments, *J. Geophys. Res.*, *65*, 1856-1857, 1960.

Cummings, W. D., R. J. O'Sullivan, and P. J. Coleman, Jr., Standing Alfvén waves in the magnetosphere, *J. Geophys. Res.*, *74*, 778-793, 1969.

Dungey, J. W., Electrodynamics of the outer atmosphere, *Ionos. Res. Lab. Sci. Rep. 69*, Pennsylvania State University, 1954.

Dungey, J. W., Effects of electromagnetic perturbations on particles trapped in the radiation belts, *Space Sci. Rev.*, *4*, 199-222, 1965.

Dungey, J. W., Hydromagnetic waves, in *Physics of Geomagnetic Phenomena*, edited by S. Matsushita and W. H. Campbell, Academic Press, New York, 913-934, 1967.

Dungey, J. W., and D. J. Southwood, Ultra low frequency waves in the magnetosphere, *Space Sci. Rev.*, *10*, 672-688, 1970.

Egeland, A., Spectral density functions of hydromagnetic emissions at high latitude, *Nature*, *208*, 539-543, 1965.

Eleman, F., Studies of giant pulsations, continuous pulsations, and pulsation trains in the geomagnetic field, *Ark. För Geof.*, *5*, 231-282, 1966.

Ellis, G. R. A., Geomagnetic micropulsations, *Austr. J. Phys.*, *13*, 625-632, 1960.

Fairfield, D. H., Average magnetic field configuration of the outer magnetosphere, *J. Geophys. Res.*, *73*, 7329-7338, 1968.

Feldstein, Y. I., and G. V. Starkov, Dynamics of auroral belt and polar geomagnetic disturbances, *Planet. Space Sci.*, *15*, 209-229, 1967.

Field, E. C., and C. Greifinger, Transmission of geomagnetic micropulsations through the ionosphere and lower exosphere, *J. Geophys. Res.*, *70*, 4885-4899, 1965.

Fowler, R. A., B. J. Kotick, and R. D. Elliot, Polarization analysis of natural and artificially induced geomagnetic micropulsations, *J. Geophys. Res.*, *72* 2871-2884, 1967.

Frank, L. A., Plasma in the earth's polar magnetosphere, *J. Geophys. Res.*, *76*, 5202-5219, 1971.

Gentleman, W. M., and G. Sande, Fast Fourier transform for fun and profit, *AFIPS proc.*, *Fall Joint Computer Conf.*, *29*, 563-578, 1966.

Greifinger, C., and P. Greifinger, Transmission of micropulsations through the lower ionosphere, *J. Geophys. Res.*, *70*, 2217-2231, 1965.

Hakura, Y., Tables and maps of geomagnetic coordinates corrected by the higher order spherical harmonic terms, *Rep. Ionos. Space Res. Japan*, *19*, 121-157, 1965.

Hirasawa, T., and T. Nagata, Spectral analysis of geomagnetic pulsations from 0.5 to 100 sec in period for the quiet sun condition, *Pure Appl. Geophys.*, *65*, 102-124, 1966.

Hirasawa, T., Long-period geomagnetic pulsations (pc 5) with typical sinusoidal waveforms, *Rep. Ionos. Space Res. Japan*, *24*, 66-79, 1970.

Holt, E. H., and R. E. Haskell, *Foundations of Plasma Dynamics*, Macmillan, New York, 1965.

Hruska, A., The magnetodynamic toroidal waves, *Planet. Space Sci.*, *16*, 1305-1309, 1968.

Hruska, A., On the interpretation of some observed features of geomagnetic pulsations, *Planet. Space Sci.*, *17*, 1937-1940, 1969.

Hultqvist, B., Plasma waves in the frequency range 0.0001-10 cps in the earth's magnetosphere and ionosphere, *Space Sci. Rev.*, *5*, 599-695, 1966.

Inoue, Y., and D. L. Shaeffer, Full wave solutions for the transmission of ULF and VLF waves through the ionosphere, *Rep. AFCRL - 70 - 0531*, University of Pittsburgh, Pennsylvania, September, 1970.

Jacobs, J. A., and K. Sinno, World-wide characteristics of geomagnetic micropulsations, *Geophys. J.*, *3*, 333-352, 1960.

Jacobs, J. A., Y. Kato, S. Matsushita, V. A. Troitskaya, Classification of geomagnetic micropulsations, *J. Geophys. Res.*, *69*, 180-181, 1964.

Jacobs, J. A., and K. O. Westphal, Geomagnetic micropulsations, in *Physics and Chemistry of the Earth*, *5*, 157-224, 1964.

Jacobs, J. A., and C. S. Wright, Geomagnetic micropulsation results from Byrd Station and Great Whale River, *Can. J. Phys.*, *43*, 2099-2122, 1965.

Jacobs, J. A., *Geomagnetic Micropulsations*, Springer-Verlag, New York, 1970.

Jenkins, G. M., and D. G. Watts, *Spectral Analysis and its Applications*, Holden-Day, San Francisco, 1968.

Jones, F. W., and A. T. Price, The perturbations of alternating geomagnetic fields by conductivity anomalies, *Geophys. J.*, *20*, 317-334, 1970.

Jones, R. H., A reappraisal of the periodogram in spectral analysis, *Technometrics*, *7*, 531-542, 1965.

Judge, D. L., and P. J. Coleman, Jr., Observations of low frequency hydromagnetic waves in the distant geomagnetic field: Explorer 6, *J. Geophys. Res.*, *67*, 5071-5090, 1962.

Kahalas, S. L., On toroidal mode eigenfrequencies, *Planet. Space Sci.*, *17*, 1281-1284, 1969.

Kaneda, E., S. Kokubun, T. Oguti, and T. Nagata, Auroral radar echoes associated with Pc-5, *Rep. Ionos. Space Res. Japan*, *18*, 165-172, 1964.

Kato, Y., and S. Akasofu, Outer atmospheric oscillation and geomagnetic micropulsation, *Sci. Rep. Tohoku Univ.*, *Ser. 5, Geophys.*, *7*, 103-123, 1955.

Kato, Y., and T. Saito, Morphological study of geomagnetic pulsations, *J. Phys. Soc. Japan, 17,* *Suppl. A-II,* 34-39, 1962.

Kato, Y., and T. Utsumi, Polarization of long period geomagnetic pulsation, pc 5, *Rep. Ionos. Space Res. Japan, 18,* 214-217, 1964.

Keller, G. V., and F. C. Frischknecht, *Electrical Methods in Geophysical Prospecting,* Pergamon Press, London, 1966.

Kimura, I., and H. Matsumoto, Hydromagnetic wave instabilities in a nonneutral plasma-beam system, *Radio Sci., 3,* 333-343, 1968.

Kitamura, T., Geomagnetic pulsations and the exosphere, part 1, statistical results, *Rep. Ionos. Space Res. Japan, 17,* 67-76, 1963.

Kurtz, R. D., *Polarization characteristics of geomagnetic micropulsations,* M.Sc. thesis, Edmonton, Department of Physics, University of Alberta, 1969.

Mather, K. B., E. J. Gauss, and G. R. Cresswell, Diurnal variations in the power spectrum and polarization of telluric currents at conjugate points, L = 2.6, *Australian J. Phys. 17,* 373-388, 1964.

Mazo, J. E., Quantizing noise and data transmission, *Bell Syst. Tech. J., 47,* 1968.

McClay, J. F., On the resonant modes of a cavity and the dynamical properties of micropulsations, *Planet. Space Sci. 18,* 1673-1690, 1970.

Nagata, T., S. Kokubun, and T. Iijima, Geomagnetically conjugate relationships of giant pulsations at Syowa Base, Antarctica and Reykjavik, Iceland, *J. Geophys. Res., 68,* 4621-4625, 1963.

Nagata, T., and H. Fukunishi, Dependence on geomagnetic activity of magnetic pulsation frequency of pc-3 and pc-4 ranges, *Geophys. J.,15,* 69-78, 1968.

Namgaladze, A. A., and B. E. Brunelli, Periods of magneto-
spheric oscillations and the plasma density,
J. Geomag. Geoelect., *22*, 383-391, 1970.

Nishida, A., A theory of irregular magnetic micropulsations
associated with a magnetic bay, *J. Geophys. Res.*,
69, 947-954, 1964.

Obayashi, T., and J. A. Jacobs, Geomagnetic pulsation and
the earth's outer atmosphere, *Geophys. J.*, *1*,
53-63, 1958.

Obertz, P., and O. M. Raspopov, Study of the spatial
characteristics of type Pc 5 geomagnetic pul-
sations, *Geomag. Aeron.*, *8*, 424-427, 1968.

Oguti, T., Inter-relations among the upper atmosphere
disturbance phenomena in the auroral zone,
JARE Sci. Rep., *Ser. A. Aeronomy*, No. 1,
1-82, 1963.

Ol', A.I., Long period gigantic geomagnetic field pulsa-
tions, *Geomag. Aeron.*, *3*, 90-95, 1963.

Parker, E. N., Effect of hydromagnetic waves in a dipole
field on the longitudinal invariant, *J. Geophys.
Res.*,*66*, 693-708, 1961.

Patel, V. L., and L. J. Cahill, Jr., Evidence of hydro-
magnetic waves in the earth's magnetosphere
and of their propagation to the earth's surface,
Phys. Rev. Lett. 12, 213-215, 1964.

Patel, V. L., Low frequency hydromagnetic waves in the
magnetosphere: Explorer 12, *Plan. Space Sci.*,
13, 485-506, 1965.

Paulson, K. V., A. Egeland, and F. Eleman, A statistical
method for quantitative analysis of geomagnetic
giant pulsations, *J. Atmospheric Terrest. Phys.*,
27, 943-967, 1965.

Peeples, W. J., *Magnetotelluric profiling over a deep
structure*, Ph.D. thesis, Edmonton, Department
of Physics, University of Alberta, 1969.

Pope, J. H., An explanation for the apparent polarization of some geomagnetic micropulsations (pearls), *J. Geophys. Res.*, *69*, 399-406, 1964.

Praus, O., J. M. DeLaurier, and L. K. Law, The extension of the Alert geomagnetic anomaly through northern Ellesmere Island, Canada, *Can. J. Earth Sci.*, *8*, 50-64, 1971.

Price, A. T., Electromagnetic induction in a semi-infinite conductor with a plane boundary, *Quart. J. Mech. Appl. Math.*, *3*, 385-410, 1950.

Price, A. T., The theory of magnetotelluric methods when the source field is considered, *J. Geophys. Res.*, *67*, 1907-1918, 1962.

Prince, C. E., Jr., and F. X. Bostick, Jr., Ionospheric transmission of transversely propagated plane waves at micropulsation frequencies and theoretical power spectrums, *J. Geophys. Res.*, *69*, 3213-3234, 1964.

Radoski, H. R., Magnetic toroidal resonances and vibrating field lines, *J. Geophys. Res.*, *71*, 1891-1893, 1966.

Radoski, H. R., Highly asymmetric MHD resonances: the guided poloidal mode, *J. Geophys. Res.*, *72*, 4026-4027, 1967.

Rankin, D., and I. K. Reddy, A magnetotelluric study of resistive anisotropy, *Geophysics*, *34*, 438-449, 1969.

Rankin, D., and R. Kurtz, A statistical study of micropulsation polarizations, *J. Geophys. Res.*, *75*, 5444-5458, 1970.

Rankin, D., and I. K. Reddy, The effect of geoelectric structure on the polarization characteristics of the geomagnetic micropulsations, *preprint*, Dept. Phys., University of Alberta, 1971.

Roman, P., Generalized Stokes parameters for waves with arbitrary form, *Nuovo Cimento, 13,* 974-982, 1959.

Roman, P., and E. Wolf, Correlation theory of stationary electromagnetic fields. Part (1) - The basic field equations, *Nuovo Cimento, 17,* 462-476, 1960a.

Roman, P., and E. Wolf, Correlation theory of electromagnetic fields. Part (2) - Conservation laws, *Nuovo Cimento, 17,* 477-490, 1960b.

Roman, P., Correlation theory of stationary electromagnetic fields. Part (3) - The presence of random sources, *Nuovo Cimento, 20,* 759-772, 1961.

Rossi, B., and S. Olbert, *Introduction to the Physics of Space,* McGraw-Hill, New York, 1970.

Rostoker, G., The frequency spectrum of Pi 2 micropulsation activity, *J. Geophys. Res., 72,* 2032-2039, 1967.

Saito, T., Mechanisms of geomagnetic continuous pulsations and physical states of the exosphere, *J. Geomag. Geoelect., 16,* 115-151, 1964.

Saito, T., Some characteristics of the dynamic spectrum of long-period geomagnetic pulsations, *J. Geophys. Res., 72,* 3895-3904, 1967.

Saito, T., Geomagnetic pulsations, *Space Sci. Rev., 10,* 319-412, 1969.

Saito, T., and T. Sakurai, Mechanism of geomagnetic Pi 2 pulsations in magnetically quiet condition, *Sci. Rep. Tohoku Univ., Ser 5, Geophys., 20,* 49-70, 1970.

Sakurai, T., Polarization characteristics of Pi 2 micropulsations, *Sci. Rep. Tohoku Univ., Ser. 5, Geophys., 20,* 107-117, 1970.

Samson, J. C., J. A. Jacobs, and G. Rostoker, Latitude-dependent characteristics of long-period geomagnetic micropulsations, *J. Geophys. Res.*, *76*, 3675-3683, 1971.

Schmucker, U., Anomalies of geomagnetic variations in the Southwestern United States, *J. Geomag. Geoelect.*, *15*, 193-221, 1964.

Sen, A. K., The stability of the magnetospheric boundary, *Planet. Space Sci.*, *13*, 131-141, 1965.

Sersen, P. H., An electrical recording magnetometer, *Can. J. Phys.*, *35*, 1387-1394, 1957.

Siebert, M., Geomagnetic pulsations with latitude dependent periods and their relation to the structure of the magnetosphere, *Planet. Space Sci.*, *12*, 137-147, 1964.

Sonett, C. P., A. R. Sims, I. J. Abrams, The distant geomagnetic field 1. Infinitesimal hydromagnetic waves, *J. Geophys. Res.*, *67*, 1191-1207, 1962.

Southwood, D. J., The hydromagnetic stability of the magnetospheric boundary, *Planet. Space Sci.*, *16*, 587-605, 1968.

Southwood, D. J., J. W. Dungey, and R. J. Etherington, Bounce resonant interaction between pulsations and trapped particles, *Planet. Space Sci.*, *17*, 349-361, 1969.

Stewart, B., On the great magnetic disturbance which extended from August 28 to September 7, 1859, as recorded by photography at the Kew Observatory, *Phil. Trans. Roy. Soc. London*, 425, 1961.

Stuart, W. F., and M. J. Usher, An investigation of micropulsations at middle latitudes, *Geophys. J. Roy. Astron. Soc.*, *12*, 71-86, 1966.

Swift, C. M., Theoretical magnetotelluric and Turam response from two-dimensional inhomogenetities, *Geophysics*, *36*, 38-52, 1971.

Swift, D. W., A new interpretation of long period micro-pulsations, *J. Geophys. Res., 72*, 4885-4898, 1967.

Tamao, T., Effects of the electron motion along magnetic field lines on torsional hydromagnetic oscillations, *J. Geomag. Geoelect., 20*, 305-313, 1968.

Tamao, T., Hydromagnetic coupling oscillations and drift instabilities in nonuniform, collisionless plasmas, *Phys. Fluids, 12*, 1458-1470, 1969.

Trigg, D. F., P. H. Serson, and P. A. Camfield, A solid-state electrical recording magnetometer, *preprint*, Earth Physics Branch, Dept. Energy, Mines and Resources, Ottawa, Canada, 1970.

Troitskaya, V. A., Micropulsations and the state of the magnetosphere, in *Solar-Terrestrial Physics*, edited by J. W. King and W. S. Newman, Academic Press, 213-274, 1967.

Vasyliunas, V. M., A survey of low-energy electrons in the evening sector of the magnetosphere with OGO 1 and OGO 3, *J. Geophys. Res., 73*, 2839-2884, 1968a.

Vasyliunas, V. M., Low energy electrons on the day side of the magnetosphere, *J. Geophys. Res., 73*, 7519-7523, 1968b.

Voelker, H., Observations of geomagnetic pulsations: pc 3, 4 and pi 2 at different latitudes, *Ann. Geophys., 24*, 245-252, 1968.

Westphal, K. O., and J. A. Jacobs, Oscillations of the earth's outer atmosphere and micropulsations, *Geophys. J., 6*, 360-376, 1962.

Whalen, J. A., Auroral oval plotter and nomograph for determing corrected geomagnetic local time, lat-itude, and longitude for high latitudes in the northern hemisphere, Air Force Cambridge Research Laboratories, Bedford, Massachusetts, 1970.

Wiener, N., Generalized harmonic analysis, *Acta. Math.*, *55*, 117-258, 1930.

Wilson, C. R., Conjugate three-dimensional polarization of high-latitude micropulsations from a hydromagnetic wave-ionospheric current model, *J. Geophys. Res.*, *71*, 3233-3249, 1966.

Wolf, E., Optics in terms of observable quantities, *Nuovo Cimento*, *12*, 884-888, 1954.

APPENDIX A1 ANALYSIS OF COMPLEX VECTOR TIME SERIES

A1.1 The general correlation matrix

A time dependent vector field is completely specified by the set of time series $x_1(\vec{r},t)$, $x_2(\vec{r},t)$, $x_3(\vec{r},t)$ where x_1, x_2, x_3 are components of the vector field measured in 3-space, $\vec{r}$ the spatial position of the measurement extending over the whole vector field, and t the time covering the duration of the event. In general these series are difficult to interpret and we find it useful to introduce a different representation of the data in the form of a correlation matrix. In three dimensions the matrix is written as

$$\phi_{ij}(\vec{r}_1,\vec{r}_2,\tau)=\begin{bmatrix} \langle x_1(\vec{r}_1,t),x_1^*(\vec{r}_2,t-\tau)\rangle & \langle x_1,x_2^*\rangle & \langle x_1,x_3^*\rangle \\ \langle x_2,x_1^*\rangle & \langle x_2,x_2^*\rangle & \langle x_2,x_3^*\rangle \\ \langle x_3,x_1^*\rangle & \langle x_3,x_2^*\rangle & \langle x_3,x_3^*\rangle \end{bmatrix} \quad (A1)$$

where * denotes the complex conjugate, $\vec{r}_1$ and $\vec{r}_2$ are varying spatial positions, and τ the lag [Wolf, 1954]. The expectation

$$\langle x_i(t), x_j^*(t-\tau)\rangle = \lim_{T\to\infty} \frac{1}{2T}\int_{-T}^{T} x_i(t)x_j^*(t-\tau)\ dt \quad (A2)$$

is a measure of the *linear* dependence of the two components x_i and x_j at lag τ.

Characteristics of this matrix for $\vec{r}_1 = \vec{r}_2$ are discussed in detail in the next section, together with a section on its frequency domain equivalent, the cross spectral matrix. A short discussion on the correlation matrix and cross spectral matrix with $\vec{r}_1 \neq \vec{r}_2$ is included in Appendix A1.4.

A1.2 The correlation matrix with $\vec{r}_1 = \vec{r}_2$: applications to vectors which are restricted to a plane

First consider the correlation matrix with $\vec{r}_1 = \vec{r}_2$. A symmetry property of the matrix can be readily shown:

$$
\phi_{ij}(\tau) = \langle x_i(t)x_j^*(t-\tau)\rangle = \langle x_i(t^1+\tau)x_j^*(t^1)\rangle
$$

$$
= \langle x_j^*(t^1)x_i(t^1+\tau)\rangle = \langle x_j(t^1)x_i^*(t^1+\tau)\rangle^*
$$

$$
= \phi_{ji}^*(-\tau) \tag{A3}
$$

Equation (A3) shows that $\phi_{ij}(0)$ is Hermitean.

Discussion here is limited to two very simple vector time series, totally random (or unpolarized) vector series and vector series restricted to a plane. Other types of vector time series lead to correlation matrices with very complicated characteristics [Roman, 1959]. In unpolar-

ized disturbances the end point of the disturbance vector moves quite irregularly. The vector shows no preferential directional properties and no predictable temporal properties. Thus the spatially orthogonal vector components must always be uncorrelated $\left[<x_i(t), x_j^*(t-\tau)>_{i \neq j} = 0 \right]$, and in order that temporal variations be purely random, $<x_i(t),$ $x_j^* (t-\tau)>_{\tau \neq 0} = 0$. The further requirement that the terms $<x_i(t), x_j^* (t-\tau)>_{i \neq j}$ be invariant under a coordinate transformation indicates that the correlation matrix U of an unpolarized vector series is a scalar. More precisely $U = A\delta_{ij}$, where A is a constant proportional to the power of the unpolarized disturbance.

In a plane polarized vector time series the vector, when measured at one point in space, is restricted to a given plane. (*Note the departure from the usual definition in optics.*) Thus there must exist a lag-independent rotation matrix R such that

$$R[\phi(\tau)]R^{-1} = \begin{bmatrix} \phi'_{11}(\tau) & \phi'_{12}(\tau) & 0 \\ \phi'_{21}(\tau) & \phi'_{22}(\tau) & 0 \\ 0 & 0 & 0 \end{bmatrix} \qquad (A4)$$

where $\phi(\tau)$ represents the correlation matrix at lag τ.

This rotation matrix can be obtained by diagonalizing $\phi(0)$ [*Cummings et al.*, 1969].

Consider now the correlation matrix $\phi(0)$ of a general vector time series. Since this matrix is Hermitean there must be a real transformation R which diagonalizes the matrix. The matrix in the new coordinate system, the principal axis system, is given by the transform

$$R[\phi(0)]R^{-1} = \begin{bmatrix} \lambda_1 & 0 & 0 \\ 0 & \lambda_2 & 0 \\ 0 & 0 & \lambda_3 \end{bmatrix} \qquad (A5)$$

where we have chosen $\lambda_3 < \lambda_2 < \lambda_1$. These eigenvalues are real and positive for any set of real time series. The trace of the matrix is invariant under coordinate transformations and represents the total intensity, or total power, of the vector disturbance. The trace elements are the intensities in the individual directions. The matrix is conveniently expanded in the form

$$\lambda_3 \begin{bmatrix} 1 & 0 & 0 \\ 0 & 1 & 0 \\ 0 & 0 & 1 \end{bmatrix} + (\lambda_2 - \lambda_3) \begin{bmatrix} 0 & 0 & 0 \\ 0 & 1 & 0 \\ 0 & 0 & 0 \end{bmatrix} + (\lambda_1 - \lambda_3) \begin{bmatrix} 1 & 0 & 0 \\ 0 & 0 & 0 \\ 0 & 0 & 0 \end{bmatrix} \qquad (A6)$$

$$\text{(A)} \qquad\qquad\qquad \text{(B)} \qquad\qquad\qquad \text{(C)}$$

If we know ápriori that the polarized part of the vector time series is confined to a plane and assume that the polarized and unpolarized components of the time series are uncorrelated, then the above expansion has a simple interpretation. (A) is the matrix of the unpolarized vector time series while (B) and (C) are the two spatial components of the plane polarized vector time series. The eigenvectors corresponding to λ_1 and λ_2 define the plane of polarization. If we require $(\lambda_1 - \lambda_3)$ and $(\lambda_2 - \lambda_3)$ to be positive then this expansion is unique. This is a reasonable requirement since, for a real time series, these two values are the two orthogonal intensities of the plane polarized vector series.

In general the polarized vector series will trace some complicated 3-dimensional shape. One helpful (though not conclusive) method to determine whether the postulate of plane polarization is correct is to determine

$$\phi'(\tau) = R[\phi(\tau)]R^{-1} \qquad (A7)$$

If $\phi'_{i,3}(\tau) \neq 0$ (where $\lambda_3 = \phi'_{33}(0)$) for any $\tau \neq 0$ then the series are not plane polarized and the above interpretation of expansion (A6) is incorrect.

A useful parameter in determining the degree of plane polarization is given by the expression

$$R_1 = \frac{(\lambda_1 - \lambda_3) + (\lambda_2 - \lambda_3)}{\lambda_1 + \lambda_2 + \lambda_3} \qquad (A8)$$

Here R_1 is the ratio of the apparent plane polarized signal intensity to the total signal intensity. If R_1 equals unity then the signal is completely plane polarized.

A1.3 The cross spectral matrix: applications to plane polarized vector fields

The information contained in the correlation matrix can also be expressed in terms of a cross spectral matrix. We use the Wiener-Khinchin relations

$$S_{ij}(f) = \int_{-\infty}^{\infty} \phi_{ij}(\tau) e^{-2\pi i f \tau} \, d\tau \qquad (A9)$$

$$\phi_{ij}(\tau) = \int_{-\infty}^{\infty} S_{ij}(f) e^{2\pi i f \tau} \, df \qquad (A10)$$

to find

$$\phi_{ij}(0) = \int_{-\infty}^{\infty} S_{ij}(f) \, df \qquad (A11)$$

The terms in (A11) may be considered to be the total auto and cross powers of the vector disturbance. Suppose now

that the disturbance has a spectral width Δf and mean frequency f_0. Then we can estimate the correlation functions $\phi_{ij}(0)$ from the equation.

$$J_{ij}(f) = \int_{f-\Delta f/2}^{f+\Delta f/2} S_{ij}(g)\,dg \qquad (A12)$$

In particular we have

$$\phi_{ij}(0) = J_{ij}(f_0) + J_{ij}(-f_0) \qquad (A13)$$

We could alternatively use the Fourier-Stieltjes transform to formulate this function [*Wiener*, 1930]. It can be shown [*Jenkins and Watts*, 1968, p467] that the matrix formed from the terms (A12) is a positive, semi-definite Hermitean matrix. As $\Delta f \rightarrow 0$, $\frac{1}{\Delta f}J_{ij}(f) \rightarrow S_{ij}(f)$ where $S_{ij}(f)$ are the auto and cross power spectral densities.

To find the apparent plane of polarization (if one exists) we diagonalize the real part of the cross spectral matrix $J(f)$ as follows:

$$R[(\text{Re } J)]R^{-1} = \begin{bmatrix} J'_{11} & 0 & 0 \\ 0 & J'_{22} & 0 \\ 0 & 0 & J'_{33} \end{bmatrix} = \text{Re}J' \qquad (A14)$$

In the expression (A14) R, J, and J', are in general functions of f. For convenience we have chosen $J'_{33} <$ $J'_{22} < J'_{11}$. The transform of the total matrix is then

$$R \; JR^{-1} = \begin{bmatrix} J'_{11} & iJ'_{12} & iJ'_{13} \\ -iJ'_{12} & J'_{22} & iJ'_{23} \\ -iJ'_{13} & -iJ'_{23} & J'_{33} \end{bmatrix} \qquad (A15)$$

Once again if $J'_{33} = J'_{23} = J'_{13} = 0$, the vector series is truly plane polarized (i.e. restricted to a plane). If only J'_{13} and J'_{23} are zero and if the non plane polarized vector series is approximately random or unpolarized, then the cross spectral matrix of the plane polarized vector series is given by

$$\begin{bmatrix} \left(J'_{11}-J'_{33}\right) & iJ'_{12} & 0 \\ -iJ'_{12} & \left(J'_{22}-J'_{33}\right) & 0 \\ 0 & 0 & 0 \end{bmatrix} \qquad (A16)$$

This matrix is found by an expansion similar to that in equation (A6). In analogy with (A8) we can also define a polarization ratio for the terms in the cross spectral matrix. This ratio is given by

$$R_1 = \frac{\left(J'_{11} - J'_{33}\right) + \left(J'_{22} - J'_{33}\right)}{J'_{11} + J'_{22} + J'_{33}} \qquad (A17)$$

Following the work of *Born and Wolf* [1959] and *Fowler et al.*, [1967] it is possible to show that the *plane polarized* part of the vector time series is composed of a vector which moves randomly in the plane and a vector series in which the two orthogonal components are completely correlated. We can accordingly expand the matrix (A16) in the form

$$
\begin{bmatrix} \left(J'_{11} - J'_{33}\right) & iJ'_{12} \\ -iJ'_{12} & \left(J'_{22} - J'_{33}\right) \end{bmatrix} = U \begin{bmatrix} 1 & 0 \\ 0 & 1 \end{bmatrix} + \begin{bmatrix} P_{11} & iP_{12} \\ -iP_{12} & P_{22} \end{bmatrix} \qquad (A18)
$$

where for simplicity we have dropped the zero terms of the matrix. U is the matrix of the random plane polarized component, and P the matrix of the completely correlated vector series with det P = 0. Consideration shows that U is simply an eigenvalue of the matrix J, although the unitary transformation is not, in general, a real rotation of the axis. The values of U are

$$\frac{1}{2}(J'_{11}+J'_{22}-2J'_{33}) \pm \frac{1}{2}\left((J'_{11}+ J'_{22}-2J'_{33})^2 - 4 \det J'\right)^{\frac{1}{2}} \qquad (A19)$$

We choose the smallest value of U since the other gives negative values for P_{11} and P_{22}.

Another useful parameter, the ratio of the completely coherent signal intensity to the plane polarized signal intensity, is given by the expression

$$R_2 = \frac{\left(J'_{11} - J'_{33} - U\right) + \left(J'_{22} - J'_{33} - U\right)}{\left(J'_{11} - J'_{33}\right) + \left(J'_{22} - J'_{33}\right)} \tag{A20}$$

Note that this expression is meaningful only if $J'_{i3} = 0$ or if the non plane polarized vector series is truly random.

When $\Delta f/f \ll 1$ the vector series has sinusoidal spatial components and the matrix P is simply the cross spectral matrix of an elliptically polarized vector time series, with the coordinate system oriented along the major and minor axes of the ellipse. The rotation eigenvectors of R corresponding to J'_{11} and J'_{22} are along the major and minor axes of the ellipse, respectively. The sense of rotation of the vector, right or left handed, is given by the sign of J'_{12} or P_{12}. The ellipticity, the ratio of the minor to the major axis of the ellipse, is given by the equation

$$E = \left(\frac{P_{22}}{P_{11}}\right)^{\frac{1}{2}} \qquad \text{(A21)}$$

The total intensity of the coherent signal is given by the equation

$$I = P_{11} + P_{22} \qquad \text{(A22)}$$

Often a vector time series will have a band-width Δf_0 such that $\Delta f_0 \gg \Delta f$ and $\Delta f_0/f_0 > 1$. In this case we might say that we are looking at the spectral components of the series and the associated frequency dependent ellipses of polarization.

A1.4 The correlation and cross spectral matrices with $r_1 \neq r_2$

The correlation matrix with $\vec{r}_1 \neq \vec{r}_2$ has none of the symmetry properties of the case when $\vec{r}_1 = \vec{r}_2$ and is very difficult to interpret in a precise manner. It is helpful, though, to redefine the elements of the correlation matrix in terms of the normalized, cross correlation function

$$\rho_{ij}(\vec{r}_1,\vec{r}_2,\tau) = \frac{\langle x_i(\vec{r}_1,\tau), x_j^*(\vec{r}_2,t-\tau)\rangle}{\left(\phi_{ii}(\vec{r}_1,\vec{r}_1,0)\phi_{jj}(\vec{r}_2,\vec{r}_2,0)\right)^{\frac{1}{2}}} \qquad \text{(A23)}$$

where $\phi_{ii}(\vec{r}_1,\vec{r}_1,0)$ is the power in the ith component at position $\vec{r}_1$. These functions have the simple characteristic

$$|\rho_{ij}(\tau)| \leq 1 \qquad \text{(A24)}$$

The parameter ρ is normally a complicated function of the lag τ and is, except in some very simple cases, difficult to interpret. A detailed study of the correlation matrix has been given by *Roman and Wolf* [1960a, 1960b] and *Roman* [1961].

The elements of the cross spectral matrix are defined by the relation

$$J_{ij}(\vec{r}_1,\vec{r}_2,f) = \int_{f-\Delta f/2}^{f+\Delta f/2} S_{ij}(\vec{r}_1,\vec{r}_2,g)dg \qquad \text{(A25)}$$

This equation is simply a generalization of equation (A12) with $\vec{r}_1 \neq \vec{r}_2$. All the terms, including the diagonal elements J_{11}, J_{22}, J_{33} are in general complex. More precisely

$$J_{ij}(f) = L_{ij}(f) + iQ_{ij}(f) \qquad \text{(A26)}$$

where $L_{ij}(f)$ and $Q_{ij}(f)$ are measures of the correlation between the in phase and out of phase components of the

two series. It is convenient to define, in analogy with equation (A23), a coherency estimator given by

$$K_{ij}(\vec{r}_1,\vec{r}_2,f) = \left[\frac{L_{ij}^2(\vec{r}_1,\vec{r}_2,f) + Q_{ij}^2(\vec{r}_1,\vec{r}_2,f)}{J_{ii}(\vec{r}_1,\vec{r}_1,f) \, J_{jj}(\vec{r}_2,\vec{r}_2,f)}\right]^{\frac{1}{2}} \qquad (A27)$$

The coherency K_{ij} can be considered as a measure of the correlation of the two series at each frequency f.

The phase spectrum estimator

$$F_{ij}(\vec{r}_1,\vec{r}_2,f) = arc \, tan \left[\frac{-Q_{ij}(\vec{r}_1,\vec{r}_2,f)}{L_{ij}(\vec{r}_1,\vec{r}_2,f)}\right] \qquad (A28)$$

is another useful parameter. F_{ij} shows to what degree the frequency components in one series lead or lag those at the same frequency in the other series.

APPENDIX A2   ESTIMATION OF THE COMPONENTS OF THE CROSS

SPECTRAL MATRIX; THE POWER SPECTRA AND

CROSS SPECTRA

In order to obtain accurate estimates of the powers and cross powers J_{ij} (equations (A12),(A25)) we need a spectral window Q which is approximately rectangular and with spectral width Δf chosen such that

$$Q(f)*S(f)_{f=f_0} \simeq \int_{f_0-\Delta f/2}^{f_0+\Delta f/2} S_{ij}(f)df \qquad (A29)$$

where the operator * denotes convolution. In our analysis the values J_{ij} were calculated by smoothing the periodogram estimates [*Jones*, 1965] which gives (as will be seen later) an approximately rectangular spectral window.

The periodogram estimates for the power spectral density are obtained from $|A(n)|^2$ where $A(n)$ is the discrete Fourier transform of the time series $X_N(t)$.

i.e. $A(n) = \frac{1}{N} \sum_{j=0}^{N-1} X_N(j)\ e^{-2\pi inj/N}$

$$n = 0,1,2,3... \qquad (A30)$$

where n represents a sample at point $n\Delta f$ ($\Delta f = (N\Delta t)^{-1}$) and Δt is the sample interval. Since the fast Fourier

transform algorithm (FFT) [*Gentleman and Sande*,1966] is used in the computation of $A(n)$, X_N normally consists of the original time series X_m (m points), with zeroes added to give N points (N being an integral power of 2). The periodogram estimates corrected for the added zeroes are then given by $\frac{N^2}{m}|A(n)|^2$.

It is possible to show [*Blackman and Tukey*,1958] that

$$\frac{N^2}{m}|A(n)|^2 = \frac{1}{m\Delta t}|a_p(n\Delta f)|^2 \qquad (A31)$$

where

$$a_p(f) = \sum_{k=-\infty}^{\infty} a(f+k\Delta t^{-1}) \qquad (A32)$$

and

$$a(f) = \int_{-\infty}^{\infty} X_m(t)\, e^{-2\pi i f t}\, dt \qquad (A33)$$

If there is no aliasing, which we now assume, then

$$a_p(f) = a(f) \qquad 0 < f < \frac{1}{2\Delta t}$$

We obtain the time series X_m from the original signal $x(t)$ by multiplying it by a data window $B(t)$,

i.e. $X_m(t) = B(t) \cdot x(t) \qquad (A34)$

Thus

$$\frac{N^2}{m} |A(n)|^2 = \frac{1}{T_m} \left| \int_0^{T_m} B(t) \cdot x(t) \ e^{-2\pi i f t} \ dt \right|^2 = P(f) \quad (A35)$$

where $A(n)$ is the function evaluated at $n\Delta f$ and T_m = $m\Delta t$. If the signal $x(t)$ is stationary, we can prove [*Blackman and Tukey*, 1958] that

$$<P(f)> = W(f)*S(f) \quad\quad (A36)$$

S, the true power spectral density, is given by the relation

$$S(f) = \lim_{T\to\infty} \frac{1}{T} \left| \int_{-T/2}^{T/2} x(t) \ e^{-2\pi i f t} \ dt \right|^2 \quad (A37)$$

The spectral window $W(f)$ is given by

$$W(f) = \frac{1}{T_m} \left| \int_{\infty}^{\infty} B(t) \ e^{-2\pi i f t} \ dt \right|^2 \quad\quad (A38)$$

To reduce the variance of the individual power estimates $\frac{N^2}{m}|A(n)|^2$, we determine the smoothed spectral estimates J from the equation

$$J(n\Delta f) = \frac{1}{N} \sum_{p=-k_1}^{k_2} \frac{N^2}{m}|A(n-p)|^2 \quad\quad (A39)$$

$$= \frac{1}{N} \sum_{p=-k_1}^{k_2} \int_{-\infty}^{\infty} W(n\Delta f - p\Delta f - g)S(g)dg \qquad (A40)$$

$$= \left[\frac{1}{N} \sum_{p=-k_1}^{k_2} W(n\Delta f - p\Delta f) \right] *S(f) \qquad (A41)$$

The expression (A41) gives the estimates of the total powers J_{ij} in equation (A12). The overall spectral window is

$$Q(f) = \frac{1}{N} \sum_{p=-k_1}^{k_2} W(f-p\Delta f) \qquad (A42)$$

We will show later that this window has an approximately rectangular shape if $B(t)$ is properly chosen.

The unsmoothed cross spectral estimates of two time series $X(t)$ and $Y(t)$ are given by

$$\frac{N^2}{m}A(n) \; C*(n) \qquad (A43)$$

where $A(n)$ and $C(n)$ are the discrete Fourier transforms of $X(t)$ and $Y(t)$ respectively. To obtain the smoothed cross powers to be used in equations (A12) and (A25) we average the real and imaginary parts of the

spectrum separately. The spectral window in each case is identical to that given in (A42).

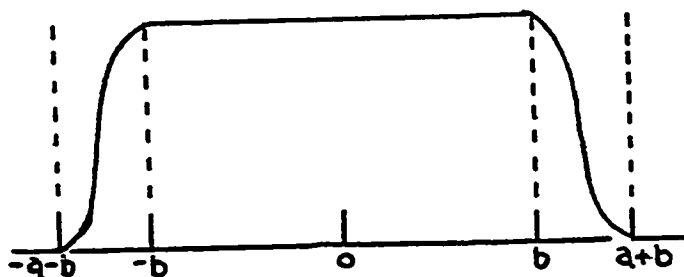In our analysis we have used the time domain window $B(t)$ shown in Figure A1.

Fig. A1. The data window $B(t)$.

$$B(t) = \frac{1}{2} \left(\cos \left(\frac{2\pi}{2a}(t+b) \right) + 1 \right) \qquad -a -b < t < -b$$

$$= \frac{1}{2} \left(\cos \left(\frac{2\pi}{2a}(t-b) \right) + 1 \right) \qquad b < t < a+b$$

$$= 1 \qquad\qquad\qquad\qquad\qquad -b < t < b \qquad \text{(A44)}$$

$$= 0 \qquad\qquad\qquad\qquad\qquad \text{otherwise}$$

The transform of this window is

$$T(f) = \frac{2b \sin \omega b}{\omega b} + 2a \frac{\sin \omega a}{\omega a} \cos \omega(a+b)$$

$$+ a \left[\cos \left\{ (\omega+\omega_0) \ a+\omega b \right\} \frac{\sin[(\omega+\omega_0)a]}{(\omega+\omega_0)a} \right.$$

$$\left. + \cos \left\{ (\omega-\omega_0)a+\omega b \right\} \frac{\sin[(\omega-\omega_0)a]}{(\omega-\omega_0)a} \right] \qquad \text{(A45)}$$

where $\omega_0 = \frac{\pi}{2a}$ and $\omega = 2\pi f$

Some simple limiting cases are

$$\lim_{b \to 0}, \quad T = 2a \, \frac{\sin 2\omega a}{2\omega a} \left[\frac{1}{1-\left(\frac{2\omega a}{\pi}\right)^2} \right] \tag{A46}$$

[*Jenkins and Watts*, p 244]

$$\lim_{a \to 0}, \quad T = \frac{2b \, \sin \omega b}{\omega b} \tag{A47}$$

[*Jenkins and Watts*, p 244]

To find the shape of the spectral window $Q(f)$ we must substitute $W(f) = |T(f)|^2$ in equation (A42). Some typical spectral windows are shown in Figures A2, A3, A4.

In our analysis of the magnetic data, the window $B(t)$ was set with $a/b = 0.2$ and the summation limits were $k_1 = k_2 = k = \frac{3N}{m}$, where k is the smallest integer closest to $3N/m$. If $\frac{N}{m} = 1$ this is a sum over 7 estimates (see equation (A39)). For convenience, the corresponding spectral window is denoted by
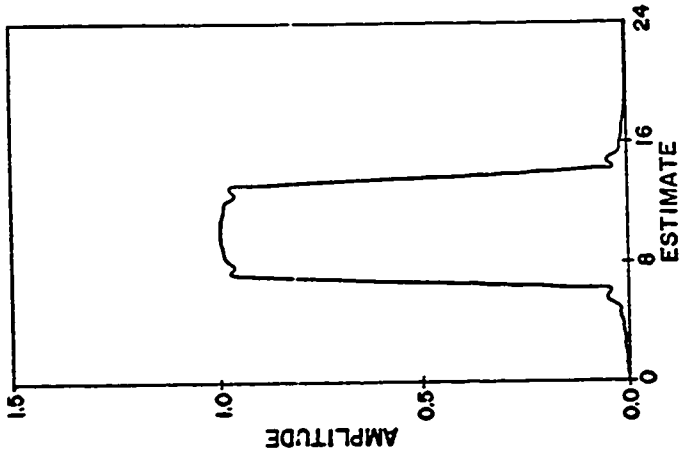
$$Q(f, a/b = 0.2, k = 3N/m).$$

Fig. A4.
The spectral window
Q(f, a/b = 0.0,
$\sum$ 10 estimates,
m/N = 0.7)
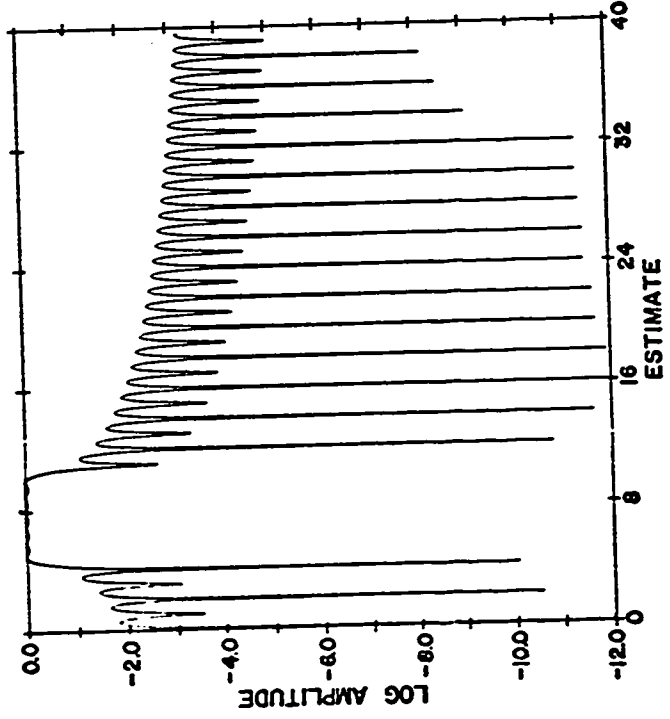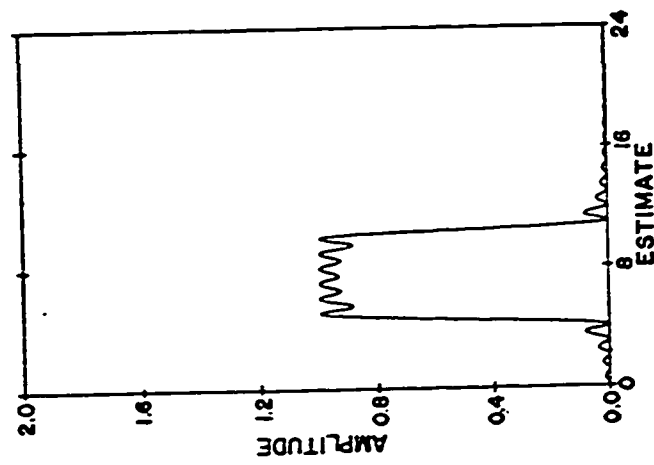
Fig. A3.
A logarithmic plot of the spectral
window in Figure A2.

Fig. A2.
The spectral window
Q(f, a/b = 0.0,
$\sum$ 6 estimates,
m/N = 1.0)

APPENDIX A3 VARIANCE OF THE SPECTRAL ESTIMATORS:
CONFIDENCE LIMITS

If a time series has an approximately normal distribution of amplitudes, then the real and imaginary parts of the discrete Fourier transform of this series also have normal distributions. In other words if

$$A(n) = a(n) + ib(n) \qquad (A48)$$

where $A(n)$ is the discrete transform, then $a(n)$ and $b(n)$ have approximately normal distributions [*Jenkins and Watts*, 1968]. The periodogram values

$$|A(n)|^2 = a^2(n) + b^2(n) \qquad (A49)$$

have χ^2_2 distributions and the smoothed periodograms (equation (A39)) have $\chi^2_{2(2k+1)}$ distributions with accordingly decreased variance.

The variance V of the spectral window $Q(f)$ (equation (A42)) can be determined from the relation

$$V = \frac{S^2(f)}{T} \int_{-\infty}^{\infty} Q^2(g) \, dg \qquad (A50)$$

[*Jenkins and Watts*, p241]

where $S(f)$ is the power spectral density at frequency f, T the length of the sample, and Q the normalized

spectral window (i.e. $\int_{-\infty}^{\infty} Q(g)dg = 1$). If we assume

that the window Q is approximately rectangular with

width $(2k+1)\Delta f = (2k+1)(N\Delta t)^{-1}$, then the variance is

$$V \sim \frac{N}{m} \frac{S^2(f)}{2k+1} \qquad (A51)$$

The calculation of the distribution functions

and associated variances of the parameters obtained from

the cross spectral matrix (see for example equations (A17),

(A20), (A21), (A22), (A27), (A28)) is of fundamental

importance in assigning confidence intervals to these

parameters, especially since the expectation and variance

of the parameters depend on the spectral window $Q(f)$.

It is particularly useful to know the distribution functions

of the polarization ratios R_1 and R_2 and the coherency

K_{ij} in order to eliminate those estimates which might

correspond to a random noise source. The calculation of

these distribution functions is not an easy task since they

are all non-linear functions of random variables.

An approximation used to assign confidence limits

to the phase and coherency spectrum is discussed by Jenkins

and Watts. They have shown, using a Taylor series expan-

sion, that the variance of the coherency estimator of a

normally distributed random variable is

$$\frac{I}{2T}(1-K_{ij}^2)^2 \qquad\qquad (A52)$$

where $I = \int_{-\infty}^{\infty} Q^2(f)df$, T the record length, and K_{ij} the expected coherency. The transformed variable $Y = \tanh^{-1}K_{ij}$ has an approximately normal distribution with a constant variance $I/2T$. The confidence limits to be used for the rejection of unwanted random noise can then be estimated from the variable Y_2, transforming back to the original scale to find K_{ij}. We find, using this method, that a 95 per cent confidence limit for the coherency of random noise is

$$0 \le K_{ij} \le 0.45 \qquad\qquad (A53)$$

where we have chosen the spectral window $Q(f,k=3)$.

The distribution functions for R_1 (equation (A17)) and R_2 (equation (A20)) were generated empirically by producing three independent, random series on a computer. Figure A5 is a histogram of the distribution of R_1 obtained using the spectral window $Q(f,a/b=0.2,k=3,N/m=1)$, and Figure A6 is a histogram for R_2 obtained using the same spectral window but with the assumption $R_1 = 1.0$ (only two non-zero time series were used). Inspection of these figures shows that in both cases 95 per cent of the estimates have values less than 0.75. Both the ratios R_1, $R_2=0.75$ can then be used as 95 per cent confidence limits for the rejection of random signals.
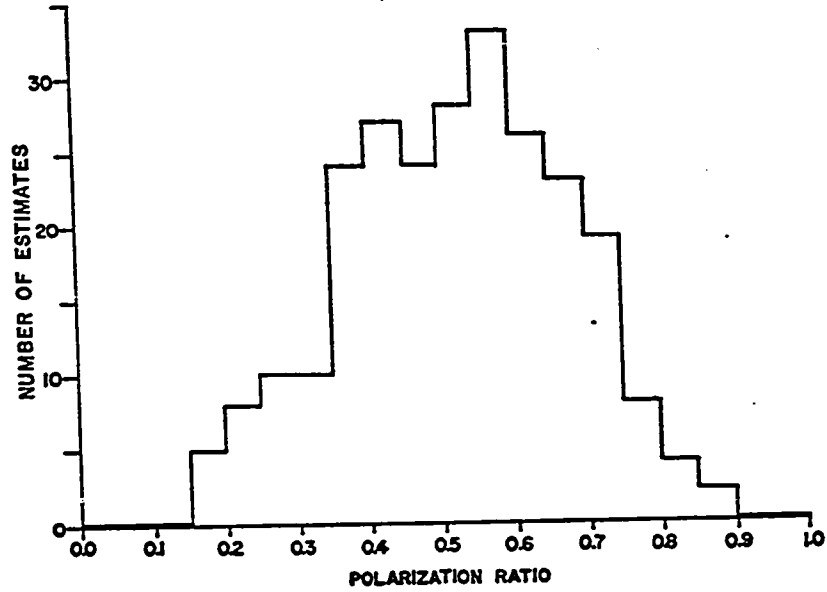
Fig. A5. Histogram of the values of R_1 which were calculated using the spectral window

$$Q(f, \text{ a/b} = 0.2, \text{ k} = 3, \text{ m/N} = 1.0).$$
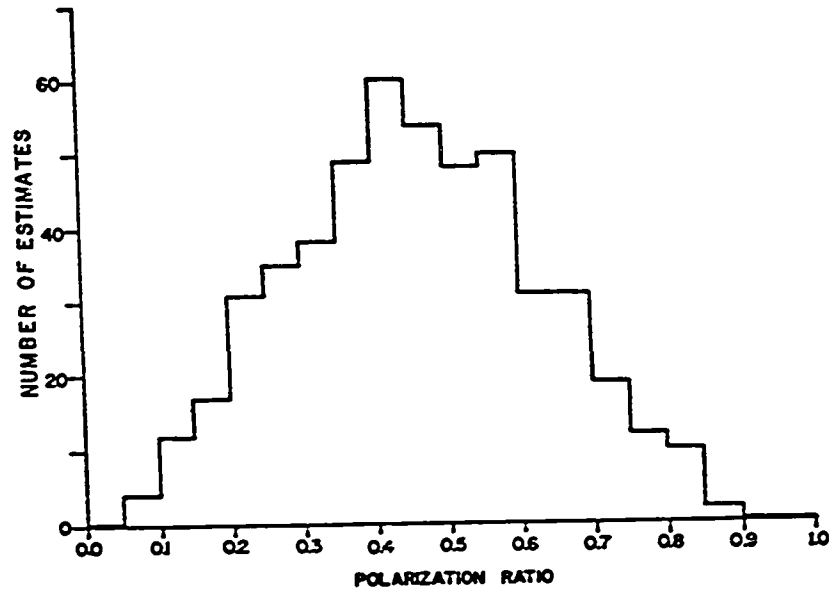

Fig. A6. Histogram of the values of R_2 which were calculated using the spectral window

$$Q(f, \text{ a/b} = 0.2, \text{ k} = 3, \text{ m/N} = 1.0).$$

APPENDIX A4 PRACTICAL CONSIDERATIONS IN ESTIMATING THE SPECTRAL PARAMETERS

A4.1 Selection of the data windows

In choosing the length and shape of the data window $B(t)$ (equation (A44)), a number of conditions must be met. First the lowest frequency and the spectral sample spacing are set by the length $m\Delta t$ of the window. More precisely the spacing of the estimates is $\Delta f = (m\Delta t)^{-1}$ (equation (A30)). Adding zeros to the time series is useful if the data have little noise since the frequency spacing is then $(N\Delta t)^{-1}$ which allows for samples at lower frequencies. This does not increase the resolution of the spectral window which actually depends on the shape of $B(t)$. All that the addition of zeros does is to give a finer spacing of the spectral estimates and in some cases the finer spacing may actually be helpful in selecting very sharp spectral peaks. If the data are noisy, which is the case for most micropulsation data, then the spectral estimates must be smoothed in the manner shown in equation (A39) to reduce the variance. Since the variance of a spectral window is proportional to $\frac{N}{m}$ (equation (A51)), the estim-ates obtained from series with added zeros must be smoothed a proportionately greater amount to achieve a variance

equivalent to estimates obtained from series with no added zeros. The end results, whether zeros are added or not, are spectral windows with the same resolution. One final condition that must be considered is that all discrete Fourier transforms obtained by the FFT must have a number of points which is an integral power of two. This constraint can place severe limitations on the length of the sample so that one normally adds zeros to make up the desired number of points.

A4.2 Detrending the data

It is sometimes apparent from inspection of spectra that much of the power is contained in a few very narrow bands, especially at low frequencies. Since spectral windows have some leakage (see for example Figure A3), these peaks cause errors in spectral estimates at lower powers. Because of this, it is usually necessary to digitally filter the data to remove power at the frequency of these bands before spectral analysis is carried out. In magnetic data recorded with fluxgate magnetometers, low frequency trends can have amplitudes hundreds of times larger than an associated micropulsation event. Consequently it is advantageous to use filters which supress the low frequency components of the magnetic signals.

A4.3 Characteristics of the data windows and detrending

filters

In the analysis of the magnetic data, two different data windows were used. The first was 60 min long and was used in conjunction with a 1-20 mHz bandpass, zero-phase shift, digital filter [*Alpaslan*, 1968]. The second was 30 min long and was used in conjunction with a 2.5-100 mHz digital filter. The frequency and impulse response functions of these filters are shown in Figures A7, A8, and A9. To eliminate the transient response of the filters the first and last 10 min of filtered data were rejected. Both data windows had a cosine taper with a/b = 0.2 (equation (A44)). This cosine taper was used to eliminate any remaining traces of the transient response of the filters and to improve the shape of the smoothed spectral window. In the analysis of the 1969 data only the 60 min data window was used and the data were sampled at every 28th point. In the analysis of the 1970 data using the 60 min window, every 16th data point was taken, and in using the 30 min window, every 8th data point. This gives a total of 117 data points for each window with the ratio N/m = 128/117. Each smoothed spectral window $Q(f)$ had k=3 (equation (A39)) with spectral window widths of
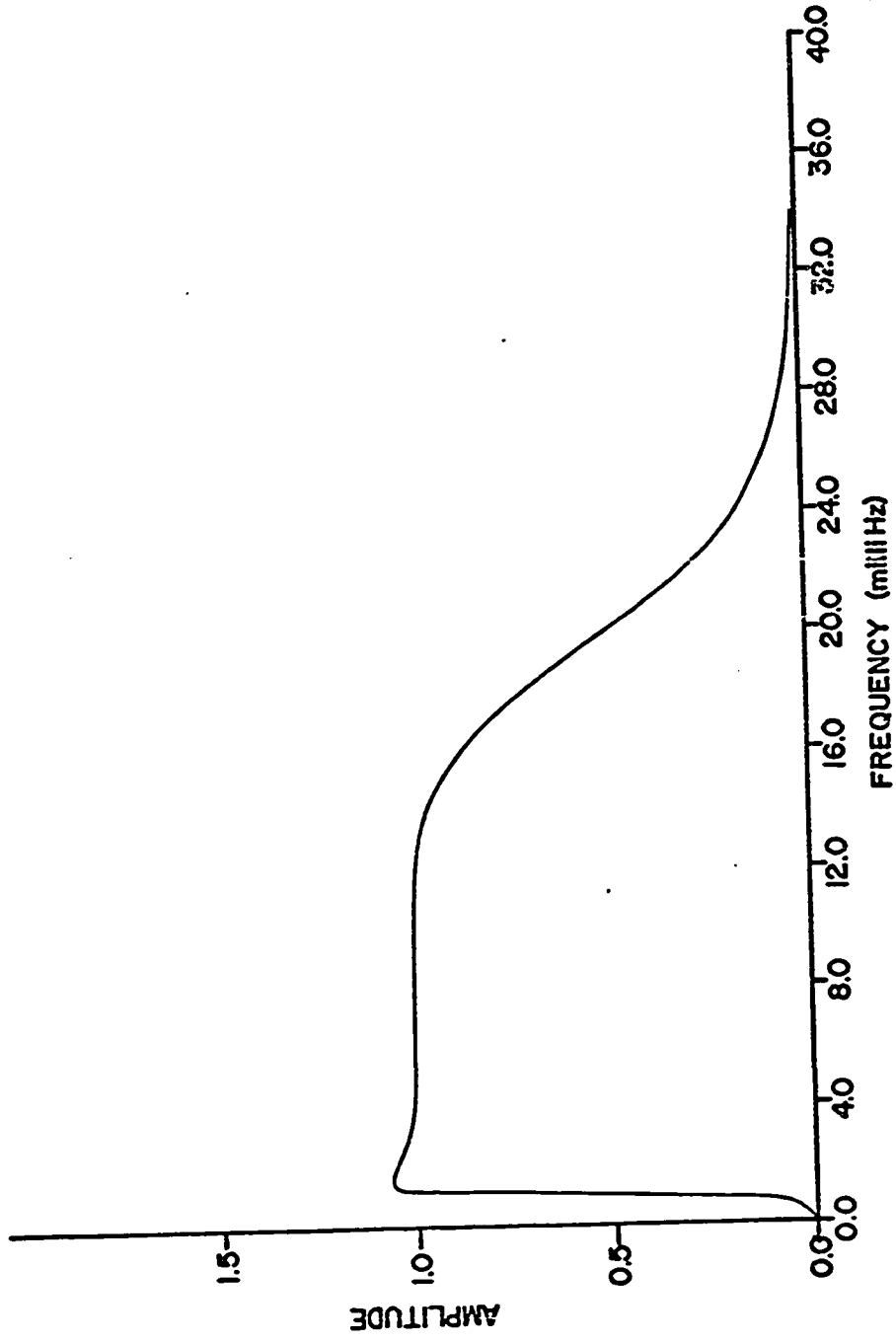
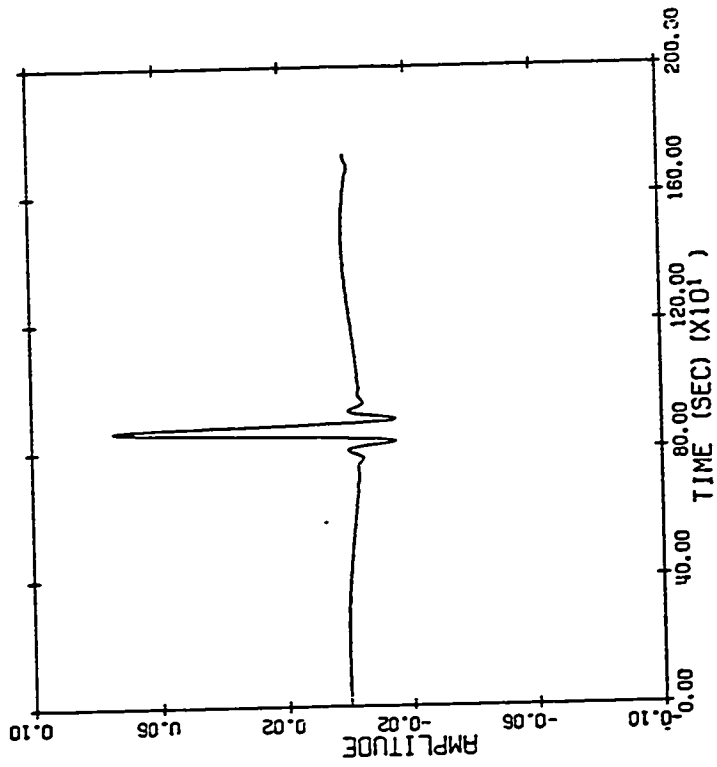Fig. A7. Frequency response of the 1-20 mHz filter.

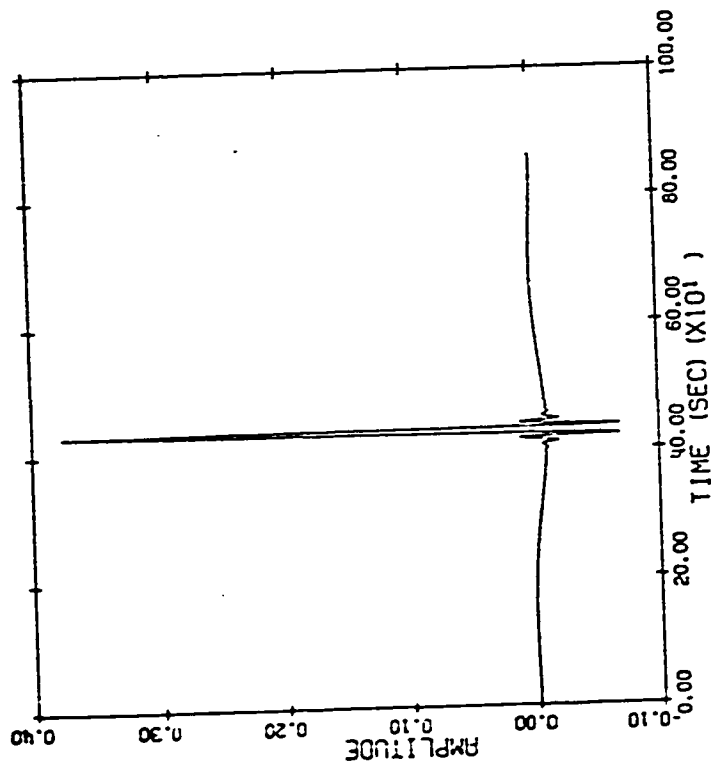Fig. A9. Impulse response of the
1-20 mHz filter.

Fig. A8. Impulse response of the
2.5-100 mHz filter.

1.78 mHz and 3.56 mHz respectively. With filtering and spectral smoothing, the 60 min data window provides a useful frequency range of 1.0-15.3 mHz,while the 30 min data window provides a range of 2.5-30.5 mHz. These ranges correspond roughly to the Pc5 and Pc 4 micropulsation bands.

A4.4 Selection of spectral peaks

The selection of spectral peaks is a difficult problem since the spectral window $Q(f, k=3)$ has very poor resolution at low frequencies. If we define the resolution of the spectral window by the ratio $\Delta f/f$ where Δf is the width of the spectral window, then we find, for example, that in using the 60 min data window $\frac{\Delta f}{f} = 1.78$ at a frequency $f = 1mHz$. A solution to this problem is to estimate the positions of the spectral peaks from the un-smoothed power (equation (A30)). A better method is to smooth the power estimates (equation (A30)) using a window $Q_2(f)$ with width $\Delta v(f)$ (Δv being a function of f) such that

$$\frac{\Delta v(f)}{f} = R \qquad (A54)$$

where R is the best resolution desired. For the interpretation of the polarization parameters it does not matter that the window $Q_2(f)$ changes its spectral width and

variance across the spectrum, since it is used only to locate the spectral peaks. We can then go back to the original spectral data, which was smoothed using $Q(f, k=3)$, to determine those estimates for which the window $Q(f, k=3)$ covered only *one* spectral peak.

APPENDIX A5 THE EFFECTS OF DIGITIZATION ON THE SPECTRUM

The digitization of data adds errors to the data field which depend on the discrete time sample interval Δt and the amplitude sample interval Δq (henceforth referred to as the quantizing interval). Under simple constraints it can be shown that the r.m.s. noise error arising from digitizing is given by $(\Delta q)^2/12$ [*Bendat and Piersol*, 1966]. In fact it is possible to prove that, independent of the data signal used, there is an upper bound to the digitizing error if the digitizing noise is assumed to be a white Gaussian noise with total power $(\Delta q)^2/12$ and bandwidth $(2\Delta t)^{-1}$ [*Mazo*, 1968]. In practice the digitizing error often has the same effect as an added noise source and the spectrum of the digitizing error is independent of the signal over a wide range of signal amplitudes. Even if the signal is so small that its amplitude covers only several quantizing intervals, there is usually enough background instrumental and magnetic noise to determine the amount of digitizing noise and hide its relation to the signal.

More precisely, *Bennett* [1948] has shown that if the digitized signal is a random noise function with a frequency spread 0 to f_o, then the power spectral density

$\Omega(f)$ of the quantizing error, with no time sampling, is given by

$$\Omega(f) = \frac{(\Delta q)^2}{2\pi^3 f_0} \left[\frac{3(\Delta q)^2}{2\pi\Omega_0}\right]^{\frac{1}{2}} \cdot B\left[\frac{3(\Delta q)^2 f^2}{8\pi^2 \Omega_0^2 f_0^2}\right] \qquad (A55)$$

where

$$B(x) = \sum_{n=1}^{\infty} \frac{e^{-x/n^2}}{n^3} \qquad (A56)$$

and Ω_0 is the r.m.s. signal value. If we include discrete time sampling, then the power spectral density function, with aliasing, becomes

$$A(f) = \sum_{n=-\infty}^{\infty} \Omega(f+2nf_N) \qquad 0 \le f \le f_N \qquad (A57)$$

where $f_N = (2\Delta t)^{-1}$ is the Nyquist or alias frequency. If the spectrum of the quantizing noise is aliased many times, $A(f)$ becomes nearly uniform between the Nyquist frequencies. Since quantizing the signal amplitude effectively spreads the bandwidth we would expect considerable aliasing of the quantizing noise. With this in mind, we find that the aliased power spectral density is approximated by the expression

$$A(f) \simeq \frac{\Delta q^2}{12} \left[\frac{1}{2f_N}\right] \qquad \text{(A58)}$$

In our experiment $f_N \simeq 0.26$ Hz, $q \simeq 1\gamma$ and the power spectral density of the quanitizing noise is $0.17\gamma^2 Hz^{-1}$. If an input signal is quasi-sinusoidal with a peak to peak amplitude of $2A\gamma$, then the ratio of the signal power to the noise power is $\sim 6A^2$.

APPENDIX   A6   A BRIEF DESCRIPTION OF THE INSTRUMENTATION

The basic components of the magnetic recording system are shown in Figure A10. Each station was equipped with a three-component magnetometer combined with a WWVB receiver, analogue-to-digital system, and digital tape recorder. Data were recorded on seven-track magnetic tapes at a rate of 3.13 samples/sec in 1969 and at a rate of 1.56 samples/sec in 1970. The records were timed by recording the WWVB radio signal directly on tape every 16 hr 23 min in 1969 and every 7 hr 38 min in the 1970 field season.

All magnetometers, except that at Leduc (where a Sharpe MFO-3 was used), were three-component fluxgate magnetometers designed by the Geomagnetic Division of the Department of Energy, Mines and Resources. The theory behind the fluxgate system has been discussed by *Sersen* [1957]. *Trigg et al.* [1970] give a complete outline of the type of magnetometer used in this experiment. The latter paper provides the general design information as well as details necessary to operate the magnetometer correctly.

The component parts of the magnetometer are displayed in Figure A11. In our experiment we mounted the sensing heads on aluminum poles set in concrete at the
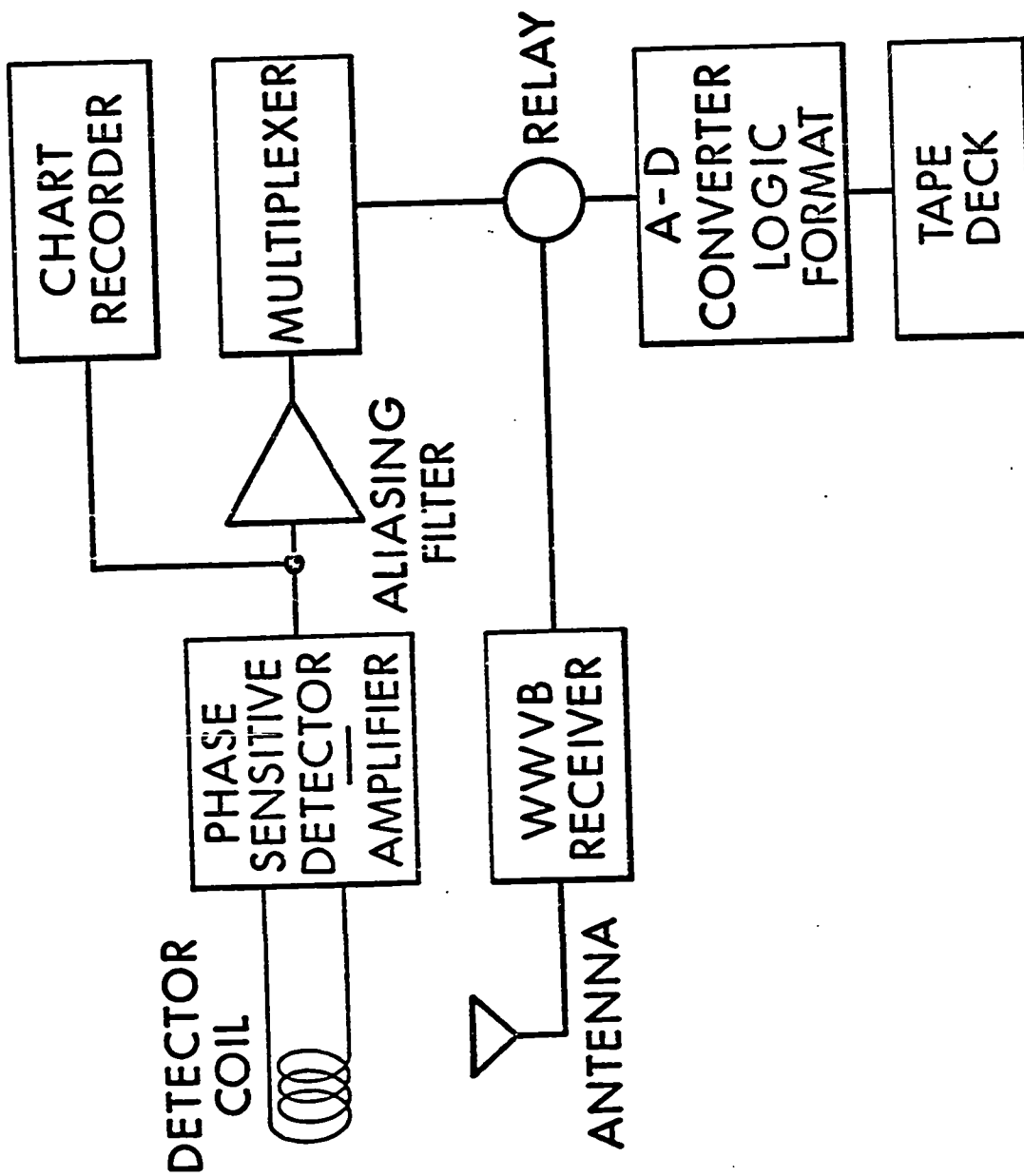
Fig. A10. The basic components of the recording system.
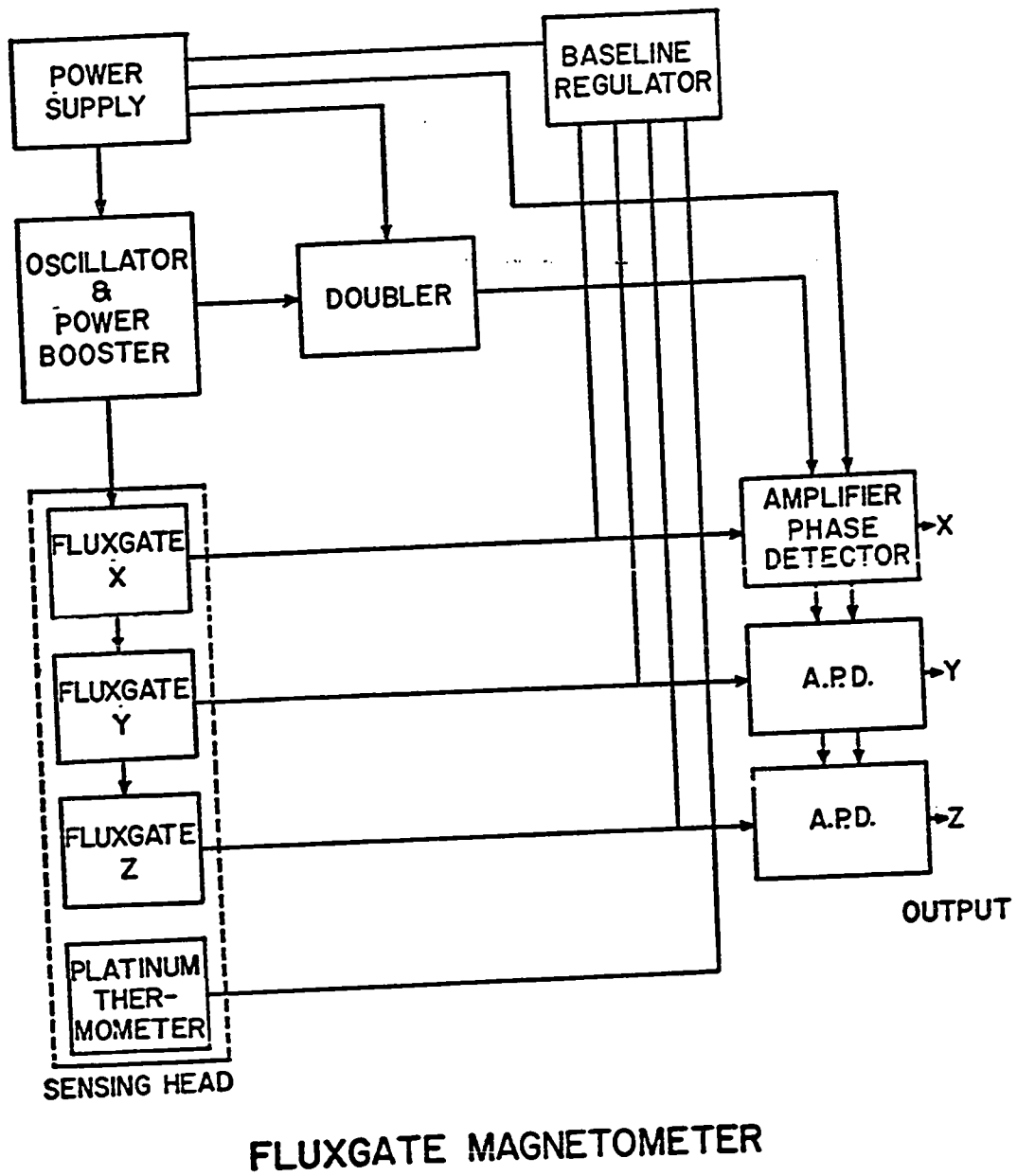
FLUXGATE MAGNETOMETER

Fig. A11. The components of the fluxgate magnetometer.

bottom of rigid plastic containers. The containers were buried with their tops at least 10-20 cm underground. The outputs (X, Y, Z) from the amplifiers had an optimal sensitivity of 10mV/γ and were linear over most of the amplifiers' ±10 V range (Figure A12). The gain and phase shift of the complete magnetometer are essentially flat to 0.1 Hz (Figure A13) which is well beyond the range of frequencies of interest in our experiment.

To prevent aliasing in the spectral analysis of the data, all magnetic signals were passed through two-stage low-pass filters. Even though the power in the natural magnetic spectrum falls off rapidly with frequency, there is often enough natural and instrumental noise at high frequencies to permit considerable aliasing. The frequency response characteristics of a typical filter are shown in Figure A14. In addition, the aliasing filters provide good protection against voltage overloads to the multiplexer since the maximum range of the filters is ±12 volts.

The analogue-to-digital system is based on the Redcor 720 A-D converter, with an added multiplexer bypass line for WWVB, an added WWVB-to-data relay, and a variable stepping rate system coupled to a crystal oscillator (Figure A15). The crystal oscillator and its associated
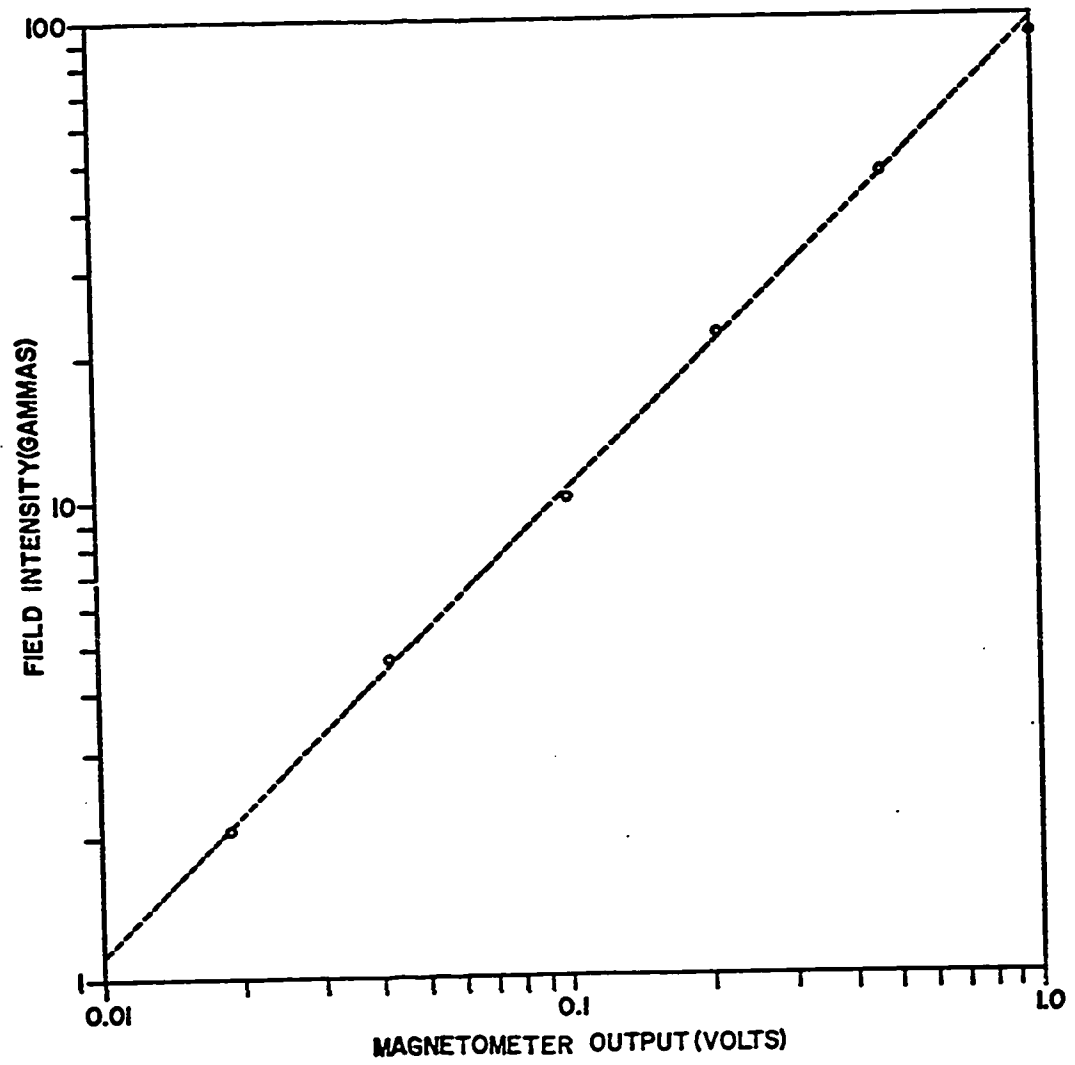
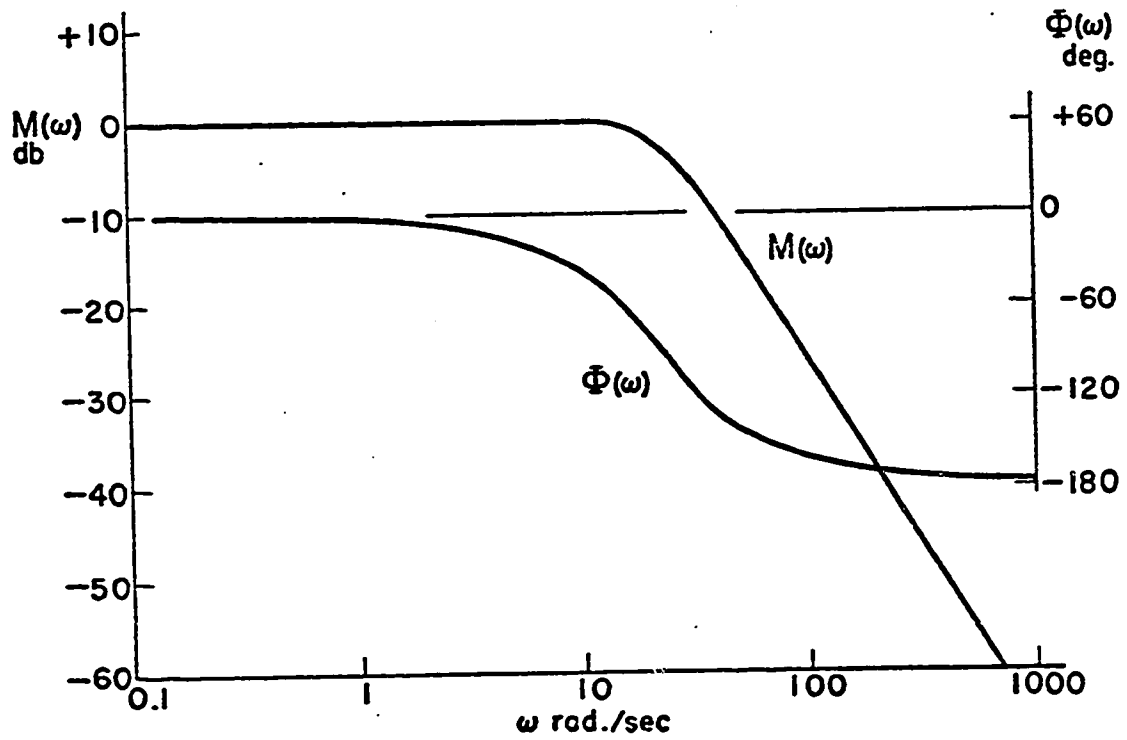Fig. A12. The gain curve of the magnetometer

Fig. A13. Gain and phase response of the magnetometer.
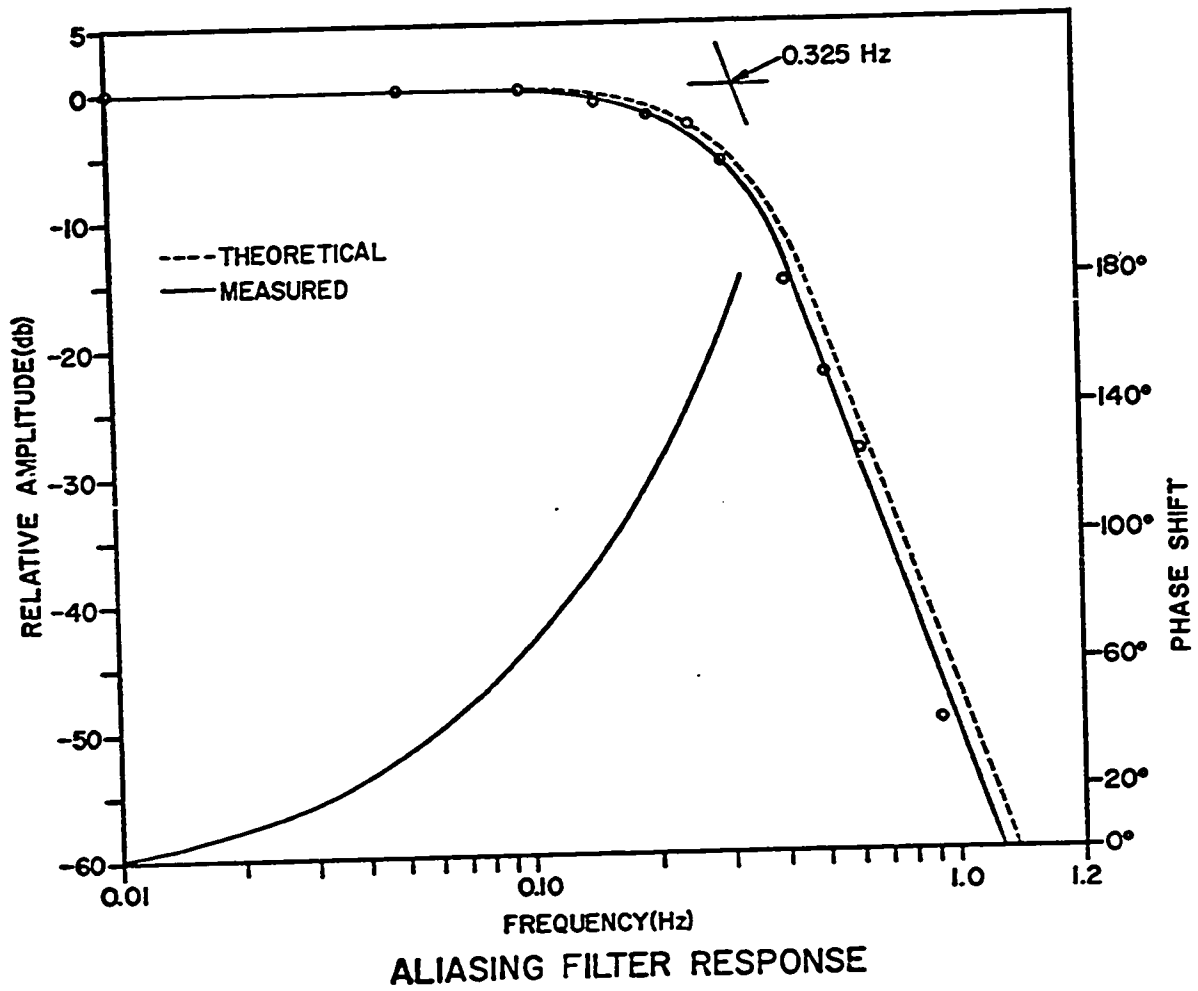(after *Trigg et el.* [1970])

Fig. A14. Gain and phase response of the aliasing filters (1969). The cutoffs of the 1970 filters were at 0.17 Hz.
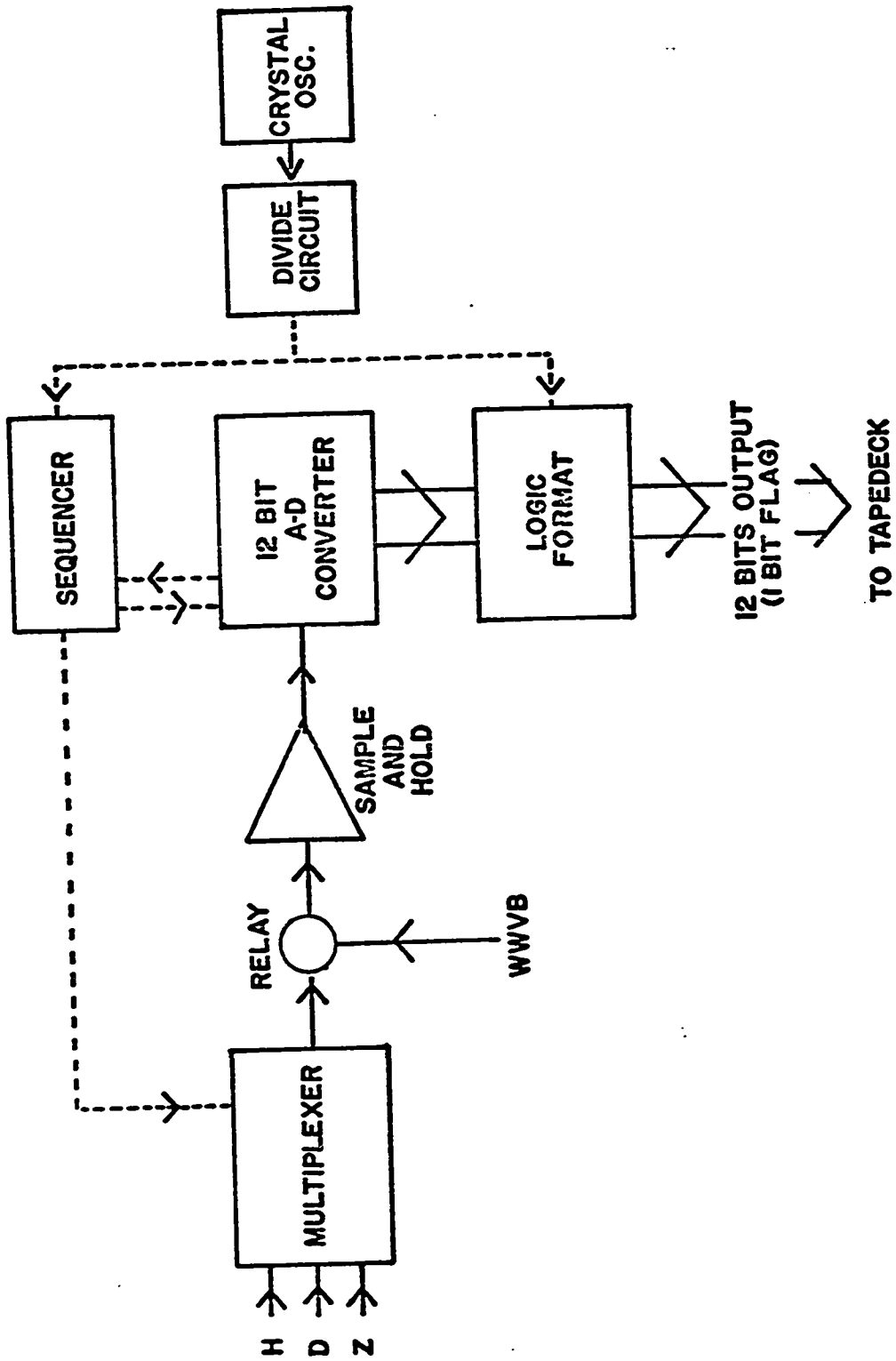
Fig. A15.   The components of the digital recording system.

divide-circuit control the sample rate of the system.
After each set of 7 data blocks (7 hr 38 min) the stepping
rate changes from 1.56/sec (corresponding to a sample
interval of 1.92 sec/component) to 50.0/sec in order to
permit an accurate recording of the WWVB time signal.
Each recording of the WWVB signal lasts 123 sec. Since
the maximum drift of the oscillators is ± 0.005 per cent,
the absolute timing should not be in error by more than
two sec over the interval between WWVB recordings. (In
1969 the interval between WWVB recordings was 16 hr 23 min,
and the sample rate was 3.13/sec). The sequencer controls
the sampling order in the multiplexer. The samples follow
a cyclic order (HDZHD...) and all the sample intervals
are of the same length. The 12 bit A-D converter uses
the successive approximation technique with an offset
binary digital coding format. The logic format board
arranges each sample into two bytes, each byte being 6
digital bits long. The least significant bit is dropped
to permit this bit position to be used as a channel flag
(the flag is utilized to identify errors in the sequential
sampling of the three input channels). Considering the
full scale input for the A-D converter (±10 volts, cor-
responding to ±1000γ) and the available 11 digital bits,

we find that the maximum range of the system is ±1000γ
with an amplitude sample interval (or quantizing interval)
of $1000/2^{10} = 0.976$γ.

The output from the analogue-to-digital system
is recorded on a seven-track Peripheral Equipment incre-
mental write tape deck. Each sample is two bytes long
(2 bytes x 6 bits) and each data block is 6144 samples
long (12288 in 1969). This block length is equivalent
to 65 min 30 sec of magnetic data and 123 sec of the
WWVB time signal.

APPENDIX A7 EARTH INDUCTION EFFECTS

In any attempt to relate ground-based magnetic fields to their sources in the ionosphere and magnetosphere we must assess the effects of induced earth currents and eliminate such effects from the data. In the discussion here we outline briefly the induction effects of uniform and simple, non-uniform earth models on low frequency electromagnetic disturbances.

Price [1950, 1962] has shown that the magnetic field at the surface of a uniform conductor (Figure A16) is given by the equation

$$H = - \left[(A+B) \left[\frac{\partial P}{\partial x} , \frac{\partial P}{\partial y} \right] , \nu P(-A+B) \right] e^{i2\pi f} \qquad (A59)$$

where the inducing field is

$$H = - \left[A \frac{\partial P}{\partial x} , A \frac{\partial P}{\partial y} , \nu AP \right] e^{i2\pi f} \qquad (A60)$$

P is the magnetic potential

$$B = \frac{\theta - \nu}{\theta + \nu} A \qquad (A61)$$

and

$$\theta^2 = \nu^2 + i2\pi\mu f\sigma \qquad (A62)$$

(M.K.S. units)

The reciprocal of the parameter ν is a measure of the horizontal scale of the source field ($\lambda = 2\pi/\nu$), f is the source frequency, μ the magnetic permitivity, and σ the conductivity of the ground
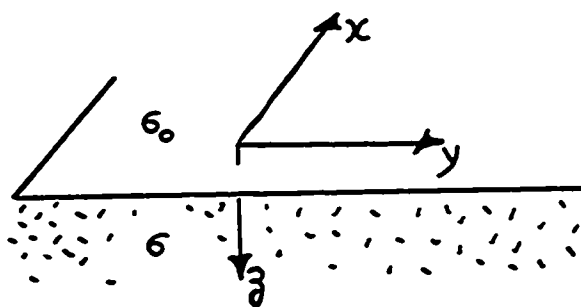

Fig. A16. The coordinate system for the uniform earth model.

The ratio $\dfrac{B}{A} = \dfrac{\theta-\nu}{\theta+\nu}$ gives a good measure of the relative induction effect.

Inspection of equation (A59) shows that uniform induction has no effect on the horizontal projection of the polarization ellipse. The case is different, however for the x-z and y-z planes. As induction increases, the z component decreases and changes phase and the major axis of the ellipse tilts toward the horizontal plane. For complete induction ($\sigma \to \infty$) the z component is zero and the two horizontal components increase by a factor of two.

Table A1 illustrates the relative induction effects for various values of $\beta = 2\pi\sigma f\mu_0\nu^{-2} = 2(10^{-7})\sigma f\lambda^2$

TABLE A1. Relative Induction Effects

β	0.01	0.25	1.0	4.0	25	100	∞
Mod[B/A]	0.0025	0.065	0.22	0.48	0.75	0.87	1.0
Arg[B/A]	90^0	77^0	66^0	39^0	16^0	8^0	0^0

Evidently induction becomes noticeable only when $\beta \geq 1$. If we take the range of values

$$10^6 < \lambda < 4(10^6)m$$
$$10^{-3} < f < 3(10^{-2})Hz \qquad \text{(A63)}$$
$$10^{-4} < \sigma < 10^{-1} mhos/m$$

then the range of β for the parameters influencing our experiment is

$$0.02 < \beta < 9600 \qquad \text{(A64)}$$

These limits show that induction will have an appreciable effect except at low frequencies (< 10 mHz) in resistive regions ($\sigma < 10^{-3}$).

The evaluation of induction effects near horizontal inhomogenieties presents a more difficult problem. In general the magnetic and electric fields are determined by numerical analysis [see e.g. *Jones*, 1970; *Swift*, 1971]. It can be easily shown [see e.g. *Jones*, 1970] that near a vertical contact of contrasting resitivities (Figure A17) the z component of the magnetic field is markedly enhanced when there is a component perpendicular to the strike (i.e. in y direction).
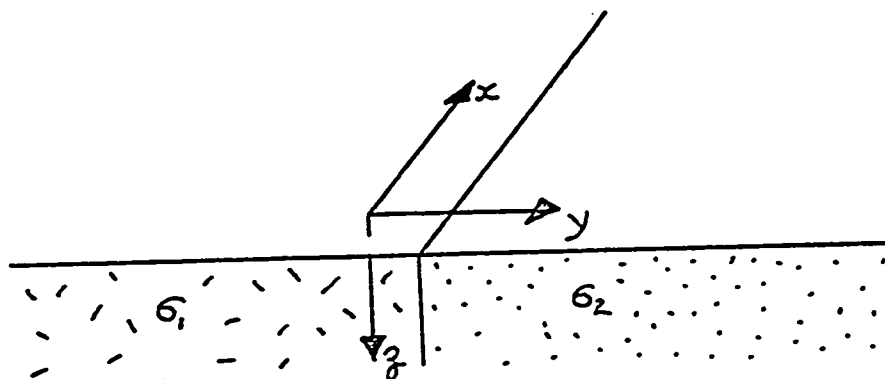

Fig. A17. The coordinate system for the model considered by *Jones* [1970].

Schmucker [1964] noticed this effect in an analysis of geomagnetic data near the coast of California. The relative phases of the y component and z component are seldom greater than 20° in this model and thus the polarization in the y-z plane is nearly linear in all regions. The

x component remains constant across the strike because

of the two dimensional character of the problem (i.e.

$\frac{\partial}{\partial x} = 0$).

Rankin and Reddy [1971] have considered a rather
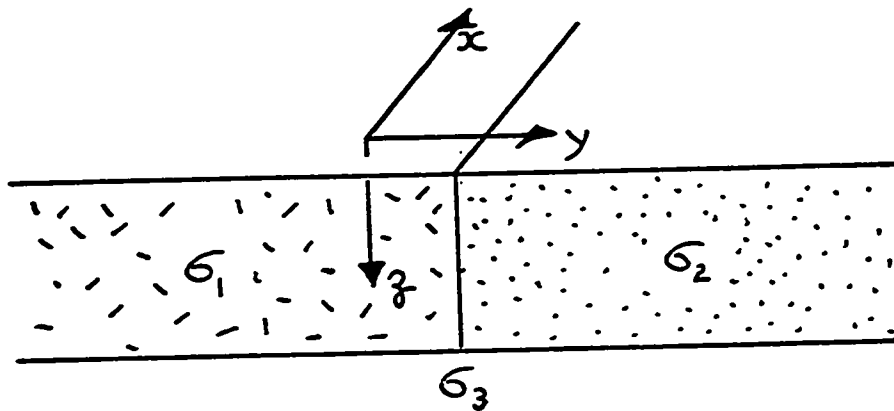
more complex earth model (Figure A18).

Fig. A18. The coordinate system for the model considered

by *Rankin and Reddy* [1971].

Figures A19-A21 show the effects of the discontinuities

in conductivity in this model on the horizontal magnetic

field components. The application of their model is

limited to sources of infinite extent but the model does

give a good indication of the induction effect of dis-

continuities similar to those found in coastal regions.

The greatest induced changes in the sense of polarization

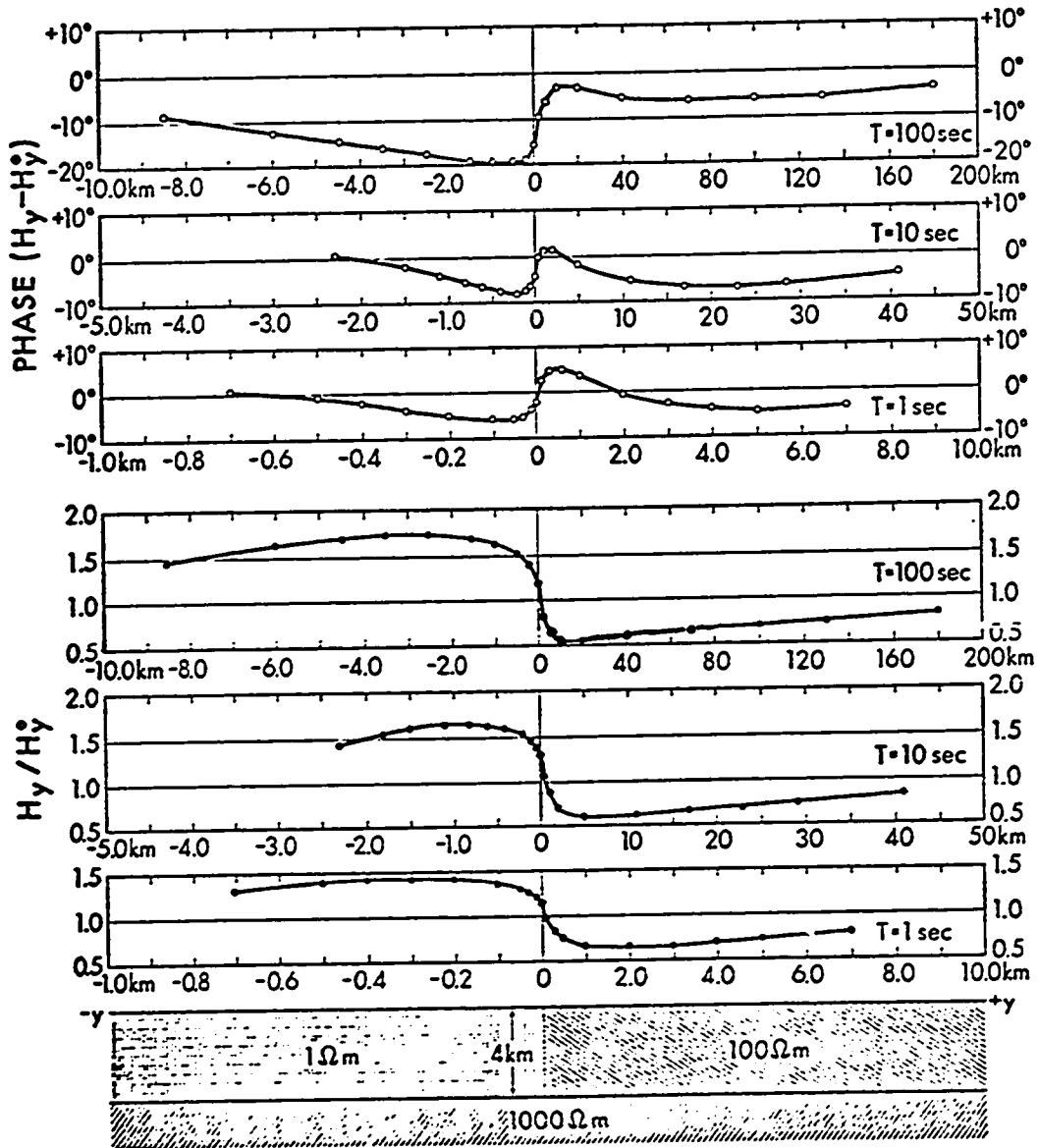occur when the source field is linearly polarized at an

Fig. A19. The relative amplitudes and phases of the y component of the magnetic field (H_y) in the model considered by Rankin and Reddy. H_y^o is the y component of the magnetic field at large distances from the vertical contact. (Note the change in scale on the abscissa; after *Rankin and Reddy* [1971]).
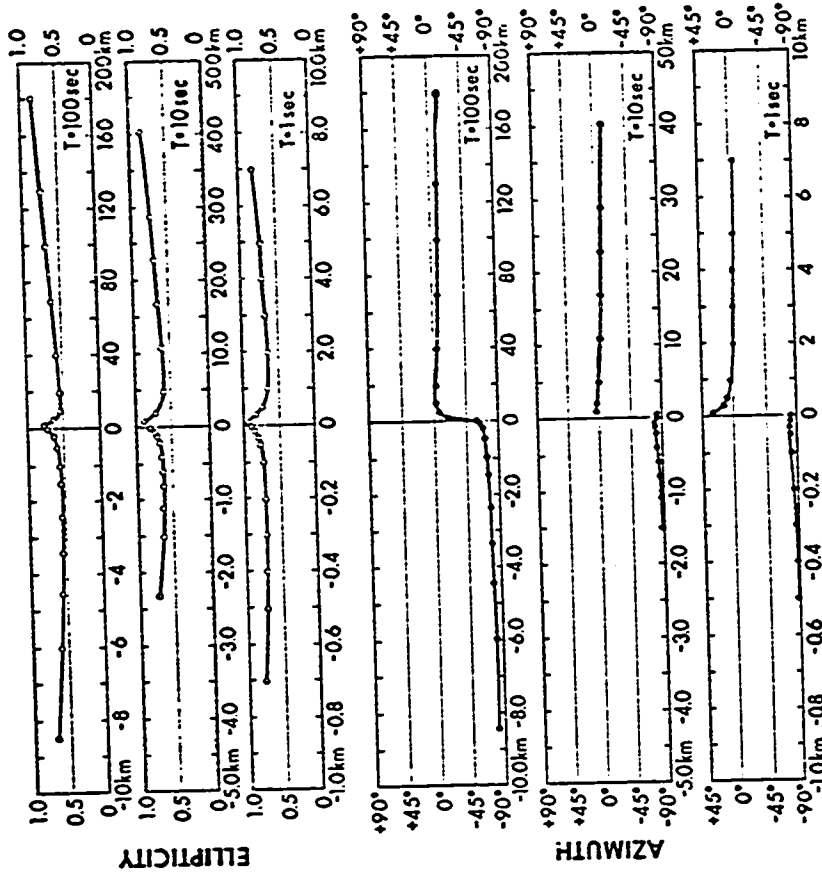
Fig. A21. The azimuth and ellipticity of the observed micropulsation field near the geoelectric structure, shown in Figure A19, for a circularly polarized incident field. (Note the change in scale on the abscissa; after *Rankin and Reddy*, [1971]).
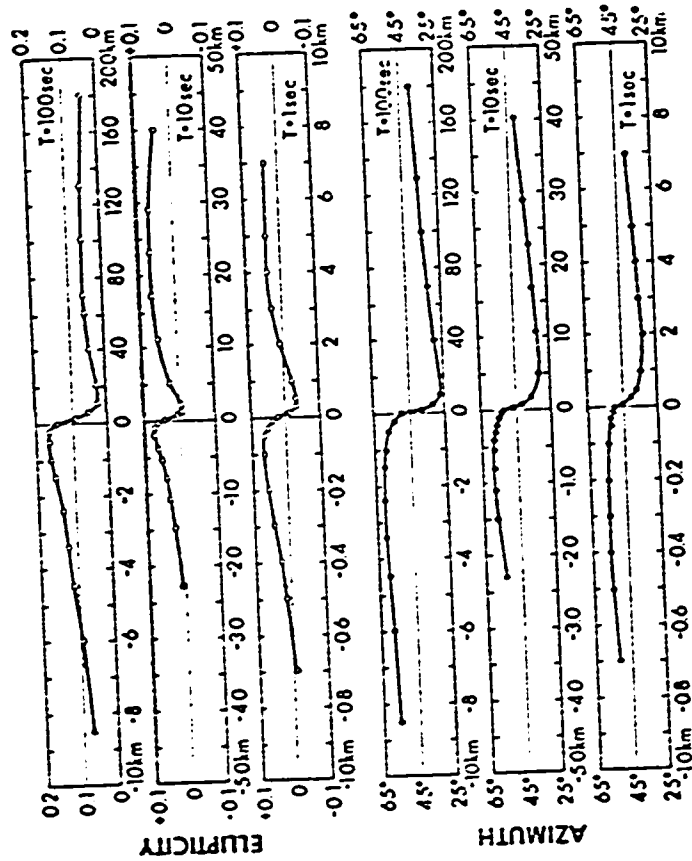
Fig. A20. The azimuth and ellipticity of the observed micropulsation field near the geoelectric structure, shown in Figure A19, for a linearly polarized incident field. (Note the change in scale on the abscissa.) The azimuth of the major axis of the ellipse is measured with respect to the x direction. A positive sign denotes a clockwise measurement (after *Rankin and Reddy*, [1971]).

angle of 45° to the strike (Figure A20). The ellipticity changes from ~ 0 on the resistive side (land) to ~ 0.1 on the conducting side (ocean). If the source is circularly polarized the apparent sense of polarization remains unchanged (Figure A21) although the magnitude of the ellipticity varies from 1.0 to 0.5. Note that the major axis of the ellipse is parallel to the strike on the resistive side and perpendicular to the strike on the conducting side.